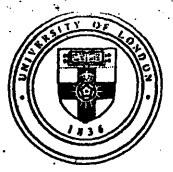

UNIVERSITY OF LONDON THESIS

Degree PhD Year 2006 Name of Author CICCIA, Alberto

THE MUS81 FAMILY OF PROTEINS

BY

ALBERTO CICCIA

Thesis submitted to the University of London,
for the degree of Doctor of Philosophy,
May 2006

ProQuest LLC
789 East Eisenhower Parkway
P.O. Box 1346
Ann Arbor, MI 48106-1346

ACKNOWLEDGEMENTS

First I would like to thank my supervisor Steve for giving me the opportunity of working in his lab and for guiding and supporting me with enthusiasm during my PhD studies. I am also grateful to my second supervisors, Irina and Simon, for their valuable suggestions on my experiments and to Razq Hakem, Weidong Wang, Johan de Winter and Shunichi Takeda for the nice and fuitful collaborations.

I would also like to thank all the lab members (Brenda, Cynthia, Fumiko, Ivan, Jean Yves, Michael, Rajvee, Stephen, Thomas, Tina, Uli, Yilun) for being always very helpful and supportive. A special thanks goes to Ivan, Michael, Steve and Yilun for valuable comments on this thesis. Moreover, I would like to thank Fumiko, for all the patience in sharing the bench (and especially the freezer) with me, Ivan for his constant support and encouragement and Yilun for all her advice and suggestions given during these four years (from experiments to car shopping).

Moreover, I am very grateful to Vincenzo for all the insightful scientific discussions and ideas and my flatmates Christian, Kristian, Michael and Neli for the nice time spent together. I would also like to thank Cell Culture and Fermentation services for providing many reagents and all the friends in Clare Hall for making my time here more pleasant and entertaining.

Finally I would like to thank my parents, my sister Laura, my brother Marco, my grandmother Caterina, my aunt Tanina and Davide for their support throughout all my studies.

ABSTRACT

The faithful and complete replication of DNA is necessary for the maintenance of genome stability. The endonuclease MUS81 has recently been implicated in the repair of blocked forks during DNA replication.

MUS81 is related to the nucleotide excision repair proteins XPF and ERCC1, due to the common ERCC4 nuclease domain that they share. Based on database searches for proteins containing the ERCC4 domain, we have identified four novel members of the MUS81 family. We named two of them EME1 and EME2, because of their similarity with *S. pombe* Eme1 protein. We showed that EME1 and EME2 interact with MUS81 and that MUS81/EME1 and MUS81/EME2 complexes are endonucleases that exhibit a high specificity for synthetic replication fork and 3'-flap structures *in vitro*. In particular, the MUS81/EME2 heterodimer is 10-fold more active than MUS81/EME1.

Besides EME1 and EME2, we have identified two additional proteins of the MUS81 family, HEF and HIP. HEF, also referred to as FANC-M, is a 250 kDa protein that is associated with the genetic disorder of Fanconi Anemia. HIP (HEF Interacting Protein) is a novel 24 KDa protein interacting with HEF/FANC-M. We showed that HIP forms a complex with HEF/FANC-M both *in vitro* and *in vivo* and that it is part of the Fanconi Anemia core complex.

HEF/FANC-M contains a DEAH helicase domain, which is required for translocase activity, and an ERCC4 nuclease domain. We showed that the ERCC4 nuclease domain of HEF/FANC-M is inactive, as suggested by sequence analysis. Based on the similarity with other members of the MUS81 family, we propose a role for the complex between HEF/FANC-M and HIP in recognising branched DNA structures, which could arise after DNA replication fork blockage. Therefore, HEF/FANC-M and HIP may be involved in targeting the Fanconi Anemia core complex to blocked replication forks.

CONTENTS

LIST OF FIGURES

CHAPTER ONE

CHAPTER TWO

CHAPTER THREE

CHAPTER FOUR

CHAPTER FIVE

CHAPTER SIX

APPENDIX ONE

APPENDIX TWO

ABBREVIATIONS

A. pernix	*Aeropyrum pernix*
ATP	adenosine triphosphate
BER	base excision repair
bp	base pair
BSA	bovine serum albumin
C. familiaris	*Canis familiaris*
CPT	camptothecin
CS	Cockayne syndrome
CV	column volume
D. melanogaster	*Drosophila melanogaster*
D. rerio	*Danio rerio*
ddH_2O	double distilled water
dHJ	double Holliday junction
DNA	deoxyribonucleic acid
dNTP	deoxynucleotide triphosphate
DSB	double-strand break
dsDNA	double-stranded DNA
DTT	dithiothreitol
E. coli	*Escherichia coli*
EDTA	ethylenediaminetetraacetic acid
ES cell	embryonic stem cell
FA	Fanconi Anemia
G. gallus	*Gallus gallus*
H. sapiens	*Homo sapiens*
HhH	helix hairpin helix
HJ	Holliday junction
HRR	homologous recombination repair
HU	hydroxyurea
ICL	interstrand cross-link
IPTG	isopropyl-β-D-thiogalactoside
IR	ionising radiation
kbp	kilobase pair

kDa	kilodalton
M. musculus	*Mus musculus*
MEF	mouse embryo fibroblast
MMC	mitomycin C
MMR	mismatch repair
MMS	methyl-methane sulfonate
NCBI	national center for biotechnology information
NER	nucleotide excision repair
NHEJ	non-homologous end joining
NP40	nonidet P40
P. furiosus	*Pyrococcus furiosus*
P. troglodytes	*Pan troglodytes*
PAGE	polyacrylamide gel electrophoresis
PBS	phosphate buffer saline
PHYRE	protein/homology/analogy recognition engine
PSI-BLAST	position specific iterated – basic local alignment search tool
R. norvegicus	*Rattus norvegicus*
rDNA	ribosomal DNA
RFB	replication fork barrier
RTS1	replication termination sequence 1
S. cerevisiae	*Saccharomyces cerevisiae*
S. pombe	*Schizosaccharomyces pombe*
S. solfataricus	*Sulfolobus solfataricus*
SDS	sodium dodecyl sulfate
SDSA	synthesis dependent strand annealing
SEI	single end invasion
SF2	superfamily 2
SSB	single-strand break
ssDNA	single-stranded DNA
T. negroviridis	*Tetraodon negroviridis*
TEMED	N,N,N',N'-(tetramethylethylenediamine)

TLS	translesion DNA synthesis
Tris	tris (hydroxymethyl) aminomethane
TTD	trichothiodystrophy
UV	ultraviolet
X. laevis	*Xenopus leavis*
X-gal	5-bromo-4-chloro-3-indolyl-beta-D-galactopyranoside
XP	xeroderma pigmentosum

CHAPTER ONE

Introduction

I. DNA DAMAGE

1.1 DNA DAMAGING AGENTS

The faithful conservation of genomic information is an essential process for cell survival. In order to maintain genomic integrity, DNA has to be protected from damage induced by environmental agents or generated spontaneously during DNA metabolism.

Environmental DNA damage can be produced by physical or chemical sources. Examples of physical genotoxic agents are ultraviolet (UV) light and ionizing radiation (IR). UV light is a component of sunlight. Extensive exposure to UV light can cause adjacent DNA bases to become covalently linked by the formation of pyrimidine dimers and (6-4) photoproducts (Cleaver et al., 1988; Setlow, 1966). IR can be generated either by natural sources (*e.g.* cosmic radiation) or by man-made sources used for medical (*e.g.* X-rays) or industrial purposes. IR exposure can induce oxidation of DNA bases and generate breaks on one or both DNA strands (Hutchinson, 1985; Teoule, 1987), referred to as single-strand and double-strand breaks, respectively. Chemical agents can cause a variety of DNA lesions: alkylating agents, such as methyl-methane sulfonate (MMS), insert alkyl groups into DNA bases (Singer, 1975), while cross-linking agents, such as mitomycin C (MMC), *cis*-platin, psoralen and nitrogen mustard (Brendel and Ruhland, 1984), introduce cross-links between bases of the same DNA strand (intrastrand cross-links) or of different DNA strands (interstrand cross-links or ICLs). Other chemical agents, such as the topoisomerase inhibitor camptothecin (CPT), induce the formation of single-strand breaks (SSBs) by trapping the topoisomerase-DNA covalent complex

(Liu et al., 2000). Hydroxyurea (HU), instead, does not induce any specific DNA lesion, but affect DNA metabolism by depleting dNTP levels through the inhibition of ribonucleotide reductase (Bianchi et al., 1986).

The main spontaneous DNA alteration arising during DNA metabolism is the misincorporation of DNA bases during DNA replication (Echols and Goodman, 1991). This can result in mismatches in the DNA sequence. DNA mismatches can also be generated by the spontaneous interconversion between DNA bases due to the loss of amino groups (*e.g.* deamination of cytosine and 5-methylcytosine into uracil and thymine, respectively) (Lindahl, 1993). Another source of spontaneous DNA damage is constituted by reactive oxygen species (hydrogen peroxide, peroxide and hydroxyl radicals) derived from normal cellular metabolism. Reactive oxygen radicals can cause fragmentation of DNA bases or sugars and induce SSBs (Imlay and Linn, 1988).

1.2 MOLECULAR AND CELLULAR EFFECTS OF DNA LESIONS

DNA lesions can interfere with basic cellular processes such as DNA replication and gene transcription. DNA damage generated during G1 and G2 phases of the cell cycle can block transcription of genes, while DNA lesions in S phase primarily affect DNA replication. It has been reported that cross-linking agents and UV radiation can block RNA polymerase (Selby et al., 1997; Tornaletti et al., 2003; Tremeau-Bravard et al., 2004) and lead to its polyubiquitination and degradation (Bregman et al., 1996; Ratner et al., 1998). Persistent blockage of RNA synthesis has been linked with induction of apoptotic cell death dependent on p53 (Latonen and Laiho, 2005).

DNA replication can be affected by the presence of DNA lesions induced by UV radiation. Early studies carried out in *E. coli*, *S. cerevisiae* and mammalian cells showed that after UV radiation, the newly synthesised DNA was significantly smaller compared to the DNA of non-irradiated cells (Lehmann, 1972; Prakash, 1981; Rupp et al., 1971). This was attributed to the presence of discontinuities left opposite the UV lesions by the DNA polymerase. Recently, these discontinuities have been visualised by electron-microscopy in

UV-irradiated *S. cerevisiae* cells (Lopes et al., 2006). Besides UV lesions, damage induced by alkylating agents, such as MMS, have been shown to slow down DNA replication in *S. cerevisiae* (Tercero and Diffley, 2001). Lesions induced by cross-linking agents cause one of the most severe blockages of DNA replication: covalently linking two DNA strands together, interstrand cross-links (ICLs) can impede strand separation and replication progression (Niedernhofer et al., 2005). Instead SSBs, which can be generated by CPT, IR or reactive oxygen species, can be converted to double-strand breaks (DSBs) during DNA replication, and therefore induce the collapse of the replication fork (Kuzminov, 2001b).

In addition to DNA replication and transcription, mitosis can also be affected by DNA lesions. The presence of DSBs in the chromosomal DNA can prevent proper chromosome segregation and can lead to uneven distribution of the genome between the two daughter cells. DSBs can also induce the formation of chromosomal deletions and translocations, which are a hallmark of cancer cells (Hoeijmakers, 2000).

II. DNA REPAIR MECHANISMS

In order to counteract the deleterious effects generated by DNA damaging agents, repair mechanisms specific for each type of DNA lesion have evolved to protect genomic integrity (Friedberg, 2003). Mispaired DNA bases are replaced with correct bases by mismatch repair (MMR) (Kunkel, 1995) and small chemical alterations of DNA bases are repaired by base excision repair (BER) through excision of the damaged base (Lindahl and Wood, 1999). More complex lesions, such as pyrimidine dimers and intrastrand cross-links, are corrected by nucleotide excision repair (NER) through the removal of a nucleotide of approximately 30 bp containing the damaged bases (Friedberg, 2001), while ICLs are excised by interstrand cross-link repair (ICL repair) with the assistance of proteins involved in the genetic syndrome Fanconi Anemia (Niedernhofer et al., 2005). DSBs are processed either by non-homologous end

joining (NHEJ) or homologous recombination repair (HRR) according to the cell cycle phase during which they are generated: during G1 phase DSBs are repaired primarily by NHEJ through the inaccurate religation of the broken ends, while during S and G2 phases sister chromatids are used as a template for the precise repair of the DSBs by HRR (West, 2003).

As previously mentioned, DNA damage during S phase can result in DNA replication blockage (Section 1.2). The processes by which stalled replication forks are repaired are referred to as DNA-damage-tolerance mechanisms (Friedberg, 2005). A DNA lesion in a replication fork can be bypassed by error-prone DNA polymerases in a process known as translesion DNA synthesis (TLS). In an alternative to TLS, the discontinuities left opposite the lesion can be repaired with high fidelity by HRR (Friedberg, 2005). NER, HRR, DNA-damage-tolerance mechanisms and ICL repair will be discussed in greater details in future sections.

1.3 NUCLEOTIDE EXCISION REPAIR

The general mechanism of NER is conserved from bacteria to humans, but the proteins involved share little similarity and many steps are more complex in the mammalian system. In bacteria, NER is catalysed by the UvrABC system (Truglio et al., 2006). In humans, defects in some of the NER components cause the genetic disorders xeroderma pigmentosum (XP), Cockayne syndrome (CS) or trichothiodystrophy (TTD) (de Boer and Hoeijmakers, 2000). XP patients exhibit more than 1000-fold incidence of sun-induced skin cancer, whereas CS and TTD patients are not predisposed to tumour development (de Boer and Hoeijmakers, 2000; Friedberg, 2001). XP is caused by mutations in one of eight genes (*XPA* - *XPG* and *XPV*) (Bootsma and Hoeijmakers, 1994). Unlike the other seven genes, *XPV* gene is involved in TLS and not in NER (Ensch-Simon et al., 1998).

NER has been reconstituted *in vitro* with purified human proteins (Aboussekhra et al., 1995; Mu et al., 1996). The DNA lesion is recognised by the complex between XPC and hHR23B (Figure 1.1, step a) (Sugasawa et al., 1998). hHR23B is the human homologue of *S. cerevisiae* NER protein Rad23

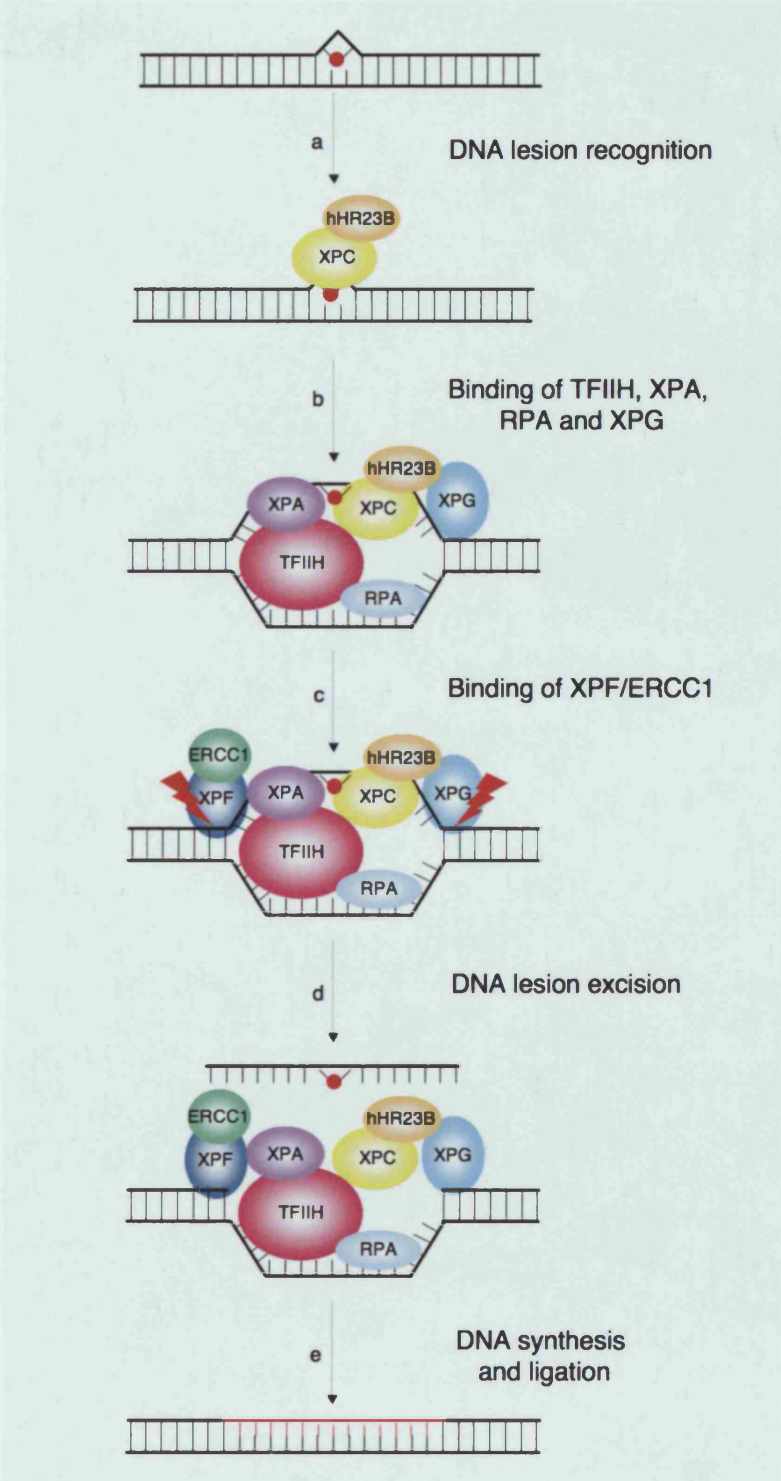

FIGURE 1.1: Schematic representation of mammalian nucleotide excision repair

See the main text in Section 1.3 for detailed description.

(Sugasawa et al., 1996). XPA, RPA, TFIIH and XPG are then recruited to the site of damage (Figure 1.1, step b) (Friedberg, 2001). XPA is able to confirm the presence of DNA damage by the recognition of an abnormal DNA structure (Buschta-Hedayat et al., 1999). TFIIH is a six subunit transcription factor required for initiation of RNA polymerase II transcription (Zurita and Merino, 2003). The TFIIH subunits XPB and XPD can unwind the duplex DNA on both sides of the lesion and create a bubble structure that can be stabilised by the single-strand binding protein RPA (Figure 1.1, step b) (Evans et al., 1997b). Following the binding of the XPF/ERCC1 complex, the damaged DNA strand is cleaved sequentially on the 3'-side of the lesion by XPG and on the 5'-side by XPF/ERCC1 (Figure 1.1, step c) (O'Donovan et al., 1994; Sijbers et al., 1996a). The double incision allows the release of an oligonucleotide approximately 30 nt long (Figure 1.1, step d) (Moggs et al., 1996). DNA integrity is then restored by DNA polymerase δ or ε and DNA ligase (Figure 1.1, step e) (Hindges and Hubscher, 1997; Mozzherin and Fisher, 1996).

1.4 HOMOLOGOUS RECOMBINATION REPAIR

HRR is responsible for the accurate repair of DNA lesions, such as ssDNA gaps or DSBs, which can be produced by DNA damaging agents such as UV and IR or can occur during DNA replication as a consequence of replication fork blockage or collapse (McGlynn and Lloyd, 2002b; Paques and Haber, 1999). Moreover, in eukaryotes DSBs are induced during meiosis by the endonuclease Spo11 in order to generate genetic diversity (Keeney et al., 1997). This section will concentrate on the repair of DSBs, whereas the repair of ssDNA gaps will be discussed in Section 1.5.

Several models have been suggested for DSB repair in eukaryotes. In the classical DSB repair model proposed in 1983 by Szostak et al. (Figure 1.2) (Szostak et al., 1983), DSBs are processed in order to generate 3'-ssDNA ends, which are required to initiate HRR. A possible candidate for the resection of DSBs ends is the MRE11/RAD50/NBS1 complex (Figure 1.2, step a) due to its reported nuclease activity on DNA ends (Paull and Gellert, 1999). However, *in vitro* MRE11/RAD50/NBS1 produces only 5'-ssDNA ends and not 3'-ssDNA

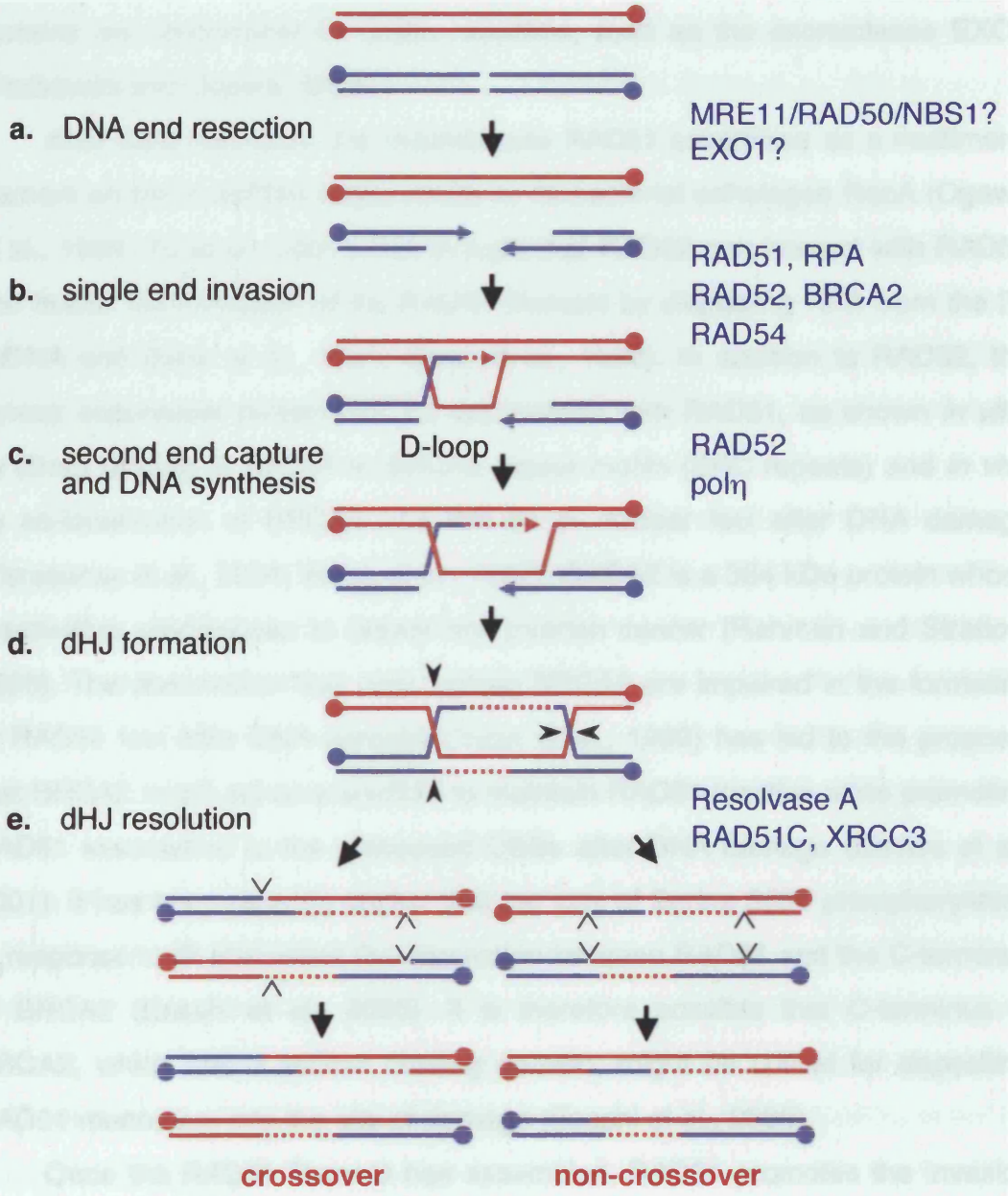

FIGURE 1.2: General model of DSB repair as suggested by Szostak et al., 1983

Proteins involved in each step of the DSB repair model are indicated in blue. See the main text in Section 1.4 for detailed description. This figure has been adapted from Hollingsworth and Brill, 2004.

ends (Paull and Gellert, 1998). It is possible that MRE11/RAD50/NBS1 *in vivo* could generate 3'-ssDNA ends by a yet unknown mechanism, or that other proteins are responsible for DSBs resection, such as the exonuclease EXO1 (Tsubouchi and Ogawa, 2000).

After DSB resection, the recombinase RAD51 assembles as a multimeric filament on the 3'-ssDNA ends, similar to its bacterial orthologue RecA (Ogawa et al., 1993; Yu et al., 2001). It is thought that RAD52 can interact with RAD51 and favour the formation of the RAD51 filament by displacing RPA from the 3'-ssDNA end (New et al., 1998; Shen et al., 1996). In addition to RAD52, the tumour suppressor protein BRCA2 can interact with RAD51, as shown *in vitro* by direct binding of RAD51 to BRCA2 repeat motifs (BRC repeats) and *in vivo* by co-localisation of BRCA2 and RAD51 in nuclear foci after DNA damage (Tarsounas et al., 2004; Wong et al., 1997). BRCA2 is a 384 kDa protein whose inactivation predisposes to breast and ovarian cancer (Rahman and Stratton, 1998). The observation that cells lacking BRCA2 are impaired in the formation of RAD51 foci after DNA damage (Yuan et al., 1999) has led to the proposal that BRCA2 might act as a scaffold to maintain RAD51 inactive while promoting RAD51 association to the processed DSBs after DNA damage (Davies et al., 2001). It has been recently shown that the loss of Serine 3291 phosphorylation in response to IR stimulates the interaction between RAD51 and the C-terminus of BRCA2 (Esashi et al., 2005). It is therefore possible that C-terminus of BRCA2, which has a ssDNA binding domain, might be critical for depositing RAD51 monomers into the site of damage (Esashi et al., 2005).

Once the RAD51 filament has assembled, RAD51 promotes the invasion of a single 3'-ssDNA end into the homologous DNA duplex (Baumann et al., 1996; Sung, 1994). This process, which is referred to as single end invasion (SEI), leads to the formation of a structure known as D-loop (Figure 1.2, step b). It has been reported that RAD54 helps to stabilise the formation of D-loop structures obtained after SEI (Mazina and Mazin, 2004; Petukhova et al., 1998). This could be explained by the ability of RAD54, a member of the family of SWI2/SNF2 chromatin remodeling proteins, to induce negative supercoils into duplex DNA and transiently separate the DNA strands (Sigurdsson et al., 2002;

Tan et al., 1999; Van Komen et al., 2000). RAD54-mediated strand separation could therefore promote the formation of D-loop by RAD51. Moreover, the ability of RAD54 to translocate along the DNA could help displace histones and facilitate the identification of homologous sequences (Ristic et al., 2001).

In the classical DNA recombination model proposed by Szostak et al., SEI is followed by the second end capture (Figure 1.2, step c). This could be promoted by RAD52, as suggested by its ability to favour single-strand annealing of complementary sequences *in vitro* (Mortensen et al., 1996). Both ends are then used as primers for DNA synthesis. The mechanism of DNA synthesis after RAD51-mediated strand invasion will be discussed in Section 1.5.

DNA ligation of the newly synthesised strands can lead to the formation of two contiguous four-way junctions, called Holliday junctions (HJs). This structure is referred to as double HJ (dHJ; Figure 1.2, step d). The existence of HJ intermediates formed by two DNA helices covalently linked (Lilley and White, 2001) was initially proposed by Robin Holliday and then confirmed by electron-microscopic studies (Benbow et al., 1975; Doniger et al., 1973; Holliday, 1964; Thompson et al., 1975).

In bacteria, HJs are processed by the RuvABC complex (West, 1997). RuvA targets RuvB to the HJ and enables RuvB to assemble as symmetrical hexameric rings on the two opposite arms of the HJ (Parsons et al., 1995; Yamada et al., 2002). The DNA is then passed through the RuvB rings as a result of the translocase activity of RuvB. This allows branch migration of the HJ along the DNA strands (Tsaneva et al., 1992). In order to separate the two DNA strands connected by the HJ, the endonuclease RuvC binds the HJ as a dimer and promotes HJ resolution by introducing symmetrical nicks in strands of the same polarity (Ariyoshi et al., 1994; Bennett et al., 1993; Dunderdale et al., 1991). The ligation of the nicked duplex products generated by HJ resolution can then restore genomic integrity.

The mechanism of HJ resolution in eukaryotes is still mysterious. No eukaryotic homologue with sequence similarity to the bacterial RuvABC resolvasome has been described (Liu et al., 2004). Nonetheless, HJ branch

migration and resolution activities similar to those of RuvABC have been identified in mammalian cells (Constantinou et al., 2001). The resolvase associated with this activity has been named Resolvase A (Figure 1.2, step e) (Constantinou et al., 2001), although its identity is still elusive. However, proteins of the RAD51 family, also known as RAD51 paralogs, have recently been associated with the HJ branch migration and resolution activity (Liu et al., 2004). In mammals, five RAD51 paralogs, named RAD51B, RAD51C, RAD51D, XRCC3 and XRCC2, have been identified (Thacker, 2005). They are known to form two main complexes: one contains RAD51B, RAD51C, RAD51D and XRCC2 and the other consists of RAD51C and XRCC3 (Masson et al., 2001). It has been reported that extracts from mammalian cells deficient for RAD51C or XRCC3 have reduced levels of HJ resolution activity (Liu et al., 2004). Moreover, depletion of RAD51C causes loss of HJ branch migration and resolution activity that can be restored by addition of purified recombinant complexes containing RAD51C (Liu et al., 2004). It has not yet been determined whether the HJ can be resolved by RAD51C itself or by an endonuclease interacting with RAD51C.

As suggested by the DSB repair model in Figure 1.2, HJ resolvases could either cleave the crossed or the non-crossed strand of the HJ (step e). Depending on the orientation in which each of the two HJs of the dHJ is cleaved, different resolution product will be obtained. If the two crossed strands of the first HJ and the two non-crossed of the second HJ are nicked, then the arms that flank the dHJ will exchange DNA strands, generating a crossover (Figure 1.2, step e) (Paques and Haber, 1999). Instead, if the nicks are introduced in the same DNA strands in both the first and the second HJ, non-crossover products will be produced (Figure 1.2, step e) (Paques and Haber, 1999).

1.5 DNA-DAMAGE-TOLERANCE MECHANISMS

As previously mentioned (Section 1.2), DNA-Damage-Tolerance Mechanisms are involved in ensuring DNA replication progression in the presence of DNA damage, such as UV lesions, SSBs and DSBs, or replication fork blocks. The

mechanism involved in this process in bacteria and eukaryotes will be discussed.

DNA Replication Restart after UV Radiation

Re-priming of DNA Synthesis

In bacteria, the recovery of DNA replication after UV radiation has been extensively studied. DNA lesions are thought to affect DNA synthesis in a manner dependent upon the DNA strand in which they are located. Models for DNA replication propose that DNA synthesis is continuous in the leading-strand and discontinuous in the lagging-strand (Benkovic et al., 2001). Therefore, DNA lesions on the lagging-strand might be bypassed by re-priming DNA synthesis downstream of the lesion, whereas lesions of the leading-strand could block the progression of DNA synthesis, due to the inability of the DNA replication apparatus to re-prime DNA synthesis on the leading-strand (Higuchi et al., 2003).

It has been reported that after UV radiation lagging-strand DNA synthesis can become transiently uncoupled from leading-strand synthesis and continue beyond the end of the leading-strand (Figure 1.3, step a) (Higuchi et al., 2003; Pages and Fuchs, 2003). This could generate ssDNA regions on the leading-strand for approximately 1 Kbp downstream of the DNA lesion before replication fork progression is blocked (Higuchi et al., 2003). According to the current model of continuous leading-strand synthesis, blocked leading-strand synthesis can exclusively be restarted from the exact position where it was interrupted, without leaving any discontinuities behind.

However, early work in *E. coli* showed that, following UV radiation of cells defective in the repair of UV lesions, DNA replication progression is continued and single-stranded DNA gaps are left opposite the UV lesions (Rupp and Howard-Flanders, 1968; Rupp et al., 1971). These observations support a discontinuous model of DNA replication in which DNA synthesis can be re-primed downstream the DNA lesion in both the leading- and the lagging-strand (Wang, 2005). This could generate DNA gaps in both newly synthesised

using the homolo

a template (temp

required to restar

responsible for th

tively. See the ma

mation.

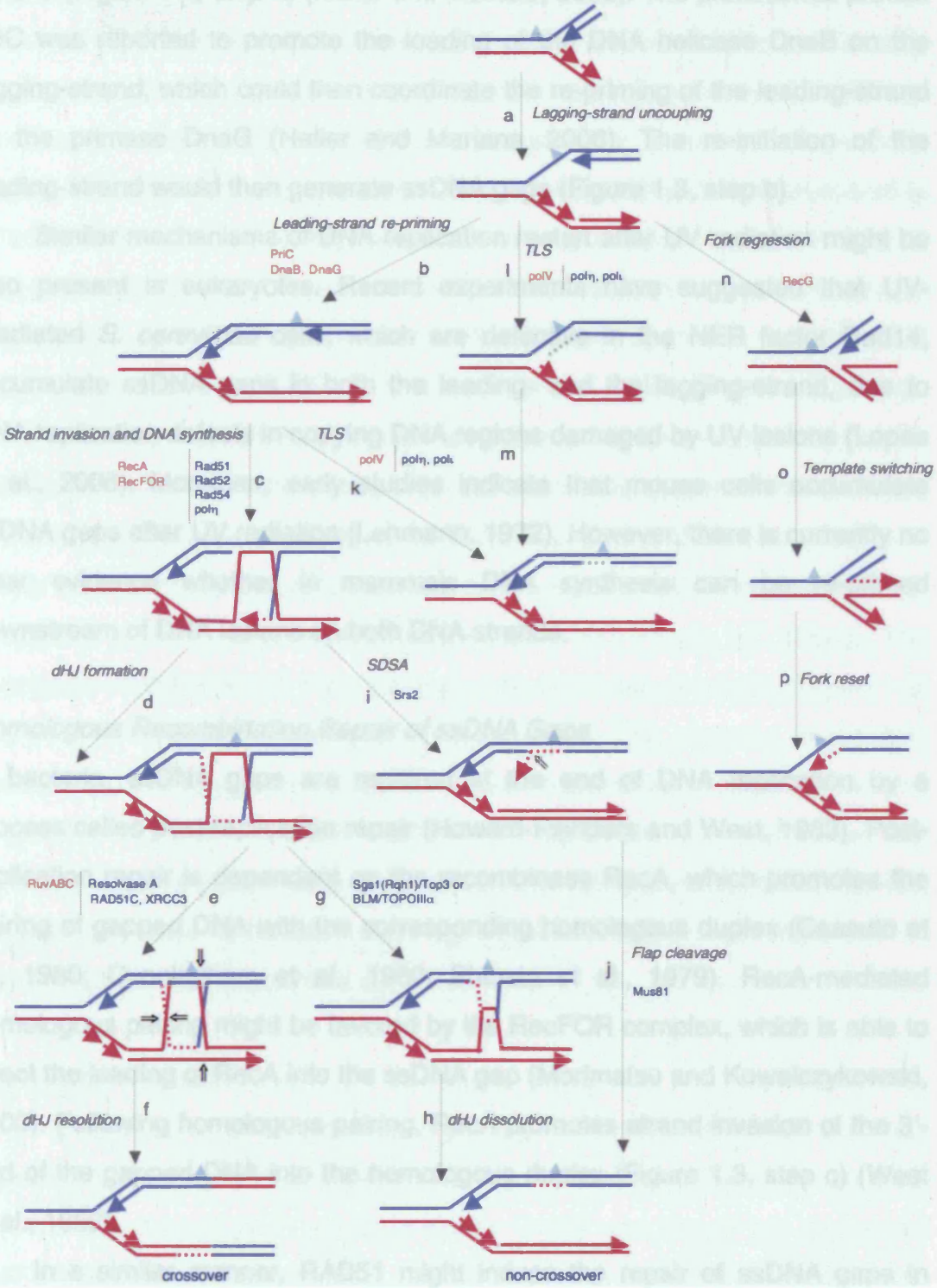
a
Lagging-strand uncoupling
Leading-strand re-priming
PriC
DnaB, DnaG
b
TLS
l
polV
polη, polι
Fork regression
n
RecG
Strand invasion and DNA synthesis
RecA
RecFOR
Rad51
Rad52
Rad54
polη
c
TLS
polV
polη, polι
k
m
o
Template switching
dHJ formation
d
SDSA
i
Srs2
p
Fork reset
RuvABC
Resolvase A
RAD51C, XRCC3
e
g
Sgs1(Rqh1)/Top3 or
BLM/TOPOIIIα
Flap cleavage
j
Mus81
dHJ resolution
f
h
dHJ dissolution
crossover
non-crossover

strands (Wang and Chen, 1992). Recent biochemical evidence supports the hypothesis that leading-strand DNA synthesis restarts downstream of DNA lesions (Figure 1.3, step b) (Heller and Marians, 2006). The primosomal protein PriC was reported to promote the loading of the DNA helicase DnaB on the lagging-strand, which could then coordinate the re-priming of the leading-strand by the primase DnaG (Heller and Marians, 2006). The re-initiation of the leading-strand would then generate ssDNA gaps (Figure 1.3, step b).

Similar mechanisms of DNA replication restart after UV radiation might be also present in eukaryotes. Recent experiments have suggested that UV-irradiated *S. cerevisiae* cells, which are defective in the NER factor Rad14, accumulate ssDNA gaps in both the leading- and the lagging-strand, due to DNA replication defects in copying DNA regions damaged by UV lesions (Lopes et al., 2006). Moreover, early studies indicate that mouse cells accumulate ssDNA gaps after UV radiation (Lehmann, 1972). However, there is currently no clear evidence whether in mammals DNA synthesis can be re-primed downstream of DNA lesions on both DNA strands.

Homologous Recombination Repair of ssDNA Gaps

In bacteria, ssDNA gaps are repaired at the end of DNA replication by a process called post-replication repair (Howard-Flanders and West, 1983). Post-replication repair is dependent on the recombinase RecA, which promotes the pairing of gapped DNA with the corresponding homologous duplex (Cassuto et al., 1980; Cunningham et al., 1980; Shibata et al., 1979). RecA-mediated homologous pairing might be favored by the RecFOR complex, which is able to direct the loading of RecA into the ssDNA gap (Morimatsu and Kowalczykowski, 2003). Following homologous pairing, RecA promotes strand invasion of the 3'-end of the gapped DNA into the homologous duplex (Figure 1.3, step c) (West et al., 1982).

In a similar manner, RAD51 might induce the repair of ssDNA gaps in eukaryotes. It is known that during S phase RAD51 co-localises in nuclear foci together with the ssDNA binding protein RPA in mammalian cells (Tarsounas et al., 2003). Some of these foci might represent sites of repair of ssDNA gaps

generated during DNA replication. HRR proteins, such as RAD52 and RAD54, might favour RAD51-mediated strand invasion, as described in Section 1.4 (Figure 1.3, step c).

After DNA synthesis and ligation, dHJs could be formed (Figure 1.3, step d). As described in Section 1.4, HJs could be resolved by RuvABC or Resolvase A (with RAD51C/XRCC3) in bacteria or mammals, respectively (Figure 1.3, step e). In situations where the two HJs of the dHJ are resolved in different orientation, crossover products would be generated (Figure 1.3, step f).

Alternatively, it has recently been proposed that in mammals dHJs might be dissolved by the concerted action of the Bloom's syndrome helicase BLM and the topoisomerase TOPOIIIα (Wu and Hickson, 2003) (Figure 1.3, step g). BLM, a member of the RecQ family of helicases, is indeed able to branch migrate *in vitro* two HJs in opposite directions and generate a catenated intermediate that can be released by TOPOIIIα (Wu and Hickson, 2003). A similar reaction might be performed also by the yeast RecQ helicases Sgs1 (*S. cerevisiae*) or Rqh1 (*S. pombe*) in complex with Top3 (Figure 1.3, step g). The dissolution of dHJs would then generate non-crossover products (Figure 1.3, step h) (Ira et al., 2003; Wu and Hickson, 2003). The absence of the dHJ dissolution pathway could lead to an increase in crossover products generated by the alternative dHJ resolution pathway. In agreement with this model, cell lines with *BLM* mutation have a hyper-recombination phenotype with 10-fold increase of sister chromatid exchanges (SCEs), which are indicative of crossover products (Chaganti et al., 1974).

Translesion Synthesis

In an alternative to leading-strand re-priming, DNA replication can progress through UV lesions by TLS (Figure 1.3, step l) (Friedberg, 2005). In bacteria, the TLS polymerase polV, whose subunits UmuC and UmuD are expressed after UV radiation (Kitagawa et al., 1985), is able to copy DNA templates with DNA lesions (Figure 1.3, step l) (Tang et al., 1999). However, polV, a member of the Y-family of DNA polymerases, has a lower fidelity than the replicative polymerase polIII, and can introduce mutations during DNA synthesis (Tang et

al., 1999). It is indeed known that polV is responsible for the majority of UV radiation-induced mutagenesis (Kato and Shinoura, 1977).

In mammals, the main polymerase responsible for the bypass of UV lesions is the Y-family polymerase polη (Figure 1.3, step l) (Lehmann, 2005). Mutation of the *POLH* gene have been associated with the XP-V variant of the genetic disorder xeroderma pigmentosum (Section 1.3) (Johnson et al., 1999b; Masutani et al., 1999). The observation that polι interacts with polη (Kannouche et al., 2002) indicates that also polι might be involved in UV lesion bypass (Vaisman et al., 2003). It is known that both polη and polι interact with monoubiquitinated PCNA through a ubiquitin binding domain (Bienko et al., 2005; Kannouche et al., 2004), which is required to promote the formation of polη and polι foci after UV radiation (Bienko et al., 2005). Therefore, polη and polι might be recruited to the site of damage by monoubiquitinated PCNA (Bienko et al., 2005; Kannouche et al., 2004). In the current polymerase switch model, PCNA is monoubiquitinated when the replication fork stalls at UV lesions present in the leading-strand (Figure 1.3, step a) (Kannouche et al., 2004; Lehmann, 2005). Under these conditions, monoubiquitinated PCNA preferentially binds polη (and possibly polι), which replaces the replicative polymerase polδ and allows bypass of the UV lesion (Figure 1.3, step l) (Bienko et al., 2005; Kannouche et al., 2004). In addition, polη might be required to repair the ssDNA gaps left opposite to the UV lesion after the re-priming of leading-strand DNA synthesis (Figure 1.3, step k).

Recent reports have indicated a role for polη also during HRR (Kawamoto et al., 2006; McIlwraith et al., 2005). It has been shown that in chicken DT40 cell lines polη is required for HRR during immunoglobulin diversification (Kawamoto et al., 2006). Moreover, RAD51 was shown to co-localise in nuclear foci with polη after UV radiation (Kannouche et al., 2001) and to stimulate the ability of polη to extend *in vitro* DNA structures mimicking D-loop recombination intermediates (McIlwraith et al., 2005). It is therefore possible that *in vivo* polη might be directly involved both in TLS and HRR (Figure 1.2, step c; Figure 1.3, steps c, k and l).

Fork Regression

In alternative to the mechanisms described above, UV lesions in the leading-strand could be bypassed by replication fork regression (McGlynn and Lloyd, 2002a). In bacteria, the helicase RecG is able to induce replication fork regression by favoring the annealing of the leading- and lagging-strand and generating a HJ structure with ssDNA extension in one of the arms (Figure 1.3, step n) (McGlynn and Lloyd, 2000; McGlynn and Lloyd, 2001; Singleton et al., 2001). This structure, also known as the "chicken foot", could allow the restart of DNA synthesis of the blocked leading-strand using the homologous sequence of the lagging-strand as a template (Figure 1.3, step o) (McGlynn and Lloyd, 2002b). The reset of the fork in its original position could then let DNA replication continue (Figure 1.3, step p).

Eukaryotic proteins able to promote fork regression have not yet been identified. Regressed forks have been visualized by electron-microscopy after HU treatment of *S. cerevisiae* cells defective in the replication checkpoint kinase Rad53 (Sogo et al., 2002). The absence of reversed fork structures in wild-type cells indicates that these structures might accumulate primarily under pathological conditions due to the absence of factors involved in the stabilisation of the replication fork (Lopes et al., 2006; Sogo et al., 2002).

DNA Replication Restart after Replication Fork Blockage or Collapse

As mentioned above, the possibility that DNA synthesis could be re-primed downstream of DNA damaged bases, such as UV lesions, suggests that DNA replication progression might be only partially affected by these lesions. Instead, DNA replication progression could be disrupted by SSBs, DSBs and replication fork blocks.

As indicated in Section 1.1, SSBs might be generated by CPT, reactive oxygen radicals or IR. During DNA synthesis, SSBs are converted into DSBs, which induce replication fork collapse (Figure 1.4, step a) (Kuzminov, 2001b). The DSBs created by fork collapse are repaired by HRR. In bacteria, the DSB ends can be resected by the RecBCD complex, which generates a 3'-end suitable for RecA-mediated strand invasion (Figure 1.4, steps b and c)

blue, respectively

detailed informati

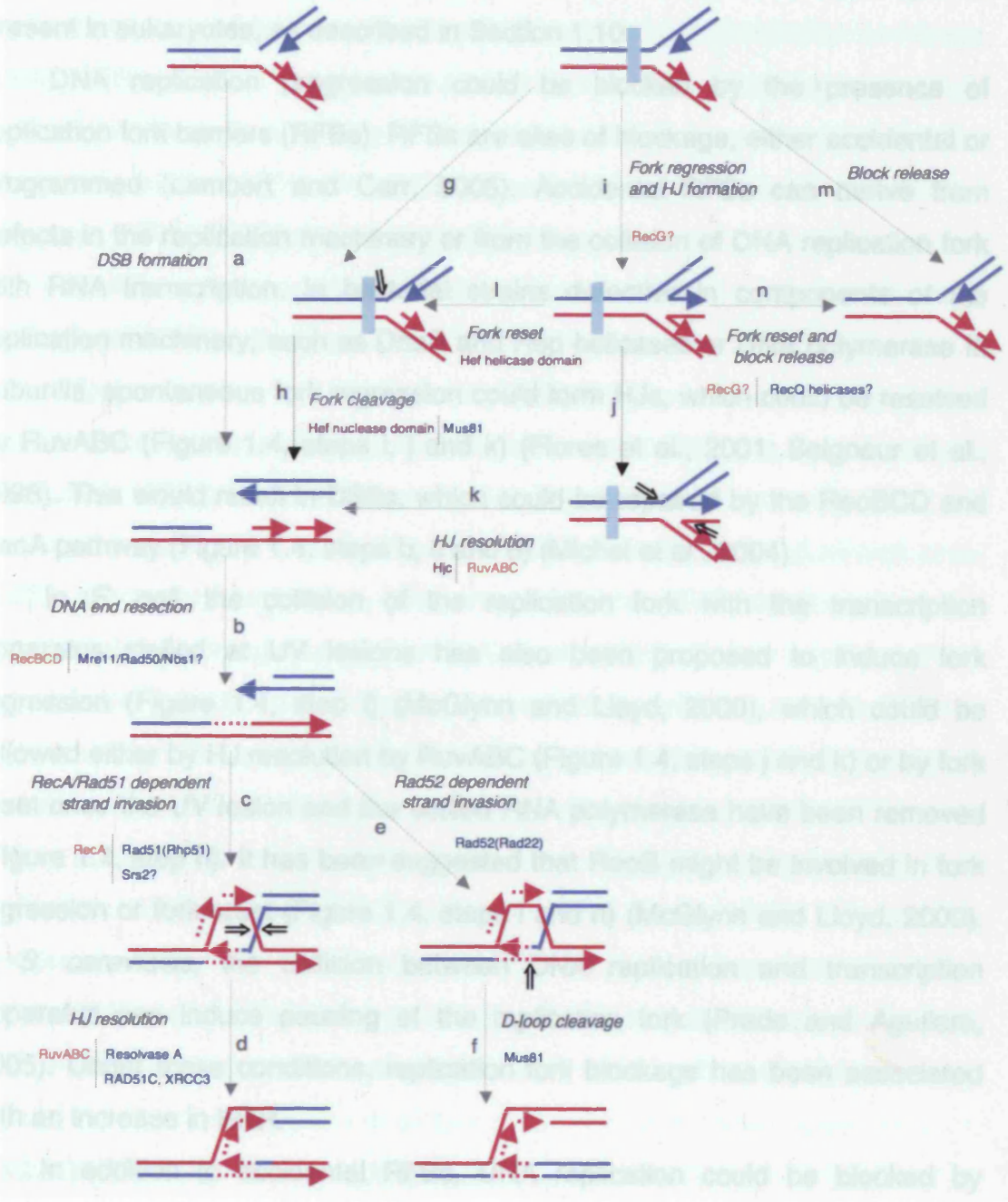
g
i
m
Fork regression
and HJ formation
Block release
RecG?
DSB formation
a
l
n
Fork reset
Hef helicase domain
Fork reset and
block release
RecG?
RecQ helicases?
h
Fork cleavage
Hef nuclease domain
Mus81
j
k
HJ resolution
Hjc
RuvABC
DNA end resection
b
RecBCD
Mre11/Rad50/Nbs1?
RecA/Rad51 dependent
strand invasion
c
Rad52 dependent
strand invasion
e
RecA
Rad51(Rhp51)
Srs2?
Rad52(Rad22)
HJ resolution
RuvABC
Resolvase A
RAD51C, XRCC3
d
D-loop cleavage
f
Mus81

(Anderson and Kowalczykowski, 1997; Kowalczykowski, 2000). The replication fork could then be re-established by RuvABC-induced resolution of the HJ formed after strand invasion (Figure 1.4, step d) (Cox et al., 2000; Kuzminov, 2001a). Similar mechanisms of repair of collapsed replication forks might be present in eukaryotes, as described in Section 1.10.

DNA replication progression could be blocked by the presence of replication fork barriers (RFBs). RFBs are sites of blockage, either accidental or programmed (Lambert and Carr, 2005). Accidental RFBs can derive from defects in the replication machinery or from the collision of DNA replication fork with RNA transcription. In bacterial strains defective in components of the replication machinery, such as DnaB and Rep helicases or DNA polymerase III subunits, spontaneous fork regression could form HJs, which could be resolved by RuvABC (Figure 1.4, steps i, j and k) (Flores et al., 2001; Seigneur et al., 1998). This would result in DSBs, which could be repaired by the RecBCD and RecA pathway (Figure 1.4, steps b, c and d) (Michel et al., 2004).

In *E. coli*, the collision of the replication fork with the transcription apparatus stalled at UV lesions has also been proposed to induce fork regression (Figure 1.4, step i) (McGlynn and Lloyd, 2000), which could be followed either by HJ resolution by RuvABC (Figure 1.4, steps j and k) or by fork reset once the UV lesion and the stalled RNA polymerase have been removed (Figure 1.4, step n). It has been suggested that RecG might be involved in fork regression or fork reset (Figure 1.4, steps i and n) (McGlynn and Lloyd, 2000). In *S. cerevisiae*, the collision between DNA replication and transcription apparatus can induce pausing of the replication fork (Prado and Aguilera, 2005). Under these conditions, replication fork blockage has been associated with an increase in HRR.

In addition to accidental RFBs, DNA replication could be blocked by programmed RFBs. Examples of programmed RFBs are present in the rDNA loci of many species, from *S. cerevisiae* (Brewer and Fangman, 1988) to mammals (Gerber et al., 1997), and in the mating-type switching *mat-1* locus of *S. pombe* (Dalgaard and Klar, 2001). Among programmed RFBs, the rDNA RFB of *S. cerevisiae* has been the most extensively studied. The function of the

rDNA RFB is to ensure that DNA replication forks move in the same direction of RNA polymerase, therefore preventing the collision between DNA replication and transcriptional apparatus (Brewer and Fangman, 1988; Takeuchi et al., 2003). It has been shown that replication forks stalled at rDNA RFBs are cleaved and successively repaired by HRR mechanisms (Burkhalter and Sogo, 2004). RFBs in the *S. pombe mat-1* locus ensure that during the mating-type switching DNA replication occurs from the telomere to centromere direction (Dalgaard and Klar, 2001). This RFB is constituted by the replication termination sequence (*RTS1*) (Dalgaard and Klar, 2001).

Recently, programmed RFBs have been exploited as a tool to study blockage of DNA replication at specific chromosome loci. In *S. pombe*, it was shown that replication fork blockage at *RTS1* sequences located in an ectopic locus promotes extensive recombination (Ahn et al., 2005). In agreement with these data, HRR proteins were reported to form foci and to be required for cell survival in response to a replication fork stalled at the *RTS1* site (Lambert et al., 2005). Moreover, replication fork processing by HRR resulted in gross chromosomal rearrangements (Lambert et al., 2005). Taken together, these experiments indicate that the repair of replication forks blocked at RFBs is dependent on HRR and that this process can generate genomic instability. In contrast, replication forks stalled at ectopic *S. cerevisiae* rDNA RFBs were shown to be stable and to maintain an intact replisome, independently from replication checkpoint or HRR proteins (Calzada et al., 2005). However, as mentioned above, rDNA RFBs induce DSB formation when located in their native rDNA region (Burkhalter and Sogo, 2004). It is therefore possible that rDNA RFBs are not processed when introduced outside of the rDNA locus.

1.6 INTERSTRAND CROSS-LINK REPAIR

As mentioned above, ICLs represent particularly toxic lesions, because they tether both DNA strands together and prevent DNA strand unwinding, which is required for DNA replication and transcription. Due to the complexity of these lesions, ICLs are repaired by a concerted action of NER, HRR and TLS. Details of these pathways will be described for bacteria, yeast and vertebrates.

Interstrand Cross-link Repair in Bacteria

In *E. coli*, the repair of ICLs induced by psoralen has been reconstituted *in vitro* (Berardini et al., 1999; Sladek et al., 1989; Van Houten et al., 1986). The NER UvrABC complex has been shown to generate nicks in one DNA strand on both sides of the ICL (Figure 1.5A, step 2) (Van Houten et al., 1986). The result is an 11 bp oligonucleotide cross-linked to the other DNA strand (Van Houten et al., 1986). The introduction of nicks is followed by the formation of a ssDNA gap on the 3'-side of the ICL due to the exonuclease activity of DNA polymerase I (Figure 1.5A, step 3) (Sladek et al., 1989). The ssDNA gap can then be repaired by HRR. RecA can promote strand invasion and displace the cross-linked oligonucleotide (Figure 1.5A, step 4) (Sladek et al., 1989). After HJ formation and resolution by RuvABC, UvrABC can introduce two additional nicks on both sides of the ICL on the DNA strand not previously cleaved (Figure 1.5A, step 5) (Sladek et al., 1989). This allows the release of the cross-linked oligonucleotide from DNA. DNA synthesis and ligation are then required to restore genomic integrity (Figure 1.5A, step 6). In the absence of HRR, the first incisions induced by UvrABC could be followed by TLS bypass of the ICL performed by DNA polymerase II (Figure 1.5B, steps 2 and 3) (Berardini et al., 1999). The ICL would then be removed after the second incisions by UvrABC (Figure 1.5B, steps 4 and 5).

Interstrand Cross-link Repair in Yeast

The mechanism of ICL repair between bacteria and yeast is similar, but in yeast more proteins participate in this pathway. In *S. cerevisiae*, ICL repair is thought to be performed by proteins involved in NER, HR and TLS (Dronkert and Kanaar, 2001). According to the phase of the cell cycle during which ICLs are generated, different ICL repair pathways might be activated, as described by the models represented in Figure 1.6. In G1, NER repair proteins can introduce nicks on both sides of the ICL (Figure 1.6A, steps 1 and 2). The NER proteins Rad1, Rad10, Rad2, Rad3 and Rad14 (orthologues of mammalian XPF, ERCC1, XPG, XPD and XPA, respectively) are thought to be involved in this step (Jachymczyk et al., 1981; McHugh et al., 1999; Miller et al., 1982). The

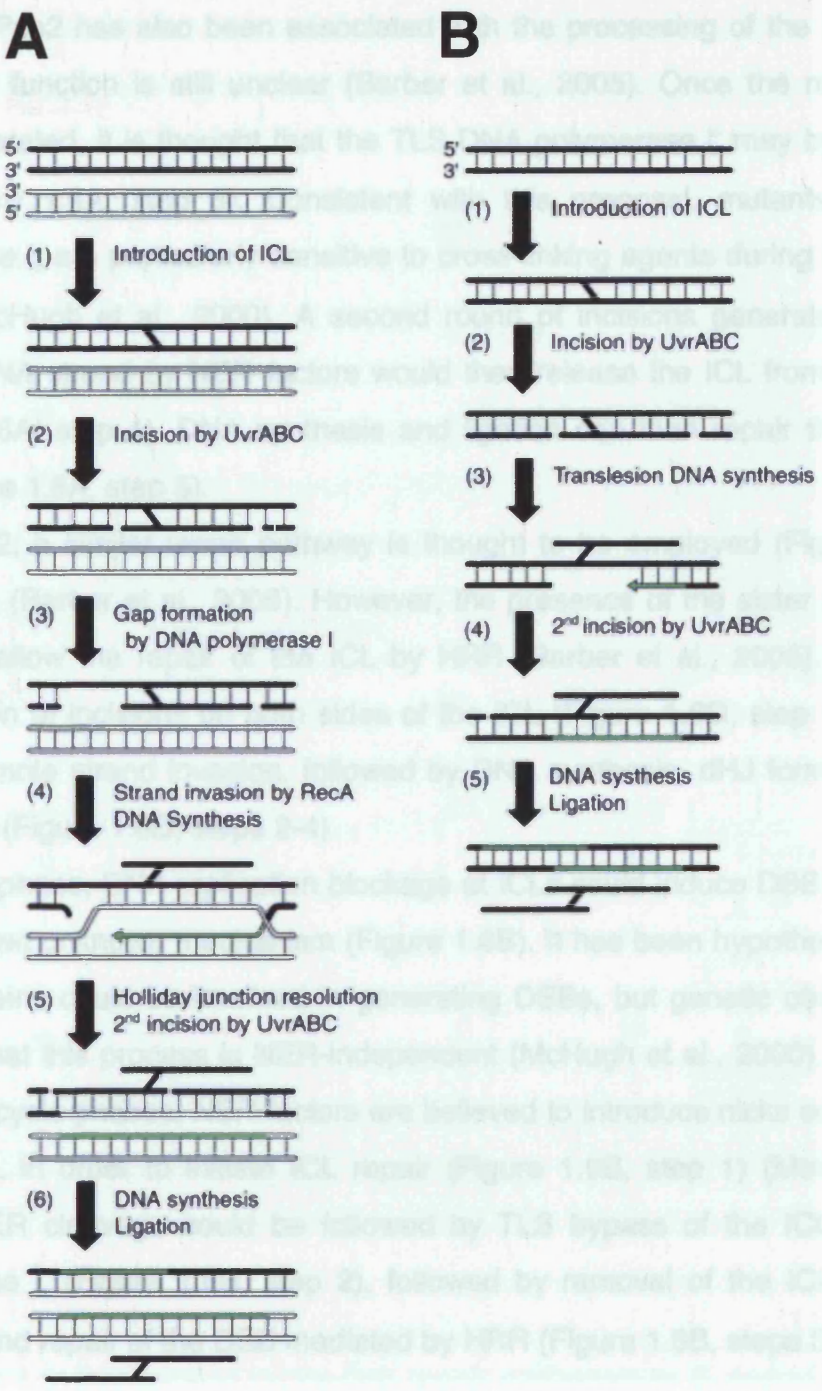

FIGURE 1.5: Interstrand cross-link repair pathways in *E. coli*

See the main text in Section 1.6 for detailed description. This figure has been taken from Dronkert and Kanaar, 2001.

nuclease Pso2 has also been associated with the processing of the ICL, even though its function is still unclear (Barber et al., 2005). Once the nicks have been generated, it is thought that the TLS DNA polymerase ζ may bypass the ICL (Figure 1.6A, step 3). Consistent with this proposal, mutants of DNA polymerase ζ are particularly sensitive to cross-linking agents during stationary phase (McHugh et al., 2000). A second round of incisions generated on the second DNA strand by NER factors would then release the ICL from the DNA (Figure 1.6A, step 4). DNA synthesis and ligation can then repair the ssDNA gap (Figure 1.6A, step 5).

In G2, a similar repair pathway is thought to be employed (Figure 1.6C, steps 1-4) (Barber et al., 2005). However, the presence of the sister chromatid can also allow the repair of the ICL by HRR (Barber et al., 2005). After the introduction of incisions on both sides of the ICL (Figure 1.6D, step 1), Rad51 could promote strand invasion, followed by DNA synthesis, dHJ formation and resolution (Figure 1.6D, steps 2-4).

In S phase, DNA replication blockage at ICLs could induce DSB formation by an as yet unknown mechanism (Figure 1.6B). It has been hypothesised that NER proteins could be involved in generating DSBs, but genetic observations suggest that this process is NER-independent (McHugh et al., 2000). As in the other cell cycle phases, NER factors are believed to introduce nicks on one side of the ICL in order to initiate ICL repair (Figure 1.6B, step 1) (Meniel et al., 1997). NER cleavage could be followed by TLS bypass of the ICL by DNA polymerase ζ (Figure 1.6B, step 2), followed by removal of the ICL by NER proteins and repair of the DSB mediated by HRR (Figure 1.6B, steps 3-4).

Fanconi Anemia and Interstrand Cross-link Repair in Vertebrates

Fanconi Anemia

In vertebrates, the repair of ICLs is dependent on the recently discovered proteins defective in the genetic syndrome Fanconi Anemia (FA) (Niedernhofer et al., 2005). FA is a rare autosomal recessive and X-linked disorder that affects less than 1 in 100,000 people (Fei et al., 2005). The clinical features of FA

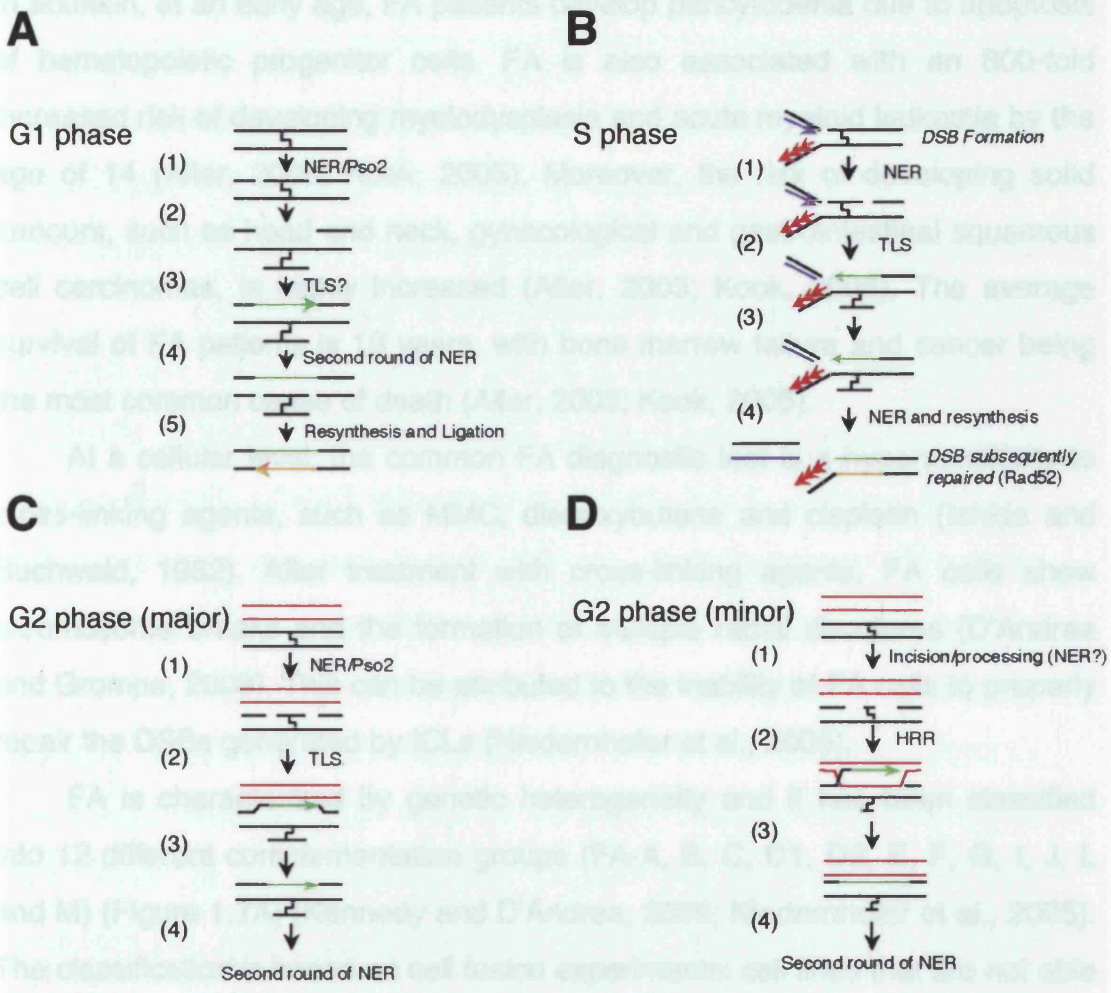

FIGURE 1.6: Interstrand cross-link repair pathways in *S. cerevisiae*

See the main text in Section 1.6 for detailed description. This figure has been adapted from Barber et al., 2005.

include early childhood skeletal abnormalities (thumb, arm, spine and hip abnormalities), cardiac, gastrointestinal and renal dysfunctions, abnormal skin pigmentation (also known as *café au lait* spots) (D'Andrea and Grompe, 2003). In addition, at an early age, FA patients develop pancytopenia due to apoptosis of hematopoietic progenitor cells. FA is also associated with an 800-fold increased risk of developing myelodysplasia and acute myeloid leukemia by the age of 14 (Alter, 2003; Kook, 2005). Moreover, the risk of developing solid tumours, such as head and neck, gynecological and gastrointestinal squamous cell carcinomas, is highly increased (Alter, 2003; Kook, 2005). The average survival of FA patients is 16 years, with bone marrow failure and cancer being the most common cause of death (Alter, 2003; Kook, 2005).

At a cellular level, the common FA diagnostic test is a hypersensitivity to cross-linking agents, such as MMC, diepoxybutane and cisplatin (Ishida and Buchwald, 1982). After treatment with cross-linking agents, FA cells show chromosome breaks and the formation of multiple radial structures (D'Andrea and Grompe, 2003). This can be attributed to the inability of FA cells to properly repair the DSBs generated by ICLs (Niedernhofer et al., 2005).

FA is characterized by genetic heterogeneity and it has been classified into 12 different complementation groups (FA-A, B, C, D1, D2, E, F, G, I, J, L and M) (Figure 1.7A) (Kennedy and D'Andrea, 2005; Niedernhofer et al., 2005). The classification is based on cell fusion experiments: cell lines that are not able to complement each other's defect are assumed to be deficient in the same gene and therefore belong to the same complementation group. The FA genes have been named according to the complementation group in which they are defective. So far 11 FA genes have been cloned: the only gene not yet identified is *FANC-I* (Niedernhofer et al., 2005). The most common genes mutated in the FA patients are *FANC-A*, *FANC-C* and *FANC-G*, affecting 60%, 15% and 10% of FA patients, respectively (Figure 1.7A) (Kennedy and D'Andrea, 2005). Mutations in *FANC-D1* or *FANC-D2* are present in 10% of FA patients (5% for each of them), whereas defects in the other FA genes are rare (Figure 1.7A) (Kennedy and D'Andrea, 2005).

dy and D'Andrea, 2

A

FA complementation group	FA gene	Approx frequency in FA patients
A	*FANC-A*	60%
B	*FANC-B*	Rare
C	*FANC-C*	15%
D1	*FANC-D1/BRCA2*	5%
D2	*FANC-D2*	5%
E	*FANC-E*	Rare
F	*FANC-F*	Rare
G	*FANC-G*	10%
I	*FANC-I*	Rare
J	*FANC-J/BRIP1*	Rare
L	*FANC-L*	Rare
M	*FANC-M/HEF*	Rare

B

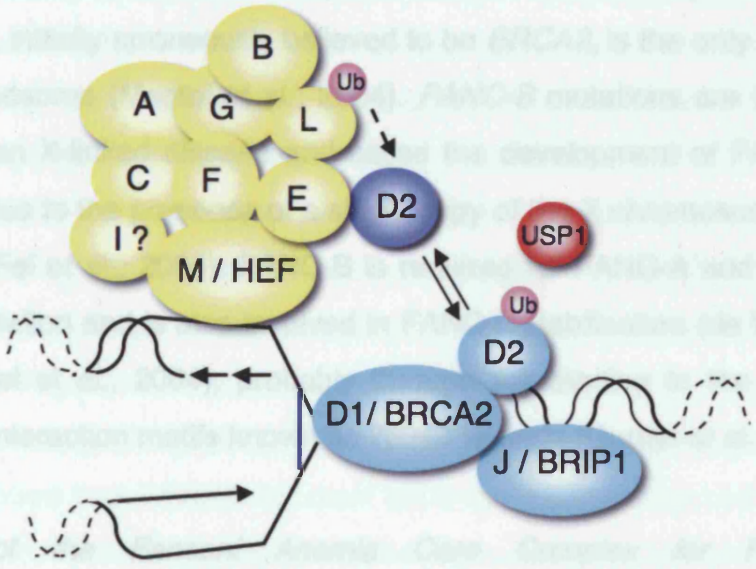

Structure of the Fanconi Anemia Core Complex

Eight of the FA proteins (FANC-A, B, C, E, F, G, L and M) associate with each other to form the FA core complex (Figure 1.7B) (Kennedy and D'Andrea, 2005). Loss of FA proteins, such as FANC-A, FANC-G or FANC-M, result in the instability of the FA core complex (Garcia-Higuera et al., 2000; Mosedale et al., 2005). The association of FANC-A with FANC-G is believed to be one of the early steps in the assembly of the FA complex (Garcia-Higuera et al., 2000). The formation of the FANC-A/FANC-G complex is dependent on the FANC-G protein-protein interaction motifs called tetratricopeptide repeats (TPRs) (Blom et al., 2004). Moreover, FANC-A and FANC-G are known to stabilise each other by reciprocally extending their half-life (Garcia-Higuera et al., 2000). Once the complex is formed, FANC-C, FANC-E and FANC-F associate with FANC-A/FANC-G (de Winter et al., 2000). FANC-E interacts with FANC-C and is required for the nuclear accumulation of FANC-C (Medhurst et al., 2001; Pace et al., 2002; Taniguchi and D' Andrea, 2002), whereas FANC-F functions as an adaptor protein by mediating the assembly of FANC-A/FANC-G and FANC-C/FANC-E complexes (Leveille et al., 2004).

Two of the remaining proteins of the FA core complex, FANC-B and FANC-L, have been proposed to directly interact with each other (Meetei et al., 2004). *FANC-B*, initially erroneously believed to be *BRCA2*, is the only FA gene on the X chromosome (Meetei et al., 2004). *FANC-B* mutations are therefore transmitted as an X-linked disease and cause the development of FA only in male patients, due to the presence of a single copy of the X chromosome in the male genome (Fei et al., 2005). FANC-B is required for FANC-A and FANC-L nuclear accumulation and is also involved in FANC-L stabilisation (de Winter et al., 2000; Meetei et al., 2004), probably through the binding to the FANC-L protein-protein interaction motifs known as WD40 repeats (Gurtan et al., 2006).

Requirement of the Fanconi Anemia Core Complex for FANC-D2 Monoubiquitination

Under DNA damaging conditions, the FA core complex is required for the monoubiquitination of the FA protein FANC-D2 on Lysine 561 (Figure 1.7B)

(Garcia-Higuera et al., 2001). Loss of any of the proteins of the FA core complex results in a lack of FANC-D2 monoubiquitination (Garcia-Higuera et al., 2001; Meetei et al., 2003a; Meetei et al., 2004; Meetei et al., 2005; Taniguchi and D' Andrea, 2002). FANC-D2 monoubiquitination is believed to be the signal of the activation of the FA pathway (Garcia-Higuera et al., 2001). This modification is induced by a variety of DNA damaging agents, such as UV, IR, HU and cross-linking agents (Garcia-Higuera et al., 2001; Howlett et al., 2005), and it also occurs during normal S phase of the cell cycle (Taniguchi et al., 2002). Therefore, the FA pathway appears to be activated in any condition of DNA stress, either caused by DNA replication or DNA damaging agents. However, the FA pathway is primarily required for ICL repair, as indicated by the exquisite sensitivity of FA cells to cross-linking agents, but not to UV, HU and IR (D'Andrea and Grompe, 2003).

The identification of the protein responsible for FANC-D2 monoubiquitination has been controversial. The initial observation that *BRCA1* mutant cell lines have lower levels of FANC-D2 monoubiquitination, compared to the same cell lines complemented by the ectopic expression of BRCA1, raised the possibility that BRCA1 could be the E3 ubiquitin ligase for FANC-D2 (Garcia-Higuera et al., 2001). BRCA1, whose inactivation predisposes individuals to the development of familial breast cancer (Easton et al., 2004), has been shown to have E3 ubiquitin ligase activity in complex with its partner protein BARD1 (Hashizume et al., 2001). The BRCA1/BARD1 complex monoubiquitinates FANC-D2 *in vitro*, but FANC-D2 monoubiquitination appears not to be affected by BRCA1 depletion (Vandenberg et al., 2003). The recent finding that FANC-L has an *in vitro* autoubiquitination activity dependent on its C-terminal RING-finger-like Plant HomeoDomain (PHD) led to the proposal that FANC-L is the E3 ubiquitin ligase for FANC-D2 (Meetei et al., 2003a). Although it has been reported that *FANC-L* deficient cell lines are defective in FANC-D2 monoubiquitination, direct evidence of *in vitro* monoubiquitination of FANC-D2 by FANC-L remains to be determined (Meetei et al., 2003a). It has been proposed that the entire FA core complex might be required for the *in vitro* monoubiquitination reaction (Fei et al., 2005). In particular, it is known that

FANC-E directly interacts with FANC-D2 (Gordon et al., 2005; Pace et al., 2002). Therefore, FANC-E might be necessary for the recruitment of FANC-D2 to the FA core complex in order to be monoubiquitinated by FANC-L. Moreover, the role of FANC-I is still unknown. It was reported that cell lines mutated for *FANC-I* are defective for FANC-D2 monoubiquitination (Levitus et al., 2004), indicating that also FANC-I could be required for FANC-D2 monoubiquitination.

Following monoubiquitination, FANC-D2 associates with chromatin (Figure 1.7B) (Garcia-Higuera et al., 2001; Montes de Oca et al., 2005). The exact mechanism by which monoubiquitinated FANC-D2 is targeted to chromatin is not yet known. It has recently been proposed that components of the FA core complex could be required for chromatin targeting of monoubiquitinated FANC-D2 (Matsushita et al., 2005). In particular, it was reported that a FANC-D2-monoubiquitin fusion protein could be targeted to chromatin in chicken cell lines defective for *FANC-D2* but not for *FANC-C*, *FANC-L* and *FANC-G* (Matsushita et al., 2005). This raises the possibility that components of the FA core complex might be required to translocate monoubiquitinated FANC-D2 to chromatin (Matsushita et al., 2005).

Fanconi Anemia Pathway and Regulation of Homologous Recombination Repair

Monoubiquitinated FANC-D2 associated with chromatin co-localises in nuclear foci with the HRR proteins BRCA1 (Garcia-Higuera et al., 2001), BRCA2 (Wang et al., 2004) and RAD51 (Hussain et al., 2004). These observations led to the proposal that the FA pathway could be involved in HRR. Data in support of this hypothesis came from the identification of *BRCA2* as the FA gene mutated in FANC-D1 patients (Howlett et al., 2002). In addition, FANC-D2 was shown to interact directly with BRCA2/FANC-D1 and to be required for the assembly of BRCA2/FANC-D1 foci after DNA damage (Hussain et al., 2004; Wang et al., 2004). In fact, FANC-D2 and BRCA2/FANC-D1 are thought to form the FA complex that is directly involved in the repair of the ICL through HRR (Figure 1.7B).

Despite the connections between FA and HRR proteins, the role of the FA pathway in HRR remains unclear. Cells deficient in *FANC-A* (Yang et al., 2005), *FANC-C* (Hirano et al., 2005; Niedzwiedz et al., 2004), *FANC-G* (Yamamoto et al., 2003) and *FANC-D2* (Houghtaling et al., 2005; Yamamoto et al., 2005) are defective in HRR. However, a recent report found that the HRR defects of *FANC-A*, *FANC-G* and *FANC-D2* mutant cell lines (Nakanishi et al., 2005) are significantly milder than those observed in *BRCA1* (Moynahan et al., 2001a; Westermark et al., 2003), *BRCA2/FANC-D1* (Moynahan et al., 2001b) and *RAD51* paralogs (Johnson et al., 1999a; Pierce et al., 1999) mutants. These results suggest a minor role of the FA core components in HRR, in contrast to that of BRCA2/FANC-D1 (Nakanishi et al., 2005; Yamamoto et al., 2003). In agreement with these conclusions, the formation of DNA damage-induced RAD51 foci, which are often considered a sign of HRR, was shown to be significantly impaired in *BRCA2/FANC-D1* cell lines (Godthelp et al., 2002a) but not in *FANC-D2* (Houghtaling et al., 2003; Ohashi et al., 2005; Yamamoto et al., 2005) or FA core complex mutants (Godthelp et al., 2002a; Godthelp et al., 2006; Yamamoto et al., 2003). Some studies, however, reported an attenuated and delayed formation of DNA damage-induced RAD51 foci in cells defective for FA core components (Digweed et al., 2002; Pichierri et al., 2002; Yang et al., 2005).

BRCA2/FANC-D1 is thought to have a late role in the FA pathway, as confirmed by the normal FANC-D2 monoubiquitination in *BRCA2/FANC-D1* mutant cell lines (Siddique et al., 2001). Similar to BRCA2/FANC-D1, cell lines mutated in the newly identified *FANC-J* (Levitus et al., 2005; Levran et al., 2005) have normal FANC-D2 monoubiquitination levels (Bridge et al., 2005; Litman et al., 2005). It has been suggested that FANC-J might be part of the FA DNA repair complex, along with FANC-D2 and BRCA2/FANC-D1 (Figure 1.7B). FANC-J was previously known as BRIP1 (BRCA1 Interacting Protein 1) or BACH1 (BRCA1 Associated C-terminal Helicase 1) (Cantor et al., 2004). As suggested by its name, BRIP1/FANC-J interacts with BRCA1 and mutations in *BRIP1* have been detected in patients with early-onset breast cancer (Cantor et al., 2004). BRIP1/FANC-J is a member of the DEAH family of helicases with

5'→3' DNA unwinding activity on forked DNA structures (Cantor et al., 2004; Gupta et al., 2005). Mammalian cell lines depleted with small interfering RNAs (siRNAs) for BRIP1/FANC-J were shown to have HRR defects similar to cell lines depleted for BRCA1 (Litman et al., 2005). However, the opposite results were obtained for chicken cell lines defective for *BRIP1/FANC-J*, where chicken BRIP1/FANC-J appeared not to be required for HRR and to function independently of BRCA1 in the FA pathway of ICL repair (Bridge et al., 2005). It has been suggested that these differences are due to the distinct role played by BRCA1 in chicken and in mammals (Kennedy and D'Andrea, 2005). Cell lines mutant for chicken *BRCA1* (Bridge et al., 2005), unlike cells defective in mammalian *BRCA1* (Moynahan et al., 2001a), are indeed proficient in ICL repair.

Role of the Fanconi Anemia Pathway in Interstrand Cross-link Repair

Studies in mammalian cells have demonstrated that processing of the ICL is more efficient in dividing cells and requires passage through S phase (De Silva et al., 2000; Rothfuss and Grompe, 2004). These observations led to the proposal that ICL repair might be activated by replication forks stalled at ICLs (Figure 1.8, step 2) (De Silva et al., 2000).

Stalled replication forks are known to activate the replication checkpoint, which is regulated primarily by the ATR (ATM and Rad3 Related) kinase (Osborn et al., 2002). Recent studies have implicated ATR in the activation of the FA pathway (Figure 1.8, centre) (Andreassen et al., 2004; Pichierri and Rosselli, 2004; Sobeck et al., 2006). Indeed, ATR was shown to be important for FANC-D2 monoubiquitination after IR and MMC treatment (Andreassen et al., 2004). The precise mechanism of ATR-dependent FANC-D2 monoubiquitination has not been determined. It is known that FANC-D2 can be phosphorylated by ATR (Figure 1.8, centre) (Pichierri and Rosselli, 2004). It is therefore possible that FANC-D2 phosphorylation could be required for FANC-D2 to be monoubiquitinated by FANC-L (Niedernhofer et al., 2005).

The observation that FANC-D2 is monoubiquitinated during normal S phase, indicates a role for the FA pathway during unperturbed DNA replication

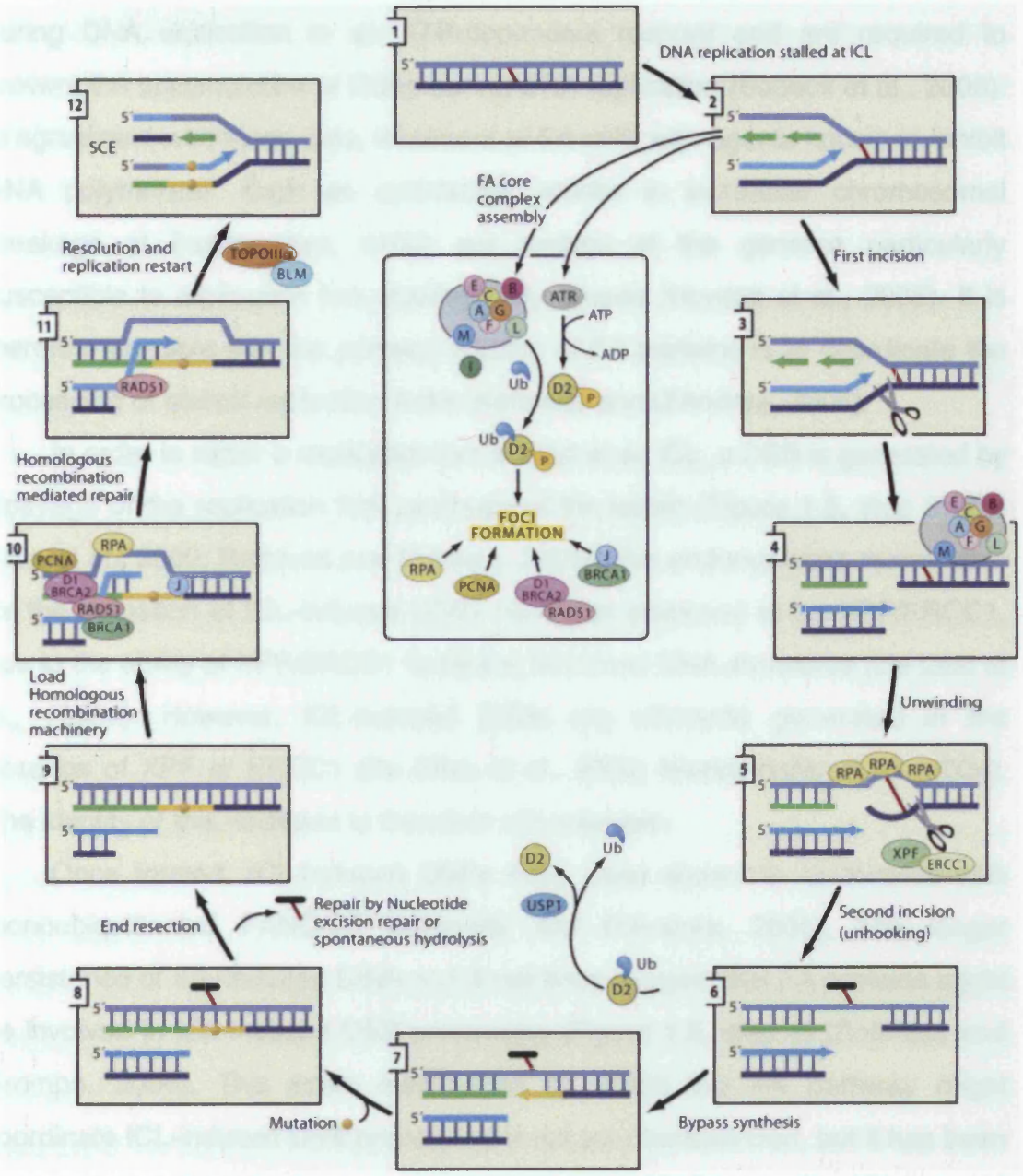

FIGURE 1.8: Interstrand cross-link repair pathways in vertebrates

See the main text in Section 1.6 for detailed description. This figure has been taken from Niedernhofer et al., 2005.

(Taniguchi et al., 2002). Indeed, FANC-A and FANC-D2 associate to chromatin during DNA replication in an ATR-dependent manner and are required to prevent the accumulation of DSBs during DNA replication (Sobeck et al., 2006). In agreement with these data, treatment of FA cells with agents known to inhibit DNA polymerase, such as aphidicolin, results in increased chromosomal breakage at fragile sites, which are regions of the genome particularly susceptible to replication fork stalling and collapse (Howlett et al., 2005). It is therefore possible that the primary function of FA proteins is to coordinate the processing of stalled replication forks (Kennedy and D'Andrea, 2005).

In order to repair a replication fork stalled at an ICL, a DSB is generated by cleavage of the replication fork upstream of the lesion (Figure 1.8, step 3) (De Silva et al., 2000; Rothfuss and Grompe, 2004). The endonuclease responsible for the formation of ICL-induced DSBs has been proposed to be XPF/ERCC1, due to the ability of XPF/ERCC1 to cleave branched DNA structures (De Laat et al., 1998a). However, ICL-induced DSBs are efficiently generated in the absence of XPF or ERCC1 (De Silva et al., 2000; Niedernhofer et al., 2004). The identity of this nuclease is therefore still unknown.

Once formed, ICL-induced DSBs have been shown to co-localise with monoubiquitinated FANC-D2 (Kennedy and D'Andrea, 2005). The longer persistence of ICL-induced DSBs in FA cell lines suggest that FA proteins might be involved in ICL-induced DSB processing (Figure 1.8, step 4) (Rothfuss and Grompe, 2004). The exact mechanism by which the FA pathway might coordinate ICL-induced DSB processing is not yet characterised, but it has been proposed that FA proteins can recruit DNA repair factors to the ICL-induced DSBs (Kennedy and D'Andrea, 2005). The nuclear foci where monoubiquitinated FANC-D2, and presumably FA core components, co-localise with DNA repair proteins RAD51 (Hussain et al., 2004), BRCA2/FANC-D1 (Wang et al., 2004), BRCA1 (Garcia-Higuera et al., 2001), NBS1/MRE11 (Pichierri et al., 2002), RPA and PCNA (Howlett et al., 2005), could visually represent the sites of repair of ICL-induced DSBs.

In order to separate the two DNA strands, a second incision is required on the opposite side of the DSB. This reaction, also known as ICL unhooking, is

likely to be performed by XPF/ERCC1 endonuclease (Figure 1.8, steps 5 and 6). In fact, XPF/ERCC1 was shown to cleave on one side of an ICL located at forked DNA structures (Kuraoka et al., 2000). In support of the involvement of XPF/ERCC1 in ICL repair, cell lines deficient for *XPF* or *ERCC1*, but not for other NER genes, are hypersensitive to cross-linking agents (Collins, 1993) and *ERCC1*$^{-/-}$ mice exhibit hematopoietic defects characteristic of FA (Prasher et al., 2005). Moreover, XPF was shown to co-localise with FANC-A (Sridharan et al., 2003) and FANC-D2 (Mace et al., 2005) after treatment with cross-linking agents.

In order to repair the gap left by the unhooking reaction, DNA synthesis is required. This is probably performed by TLS DNA polymerases that are able to bypass the residual cross-link adduct present on the opposite strand (Figure 1.8, step 7). Evidence for a role of TLS in ICL repair came from experiments showing that chicken cell lines deficient for the TLS polymerases *Rev1* or *Rev3* are hypersensitive to cross-linking agents (Niedzwiedz et al., 2004). The observations that *Rev1* and *Rev3* mutants are epistatic with *FANC-C* for *cis*-platin sensitivity and that Rev1 co-localises with FANC-D2 after DNA damage further suggests that the FA pathway and TLS are interconnected (Niedzwiedz et al., 2004). In addition, FA cell lines have been demonstrated to generate fewer rather than more mutations after cross-linking agents treatment (Papadopoulo et al., 1990a; Papadopoulo et al., 1990b). This correlates well with the hypothesis of defective TLS, which is an error-prone pathway, in the absence of FA proteins (Niedzwiedz et al., 2004).

After removal of the residual cross-link adduct by NER or by spontaneous hydrolysis (Figure 1.8, step 8), the DSB might be repaired by HRR (Figure 1.8, step 10). The involvement of HRR in ICL repair was initially suggested by the hypersensitivity of mutants for HRR proteins, such as BRCA1 (Yun et al., 2005) and RAD51 paralogs RAD51C (Godthelp et al., 2002b), RAD51D (Gruver et al., 2005), XRCC2 and XRCC3 (Cui et al., 1999), to cross-linking agents. As previously mentioned, the identification of *FANC-D1* as *BRCA2* (Howlett et al., 2002) and the colocalisation of FANC-D2 with HRR proteins have suggested a relationship between HRR and FA pathways (Kennedy and D'Andrea, 2005).

However, the link between HRR and FA pathway might be restricted to the repair of a particular subset of DNA lesions, such as ICLs. In agreement with this, it was shown that chicken *XRCC3* and *FANC-C* deletions are epistatic for *cis*-platin sensitivity (Hirano et al., 2005), even though *XRCC3* mutants have considerably higher defects in HRR than *FANC-C* mutants (Niedzwiedz et al., 2004).

It has been proposed that BRIP1/FANC-J might participate during the repair of the ICL-induced DSB by HRR (Figure 1.8, step 10) (Litman et al., 2005). The exact role of BRIP1/FANC-J is uncertain, but BRIP1/FANC-J could permit the efficient pairing of the invading strand with homologous DNA by unwinding non-productive D-loops formed by partial annealing of the invading strand with homeologous sequences. Consistent with this proposal, BRIP1/FANC-J is able to unwind D-loop structures *in vitro* (Gupta et al., 2005).

The replication fork could then be re-established by resolution of the HJ formed after RAD51-mediated strand invasion (Figure 1.8, step 11). Alternatively, BLM/TOPOIIIα complex could promote the dissolution of dHJs that might be generated (Figure 1.8, step 12) (Wu and Hickson, 2003). The identification of BLM and TOPOIIIα in a complex with FA core proteins is suggestive of a connection between BLM/TOPOIIIα and the FA pathway (Meetei et al., 2003b). Further studies have shown that FANC-D2 co-localises in nuclear foci with BLM after treatment with cross-linking agents and that the FA pathway is required for the efficient formation of BLM foci (Hirano et al., 2005; Pichierri et al., 2004). Altogether, these observations provide some evidence of the possible involvement of BLM/TOPOIIIα in ICL repair.

Once the ICL has been repaired, the deubiquitinating enzyme USP1 can inactivate the FA pathway by removing the ubiquitin moiety from FANC-D2 (Figure 1.8, bottom centre) (Nijman et al., 2005). Moreover, it has been suggested that USP1 might be responsible for deubiquitinating FANC-D2 at the end of S phase after DNA replication (Nijman et al., 2005). This observation further supports the possible role of the FA pathway in the repair of stalled forks during an unperturbed cell cycle.

III. DNA REPAIR STRUCTURE-SPECIFIC NUCLEASES

1.7 HOLLIDAY JUNCTION RESOLVASES

HJ resolvases are endonucleases that cleave HJs by introducing symmetrical nicks (Lilley and White, 2001). As described in Section 1.4, HJs are four-way junctions, in which two DNA double helices are covalently connected (Figure 1.9A, panels 1 and 3). Four-way junctions can adopt different conformations. In the presence of cations, such as Mg^{2+}, HJs assume an X-shape conformation with the DNA helices stacked antiparallel to each other (Figure 1.9A panel 4) (Duckett et al., 1988). In the absence of cations, the electrostatic repulsion between the DNA backbone of the helices induces the HJ to adopt an unstacked open planar structure (Figure 1.9A panel 4) (Clegg et al., 1994). This structure can be stabilised by the binding of HJ processing enzymes (Liu and West, 2004).

HJ resolvases have been identified in bacteriophage, bacteria and archaea (Sharples, 2001). Examples are phage T4 endonuclease VII (Mizuuchi et al., 1982), *E. coli* RuvC and RusA (Dunderdale et al., 1991; Sharples et al., 1994), archaeal Hjc (Holliday junction cleavage) and Hje (Holliday junction endonuclease) (Komori et al., 1999; Kvaratskhelia and White, 2000). In eukaryotes, the mitochondrial HJ resolvases *S. cerevisiae* Cce1 and *S. pombe* Ydc2 have been identified (Evans and Kolodner, 1988; Symington and Kolodner, 1985; Whitby and Dixon, 1997; White and Lilley, 1997). Most of the HJ resolvases belong to two groups: the integrase superfamily or the nuclease superfamily (Figure 1.9B) (Lilley and White, 2000). RuvC, Cce1 and Ydc2 are part of integrase superfamily (Aravind et al., 2000; Ariyoshi et al., 1994; Ceschini et al., 2001), whereas Hjc and Hje belong to the nuclease superfamily (Middleton et al., 2004; Nishino et al., 2001). On the contrary, T4 endonuclease VII and RusA have evolved independently from these two groups (Figure 1.9B) (Raaijmakers et al., 1999; Rafferty et al., 2003). A more detailed description of RuvC will follow.

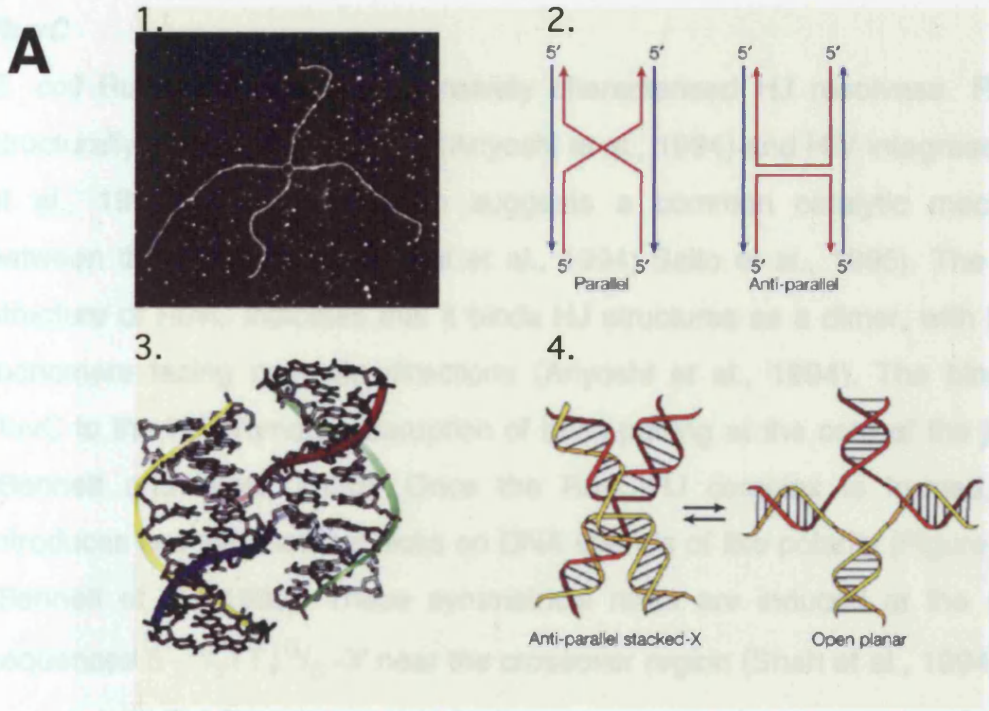
A
1.
2.
5′
5′
5′
5′
Parallel
Anti-parallel
3.
4.
Anti-parallel stacked-X
Open planar

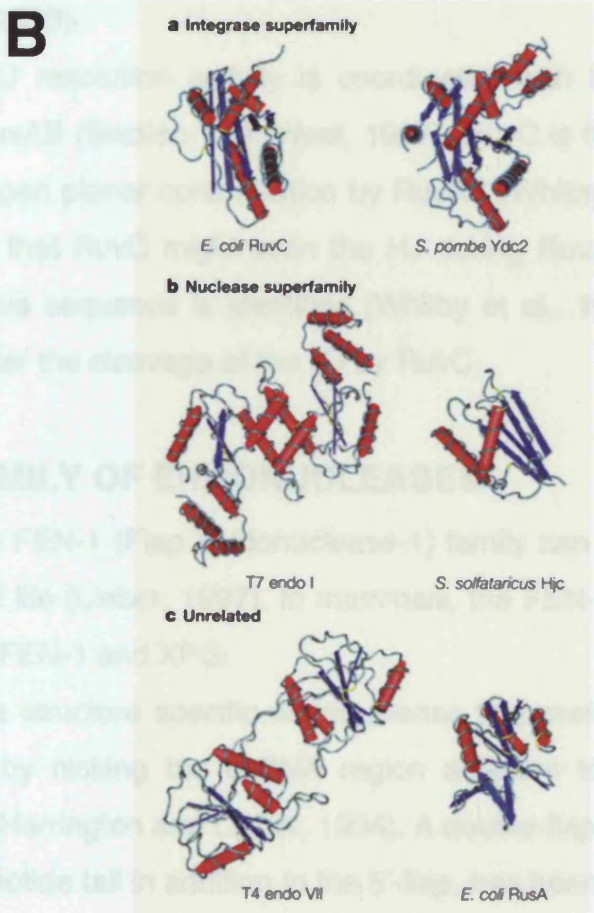
B
a Integrase superfamily
E. coli RuvC
S. pombe Ydc2
b Nuclease superfamily
T7 endo I
S. solfataricus Hjc
c Unrelated
T4 endo VII
E. coli RusA

RuvC

E. coli RuvC is the most extensively characterised HJ resolvase. RuvC is structurally similar to RNAse H1 (Ariyoshi et al., 1994) and HIV integrase (Dyda et al., 1994). This observation suggests a common catalytic mechanism between these proteins (Ariyoshi et al., 1994; Saito et al., 1995). The crystal structure of RuvC indicates that it binds HJ structures as a dimer, with the two monomers facing opposite directions (Ariyoshi et al., 1994). The binding of RuvC to the HJ promotes disruption of base pairing at the core of the junction (Bennett and West, 1995). Once the RuvC-HJ complex is formed, RuvC introduces two symmetrical nicks on DNA strands of like polarity (Figure 1.10A) (Bennett et al., 1993). These symmetrical nicks are induced at the specific sequences 5'- $^{A}/_{T}TT\downarrow^{G}/_{C}$ -3' near the crossover region (Shah et al., 1994). Each monomer of RuvC is responsible for the introduction of one of the two incisions, which occur independently from each other (Shah et al., 1997). The linear duplexes that are generated by RuvC contain nicks that are re-ligatable (Bennett et al., 1993).

RuvC's HJ resolution activity is coordinated with HJ branch migration promoted by RuvAB (Section 1.4) (West, 1997). RuvC is thought to bind to the HJ held in an open planar conformation by RuvAB (Whitby et al., 1996). It has been proposed that RuvC might scan the HJ during RuvAB branch migration until a consensus sequence is identified (Whitby et al., 1996). This sequence would then trigger the cleavage of the HJ by RuvC.

1.8 FEN-1 FAMILY OF ENDONUCLEASES

Members of the FEN-1 (Flap ENdonuclease-1) family can be identified in all of the kingdoms of life (Lieber, 1997). In mammals, the FEN-1 family includes the endonucleases FEN-1 and XPG.

FEN-1 is a structure specific endonuclease that preferentially cleaves 5'-flap structures by nicking the dsDNA region adjacent to the 5'-ssDNA arm (Figure 1.10B) (Harrington and Lieber, 1994). A double flap structure, which has a 3'-single nucleotide tail in addition to the 5'-flap, has been suggested to be the preferred substrate of FEN-1 (Figure 1.10B) (Kao et al., 2002). The 5'-flap

HOLLIDAY JUNCTION RESOLVASES

A) RuvC

FEN-1 FAMILY OF ENDONUCLEASES

B) FEN-1

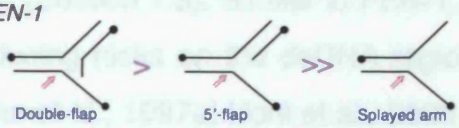

C) XPG

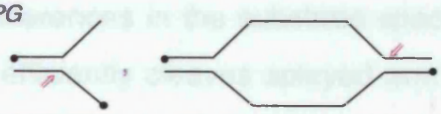

SLX ENDONUCLEASES

D) Slx1/Slx4

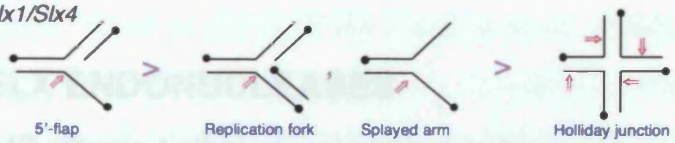

MUS81 FAMILY OF ENDONUCLEASES

E) P. furiosus Hef

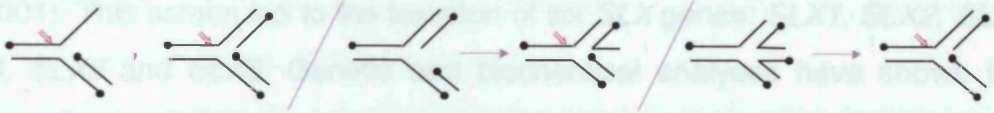

F) S. solfataricus XPF

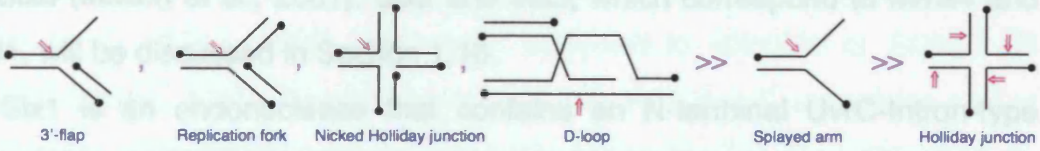

G) H. sapiens XPF/ERCC1

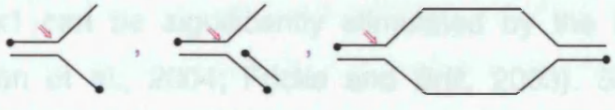

H) Yeast Mus81/Eme1(Mms4)

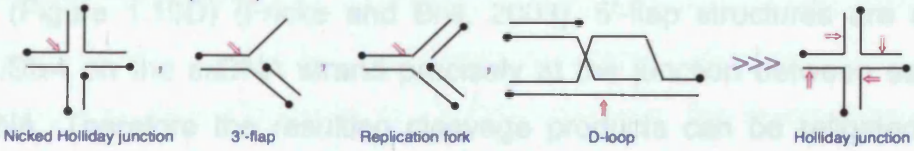

activity of FEN-1 is important for Okazaki fragment maturation during DNA replication (Hubscher and Seo, 2001). In the current model of Okazaki fragment processing, DNA extension synthesis catalysed by DNA polymerase δ can displace the RNA primer of the downstream Okazaki fragment, thus creating a 5'-flap that can be cleaved by FEN-1 (Henneke et al., 2003).

XPG is required during NER to nick the 3'-side of the damaged DNA strand (Section 1.3). Similar to FEN-1, XPG cleaves ssDNA/dsDNA junctions by introducing nicks on the dsDNA region near the 5'-ssDNA arm (Figure 1.10C) (Evans et al., 1997a; Hohl et al., 2003; O'Donovan et al., 1994). However, there are differences in the substrate specificity between XPG and FEN-1. Whereas XPG efficiently cleaves splayed arm and bubble structures (O'Donovan et al., 1994), FEN-1 prefers 5'-flap structures (Figure 1.10, compare B and C) (Harrington and Lieber, 1994).

1.9 SLX ENDONUCLEASES

SLX (Synthetic Lethal of unknown function) genes have been identified in a genetic screen for mutations that are lethal in combination with *sgs1* (Mullen et al., 2001). This screen led to the isolation of six *SLX* genes: *SLX1*, *SLX2*, *SLX3*, *SLX4*, *SLX5* and *SLX8*. Genetic and biochemical analyses have shown that these proteins form three heterodimeric complexes: Slx1/Slx4, Slx2/Slx3 and Slx5/Slx8 (Mullen et al., 2001). Slx2 and Slx3, which correspond to Mms4 and Mus81, will be discussed in Section 1.10.

Slx1 is an endonuclease that contains an N-terminal UvrC-Intron-type (URI) nuclease domain (Aravind and Koonin, 2001). The endonuclease activity of Slx1 can be significantly stimulated by the interaction of Slx1 with Slx4 (Coulon et al., 2004; Fricke and Brill, 2003). Slx1/Slx4 has been shown to cleave 5'-flap, splayed arm and replication fork structures more efficiently than HJs (Figure 1.10D) (Fricke and Brill, 2003). 5'-flap structures are nicked by Slx1/Slx4 on the ssDNA strand precisely at the junction between ssDNA and dsDNA. Therefore the resulting cleavage products can be religated by DNA ligase (Fricke and Brill, 2003). In contrast, the HJ cleavage products are not

religatable. Unlike classical HJ resolvases, Slx1/Slx4 does not introduce symmetrical nicks at the crossover of the junction (Fricke and Brill, 2003).

Yeast cells deficient for *SLX1* or *SLX4* do not exhibit any obvious phenotype after treatment with DNA damaging agents (Mullen et al., 2001). However, *S. cerevisiae slx4* mutants containing a temperature-sensitive allele of *SGS1* are defective in rDNA replication (Kaliraman and Brill, 2002). Similar results were obtained in *S. pombe* for *slx1* or *rqh1* mutants (Coulon et al., 2004). However, no defects in bulk DNA replication have been detected in the absence of *SGS1* or *SLX4* (Kaliraman and Brill, 2002). These data indicate that Slx1/Slx4 might be specifically required during rDNA replication.

The observation that *slx1* or *slx4* are synthetic lethal with *sgs1(rqh1)* or *top3* (Coulon et al., 2004; Mullen et al., 2001), suggests that Slx1/Slx4 and Sgs1(Rqh1)/Top3 might provide alternative pathways to process stalled replication forks at rDNA RFBs (Coulon et al., 2006; Fricke and Brill, 2003). It has been proposed that converging replication forks at RFBs could be either cleaved by Slx1/Slx4 or dissolved by Sgs1(Rqh1)/Top3 (Coulon et al., 2006; Fricke and Brill, 2003). The absence of both Sgs1(Rqh1) and Slx1/Slx4 could prevent stalled fork processing and completion of rDNA replication and therefore be incompatible with cell survival.

In contrast to Slx1/Slx4 and Slx2/Slx3, neither Slx5 nor Slx8 contain known nuclease domains. Instead, both Slx5 and Slx8 contain RING finger domains (Mullen et al., 2001), which have been identified in ubiquitin or SUMO E3 ligases (Jackson, 2001). It has recently been reported that *S. cerevisiae slx5* or *slx8* mutants are synthetic lethal with SUMO conjugating enzymes (Wang et al., 2005). This has raised the possibility that Slx5 and Slx8 might be SUMO E3 ligases. However, no activity has yet been reported for the Slx5/Slx8 complex.

Among the *SLX* genes, *SLX5* and *SLX8* have been recently shown to be particularly critical for the suppression of spontaneous gross chromosomal rearrangements, such as translocations, large deletions and loss of chromosomal arms (Zhang et al., 2006). However, the mechanism by which Slx5 and Slx8 ensure genomic stability is still unknown and no clear explanation is available for the synthetic lethality of *slx5* or *slx8* with *sgs1* mutants.

1.10 MUS81 FAMILY OF ENDONUCLEASES

The MUS81 family derives its name from the endonuclease MUS81, initially identified in yeast (Boddy et al., 2000; Interthal and Heyer, 2000). Members of this family can be found both in archaea and in eukaryotes (Nishino et al., 2006). The single archaeal member of the MUS81 family has been named XPF in *Aeropyrum pernix* (or *Sulfolobus solfataricus*) and Hef in *Pyrococcus furiosus* (Figure 1.11). In *S. pombe,* four MUS81 family proteins are known: Mus81, Eme1, Rad16 and Swi10. The *S. cerevisiae* orthologues of Eme1, Rad16 and Swi10 are Mms4, Rad1 and Rad10, respectively. Rad16(Rad1) and Swi10 (Rad10) correspond to human XPF and ERCC1, respectively.

Proteins of the MUS81 family are characterised by the presence of the ERCC4 nuclease domain (Enzlin and Scharer, 2002), which is structurally related to the nuclease domain of type II restriction endonucleases (Nishino et al., 2003). Indeed, the catalytic motif of the ERCC4 domain, $ERKX_3D$, with an extension at the N-terminal GDX_n (GDX_nERKX_3D), is similar to the sequence $PDX_n(D/E)XK$ required for restriction endonuclease activity. Interestingly, some MUS81 family proteins, such as Eme1(Mms4), Swi10(Rad10) and ERCC1 contain an inactive ERCC4 domain, due to the absence of the catalytic motif $ERKX_3D$ (Figure 1.11) (Aravind et al., 1999). The characteristics of the MUS81 family proteins will be described in following sections.

Archaeal MUS81 Family Proteins

P. furiosus Hef was the first archaeal member of the MUS81 family identified. In the initial report, Hef was discovered as a stimulatory factor of the nuclease activity of the HJ resolvase Hjc (Komori et al., 2002). In addition to the ERCC4 nuclease domain, Hef contains a DEAH helicase domain typical of DNA/RNA helicases of the superfamily II (SF2) (Figure 1.11) (Nishino et al., 2005b). SF2 helicases, which also include RecG and RecQ (Bernstein et al., 2003; Singleton et al., 2001), are characterised by the presence of seven helicase motifs (I-Ia-II-III-IV-V-VI) (Singleton and Wigley, 2002). Motifs I and II contain the conserved Walker A and B sequences typical of ATPases (Walker et al., 1982).

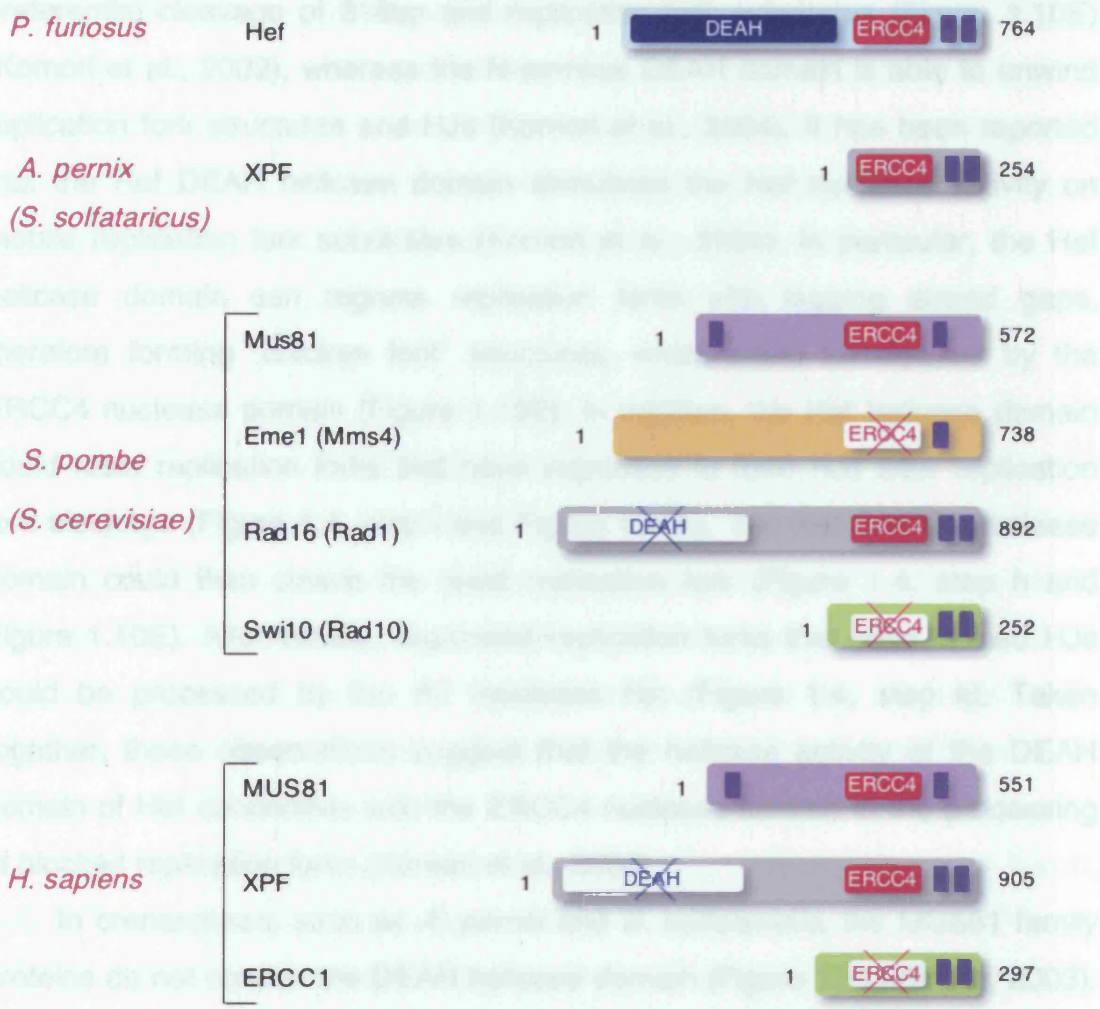

FIGURE 1.11: Evolutionary relationship of the MUS81 family of proteins

The MUS81 family of proteins in *Pyrococcus furiosus*, *Aeropyrum pernix*, *Schizosaccharomyces pombe* and *Homo sapiens* are represented. *Sulfolobus solfataricus* XPF has the same domain organisation of *Aeropyrum pernix* XPF. *Saccharomyces cerevisiae* orthologues of *Schizosaccharomyces pombe* proteins are shown in brackets. ERCC4 nuclease domains (red), HhH motifs (dark violet), DEAH helicase domains (blue) are indicated with boxes. Inactive ERCC4 and DEAH domains are indicated with red and blue crosses, respectively.

In vitro experiments using truncated mutant proteins have shown that the C-terminal fragment of Hef containing the ERCC4 nuclease domain exhibits preferential cleavage of 3'-flap and replication fork substrates (Figure 1.10E) (Komori et al., 2002), whereas the N-terminal DEAH domain is able to unwind replication fork structures and HJs (Komori et al., 2004). It has been reported that the Hef DEAH helicase domain stimulates the Hef nuclease activity on mobile replication fork substrates (Komori et al., 2004). In particular, the Hef helicase domain can regress replication forks with lagging strand gaps, therefore forming "chicken foot" structures, which could be cleaved by the ERCC4 nuclease domain (Figure 1.10E). In addition, the Hef helicase domain could reset replication forks that have regressed to form HJs after replication fork blockage (Figure 1.4, step I and Figure 1.10E). The Hef ERCC4 nuclease domain could then cleave the reset replication fork (Figure 1.4, step h and Figure 1.10E). Alternatively, regressed replication forks that have formed HJs could be processed by the HJ resolvase Hjc (Figure 1.4, step k). Taken together, these observations suggest that the helicase activity of the DEAH domain of Hef cooperates with the ERCC4 nuclease domain in the processing of blocked replication forks (Komori et al., 2004).

In crenarchaea, such as *A. pernix* and *S. solfataricus*, the MUS81 family proteins do not contain the DEAH helicase domain (Figure 1.11) (White, 2003). The observation that *S. solfataricus* XPF is active only in complex with the sliding clamp PCNA (Roberts et al., 2003), has suggested that PCNA could be functionally equivalent to the DEAH helicase domain of *P. furiosus* Hef (Roberts et al., 2003). *S. solfataricus* XPF preferentially cleaves 3'-flap, replication fork, nicked HJ and D-loop structures, with splayed arm structures and intact HJs processed 10- and 100-fold less efficiently, respectively (Figure 1.10F) (Roberts and White, 2005).

Archaeal proteins of the MUS81 family form homodimers in order to be active (Komori et al., 2002). In *P. furiosus*, the dimerisation of the Hef protein is mediated by the ERCC4 nuclease domain and the two adjacent Helix hairpin Helix (HhH) motifs (Figure 1.11) (Nishino et al., 2003; Nishino et al., 2005a). The HhH motifs are commonly found in DNA repair proteins and are thought to

be important for DNA substrate recognition (Doherty et al., 1996). It has been proposed that the HhH motifs of *P. furiosus* Hef form a bridge between the duplex arms of the fork structure allowing the ERCC4 nuclease domain to bind and cleave near the centre of the fork (Nishino et al., 2005a). Although *P. furiosus* Hef homodimer has two ERCC4 nuclease domains, one is sufficient to have a fully active complex (Nishino et al., 2005a). A similar model has been suggested for *A. pernix* XPF (Figure 1.12) (Newman et al., 2005).

XPF and ERCC1

Structural Organisation of XPF and ERCC1

In contrast to the archaeal members of the MUS81 family, mammalian XPF does not homodimerise, but forms a heterodimer with ERCC1 (Sijbers et al., 1996a). The interaction between XPF and ERCC1 is mediated by their C-terminal regions (De Laat et al., 1998b), which contain the two HhH motifs (Figure 1.11) (Gaillard and Wood, 2001). The similarity between the C-termini of XPF and ERCC1 had suggested that *ERCC1* might have derived by gene duplication of the 3'-region of *XPF* (Aravind et al., 1999; Gaillard and Wood, 2001). The crystal structure of the complex between the C-termini of XPF and ERCC1 showed that the interaction between XPF and ERCC1 is mediated by hydrophobic contacts between the HhH motifs of XPF and ERCC1 (Tripsianes et al., 2005). In particular, Phe894 of XPF and Phe293 of ERCC1 (Figure 1.13A, green amino acid residues) interact with hydrophobic pockets formed by the HhH motifs of ERCC1 and XPF, respectively. The importance of Phe293 of ERCC1 is indicated by the observation that Phe293 is required for the stability and function of XPF/ERCC1 complex (De Laat et al., 1998b; Sijbers et al., 1996b).

The XPF/ERCC1 complex functions as an endonuclease that preferentially cleaves splayed arm, 3'-flap and bubble structures on dsDNA regions near the transition between dsDNA and ssDNA (Figure 1.10G) (De Laat et al., 1998a). The critical residues for endonuclease activity reside in the ERCC4 domain of XPF (Enzlin and Scharer, 2002), whereas they are absent in the ERCC4

FIGURE 1.12: Structural model of *Aeropyrum pernix* XPF bound to a 3'-flap substrate

A. Crystal structure of the nuclease domains and the HhH motifs of *Aeropyrum pernix* XPF dimeric complex bound to DNA. The nuclease domain and the HhH motifs of the XPF monomer A are in blue and green, respectively, whereas the corresponding domains of the XPF monomer B are in light blue and yellow. A schematic model of XPF interacting with a 3'-flap structure is shown on the right. The interaction of XPF with site I of the 3'-flap was determined by crystallographic data, whereas the binding of XPF to the site II is modelled. Taken from Newman et al., 2005.

B. Representation of the catalytically active (red) and inactive (green) subunits of *A. pernix* XPF dimeric complex. The DNA strand that is cleaved by XPF is indicated by a black line, which continues into the active site of XPF and beyond (dashed black and red lines). Note that the active XPF monomer is in contact with the DNA strand to be cleaved. Taken from Newman et al., 2005.

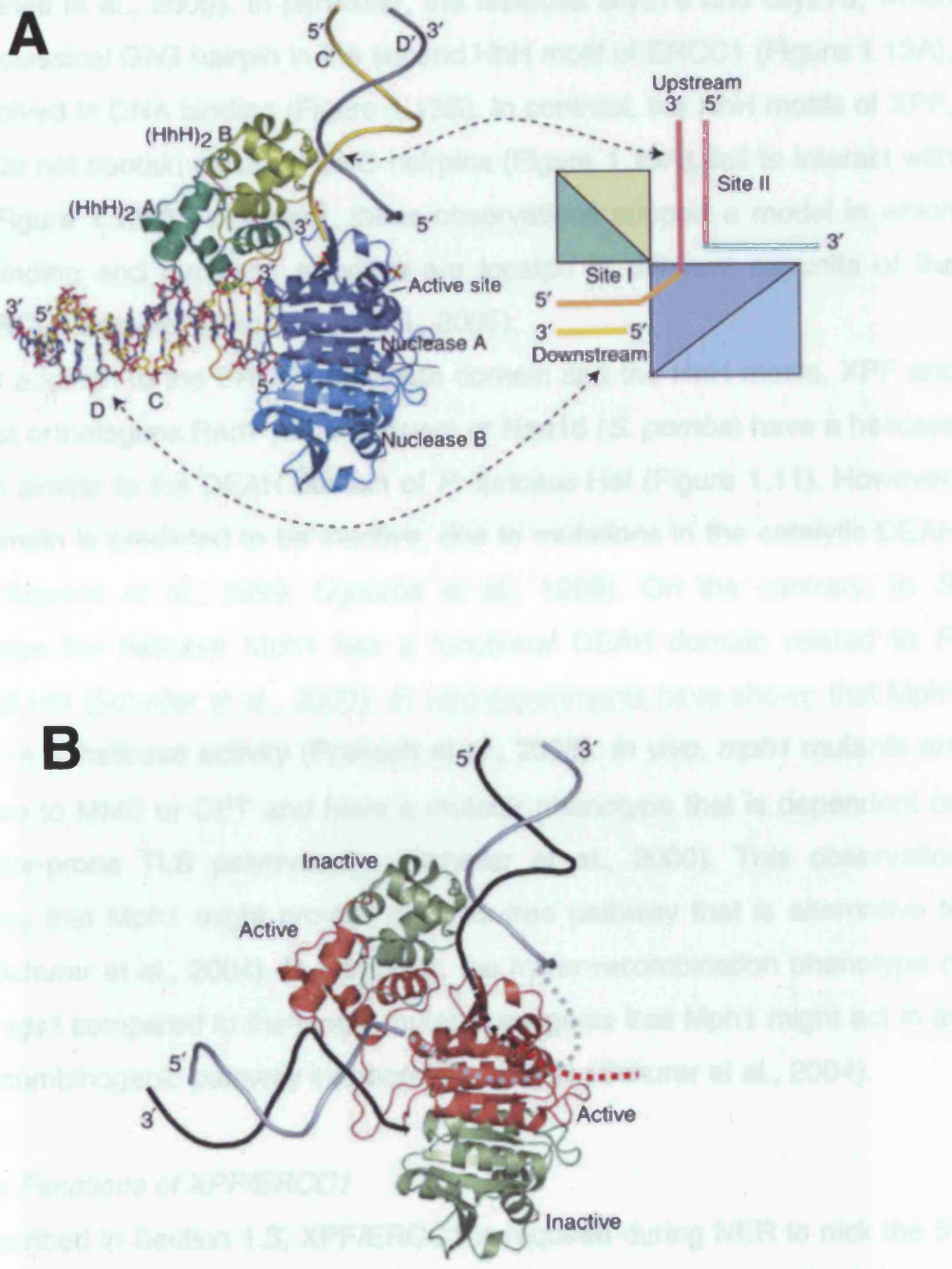
A
5′
C′
D′
3′
(HhH)2 B
(HhH)2 A
3′
5′
3′
Active site
3′
5′
Nuclease A
5′
D
C
Nuclease B
Upstream
3′ 5′
Site II
3′
Site I
5′
3′ 5′
Downstream
B
5′
3′
Inactive
Active
5′
3′
Active
Inactive

domain of ERCC1, which is inactive (Figure 1.11) (Aravind et al., 1999). Therefore, as observed with archaeal Hef and XPF proteins, a single active ERCC4 domain is sufficient for endonuclease activity.

Recent data indicate that ERCC1 is required to target XPF to DNA (Tripsianes et al., 2005). In particular, the residues Gly276 and Gly278, which form a classical GhG hairpin in the second HhH motif of ERCC1 (Figure 1.13A), are involved in DNA binding (Figure 1.13B). In contrast, the HhH motifs of XPF, which do not contain classical GhG hairpins (Figure 1.13A), fail to interact with DNA (Figure 1.13B). Altogether, these observations support a model in which DNA binding and nuclease activities are located in different subunits of the XPF/ERCC1 complex (Tripsianes et al., 2005).

In addition to the ERCC4 nuclease domain and the HhH motifs, XPF and its yeast orthologues Rad1 (*S. cerevisiae*) or Rad16 (*S. pombe*) have a helicase domain similar to the DEAH domain of *P. furiosus* Hef (Figure 1.11). However, this domain is predicted to be inactive, due to mutations in the catalytic DEAH motif (Aravind et al., 1999; Sgouros et al., 1999). On the contrary, in *S. cerevisiae* the helicase Mph1 has a functional DEAH domain related to *P. furiosus* Hef (Scheller et al., 2000). *In vitro* experiments have shown that Mph1 has 3' → 5' helicase activity (Prakash et al., 2005). *In vivo*, *mph1* mutants are sensitive to MMS or CPT and have a mutator phenotype that is dependent on the error-prone TLS polymerases (Scheller et al., 2000). This observation indicates that Mph1 might provide an error-free pathway that is alternative to TLS (Schurer et al., 2004). In particular, the hyper-recombination phenotype of *mph1 sgs1* compared to the single mutants suggests that Mph1 might act in an anti-recombinogenic pathway independent of Sgs1 (Schurer et al., 2004).

In Vivo Functions of XPF/ERCC1

As described in Section 1.3, XPF/ERCC1 is required during NER to nick the 5'-side of the damaged DNA strand. The concerted action of XPF/ERCC1 and XPG, which cleaves the 3'-side of the damaged DNA strand, is responsible for the release of an oligonucleotide containing the DNA lesion (Figure 1.1).

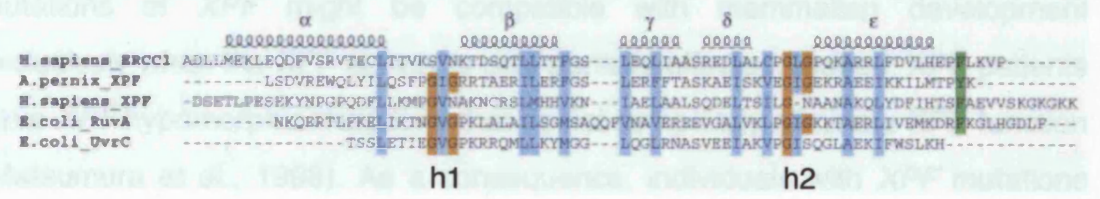
A
α
β
γ
δ
ε
H.sapiens_ERCC1 ADLLMEKLEQDFVSRVTECLTTVKSVNKTDSQTLLTTFGS---LEQLIAASREDLALCPGLGPQKARRLFDVLHEPLKVP-------
A.pernix_XPF --------LSDVREWQLYILQSFPGIGRRTAERILERFGS---LERFFTASKAEISKVEGIGEKRAEEIKKILMTPYK----------
H.sapiens_XPF -DSETLPESEKYNPGPQDFLLKMPGVNAKNCRSLMHHVKN---IAELAALSQDELTSILG-NAANAKQLYDFIHTSFAEVVSKGKGKK
E.coli_RuvA ---------NKQERTLFKELIKTNGVGPKLALAILSGMSAQQFVNAVEREEVGALVKLPGIGKKTAERLIVEMKDRFKGLHGDLP---
E.coli_UvrC ----------------TSSLETIEGVGPKRRQMLLKYMGG---LQGLRNASVEEIAKVPGISQGLAEKIFWSLKH------------
h1
h2

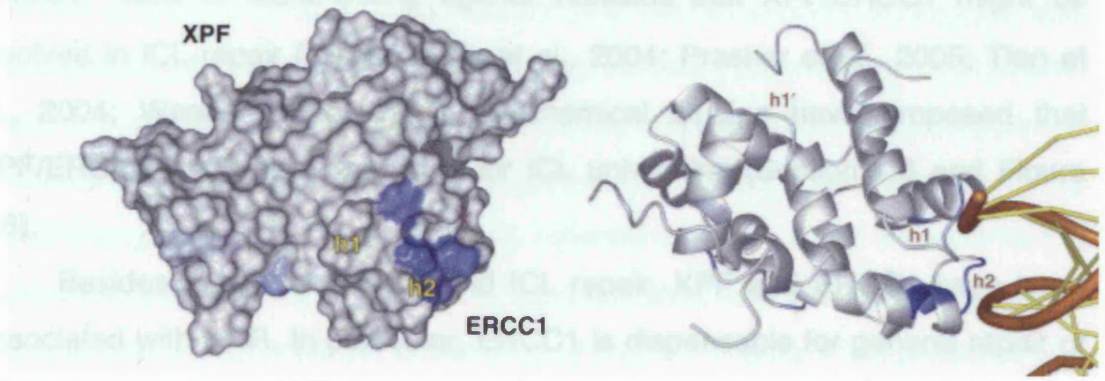
B
XPF
h1
h2
ERCC1
h1'
h1
h2

Mutations in *XPF* have been identified in XP patients of the complementation group F (Section 1.3) (Sijbers et al., 1996a). However, no complementation groups of XP patients are defective for ERCC1 (Cleaver, 2005). This could be a result of the apparent requirement of ERCC1 for postnatal survival, as suggested by the death of *ERCC1*$^{-/-}$ mice 3 weeks after birth (Weeda et al., 1997). Similar results obtained for *XPF*$^{-/-}$ mice indicate that XPF is also necessary for postnatal survival (Tian et al., 2004). Therefore, mutations of *XPF* might be compatible with mammalian development exclusively when the XPF activity is only partially affected. Indeed, XPF patients have *XPF* hypomorphic mutations that do not completely eliminate XPF function (Matsumura et al., 1998). As a consequence, individuals with *XPF* mutations show mild symptoms of photosensitivity, compared to XP patients of other complementation groups (Kondo et al., 1989).

XPF$^{-/-}$ or *ERCC1*$^{-/-}$ mice have a distinct phenotype from *XPA*$^{-/-}$ or *XPC*$^{-/-}$ mice, which develop normally (de Vries et al., 1995; Nakane et al., 1995; Sands et al., 1995). This indicates that XPF/ERCC1 complex has an additional function outside NER. As described in Section 1.6, the hypersensitivity of *XPF*$^{-/-}$ or *ERCC1*$^{-/-}$ cells to cross-linking agents indicates that XPF/ERCC1 might be involved in ICL repair (Niedernhofer et al., 2004; Prasher et al., 2005; Tian et al., 2004; Weeda et al., 1997). Biochemical studies have proposed that XPF/ERCC1 could be responsible for ICL unhooking (Section 1.6 and Figure 1.8).

Besides their role in NER and ICL repair, XPF and ERCC1 have been associated with HRR. In particular, ERCC1 is dispensable for general repair of DSBs (Adair et al., 2000), but is essential in ES cells for a particular subset of HRR, such as targeted gene replacement (Adair et al., 2000; Niedernhofer et al., 2001). In addition to a role in gene targeting, XPF/ERCC1 has been implicated in HRR during meiosis. In *Drosophila melanogaster*, MEI-9, which is the orthologue of XPF, is required for NER, ICL repair and meiotic recombination (Yildiz et al., 2004). It has been shown that *mei-9* mutants exhibit 90-95% decrease of the number of crossover products and extensive

chromosomal non-disjunctions (Baker and Carpenter, 1972). These observations indicate that MEI-9 might be involved in HJ resolution (Yildiz et al., 2004). It has been reported that MEI-9 has two different partners, MUS312 and ERCC1 (Yildiz et al., 2002). MUS312, a protein identified exclusively in *D. melanogaster*, is required for the formation of crossover products (Yildiz et al., 2002), whereas ERCC1 is only partially involved in meiotic recombination (Radford et al., 2005). It is not known whether MEI-9/MUS312 complex is able to generate crossovers by cleaving HJs (Yildiz et al., 2002). In mouse, XPF and ERCC1 are highly expressed in testis and ERCC1 is required for normal spermatogenesis and oogenesis (Hsia et al., 2003; Shannon et al., 1999). However, no direct evidence of a role for XPF or ERCC1 in meiotic recombination has been obtained.

MUS81

Structural Organisation of MUS81 and its Partner Protein

Mus81 was initially identified as an interactor of the HRR protein Rad54 in *S. cerevisiae* (Interthal and Heyer, 2000) and the replication checkpoint kinase Cds1 in *S. pombe* (Boddy et al., 2000). The human MUS81 orthologue was subsequently found based on a homology search (Chen et al., 2001). Both yeast and human MUS81, similar to *A. pernix* and *S. solfataricus* XPF, do not contain the helicase DEAH domain (Figure 1.11). Moreover, the analysis of the MUS81 sequence has suggested that, different from the other member of the family, the C-terminal two HhH motifs are separated, with a HhH motif at the N-terminus and the other at the C-terminus of MUS81 (Figure 1.11) (Interthal and Heyer, 2000). Knowing that the HhH motifs cooperate in promoting DNA binding in the archaeal MUS81 family proteins, it is possible that the 2 HhH motifs of MUS81 might be in close proximity in the MUS81 three-dimentional structure.

Yeast Mus81 forms a heterodimer with Mms4 in *S. cerevisiae* (Mullen et al., 2001) and Eme1 in *S. pombe* (Boddy et al., 2001). Both Mms4 and Eme1, like Rad10 and Swi10, contain in their C-termini a ERCC4 domain, which is inactive due to the absence of the catalytic motif $ERKX_3D$, and a single HhH

motif (Figure 1.11). The observation that the C-terminal regions of Mus81 and Eme1(Mms4) are required for the formation of the Mus81/Eme1(Mms4) complex, suggests that, similar to the archaeal MUS81 family proteins (Nishino et al., 2003; Nishino et al., 2005a), the ERCC4 domain and the HhH motifs might be responsible for the interaction between Mus81 and Eme1(Mms4) (Boddy et al., 2001; Fu and Xiao, 2003). The formation of the heterodimeric complex is necessary for the endonuclease activity of Mus81/Eme1(Mms4) (Boddy et al., 2001; Kaliraman et al., 2001), both during meiosis and mitosis.

Role of MUS81 in Meiosis

Initial experiments in *S. pombe* showed that *mus81* or *eme1* mutants exhibit very pronounced meiotic defects consistent with problems with the processing of recombination intermediates, and that this phenotype could be at least partially rescued by the expression of the RusA HJ resolvase (Boddy et al., 2001). These studies raised the possibility that Mus81/Eme1 possessed HJ resolution activity, a proposal that was supported by *in vitro* studies with Mus81/Eme1 protein (Boddy et al., 2001). However, the ability of Mus81/Eme1 to cleave HJs was subsequently shown to be considerably lower than that observed with other DNA substrates such as 3'-flaps and replication fork structures (Figure 1.10H) (Boddy et al., 2001; Doe et al., 2002; Whitby et al., 2003). The recent *in vitro* observation that Mus81/Eme1 efficiently cleaves D-loops and nicked HJs (Figure 1.10H) (Gaillard et al., 2003; Osman et al., 2003) led to the suggestion that D-loops and nicked HJs might be the substrates cleaved by Mus81/Eme1 *in vivo* during meiosis (Osman et al., 2003). In the current model, Mus81/Eme1 is proposed to nick the D-loop structure formed by strand invasion and the unligated HJ generated after second end capture (Figure 1.14, steps 3c and 5c). By this mechanism, Mus81 would generate crossover products, without resolving intact HJs (Figure 1.14, step 6c). This model is in agreement with the observation that *S. pombe mus81* cells have defects in generating crossover products, whereas non-crossovers are unaffected by the absence of Mus81 (Osman et al., 2003; Smith et al., 2003). Therefore, the extensive meiotic defect of *mus81* or *eme1* mutants (Boddy et

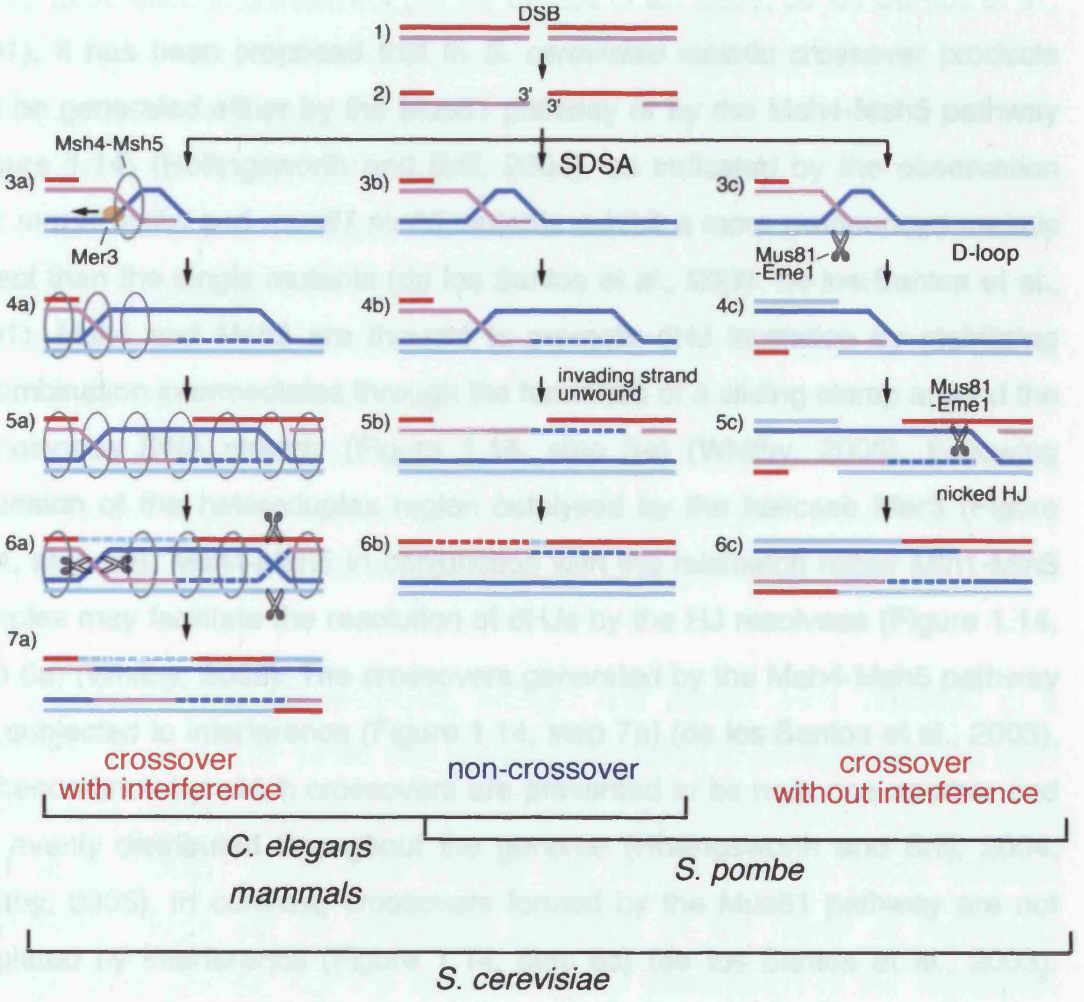
DSB
1)
2)
3'
3'
SDSA
Msh4-Msh5
3a)
3b)
3c)
Mer3
Mus81
-Eme1
D-loop
4a)
4b)
4c)
invading strand
unwound
Mus81
-Eme1
5a)
5b)
5c)
nicked HJ
6a)
6b)
6c)
7a)
crossover
with interference
non-crossover
crossover
without interference
C. elegans
mammals
S. pombe
S. cerevisiae

al., 2001; Osman et al., 2003) indicates that Mus81 is responsible for the major pathway that leads to meiotic crossover products in *S. pombe* (Figure 1.14) (Hollingsworth and Brill, 2004).

In *S. cerevisiae*, however, the mild crossover defects of *mus81* and *mms4* cells has suggested the presence of an alternative Mus81-independent pathway for the generation of crossovers (de los Santos et al., 2003; de los Santos et al., 2001). It has been proposed that in *S. cerevisiae* meiotic crossover products can be generated either by the Mus81 pathway or by the Msh4-Msh5 pathway (Figure 1.14) (Hollingsworth and Brill, 2004), as indicated by the observation that *mms4 msh5* and *mus81 msh5* mutants exhibit a more pronounced meiotic defect than the single mutants (de los Santos et al., 2003; de los Santos et al., 2001). Msh4 and Msh5 are thought to promote dHJ formation by stabilising recombination intermediates through the formation of a sliding clamp around the homologous DNA strands (Figure 1.14, step 3a) (Whitby, 2005). Following extension of the heteroduplex region catalysed by the helicase Mer3 (Figure 1.14, step 4a), Msh4-Msh5 in conjunction with the mismatch repair Mlh1-Mlh3 complex may facilitate the resolution of dHJs by the HJ resolvase (Figure 1.14, step 6a) (Whitby, 2005). The crossovers generated by the Msh4-Msh5 pathway are subjected to interference (Figure 1.14, step 7a) (de los Santos et al., 2003), a phenomenon by which crossovers are prevented to be near one another and are evenly distributed throughout the genome (Hollingsworth and Brill, 2004; Whitby, 2005). In contrast, crossovers formed by the Mus81 pathway are not regulated by interference (Figure 1.14, step 6c) (de los Santos et al., 2003). Whereas in *S. cerevisiae* crossovers result from both the interference-dependent Msh4-Msh5 pathway and the interference-independent Mus81 pathway, in *C. elegans* crossovers are exclusively generated by the interference-dependent Msh4-Msh5 pathway (Figure 1.14) (Hollingsworth and Brill, 2004).

In mammals, as observed with *C. elegans*, crossovers might be formed only by the interference-dependent MSH4-MSH5 pathway (Figure 1.14) (Whitby, 2005). Indeed, *MSH4*$^{-/-}$ and *MSH5*$^{-/-}$ mice are infertile (de Vries et al.,

1999; Edelmann et al., 1999; Kneitz et al., 2000), whereas *MUS81*$^{-/-}$ mice do not exhibit any meiotic defects (Dendouga et al., 2005; McPherson et al., 2004). Altogether, these observations suggest that mammalian MUS81 might function exclusively during mitosis.

Mus81 and Replication Fork Cleavage in Yeast

In vivo studies have shown that yeast *mus81* mutants are sensitive to DNA damaging agents that cause replicative damage, such as UV, HU, MMS or CPT (Bastin-Shanower et al., 2003; Boddy et al., 2000; Doe et al., 2002; Interthal and Heyer, 2000). In contrast, *mus81* mutants do not show defects in DSB repair, as indicated by the normal growth after IR (Boddy et al., 2000; Interthal and Heyer, 2000). In agreement with a role for Mus81 during DNA replication, yeast Mus81/Eme1(Mms4) was shown to efficiently cleave replication fork and 3'-flap substrates *in vitro* (Doe et al., 2002; Kaliraman et al., 2001; Whitby et al., 2003). Taken together, these observations suggest that Mus81 might be involved during DNA replication in repairing blocked or collapsed replication forks.

Consistent with this proposal, *MUS81* and *MMS4* were identified in a screen for *S. cerevisiae* genes that are synthetic lethal in combination with *sgs1* (Mullen et al., 2001). Similarly, *S. pombe rqh1 mus81* cells proved to be inviable (Doe et al., 2002). These data indicate that Mus81 and the RecQ helicase Sgs1(Rqh1) might act on alternative pathways in the repair of replicative damage. In *S. pombe*, Rqh1 is required for the stabilisation of the replication fork, as indicated by the formation of DSBs in replication forks blocked at the *RTS1* RFB in the absence of Rqh1 (Ahn et al., 2005). RecQ helicases could maintain fork integrity by resetting replication forks that have regressed at DNA replication blocks (Figure 1.4, step n) (Doe et al., 2000; Karow et al., 2000). This could allow DNA replication restart when the block has been removed (Figure 1.4, step n). In the absence of RecQ helicases, Mus81/Eme1 could be required in order to cleave blocked replication forks (Figure 1.4, step h). Mus81/Eme1 cleavage activity might be favoured by helicases that could reset replication forks that have regressed (Figure 1.4, step l), similar to the

mechanism described for the helicase and nuclease domain of *P. furiosus* Hef (Komori et al., 2004). As a consequence of Mus81/Eme1 cleavage, DNA replication could restart after the DSBs are repaired by HRR (Figure 1.4, steps b-f). However, the observation that DSBs at the *RTS1* RFB are not detected in wild-type cells (Ahn et al., 2005) indicates that, in physiological conditions, replication fork cleavage might not represent the primary mechanism of replication fork restart after replication fork blockage.

Replication fork breakage might be deleterious, as it could induce genomic rearrangements (Kai et al., 2005; Lambert et al., 2005). It has been proposed that, in order to avoid replication fork cleavage when replication forks stall because of HU-induced dNTP depletion, *S. pombe* Mus81 might dissociate from the chromatin after being phosphorylated in a Cds1-dependent manner (Kai et al., 2005). Following Mus81 release from the chromatin, replication fork progression could resume once dNTP levels are restored. These observations may indicate that Mus81 is not a critical factor for survival after HU treatment. In contrast, Mus81 might be required when DNA replication progression is compromised by mutations of replicative genes (Kai et al., 2005). In these mutants, Mus81 is only partially phosphorylated, due to moderate activation of Cds1, and remains associated to chromatin. In the proposed model, chromatin-associated Mus81 could promote the cleavage of blocked replication forks in order to restart DNA replication. As a consequence, chromosomal deletions might be generated by inaccurate DSB repair. These chromosomal rearrangements are the price that replication mutants might have to pay in order to complete DNA replication and survive. Taken together, these experiments suggest that Cds1 might restrict Mus81 activity to situations in which it is required for cell survival (Kai et al., 2005). The absence of checkpoint kinases is predicted to result in hyperactivation of Mus81. It is possible that the replication fork collapse observed in *S. cerevisiae rad53* strains after HU and MMS treatment (Lopes et al., 2001; Tercero and Diffley, 2001) could be partly due to abnormal activation of Mus81.

Mus81 and the Repair of ssDNA Gaps and DSBs during DNA Replication in Yeast

In addition to replication fork breakage, Mus81/Eme1(Mms4) could promote the cleavage of HRR intermediates generated by the repair of ssDNA gaps during DNA replication (Figure 1.3) (Fabre et al., 2002). As an alternative to dHJ formation, the yeast Srs2 helicase could promote the synthesis dependent strand annealing (SDSA) pathway by disassembling the Rad51 filament and therefore dissociating the D-loop intermediate (Figure 1.3, step i) (Ira et al., 2003; Krejci et al., 2003; Veaute et al., 2003). In case DNA synthesis extends over the length of the ssDNA gap, 3'-flap structures would be generated when the displaced invading strand re-anneals to the original DNA filament (Figure 1.3, step i). These 3'-flap structures could be efficiently cleaved by Mus81/ Eme1(Mms4) (Figure 1.3, step j) (Fabre et al., 2002), as indicated by *in vitro* experiments (Kaliraman et al., 2001; Whitby et al., 2003). The involvement of Mus81 in the Srs2-dependent SDSA pathway has been suggested by the epistatic relationship between *srs2* and *mus81* after UV radiation (Doe and Whitby, 2004).

Mus81 and Srs2, instead, do not appear to function in the same pathway in the repair of replication forks collapsed at CPT-induced SSBs, as indicated by the hypersensitivity to CPT of *mus81 srs2* cells compared to either *mus81* or *srs2* mutants (Doe and Whitby, 2004). The exquisite sensitivity of *mus81* to CPT indicates that Mus81 has an important role in repairing collapsed forks (Bastin-Shanower et al., 2003; Doe et al., 2002; Kai et al., 2005). In *S. pombe* collapsed forks can be repaired by mechansims dependent or independent of Rhp51 (*S. pombe* Rad51 orthologue) (Doe et al., 2004). Mus81 has been shown to function in the Rhp51-independent pathway, while Srs2 belongs to the Rhp51-dependent pathway (Doe et al., 2004; Doe and Whitby, 2004). It has been proposed that Mus81/Eme1 might restart the collapsed fork by cleaving a D-loop formed by Rad22 (*S. pombe* Rad52 orthologue) (Figure 1.4, steps e and f) (Doe et al., 2004). Instead, the repair of the collapsed fork by Srs2 might involve the formation of a D-loop by Rhp51 and subsequent HJ resolution

(Figure 1.4, steps c and d) (Doe and Whitby, 2004). The differences between the two mechanisms are not yet defined.

MUS81 and Genomic Integrity in Mammals

In mammals, *MUS81*$^{-/-}$ mouse embryo fibroblasts (MEFs) and *MUS81*$^{-/-}$ human colon cancer HCT116 cell lines exhibit proliferation defects, due to the activation of the checkpoint kinases CHK1 and CHK2 and subsequent delay of the cell cycle (Dendouga et al., 2005; Hiyama et al., 2006). Consistent with the hypothesis that the checkpoint might be activated by spontaneous generation of DNA damage, *MUS81*$^{-/-}$ MEFs accumulate chromosomal aberrations, including breaks, fusions, triradials (Dendouga et al., 2005). Other studies have reported equal numbers of chromosome abnormalities in both *MUS81*$^{+/-}$ and *MUS81*$^{-/-}$ activated T cells or *MUS81*$^{+/-}$ and *MUS81*$^{-/-}$ HCT116 cell lines (Hiyama et al., 2006; McPherson et al., 2004). Therefore inactivation of a single copy of *MUS81* appears to be sufficient to cause genomic instability (McPherson et al., 2004).

According to these data, *MUS81*$^{+/-}$ and *MUS81*$^{-/-}$ mice were reported to develop tumours, in particular non-Hodgkin's lymphomas, during the first year of life (McPherson et al., 2004). On the contrary, a second study demonstrated that *MUS81*$^{+/-}$ and *MUS81*$^{-/-}$ mice are healthy and viable during the first 15 months of life (Dendouga et al., 2005). The basis of this discrepancy is not clear. Although similar mouse strains were used in both studies, the distinct phenotypes might be due to different disruption strategy of the *MUS81* gene. Future experiments are required to test whether *MUS81* is a tumour suppressor gene.

MUS81 plays a role during normal DNA replication, as indicated by MUS81 accumulation during unperturbed S phase (Gao et al., 2003). The majority of MUS81 protein during normal conditions is retained in the nucleoli, where the repetitive rDNA is located (Gao et al., 2003). Following UV radiation, MUS81 is recruited to the site of UV lesions (Gao et al., 2003). Similarly, in HU-

treated cells, MUS81 has been reported to co-localise in nuclear foci with BLM and RAD51 (Zhang et al., 2005). The interaction between MUS81 and BLM has been confirmed *in vitro* (Zhang et al., 2005).

Despite being recruited to site of replicative damage after HU treatment and UV radiation, mammalian MUS81 appears to be required exclusively for recovery from treatment with cross-linking agents, as indicated by the hypersensitivity of *MUS81*$^{-/-}$ cells to MMC and *cis*-platin, but not to HU, UV and IR (Dendouga et al., 2005; Hiyama et al., 2006; McPherson et al., 2004). Moreover, in contrast to yeast *mus81* cells, no sensitivity to CPT has been observed for mammalian *MUS81*$^{-/-}$ cells (Dendouga et al., 2005). These data indicate that the primary role of mammalian MUS81 could be in ICL repair.

It has been proposed that MUS81 might promote the formation of crossover products during mitosis (Blais et al., 2004). In fact, depletion of MUS81 in human somatic cells was reported to induce a two-fold reduction of mitotic recombination. Similar to yeast cells, this recombination defect could be rescued by overexpression of RusA (Blais et al., 2004). However, human somatic cells possess the unknown Resolvase A, which is distinct from MUS81 (Constantinou et al., 2002) and it has been shown to be associated with the RAD51 paralogs RAD51C and XRCC3 (Section 1.4) (Liu et al., 2004). It is therefore possible that Resolvase A might be primarily responsible for crossover formation in mitosis (and also in meiosis).

Taken together, these data suggest that mammalian MUS81 is required for the maintanance of genomic stability, during both normal cell growth and after treatment with cross-linking agents. Characterisation of the biochemical properties of human MUS81 has been hampered by the lack of obvious human orthologues of *S. pombe* Eme1 or *S. cerevisiae* Mms4.

In the work described in this thesis, we report the identification of two human othologues of *S. pombe* Eme1, which we named human EME1 and EME2. We showed that EME1 and EME2 interact with MUS81 and are novel members of the MUS81 family. The biochemical properties of MUS81/EME1 and MUS81/EME2 complexes have been characterised. Moreover, we have

identified two more human members of the MUS81 family, which we have called HEF and HIP. We demonstrate that HEF and HIP form a complex both *in vitro* and *in vivo*. Consistent with the recent identification of HEF as FANC-M, we show that HIP is a novel member of the Fanconi Anemia core complex.

CHAPTER TWO

Materials and Methods

I. ENZYMES AND REAGENTS

2.1 ENZYMES

Enzymes were purchased from the following companies:

New England Biolabs Inc. (NEB): restriction enzymes, T4 polynucleotide kinase, T4 DNA ligase

Sigma Aldrich: Proteinase K

2.2 REAGENTS

Reagents were obtained from Sigma or BDH unless indicated otherwise. Other materials were obtained as follows: radiolabelled reagents, ECL western blotting detection reagents, GST-sepharose 4 Fast Flow, HiPrep 16/60 Sephracryl S-200 HR gel filtration column, HiTrap chelating and Heparin columns, Thrombin (Amersham); Talon metal affinity resin (BD bioscience); Bradford reagent, bromophenol blue, xylene cyanol, ammonium persulfate and 30% acrylamide solution (Biorad); ethidium bromide (International Biotechnologies Inc.); Cellfectin, Mark 12 Unstained Standard, NuPAGE 4-12% Bis-Tris gradient gels, SeeBlue Plus2 Pre-Stained Standard, ProQuest HeLa Cell cDNA library, ProQuest Human Fetal Brain cDNA library and SuperScript Human Testis cDNA library (Invitrogen); Biomax MR and X-Omat films (Kodak); urea (MP Biomedicals); 10x BugBuster (Novagen); Imject Maleimide Activated KeyHole Limpet Hemocyanin (KLH), ImmunoPure gentle Ag/Ab elution buffer, Snakeskin dialysis bag and SulfoLink kit (Pierce); Nickel-NTA Agarose (Qiagen); complete EDTA-free protease inhibitor cocktail (Roche); anti-ERCC1 FL-297 polyclonal antibody (Santa Cruz); BA85 cellulose-nitrate membrane (Schleicher and Schuell); anti-FLAG M2 mouse monoclonal antibody and anti-FLAG M2 Affinity Gel Resin (Sigma).

2.3 BUFFERS AND SOLUTIONS

2.3.1 MEDIA AND PROTEIN BUFFERS

Blocking buffer: 4% (w/v) milk in PBS

Coomassie blue staining solution: 40% (v/v) methanol, 10% (v/v) glacial acetic acid, 0.1% (w/v) Coomassie brilliant blue

Denaturing lysis buffer: 100 mM sodium phosphate pH 7.0, 10% (v/v) glycerol, 8 M urea

Destaining solution: 40% (v/v) methanol, 10% (v/v) glacial acetic acid

Developing solution: 2% (w/v) sodium carbonate, 0.04% (v/v) formaldehyde

FLAG buffer: 50 mM Tris-HCl pH 7.5, 10% (v/v) glycerol, 0.1% (v/v) NP40, 0.5 mM EDTA

GST buffer: 50 mM Tris-HCl pH 7.5, 10% (v/v) glycerol, 0.5% (v/v) triton X-100, 500 mM KCl, 1 mM DTT, 1 mM EDTA

Heparin buffer: 50 mM Tris-HCl pH 7.5, 10% (v/v) glycerol, 0.1% (v/v) triton X-100, 1 mM EDTA, 1 mM DTT

Insect cell medium: Grace's medium supplemented with 3.3 g/l TC-yeastolate, 3.3 g/l TC-lactalbumin, 10% (v/v) heat inactivated fetal calf serum and 1% (v/v) antibiotic/antimycotic solution

Luria broth: 1% (w/v) bactotryptone, 0.5% (w/v) yeast extract, 0.05% (w/v) NaCl

Lysis buffer: 50 mM Tris-HCl pH 7.5, 10% (v/v) glycerol, 0.5 mM EDTA

Nickel buffer: 50 mM Tris-HCl pH 7.5, 10% (v/v) glycerol, 0.5% (v/v) triton, 500 mM KCl, 1 mM β-mercaptoethanol

PBS: 140 mM NaCl, 3.4 mM KCl, 10 mM Na_2HPO_4, 18 mM KH_2PO_4

Phosphate buffer: 50 mM sodium phosphate pH 7.0, 0.01% (v/v) NP40 and 10% (v/v) glycerol

SDS gel buffer A (2x): 750 mM Tris-NaOH (pH 8.8), 0.2% (w/v) SDS

SDS gel buffer B (2x): 250 mM Tris-HCl (pH 6.8), 0.2% (w/v) SDS

SDS sample buffer (4x): 125 mM Tris-HCl (pH 6.8), 10% (v/v) glycerol, 2% (w/v) SDS, 0.01% (w/v) bromphenol blue,10% (v/v) β-mercaptoethanol

Storage buffer: phosphate buffer containing 0.1 M NaCl, 1 mM DTT and 0.5 mM EDTA

SDS gel running buffer: 25 mM Tris base, 190 mM glycine, 1 mg/ml SDS

SulfoLink coupling buffer: 50 mM Tris-NaOH (pH 8.5), 5 mM EDTA

SulfoLink wash buffer: 1 M NaCl, 0.05% NaN_3

Transfer buffer: 25 mM Tris base, 190 mM glycine, 20% (v/v) methanol

2.3.2 DNA BUFFERS:

Formamide loading buffer: 80% (v/v) deionised formamide, 89 mM Tris base, 89 mM boric acid, 2 mM EDTA, 0.2% (w/v) bromophenol blue, 0.2% (w/v) xylene cyanol

Sample loading buffer (5x): 50 mM Tris-HCl (pH 8.0), 50 % (v/v) glycerol, 1 mg/ml bromophenol blue

Stains-all solution: 20% (v/v) isopropanol, 10% (v/v) formamide, 0.01% (w/v) Stains-all

TAE buffer: 40 mM Tris base, 1.1% (v/v) glacial acetic acid, 1mM EDTA

TBE buffer: 89 mM Tris base, 89 mM boric acid, 2 mM EDTA

TE: 10 mM Tris-HCl (pH 8.0), 1 mM EDTA

TNM buffer: 10 mM Tris-HCl (pH 8.0), 50 mM NaCl, 10 mM $MgCl_2$

2.3.3 ENZYME BUFFERS:

Cleavage buffer: 60 mM sodium phosphate (pH 7.4), 5 mM $MgCl_2$, 1 mM DTT, 100 μg/ml BSA

Stop buffer (5x): 2% (w/v) SDS, 10 mg/ml Proteinase K

2.4 BACTERIAL STRAINS

E. coli competent cells XL1-Blue cells (Stratagene) were used for DNA cloning. *E. coli* competent cells DH10BAC (Invitrogen), which contain a baculovirus shuttle vector, also known as bacmid, were used to generate recombinant baculovirus DNA, as described in Section 2.23.

E. coli competent cells BL21-CodonPlus (DE3)-RIL (Stratagene), BL21-CodonPlus (DE3)-PR (Stratagene) and *E. coli* STL5827 BL21-(DE3)-ExoI$^-$

Endol$^-$ were used for protein expression. *E. coli* STL5827 BL21-(DE3)-Exol$^-$ Endol$^-$ strain was a gift of Bob Lloyd.

2.5 DNA OLIGONUCLEOTIDES

TABLE 2.1: List of DNA oligonucleotides

1) $^{5'}$CATCATGCCATGGCTCACCATCACCACCATCACCATCATCACCACGGCGGCCTGGAAGTTCTGTTCCAGGG GCCCCATATG TCGCATGGTGGTGGAAAGGAGGTCT$^{3'}$
2) $^{5'}$CATATAAGAATGCGGCCGCGCTAGCGGTACCTTACTTGTCATCGTCGTCCTTGTAGTCTCCTCCGGGCCCC TGGAACAGAACTTCCAGTATATCAGATTTCAGTCTATCTTGGTTAAGATCATTTG$^{3'}$
3) $^{5'}$CATATAAGAATGCGGCCGCGCTAGCGGTACCTTATTTTTCGAACTGCGGGTGGCTCCAAGCGCTGGGCCCC TGGAACAGAACTTCCAGTATATCAGATTTCAGTCTATCTTGGTTAAGATCATTTG$^{3'}$
4) $^{5'}$ GGGGACAAGTTTGTACAAAAAAGCAGGCTTCCATATGAGCGGACGGCAAAGA$^{3'}$
5) $^{5'}$ CATCATCCGCTCGAGTTATTTACCATCCCTATAGGAAA$^{3'}$
6) $^{5'}$CATGGGAATTCATCGATGGTACCAAGCTTC$^{3'}$
7) $^{5'}$GGAATTCCATATGGCTCTAAAGAAGTCATCACCC$^{3'}$
8) $^{5'}$CATCCCAAGCTTTCAGTCAGCACTATCTAAAGAGAG$^{3'}$
9) $^{5'}$GGGGACAAGTTTGTACAAAAAAGCAGGCTTCCATATGGCGCGGGTTGGAC$^{3'}$
10) $^{5'}$GGGGACCACTTTGTACAAGAAAGCTGGGTAAAGCTTTCAGGAGCCCAGGTCCAG$^{3'}$
11) $^{5'}$GGAATTCCATATGGACCCTGGGAAGGAC$^{3'}$
12) $^{5'}$CATCCCAAGCTTTCAGGGTACTTTCAAGAAGGG$^{3'}$
13) $^{5'}$GGGGACAAGTTTGTACAAAAAAGCAGGCTTCCATATGGAAAAGAACCCCCCTG$^{3'}$
14) $^{5'}$GGGGACCACTTTGTACAAGAAAGCTGGGTAAAGCTTTCACCTGGGCTGTGTGAAG$^{3'}$
15) $^{5'}$CATCATGAATTCTGGATCCATGGAAAAGAACCCCCCTG$^{3'}$
16) $^{5'}$CATCATGGATCCGCGGCCGCTCACCTGGGCTGTGTGAAG$^{3'}$
17) $^{5'}$ATGGCGCGGGTTGGAC$^{3'}$
18) $^{5'}$TCAGGAGCCCAGGTCCA$^{3'}$
19) $^{5'}$GGGGACAAGTTTGTACAAAAAAGCAGGCTTCCATATGGGATCCTTAGCAAAGCAGAGCAAACAGA$^{3'}$
20) $^{5'}$GGGGACCACTTTGTACAAGAAAGCTGGGTAGCGGCCGCCTCGAGTTATATATCAGATTTCAGTCTATCTT$^{3'}$
21) $^{5'}$CATGAATTCTAATGGCGGCCCCGGTCCG$^{3'}$
22) $^{5'}$CATGGATCCCTCGAGTCAGGTCAAGGGGCCGTAGC$^{3'}$
23) $^{5'}$CATCGGAATTCTACAACGCTATCTCACTGCTTTG$^{3'}$
24) $^{5'}$CATCATCCGCTCGAGTCACTTTTTCCCTTTTCCTTTTG$^{3'}$
25) $^{5'}$GGGGACAAGTTTGTACAAAAAAGCAGGCTTCATGGCTCTAAAGAAGTCATCACCC$^{3'}$
26) $^{5'}$GGGGACCACTTTGTACAAGAAAGCTGGGTATCAGTCAGCACTATCTAAAGAGAG$^{3'}$
27) $^{5'}$ GGGGACAAGTTTGTACAAAAAAGCAGGCTTCCATATGCCCACAGCAGGGCTG$^{3'}$
28) $^{5'}$ GGGGACCACTTTGTACAAGAAAGCTGGGTAAAGCTTTCAGGAGCCCAGGTCCAGC$^{3'}$
29) $^{5'}$GGGGACAAGTTTGTACAAAAAAGCAGGCTTCATGGCGGCCCCGGTCCG$^{3'}$
30) $^{5'}$GGGGACCACTTTGTACAAGAAAGCTGGGTATCAGGTCAAGGGGCCGTAGC$^{3'}$

2.6 PLASMIDS

TABLE 2.2: List of plasmids constructed

PLASMID	DESCRIPTION
pDEST8-10HISHEF	Gateway vector for baculovirus expression generated by Gateway recombination between pDEST8 (Invitrogen) and pENTR4-10HISHEF
pDEST8-10HISHEFFLAG	Gateway vector for baculovirus expression generated by Gateway recombination between pDEST8 (Invitrogen) and pENTR4-10HISHEFFLAG
pDEST8-10HISHEFSTREP	Gateway vector for baculovirus expression generated by Gateway recombination between pDEST8 (Invitrogen) and pENTR4-10HISHEFSTREP
pDEST15-GSTMUS81	Gateway vector for *E. coli* expression generated by Gateway recombination between pDEST15 (Invitrogen) and p221-MUS81
pDEST17-HISEME1	Gateway vector for *E. coli* expression generated by Gateway recombination between pDEST17 (Invitrogen) and p221-EME1
pDEST17-HISMUS81	Gateway vector for *E. coli* expression generated by Gateway recombination between pDEST17 (Invitrogen) and p221-MUS81
pENTR4-10HIS-FLAG	Gateway entry vector obtained by inserting into the *Nco* I and *Not* I sites of pENTR4 (Invitrogen) a PCR fragment (amplified with

	DNA oligonucleotides 1 and 2 described in Table 2.1) coding for amino acids 1859-2048 of HEF in frame with a N-terminus 10HIS tag and a C-terminus FLAG tag (Figure 5.3)
pENTR4-10HIS-STREP	Gateway entry vector obtained by inserting into the *Nco* I and *Not* I sites of pENTR4 (Invitrogen) a PCR fragment (amplified with DNA oligonucleotides 1 and 3 described in Table 2.1) coding for amino acids 1859-2048 of HEF in frame with a N-terminus 10HIS tag and a C-terminus Strep tag
pENTR4-10HISHEF	Gateway entry vector obtained by cloning HEF (*Nco* I and *Not* I cut from pET16b-HEF) into the *Nco* I and *Not* I sites of pENTR4 (Invitrogen)
pENTR4-10HISHEFFLAG	Gateway entry vector obtained by inserting a fragment coding for amino acids 1-2018 of HEF from pET16b-HEF (*Nde* I and *Bgl* II digested) into the *Nde* I and *Bgl* II sites of pENTR4-10HIS-FLAG (Figure 5.3)
pENTR4-10HISHEFSTREP	Gateway entry vector obtained by inserting a fragment coding for amino acids 1-2018 of HEF from pET16b-HEF (*Nde* I and *Bgl* II digested) into the *Nde* I and *Bgl* II sites of pENTR4-10HIS-STREP
pET16b-HEF	*E. coli* expression vector generated by cloning HEF from Origene clone TC125463 (*Sac* II and *Not* I digested) into the *Sac* II and *Not* I sites of pET16b- HEF_{1-669}
pET16b-HEF_{1-669}	*E. coli* expression vector generated by cloning a fragment coding for amino acids 1-669 of HEF (PCR amplified from the IMAGE

	clone 5270515 with DNA oligonucleotides 4 and 5 described in Table 2.1) into the *Nde* I and *Xho* I sites of pET16b (Novagen). The *Not* I site was introduced before *Xho* I
pET21d-linker	*E. coli* expression vector generated by introducing a polylinker (DNA oligonucleotide 6 described in Table 2.1) into the *Nco* I and *Xho* I sites (Figure 3.4) of pET21 (Novagen)
pET21d-MUS81/HISEME1	Bicistronic vector for *E. coli* expression constructed by inserting an *Eco*R I-*Hin*d III fragment encoding MUS81/HISEME1 from pGex-GSTMUS81/HISEME1 into the *Eco*R I and *Hin*d III sites of pET21d-linker (Figure 3.4)
pET21d-MUS81/HISEME2	Bicistronic vector for *E. coli* expression constructed by inserting an *Eco*R I-*Hin*d III fragment encoding MUS81/HISEME2 from pGex-GSTMUS81/HISEME2 into the *Eco*R I and *Hin*d III sites of pET21d-linker
pET28-EME1	*E. coli* expression vector generated by cloning *EME1* (PCR amplified from IMAGE clone 2899969 with DNA oligonucleotides 7 and 8 described in Table 2.1) into the *Nde* I and *Hin*d III of pET28 (Novagen)
pET28-EME2	*E. coli* expression vector generated by cloning *EME2* (PCR amplified from pGEMT-EME2_HeLa with DNA oligonucleotides 9 and 10 described in Table 2.1) into the *Nde* I and *Hin*d III of pET28 (Novagen)
pET28-ERCC1	*E. coli* expression vector generated by cloning *ERCC1* (PCR amplified from Invitrogen SUPERSCRIPT Human testis

	cDNA library with DNA oligonucleotides 11 and 12 described in Table 2.1) into the *Nde* I and *Hind* III of pET28 (Novagen)
pET28-HIP	*E. coli* expression vector generated by cloning *HIP* (PCR amplified from the IMAGE clone 3609326 with DNA oligonucleotides 13 and 14 described in Table 2.1) into the *Nde* I and *Hind* III of pET28 (Novagen)
pFAST-BAC-DUAL-10HISHEFFLAG/HIP	Bicistronic vector for baculovirus expression generated by cloning *HIP* (PCR amplified from IMAGE clone 3609326 with DNA oligonucleotides 15 and 16 described in Table 2.1) into the *Bam*H I and *Not* I sites of pFAST-BAC-DUAL (Invitrogen), followed by the insertion of *HEF* (*Nco* I and *Kpn* I cut from pENTR4-10HISHEFFLAG) into the *Nco* I and *Kpn* I sites (Figure 5.5).
pGEMT-EME2_HeLa	Cloning vector constructed by inserting EME2_HeLa (PCR amplified from Invitrogen ProQuest HeLa Cell cDNA library with DNA oligonucleotides 17 and 18 described in Table 2.1) into TT overhangs of pGEMT (Promega)
pGEMT-EME2_testis	Cloning vector constructed by inserting EME2_testis (PCR amplified from Invitrogen SuperScript Human Testis cDNA library with DNA oligonucleotides 17 and 18 described in Table 2.1) into TT overhangs of pGEMT (Promega)
pGex-BICIS-HIS	Bicistronic vector for *E. coli* co-expression of one GST-tagged and one HIS-tagged protein (Figure 3.2). Gift from Frank Uhlmann

	(CRUK, LIF)
pGex-GSTHEF$_{1727-2048}$	Bicistronic vector for *E. coli* expression constructed by cloning HEF$_{1727-2048}$ (fragment coding for amino acids 1727-2048 of HEF, PCR amplified from Origene clone TC125463 with DNA oligonucleotides 19 and 20 described in Table 2.1) into the *Bam*H I and *Xho* I sites of pGex-BICIS-HIS
pGex-GSTHEF$_{1727-2048}$/ HISEME1	Bicistronic vector for *E. coli* expression generated by cloning *EME1* (*Nde* I and *Not* I cut from pET28-EME1) into the *Nde* I and *Not* I sites of pGex-GSTHEF$_{1727-2048}$
pGex-GSTHEF$_{1727-2048}$/ HISEME2	Bicistronic vector for *E. coli* expression generated by cloning *EME2* (*Nde* I and *Not* I cut from pET28-EME2) into the *Nde* I and *Not* I sites of pGex-GSTHEF$_{1727-2048}$
pGex-GSTHEF$_{1727-2048}$/ HISERCC1	Bicistronic vector for *E. coli* expression generated by cloning *ERCC1* (*Nde* I and *Not* I cut from pET28-ERCC1) into the *Nde* I and *Not* I sites of pGex-GSTHEF$_{1727-2048}$
pGex-GSTHEF$_{1727-2048}$/ HISHIP	Bicistronic vector for *E. coli* expression generated by cloning *HIP* (*Nde* I and *Not* I cut from pET28-HIP) into the *Nde* I and *Not* I sites of pGex-GSTHEF$_{1727-2048}$
pGex-GSTMUS81	Bicistronic vector for *E. coli* expression constructed by cloning *MUS81* (PCR amplified from the IMAGE clone 4135990 with DNA oligonucleotides 21 and 22 described in Table 2.1) into the *Eco*R I and *Xho* I sites of pGEX-BICIS-HIS (Figure 3.2)
pGex-GSTMUS81/HISEME1	Bicistronic vector for *E. coli* expression

	generated by cloning *EME1* (PCR amplified from the IMAGE clone 2899969 with DNA oligonucleotides 7 and 8 described in Table 2.1) into the *Nde* I and *Hind* III sites of pGex-GSTMUS81 (Figure 3.2)
pGex-GSTMUS81/HISEME2	Bicistronic vector for *E. coli* expression generated by cloning *EME2* (*Nde* I and *Hind* III cut from pET28-EME2) into the *Nde* I and *Hind* III sites of pGex-GSTMUS81
pGex-GSTMUS81/ HISEME2_predicted	Bicistronic vector for *E. coli* expression generated by cloning *EME2_predicted* (*Nde* I and *Hind* III cut from p221-EME2_predicted) into the *Nde* I and *Hind* III sites of pGex-GSTMUS81
pGex-GSTMUS81/HISERCC1	Bicistronic vector for *E. coli* expression generated by cloning *ERCC1* (*Nde* I and *Not* I cut from pET28-ERCC1) into the *Nde* I and *Not* I sites of pGex-GSTMUS81
pGex-GSTMUS81/HISHIP	Bicistronic vector for *E. coli* expression generated by cloning *HIP* (*Nde* I and *Not* I cut from pET28-HIP) into the *Nde* I and *Not* I sites of pGex-GSTMUS81
pGex-GSTXPF$_{606-905}$	Bicistronic vector for *E. coli* expression constructed by cloning XPF$_{606-905}$ (fragment coding for amino acids 606-905 of XPF, PCR amplified from Invitrogen SUPERSCRIPT human testis cDNA library with DNA oligonucleotides 23 and 24 described in Table 2.1) into the *Eco*R I and *Xho* I sites of pGEX-BICIS-HIS
pGex-GSTXPF$_{606-905}$/HISEME1	Bicistronic vector for *E. coli* expression generated by cloning *EME1* (*Nde* I and *Not* I

	cut from pET28-EME1) into the *Nde* I and *Not* I sites of pGex- $_{GST}XPF_{606-905}$
pGex-$_{GST}XPF_{606-905}$/$_{HIS}$EME2	Bicistronic vector for *E. coli* expression generated by cloning *EME2* (*Nde* I and *Not* I cut from pET28-EME2) into the *Nde* I and *Not* I sites of pGex- $_{GST}XPF_{606-905}$
pGex-$_{GST}XPF_{606-905}$/ $_{HIS}$ERCC1	Bicistronic vector for *E. coli* expression generated by cloning *ERCC1* (*Nde* I and *Not* I cut from pET28-ERCC1) into the *Nde* I and *Not* I sites of pGex- $_{GST}XPF_{606-905}$
pGex- $_{GST}XPF_{606-905}$/ $_{HIS}$HIP	Bicistronic vector for *E. coli* expression generated by cloning *HIP* (*Nde* I and *Not* I cut from pET28-HIP) into the *Nde* I and *Not* I sites of pGex- $_{GST}XPF_{606-905}$
p221-EME1	Gateway entry vector obtained by inserting through Gateway recombination *EME1* (PCR amplified from the IMAGE clone 2899969 with DNA oligonucleotides 25 and 26 described in Table 2.1) into p221 (Invitrogen)
p221-EME2_predicted	Gateway entry vector obtained by inserting through Gateway recombination *EME2_predicted* (PCR amplified from the cDNA # AK074080 with DNA oligonucleotides 27 and 28 described in Table 2.1) into p221 (Invitrogen)
p221-MUS81	Gateway entry vector obtained by inserting through Gateway recombination *MUS81* (PCR amplified from the IMAGE clone 4135990 with DNA oligonucleotides 29 and 30 described in Table 2.1) into p221 (Invitrogen)

II. GEL ELECTROPHORESIS

2.7 SDS-PAGE

Gels were prepared according to the Laemmli procedure (Laemmli, 1970). Running gels typically contained 10 or 12% polyacrylamide, supplied as a 30% stock (29:1 acrylamide : bisacrylamide ratio; Section 2.2) and 1x SDS gel buffer A (Section 2.3.1). Stacking gels contained 4% polyacrylamide and 1x SDS gel buffer B (Section 2.3.1). Polymerisation was induced by addition of 0.1% (w/v) ammonium persulfate and 0.1% (v/v) TEMED. Protein samples were prepared by adding 1/3 volume of SDS sample buffer (4x; Section 2.3.1) and were boiled for 3 minutes before gel loading. Gel electrophoresis was performed in SDS gel running buffer (Section 2.3.1) at 150 V for 90 minutes (Mini PROTEAN II) or 200 V for 2 hours (20 x 12 cm Cambridge gel apparatus). Proteins were visualized by western blotting, Coomassie blue staining or silver staining (Sections 2.18, 2.19 and 2.22).

2.8 AGAROSE GEL ELECTROPHORESIS

Gels were prepared in ANACHEM Mini Cell gel trays and contained 0.8-1% (w/v) agarose in TAE buffer (Section 2.3.2). Approximately 1/4 volume sample loading buffer (5x; Section 2.3.2) was added to samples and gels were run in TAE at 7 V/cm. DNA samples were visualised by staining with 0.5 μg/ml ethidium bromide (Sharp et al., 1973). Stained gels were imaged and photographed using a digital camera on a BIORAD GelDoc 2000 setup.

2.9 NEUTRAL PAGE

Gels were prepared using a BIORAD PROTEAN II gel apparatus or Cambridge gel apparatus and contained 10% polyacrylamide (acrylamide/bisacrylamide 19:1) in TBE buffer (Section 2.3.2). Samples were supplemented with sample loading buffer (5x) and gels were run in TBE at 150 V for 2 hours. Gels were dried onto 3MM filter paper (Whatman) and ^{32}P-labelled DNA was detected by autoradiography (Section 2.11).

2.10 DENATURING PAGE

Gels were prepared in a BIORAD Sequi-Gen nucleic acid sequencing apparatus (21 x 50 cm) and contained 7 M urea and 10% polyacrylamide (acrylamide/bis-acrylamide 19:1) in TBE buffer. Samples were resuspended in formamide loading buffer (Section 2.3.2) and boiled for 3 minutes before gel loading. Gels were preheated to 50°C, and run in TBE buffer for 2 hours at 65 W. Gels were dried onto 3MM filter paper (Whatman) and ^{32}P-labelled DNA was detected by autoradiography (Section 2.11).

2.11 AUTORADIOGRAPHY

Dried agarose or polyacrylamide gels were exposed to Biomax MR films (Section 2.2). Intensifying screens were used at -80°C when necessary. Films were developed using an IGP Compact2 X-ray film processor.

2.12 PHOSPHORIMAGER ANALYSIS

Dried gels plates were exposed to Molecular Dynamics storage phosphor screens up to 12 hours. Screens were analysed on a Molecular Dynamics PhosphorImager (model 425E) and ImageQuant software.

III. GENERAL METHODS OF DNA MANIPULATION

2.13 DNA CONCENTRATION DETERMINATION

DNA concentrations were determined by measuring the absorbance at 260 nm using quartz cuvettes and a UltroSpec 2000 Spectrophotometer (Pharmacia). Calculations were based on the assumption that the absorbance at 260 nm equals 1 (A_{260}=1) for a solution of 36 μg/ml single-stranded or 50 μg/ml duplex DNA.

2.14 SOLVENT EXTRACTION

Samples were mixed with an equal volume of solvent, mixed thoroughly and the

phases were separated by low speed centrifugation. The aqueous phase was retained for further processing. Solvents used were phenol and chloroform (supplemented with 1/25 volume of isoamyl alcohol).

2.15 ETHANOL PRECIPITATION

DNA samples were mixed with 1/10 volume of 3 M sodium acetate (pH 7.0) and 2.6 volumes of ethanol. After 30 minutes in dry ice, precipitated DNA was collected by centrifugation. The DNA pellet was washed with 70% ethanol, air-dried and resuspended in TE buffer (pH 8.0; Section 2.3.2).

IV. GENERAL METHODS OF PROTEIN MANIPULATION

2.16 PROTEIN CONCENTRATION DETERMINATION

Protein concentrations were determined by the Bradford method (Bradford, 1976). The Bradford reagent was diluted 5-fold with ddH_2O and 5 to 10 µl of protein were added. The colour was allowed to develop for 10 minutes at room temperature. The absorbance at 595 nm was then measured and it was compared to a standard curve obtained with known concentrations of BSA.

2.17 MOLECULAR WEIGHT STANDARDS

Molecular weight Mark 12 Unstained Standard and SeeBlue Plus2 Pre-Stained Standard were used (Section 2.2). Mark 12 Unstained Standard contains myosin (200 kDa), β-galactosidase (116 kDa), phosphorylase (97 kDa), BSA (66 kDa), glutamic dehydrogenase (55 kDa), lactate dehydrogenase (36 kDa), carbonic anhydrase (31 kDa), tripsin inhibitor (21 kDa) and lysozyme (14 kDa). SeeBlue Plus2 Pre-Stained Standard was used as a guideline for SDS-PAGE and western blotting. Approximate molecular weights are: myosin (250 kDa), phosphorylase (148 kDa), BSA (98 kDa), glutamic dehydrogenase (64 kDa),

alcohol dehydrogenase (50 kDa), carbonic anhydrase (36 kDa) and myoglobin red (30 kDa).

2.18 COOMASSIE BLUE STAINING

After SDS-PAGE, gels were soaked overnight in Coomassie blue staining solution (Section 2.3.1). Gels were then destained with 5-6 washes in destaining solution (Section 2.3.1) and subsequently dried between two sheets of cellophane with GelAir Dryer (Biorad).

2.19 SILVER STAINING

Silver staining was performed as described (Shevchenko et al., 1996). After electrophoresis, gels were fixed overnight in 100 ml 40% (v/v) ethanol and 10% (v/v) acetic acid. Gels were then soaked for 10 minutes in 100 ml 50% (v/v) methanol and for 10 minutes in 100 ml ddH_2O. Gels were sensitised by 1 minute incubation in 100 ml 0.02% (w/v) sodium thiosulfate and, after 2 washes with ddH_2O, were incubated in 50 ml 0.1 % (w/v) silver nitrate for 20 minutes at 4°C. Gels were subsequently rinsed in ddH_2O and developed in 50 ml developing solution (Section 2.3.1). Incubation was continued until the bands had reached the desired intensity. After discarding the developing solution, gels were stored in 1% (v/v) acetic acid at 4°C until they were dried between two sheets of cellophane with GelAir Dryer.

2.20 GENERATION OF MONOCLONAL AND POLYCLONAL ANTIBODIES

a) *Mouse Monoclonal Antibodies*

Recombinant HISMUS81 and HISEME1 were purified under denaturing conditions from *E. coli* (Sections 2.27 and 2.29). Four protein aliquots (50 μg each) were diluted to 300 μl with PBS to immunise mice (two per antigen). Mice test bleeds received after 3 months were assayed by western blotting (Section 2.22) on HISMUS81 or HISEME1 and on HeLa extract. Spleen tissue was then removed from mice showing positive by western blotting, and hybridoma cells were generated from single antibody producing cells. The hybridomas were then screened by western blotting on HISMUS81 or HISEME1 and on HeLa

extract, positive clones were expanded, and antibodies were purified using affinity chromatography. Anti-MUS81 antibody was designated MTA30 2G10 and anti-EME1 antibody MTA31 7H2.

b) Rabbit Polyclonal Antibodies

Synthetic peptides for EME2 (amino acids 271-290) and HIP (amino acids 16-34) were generated. Peptides (1 mg) were cross-linked to 2 mg of Imject Maleimide Activated KeyHole Limpet Hemocyanin (KLH; Section 2.2) for 4 hours at room temperature. Conjugated peptides-KLH were dialysed against 83 mM sodium phosphate pH 7.0 and 450 mM NaCl for 1 hour at 4°C, aliquoted (200 μg for the first aliquot, 100 μg for 5 aliquots), and injected into a single rabbit. Test bleeds were assayed by western blotting against HISEME2 or HISHIP, and against HeLa extract. The final bleed was then used as a stock antibody. Anti-$EME2_{271-290}$ antibody was designated SWE57 and anti-HIP_{16-34} SWE92.

Recombinant HISHIP and GSTHEF$_{1727-2048}$ were purified from *E. coli* (Sections 2.34 and 2.35, respectively). Six aliquots of 300 μg HISHIP or GSTHEF$_{1727-2048}$ were used to immunise one rabbit. The final bleed was used as stock antibody. Anti-GSTHEF$_{1727-2048}$ and anti-HISHIP antibodies were designated SWE98 and SWE94, respectively.

2.21 PURIFICATION OF POLYCLONAL ANTIBODIES

SWE57 anti-EME2 polyclonal antibody was purified using SulfoLink kit (Section 2.2). EME2 peptide (amino acids 271-290; 5 mg) was dissolved in SulfoLink coupling buffer (Section 2.3.1). Peptide solution was added to a pre-packed column containing SulfoLink resin that immobilises any peptide containing cystein sulfhydryl groups (-SH). The column was then sealed and rotated overnight at 4°C. EME2 peptide was then dripped through the column followed by 8 ml wash with coupling buffer and L-cysteine (15.8 mg) to block non-specific binding to the resin. After adding 12 ml of SulfoLink wash buffer (Section 2.3.1), 15 ml of SWE57 serum was loaded on the column. The flow-through was

reloaded to the column 2 more times. The remaining flow-through (5 ml) was mixed with SulfoLink column resin overnight and applied to the column followed by 12 ml wash with coupling buffer. Bound antibody was eluted from the resin with 8 x 1 ml fractions of ImmunoPure gentle Ag/Ab elution buffer (Section 2.2). Fractions with highest OD_{280} readings were stored at –20°C and used for western blotting.

2.22 WESTERN BLOTTING

Protein samples were subjected to SDS-PAGE as described in Section 2.7 and transferred onto BA85 cellulose-nitrate membrane in transfer buffer (Section 2.3.1) at 100 V for 2 hours. Membranes were then incubated in blocking buffer for 30 minutes, followed by the addition of primary antibody diluted in blocking buffer. Primary antibodies used were: mouse monoclonal anti-MUS81 MTA30 2G10 (1:1000), anti-EME1 MTA31 7H2 (1:1000) and anti-FLAG (1:1000; Section 2.2) or rabbit polyclonal purified anti-EME2 SWE57 (1:500), anti-HIP SWE92 and SWE94 (1:500), anti-GSTHEF$_{1727-2048}$ SWE98 (1:500), anti-GST (1:1000) and anti-ERCC1 FL-297 (1:1000; Section 2.2). The anti-GST antibody was a gift of Tim Hunt. Incubation with the primary antibody was continued overnight and then membranes were washed 3 times with 0.05% Tween and PBS. Peroxidase-conjugated goat anti-mouse (for MTA30, MTA31 and anti-FLAG) or swine anti-rabbit (for purified SWE57, SWE92, SWE93, SWE98 and anti-GST) secondary antibody was then diluted 1:5000 in blocking buffer. After one hour incubation with secondary antibody, the blots were washed three times with 0.05% Tween and PBS. Following application of ECL western blotting detection reagents (Section 2.2) membranes were exposed to X-Omat film (Section 2.2) for 1 to 10 minutes.

V. BACULOVIRUS AND INSECT CELLS

2.23 BACULOVIRUS PRODUCTION

E. coli DH10BAC cells (Section 2.4) were transformed with pDEST8-10HISHEF, pDEST8-10HISHEFFLAG, pDEST8-10HISHEFSTREP or pFAST-BAC-DUAL-10HISHEF FLAG/HIP (Section 2.6). Recombinant bacmids were generated by transposing a DNA fragment flanked by Transposon 7 (Tn7) sites (containing 10HISHEF, 10HISHEFFLAG, 10HISHEFSTREP or 10HISHEFFLAG/HIP) into the mini Tn7 attachment sites of the bacmid DNA. Clones were grown on LB plates with kanamycin (50 μg/ml), tetracycline (10 μg/ml), gentamicin (7 μg/ml), IPTG (40 μg/ml) and X-gal (100 μg/ml). Successful transposition generated white colonies (due to the disruption of the *lacZ* gene in the bacmid DNA). DNA extracted from white colonies was amplified with one DNA primer annealing to the bacmid DNA and one to the *HEF* gene in order to verify the recombination of 10HISHEF, 10HISHEFFLAG, 10HISHEFSTREP or 10HISHEFFLAG/HIP into the bacmid DNA.

2.24 TRANSFECTION OF INSECT CELLS

Spodoptera frugiperda Sf9 cells were grown on 6 well plates (1 x 10^6 cells per well) with complete insect cell medium (Section 2.3.1). Bacmid DNA for 10HISHEF, 10HISHEFFLAG, 10HISHEFSTREP or 10HISHEFFLAG/HIP (5 μg) and lipid reagent Cellfectin (6 μl; Section 2.2) were diluted separately in 100 μl of insect cell medium without serum. The 2 solutions were mixed and left 20 minutes at room temperature. The transfection solution, containing bacmid DNA and Cellfectin, was then added to Sf9 cells incubated in medium without serum. After 6 hours 2 ml of medium with serum were added. Cell medium containing baculovirus particles released from the insect cells was collected after 5 days (P1 viral stock).

2.25 AMPLIFICATION OF BACULOVIRUS

P1 stock (0.5 ml, approximately 1 x 10^6 plaque forming units or pfu) was used to infect a medium flask containing 20 ml of Sf9 cells (1 x 10^6 cells/ml). The

medium was then collected after 7 days (P2 viral stock). P2 stock (2 ml) was amplified by infecting a large flask containing 100 ml of Sf9 cells (1 x 10^6 cells/ml) and the medium was collected after 7 days (P3 viral stock). P3 stock was tested for protein expression by western blotting using antibodies raised against HEF and the FLAG tag (for 10HISHEF, 10HISHEFFLAG and 10HISHEFSTREP).

VI. PROTEIN PURIFICATION

2.26 PURIFICATION OF HISMUS81

pDEST17-HISMUS81 (Section 2.6) was grown at 30°C in *E. coli* BL21-CodonPlus (DE3)-PR in LB medium supplemented of ampicillin (50 μg/ml) to an OD_{600} = 1, and expression was induced by addition of 10 μM IPTG. Growth was then continued for a further 3 hours. Cultures (1 litre) were collected by centrifugation and the pellet was resuspended in 50 ml of phosphate buffer (Section 2.3.1) containing 0.1 M NaCl and 1 tablet of complete EDTA-free protease inhibitor cocktail (Section 2.2). The cells were then lysed using a French press. The mixture was centrifuged for 1 hour at 35,000 rpm in a Beckman 45 Ti rotor, and the clear supernatant was loaded on a 5 ml phosphocellulose column equilibrated with the same buffer. Proteins were eluted using a 50 ml gradient of phosphate buffer containing 0.1 – 1.0 M NaCl and identified by SDS-PAGE. Peak fractions of HISMUS81 were pooled (approximately 40 ml) and mixed with 0.5 ml of Talon metal affinity resin (Section 2.2). After 2 hours at 4°C, the beads were washed with 5 ml of phosphate buffer containing 0.5 M NaCl and 25 mM imidazole. Bound proteins were then eluted with 4 x 0.5 ml washes with the same buffer containing 0.5 M imidazole. Eluted proteins were identified by SDS-PAGE, pooled and dialysed for 2 hours against 4 litres of storage buffer (Section 2.3.1) and frozen in 25 μl aliquots at –80°C. The final HISMUS81 yield was 210 μg.

2.27 PURIFICATION OF DENATURED HISMUS81

pDEST17-HISMUS81 (Section 2.6) was grown at 37°C in *E. coli* BL21-CodonPlus (DE3)-PR to an OD_{600} = 0.6, and expression was induced by addition of 1 mM IPTG. Growth was then continued for a further 4 hours. Cultures (1 litre) were collected by centrifugation and resuspended in 20 ml of denaturing lysis buffer (Section 2.3.1). The cell lysate was sonicated 3 x 30 seconds using a Soniprep 150 sonicator (Jencons) and then stirred at room temperature for 4 hours. After centrifugation for 1 hour at 35,000 rpm in a Beckman 70 Ti rotor, the cleared supernatant was collected and incubated with Talon metal affinity resin (1 ml) for 2 hours at room temperature. Bound HISMUS81 was eluted with SDS sample buffer and run on a single well 10% SDS-PAGE gel for 2 hours at 150 V in a Cambridge apparatus. Strips corresponding to both ends of the gel were cut and stained with Coomassie blue to visualise HISMUS81. After destaining, the strips were aligned to the unstained gel and the portion of the unstained gel matching with the position of HISMUS81 was cut into small pieces. HISMUS81 was then electro-eluted from the gel into a Snakeskin dialysis bag (Section 2.2) for 2 hours at 100 V in SDS gel running buffer with the addition of transfer buffer (0.5x). Eluted HISMUS81 was divided in 50 μg aliquots and used for mice immunisation (Section 2.20).

2.28 PURIFICATION OF HISEME1

pDEST17-HISEME1 (Section 2.6) was grown at 30°C in *E. coli* BL21-CodonPlus (DE3)-PR in LB medium supplemented of ampicillin (50 μg/ml) to an OD_{600} = 1, and expression was induced by addition of 10 μM IPTG. Purification of HISEME1 was performed according to the protocol described in Section 2.26 for HISMUS81. The final HISEME1 yield was 130 μg.

2.29 PURIFICATION OF DENATURED HISEME1

pDEST17-HISEME1 (Section 2.6) was grown at 37°C in *E. coli* BL21-CodonPlus (DE3)-PR to an OD_{600} = 0.6, and expression was induced by addition of 1 mM IPTG. Growth was then continued for a further 4 hours. Purification of HISEME1

was performed according to the protocol described in Section 2.27 for HISMUS81. Electro-eluted HISEME1 was divided in 50 μg aliquots and used for mice imunisation (Section 2.20).

2.30 PURIFICATION OF GSTMUS81

E. coli BL21-CodonPlus (DE3)-PR carrying pDEST15-GSTMUS81 (Section 2.6; 1 litre) were grown at 30°C to an an OD_{600} = 1 and induced with 10 μM IPTG for 3 hours. Cell pellets were resuspended in 50 ml of phosphate buffer (Section 2.3.1) containing 0.1 M NaCl, 1 tablet of complete EDTA-free protease inhibitor cocktail and 1 mM DTT and lysed using a French press. Following high speed centrifugation, as described in Section 2.26, the supernatant was loaded on a 5 ml phosphocellulose column and eluted using a 50 ml 0.1 – 1.0 M NaCl gradient in the same buffer. Peak fractions were identified by SDS-PAGE, pooled, and incubated with 0.5 ml of GST-sepharose 4 Fast Flow beads (Section 2.2) for 2 hours at 4°C. The beads were washed with 5 ml of phosphate buffer containing 0.3 M NaCl, and 1 mM DTT, and bound proteins were eluted with 4 washes of 0.5 ml of the same buffer containing 20 mM glutathione. Proteins were identified by SDS-PAGE, pooled and dialysed for 2 hours against 4 litres of storage buffer and frozen in 25 μl aliquots at –80°C. The final yield of GSTMUS81was 260 μg.

2.31 PURIFICATION OF MUS81/HISEME1

E. coli BL21-CodonPlus (DE3)-PR carrying pET21d-MUS81/HISEME1 (Section 2.6; 4 litres) were grown at 30°C to an an OD_{600} = 1 and induced with 10 μM IPTG for 3 hours. Cell pellet was resuspended in 100 ml of phosphate buffer (Section 2.3.1) containing 0.5 M NaCl and 2 tablets of complete EDTA-free protease inhibitor cocktail and lysed using a French press. After high speed centrifugation, the supernatant was loaded on a 10 ml phosphocellulose column and eluted using 100 ml 0.5 – 1.5 M NaCl gradient in the same buffer. Peak fractions were supplemented with 1.5 ml of Talon metal affinity resin and incubated for 2 hours at 4°C. The beads were then washed with 10 ml of phosphate buffer containing 50 mM imidazole and eluted with 4 x 1.5 ml of buffer containing 0.5 M imidazole. Proteins were identified by SDS-PAGE,

pooled and dialysed for 2 hours against 4 litres of storage buffer and frozen in 25 µl aliquots at –80 °C. The final yield of MUS81/HISEME1 was 215 µg.

2.32 PURIFICATION OF MUS81/HISEME2

E. coli BL21-CodonPlus (DE3)-PR carrying pET21d-MUS81/HISEME2 (Section 2.6; 4 litres) were grown at 30°C to an an OD_{600} = 1 and induced with 10 µM IPTG for 3 hours. Purification of MUS81/HISEME2 was performed according to the protocol described for MUS81/HISEME1 in Section 2.31. The final yield of MUS81/HISEME2 was 175 µg.

2.33 PURIFICATION OF HISHIP

E. coli BL21-CodonPlus (DE3)-RIL carrying pET28-HISHIP (Section 2.6) were grown at 30°C to an OD_{600} = 0.6 and were induced with 1 mM IPTG for 5 hours. The cell pellet (1 litre) was lysed in 10 ml Nickel buffer (Section 2.3.1) with the addition of 5 mM imidazole and 1/2 tablet of complete EDTA-free protease inhibitor cocktail. Cell lysate was supplemented with 1 ml of BugBuster (10x; Section 2.2) and 100mg of lysozyme. The mixture was incubated at 4°C for 3 hours under constant agitation and then centrifuged for 1 hour at 35,000 rpm in a Beckman 70.1 Ti rotor. The clear supernatant was loaded onto a 1 ml HiTrap chelating column (Section 2.2) pre-charged with 0.1 M $NiSO_4$. After 20 column volumes (CV) wash with Nickel buffer containing 50 mM imidazole, the bound protein was eluted with 20 x 1 ml fractions of Nickel buffer containing 0.05 M – 1 M imidazole gradient. Peak fractions of HISHIP were then pooled, diluted 1:10 in Heparin buffer (Section 2.3.1) containing 100 mM KCl and were loaded onto a 1ml HiTrap Heparin column (Section 2.2). The column was washed with 20 CV of Heparin buffer with 200 mM KCl and HISHIP was eluted with 15 ml of Heparin buffer containing 1 M KCl. Eluted protein was identified by SDS-PAGE, pooled, dialysed for 2 hours against 4 litres of Heparin buffer with 200 mM KCl and frozen in 250 µl aliquots at –80°C. The final yield of HISHIP was 1.5 mg.

2.34 PURIFICATION OF DENATURED HISHIP

E. coli BL21-CodonPlus (DE3)-RIL carrying pET28-HISHIP (1 litre) were grown

at 30°C to an OD_{600} = 0.6 and were induced with 1 mM IPTG for 5 hours. Cell pellet was lysed and clear supernatant was subjected to Nickel chromatography as indicated in Section 2.33. Peak fractions containing HISHIP were pooled and run on a single well 10% SDS-PAGE gel for 2 hours at 150 V in a Cambridge apparatus. HISHIP was then cut from the gel as described for HISMUS81 (Section 2.27). Electro-elution was performed overnight using a Biotrap apparatus at 100 V in SDS gel running buffer with the addition of transfer buffer (0.5x). Eluted HISHIP was divided in 300 µg aliquots and used for rabbit immunisation (Section 2.20).

2.35 PURIFICATION OF DENATURED GSTHEF$_{1727-2048}$

E. coli BL21-CodonPlus (DE3)-RIL carrying pGex-GSTHEF$_{1727-2048}$/HISHIP (Section 2.6) were grown at 37°C to an OD_{600} = 0.6 and induced with 50 µM IPTG for 4 hours. For this experiment, the pGex-GSTHEF$_{1727-2048}$/HISHIP plasmid was preferred to pGex-GSTHEF$_{1727-2048}$ because of the higher solubility of GSTHEF$_{1727-2048}$ when in complex with HISHIP. The cell pellet (1 litre) was lysed in 20 ml GST buffer (Section 2.3.1) supplemented with 1 tablet of complete EDTA-free protease inhibitor cocktail, 2 ml of 10x BugBuster and 200 mg of lysozyme. The mixture was incubated at 4°C for 2 hours under agitation and centrifuged 1 hour at 35,000 rpm in a Beckman 70 Ti rotor. The clear supernatant was mixed with 0.5 ml of GST-sepharose 4 Fast Flow beads for 2 hours at 4°C. Bound proteins were eluted with SDS sample buffer and were run on a single well 10% SDS-PAGE gel for 2 hours at 150 V in a Cambridge apparatus. GSTHEF$_{1727-2048}$ was then cut from the gel as described for HISMUS81 (Section 2.27). Electro-elution was performed as indicated for HISHIP in Section 2.34. The eluted GSTHEF$_{1727-2048}$ was divided in 300 µg aliquots and used for rabbit immunisation (Section 2.20).

2.36 PURIFICATION OF 10HISHEFFLAG

High Five cells (2 litres) were infected with 100 ml 10HISHEFFLAG P3 viral stock (Section 2.25). High Five cells were preferred to Sf9 cells because of a higher

expression level of 10HISHEFFLAG. After 2 days of infection, cells were harvested and the cell pellet was resuspended in 6 ml of FLAG buffer (Section 2.3.1) supplemented with 1 tablet of complete EDTA free protease inhibitor cocktail. Cells were kept in ice for 10 minutes, and 6 ml of FLAG buffer containing 500 mM KCl was added (the final KCl concentration was 250 mM). The cell mixture was then lysed with an "A" pestel (40 strokes) and sonicated 2 x 30 seconds using a Soniprep 150 sonicator. The whole cell extract was centrifuged for 1 hour at 35,000 rpm in a Beckman 70 Ti rotor. The supernatant was collected and the pellet resuspended in 20 ml of FLAG buffer containing 500 mM KCl (supplemented with 1 tablet of complete EDTA-free protease inhibitor cocktail) to extract proteins bound to chromatin. Chromatin extraction was performed at 4°C for 1 hour under constant agitation. After centrifugation, the supernatant from the chromatin extract was collected and pooled with the supernatant from the whole cell extract (the final KCl concentration in the extract was approximately 300 mM). Anti-FLAG M2 Affinity Gel Resin (750 µl; Section 2.2) was mixed with the pooled supernatant overnight at 4°C. After washing with 5 x 20 ml of FLAG buffer containing 300 mM KCl, proteins were released from beads with 5 x 750 µl elutions of FLAG buffer (without EDTA) supplemented with 0.5 mg/ml FLAG peptide (amino acid sequence DYKDDDDK). Each elution was continued for 1 hour under constant agitation. Peak fractions of 10HISHEFFLAG were pooled and diluted 1:10 in Nickel buffer (Section 2.3.1) containing 5 mM imidazole. Pooled fractions were incubated with Nickel-NTA Agarose (300 µl; Section 2.2) overnight at 4°C and then poured into a Biorad 10 ml disposable column. After 50 CV wash with Nickel buffer containing 30 mM imidazole, bound 10HISHEFFLAG was eluted with 10 x 300 µl of Nickel buffer containing 0.5 M imidazole. Proteins were identified by western blotting against HEF (Section 2.22). Peak fractions were pooled, run on a NuPAGE 4-12% Bis-Tris gradient gel (Section 2.2) and silver stained (Section 2.19).

2.37 PURIFICATION OF 10HISHEFFLAG/HIP

High Five cells (2 litres) were infected with 100 ml 10HISHEFFLAG/HIP P3 viral stock (Section 2.25). Purification of 10HISHEFFLAG/HIP was performed according

to the protocol for the purification of 10HISHEFFLAG (Section 2.36). Proteins were identified by western blotting against HEF and HIP (Section 2.22). Peak fractions were pooled, run on a NuPAGE 4-12% Bis-Tris gradient gel and silver stained (Section 2.19).

2.38 PURIFICATION OF $HEF_{1727-2048}$/HIP

E. coli BL21-CodonPlus (DE3)-PR or *E. coli* STL5827 BL21-(DE3)-ExoI$^-$ EndoI$^-$ carrying pGex-GSTHEF$_{1727-2048}$/HISHIP (Section 2.6) were grown at 30°C to an an OD_{600} = 0.6 and induced with 0.1 mM IPTG for 5 hours. The cell pellet (1 litre) was lysed in 10 ml GST buffer (Section 2.3.1) supplemented with 1/2 tablet of complete EDTA-free protease inhibitor cocktail, 1 ml of 10x BugBuster and 100 mg of lysozyme. The mixture was incubated at 4°C for 2 hours under agitation and centrifuged 1 hour at 35,000 rpm in a Beckman 70 Ti rotor. The clear supernatant was mixed with 0.5 ml of GST-sepharose 4 Fast Flow beads for 2 hours at 4°C. The beads were washed 6 x 10 ml washes with GST buffer and 2 x 10 ml with PBS. Proteins were eluted from the GST beads by the addition of 450 µl of PBS with 50 units of Thrombin (Section 2.2). The cleavage reaction was incubated for 4 hours at 4°C. Two additional elutions were performed as before. Eluted fractions were pooled and injected onto a HiPrep 16/60 Sephracryl S-200 HR gel filtration column (Section 2.2) equilibrated in GST buffer. Following the injection of the pooled fractions (1.5 ml) at 0.5 ml/min, 120 ml (1 CV) of GST buffer were loaded on the column at 0.5 ml/min. The first 40 fractions (2 ml each) were collected. Proteins were identified by SDS-PAGE, pooled and dialysed for 2 hours against 4 litres of storage buffer and frozen in 200 µl aliquots at –80°C. The final protein yield was 120 µg from *E. coli* BL21-CodonPlus (DE3)-PR or 50 µg from *E. coli* STL5827 BL21-(DE3)- EndoI$^-$ ExoI$^-$.

2.39 CO-PRECIPITATION ASSAYS FOR GSTMUS81/HISEME1 AND GSTMUS81/HISEME2

E. coli BL21-CodonPlus (DE3)-PR carrying pGex-GSTMUS81/HISEME1 or pGex-GSTMUS81/HISEME2 (Section 2.6) were grown at 30°C to an an OD_{600} = 1 and

induced with 10 μM IPTG for 3 hours. A cell-free extract (50 ml), prepared in phosphate buffer (Section 2.3.1) containing 0.5 M NaCl, was incubated with 0.5 ml of beads (either GST-sepharose 4 Fast Flow or Talon metal affinity resin) for 2 hours at 4°C and eluted with 4 x 0.5 ml of the same buffer supplemented 20 mM glutathione or 0.5 M imidazole, respectively.

2.40 GST PULL-DOWNS FOR MUS81 FAMILY PROTEINS

E. coli BL21-CodonPlus (DE3)-RIL (100 ml) carrying pGex-GSTXPF$_{606-905}$/HISEME1, pGex-GSTXPF$_{606-905}$/HISEME2, pGex-GSTXPF$_{606-905}$/HISHIP, pGex-GSTXPF$_{606-905}$/HISERCC1, pGex-GSTHEF$_{1727-2048}$/HISEME1, pGex-GSTHEF$_{1727-2048}$/HISEME2, pGex-GSTHEF$_{1727-2048}$/HISHIP, pGex-GSTHEF$_{1727-2048}$/HISERCC1, pGex-GSTMUS81/HISEME1, pGex-GSTMUS81/HISEME2, pGex-GSTMUS81/HISHIP or pGex-GSTMUS81/HISERCC1 (Section 2.6) were grown at 37°C to an OD_{600} = 0.3 and induced with 50 μM IPTG for 7 hours at 25°C. Cell pellets were resuspended in 10 ml GST buffer (Section 2.3.1) supplemented with 1/2 tablet of complete EDTA-free protease inhibitor cocktail, 1 ml of 10x BugBuster and 100 mg of lysozyme. The mixture was incubated for 2 hours at 4°C under agitation and then centrifuged for 30 minutes at 35,000 rpm in a Beckman 70.1 Ti rotor. The supernatant was mixed with 200 μl GST-sepharose 4 Fast Flow beads. After 2 hours at 4°C, the beads were washed with 5 x 10 ml GST buffer, transferred to Eppendorf tubes and washed twice with PBS. The beads (50 μl) were resuspended in SDS sample buffer and aliquots were run on a 10% SDS-PAGE gel to visualise protein complexes. The remaining beads were stored at –20°C.

2.41 MAMMALIAN CELL EXTRACT FRACTIONATION

Mammalian cell extracts were prepared from HeLa S3 cells and were a gift from Yilun Liu (Liu et al., 2004). Peak MonoQ fractions with either 3'-flap or Holliday junction resolution activity were used as positive controls in cleavage assays (Section 2.45). The fraction partially purified from HeLa having Holliday junction resolution activity was designated Resolvase A fraction (due to the presence of

the unidentified Resolvase A (Constantinou et al., 2002)) and the 3'-flap fraction was called MUS81 fraction (because it contains MUS81). The Resolvase A fraction and the MUS81 fraction used in the experiments described in Chapter 3 were a gift from Angelos Constantinou and were purified as described (Constantinou et al., 2002). The Resolvase A fraction and the MUS81 fraction used in the experiments described in Chapters 4 and 5 were a gift from Yilun Liu and were purified as described (Liu et al., 2004).

Small scale cell extracts were prepared from HeLa S3 cells (50 ml at 1 x 10^6 cells/ml). The cell pellet was resuspended in one volume of lysis buffer (Section 2.3.1) in the presence of complete EDTA-free protease inhibitor cocktail, left on ice for 10 min and lysed by the addition of 0.1% NP40. The cell lysate was then vortexed for 30 sec and 0.5 volume of lysis buffer containing 0.5 M KCl was added. After 30 min incubation at 4°C, cell mixture was centrifuged for 10 min at 14,000 rpm. The supernatant was retained and the pellet was resuspended in 2 volumes of lysis buffer containing 0.5 M KCl to extract nuclear proteins. After 1 hour at 4°C under agitation, nuclear extract was centrifuged for 10 min at 14,000 rpm and the supernatant was mixed with whole cell extract supernatant. The pooled supernatant (10 µl) was then used for western blotting using antibodies against EME2, HEF and HIP (Section 2.22).

VII. PREPARATION OF DNA SUBSTRATES AND CLEAVAGE ASSAYS

2.42 GEL PURIFICATION OF OLIGONUCLEOTIDES

Oligonucleotides were purchased from SIGMA-Genosys. The dried pellet was resuspended in TE buffer to give a final concentration of 1 mg/ml. Approximately 100 µg of oligonucleotide was loaded on a 15% polyacrylamide denaturing gel that was run at 400 V for 2 hours. The gel was then stained using Stains-all solution (Section 2.3.2) for 15 minutes and destained in water for 20 minutes. The oligonucleotide bands were excised from the gel, cut in

small pieces, and soaked in 1 ml of TE buffer overnight. After spinning down the gel particles, the supernatant was removed and ethanol precipitated (Section 2.15). The DNA pellet was resuspended in 100 µl of TE buffer and the oligonucleotide concentration was determined by spectrophotometry (Section 2.13).

2.43 5'-^{32}P-END LABELLING OF OLIGONUCLEOTIDES

Reactions contained 200 ng oligonucleotide, 20 µCi [γ-^{32}P] ATP and 10 units of T4 polynucleotide kinase in NEB T4 polynucleotide kinase buffer. After incubation for 45 minutes at 37°C, reactions were stopped by the addition of EDTA to 25 mM.

2.44 OLIGONUCLEOTIDE SUBSTRATE PREPARATION

Labelled oligonucleotides were boiled and annealed overnight with appropriate combinations of unlabelled oligonucleotides to generate the DNA substrates required (Table 2.3) for the biochemical assays. Annealed substrates were run on 10% polyacrylamide gels for 2 hours at 200 V. The gels were exposed to Biomax MR film and the ^{32}P-labelled DNA bands were cut from the gel. The substrates were electro-eluted from the gel at 100 V for 2 hours using a Biotrap apparatus (Schleicher & Schuell). The eluted DNA substrates were dialysed for 2 hours against TNM buffer (Section 2.3.2), divided in 50 µl aliquots and stored at –20°C.

2.45 CLEAVAGE ASSAY

Reactions (20 µl) contained 5'-^{32}P-labelled substrate (approximately 3 ng) in cleavage buffer (Section 2.3.3). Reactions were initiated by the addition of various concentrations of human HISMUS81, HISEME1, MUS81/HISEME1, MUS81/HISEME2 or $HEF_{1727-2048}$/HIP. Murine HAEME1 or FLAGMUS81/HAEME1 were also tested for activity. Following incubation for 30 minutes at 37°C, the cleavage reactions were stopped and samples deproteinized by 15 min

incubation in the presence of stop buffer (5x; Section 2.3.3). In time course experiments, reactions started by MUS81/HISEME1 or MUS81/HISEME2 were stopped and deproteinised after 3 min, 10 min or 30 min. Labelled DNA products were analysed by electrophoresis through 10% neutral polyacrylamide gels followed by autoradiography (Section 2.11).

In order to visualise the cleavage pattern produced by MUS81/HISEME1 and MUS81/HISEME2, cleavage reactions were performed in 10 µl volume. Aliquots (5 µl) were resuspendend in formamide loading buffer (Section 2.3.2) and analysed by denaturing PAGE (Section 2.10) followed by autoradiography (Section 2.11).

SUBSTRATE	OLIGONUCLEOTIDES
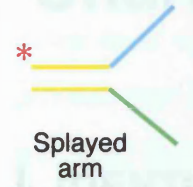 Splayed arm	(XO1) 5'GACGCTGCCGAATTCTACCAGTGCCTTGCTAGGACATCTTTGCCCACCTGCAGGTTCACCC3' (XO4) 5'ATCGATAGTCGGATCCTCTAGACAGCTCCATGTAGCAAGGCACTGGTAGAATTCGGCAGCGT3'
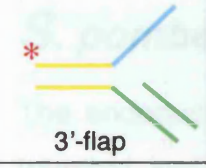 3'-flap	(XO1) 5'GACGCTGCCGAATTCTACCAGTGCCTTGCTAGGACATCTTTGCCCACCTGCAGGTTCACCC3' (XO3.1/2) 5'CATGGAGCTGTCTAGAGGATCCGACTATCGA3' (XO4) 5'ATCGATAGTCGGATCCTCTAGACAGCTCCATGTAGCAAGGCACTGGTAGAATTCGGCAGCGT3'
 Replication fork	(XO1) 5'GACGCTGCCGAATTCTACCAGTGCCTTGCTAGGACATCTTTGCCCACCTGCAGGTTCACCC3' (XO2.1/2) 5'TGGGTGAACCTGCAGGTGGGCAAAGATGTCC3' (XO3.1/2) 5'CATGGAGCTGTCTAGAGGATCCGACTATCGA3' (XO4) 5'ATCGATAGTCGGATCCTCTAGACAGCTCCATGTAGCAAGGCACTGGTAGAATTCGGCAGCGT3'
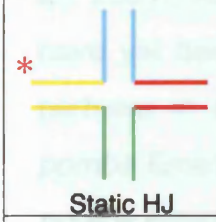 Static HJ	(XO1) 5'GACGCTGCCGAATTCTACCAGTGCCTTGCTAGGACATCTTTGCCCACCTGCAGGTTCACCC3' (XO2) 5'TGGGTGAACCTGCAGGTGGGCAAAGATGTCCATCTGTTGTAATCGTCAAGCTTTATGCCGTT3' (XO3) 5'GAACGGCATAAAGCTTGACGATTACAACAGATCATGGAGCTGTCTAGAGGATCCGACTATCGA3' (XO4) 5'ATCGATAGTCGGATCCTCTAGACAGCTCCATGTAGCAAGGCACTGGTAGAATTCGGCAGCGT3'
 Mobile HJ	(SW315) 5'CCGCTACCAGTGATCAGCAATGGATTGCTAGGACATCTTTGCCCACCTGCAGGTTCACCC3' (SW316) 5'TGGGTGAACCTGCAGGTGGGCAAAGATGTCCTAGCAATCCATTGTCTATGACGTCAAGCT3' (SW317) 5'GAGCTTGACGTCATAGACAATGGATTGCTAGGACATCTTTGCCGTCTTGTCAATATCGGC3' (SW318) 5'TGCCGATATTGACAAGACGGCAAAGATGTCCTAGCAATCCATTGGTGATCACTGGTAGCGG3'

TABLE 2.3: Oligonucleotide sequences of synthetic DNA substrates

Identical colours indicate DNA strands in the substrates and their corresponding sequences. Complementary sequences are highlighted by the same colours. Note that splayed arm, 3'-flap, replication fork and static HJ have oligonucleotides X0.1 and X0.4 in common. ^{32}P label is indicated by an asterisk on each DNA structure.

CHAPTER THREE

Identification and Characterisation of Human EME1

I. IDENTIFICATION OF A HUMAN ORTHOLOGUE OF *S. pombe* EME1

The endonuclease Mus81 was initially identified in yeast (Boddy et al., 2000; Interthal and Heyer, 2000). A human MUS81 orthologue was subsequently found by database searches for human proteins similar to yeast Mus81 (Chen et al., 2001). Yeast Mus81 is active in the presence of a partner protein, called Eme1 in *S. pombe* and Mms4 in *S. cerevisiae* (Boddy et al., 2001; Kaliraman et al., 2001). No human orthologues of *S. pombe* Eme1 and *S. cerevisiae* Mms4 have yet been reported. This could be due to the high divergence of Mus81 partners in eukaryotes, as suggested by the minimal similarity between *S. pombe* Eme1 and *S. cerevisiae* Mms4. As shown in Appendix 1, Figure 1, *S. pombe* Eme1 and *S. cerevisiae* Mms4 share only 15% and 19% of identical and similar residues, respectively.

In order to identify a partner for human MUS81, a search of the National Center for Biotechnology Information (NCBI) database was performed. PSI-BLAST (Position Specific Iterated - Basic Local Alignment Search Tool) software was utilised to identify similarities between proteins. PSI-BLAST searches of the NCBI database to identify a human orthologue of *S. cerevisiae* Mms4 were unsuccessful, but similar attempts to identify a human orthologue of *S. pombe* Eme1 proved to be fruitful. Among the sequences similar to *S. pombe* Eme1, we observed *S. cerevisiae* Mms4 and a *Neurospora crassa* Mms4/Eme1 orthologue (NCBI # CAD21209), as previously reported {Mullen, 2001 #7193; Boddy, 2001 #7592}. Additionally, one human protein was identified which we designated EME1 (NCBI # BC016470). Human EME1 is a weak homologue of

S. pombe Eme1, since it exhibits just 17% identity and 26% similarity to *S. pombe* Eme1 (Figure 3.1) (Ciccia et al., 2003).

Human EME1 is a 583 amino acid protein with a molecular weight of 65 kDa. The *EME1* gene is located on chromosome 17. In the NCBI database there is a second version of the gene (NCBI # AK055926) that encodes a protein that is 13 amino acids shorter (residues 372 to 384 are missing). It is possible that these are two tissue-specific splicing variants, as the long version of *EME1* was cloned from choriocarcinoma cell cDNA whereas the shorter variant was isolated from neuroblastoma cells. *EME1* cloned from HeLa cell cDNA library corresponds to the shorter isoform of EME1 (Blais et al., 2004). A third *EME1* splice variant has been retrieved from the ATCC database. This EME1 isoform is 42 amino acid shorter than the long EME1 splice variant (Blais et al., 2004).

EME1 is conserved among all eukaryotes (Appendix 1, Figure 2): orthologues for human EME1 could be found in *Canis familiaris* (NCBI # XP_548199), *Mus musculus* (NCBI # AAH89459), *Rattus norvegicus* (NCBI # XP_220879), *Gallus gallus* (NCBI #XP_420107), *Danio rerio* (NCBI # XP_707096), *Ustilago maydis* (NCBI # XP_761348) and *Arabidopsis thaliana* (NCBI # AAP21264).

II. INTERACTION OF HUMAN EME1 WITH MUS81

In order to test the possible interaction between human EME1 and MUS81, a bicistronic vector containing *MUS81* and the long isoform of *EME1* was constructed (Figure 3.2). *MUS81* and *EME1* were cloned in the vector pGex-BICIS-HIS (Section 2.6) to co-express GSTMUS81 and HISEME1 in *E. coli* BL21-CodonPlus (DE3)-PR. Following expression of the two proteins, GST-sepharose beads were used in pull-down assays carried out with cell-free extracts containing GSTMUS81 and HISEME1 (Section 2.39). We observed that the GST beads pulled out both GSTMUS81 and HISEME1 (Figure 3.3, lane c), as determined by SDS-PAGE followed by Coomassie blue staining. Similarly,

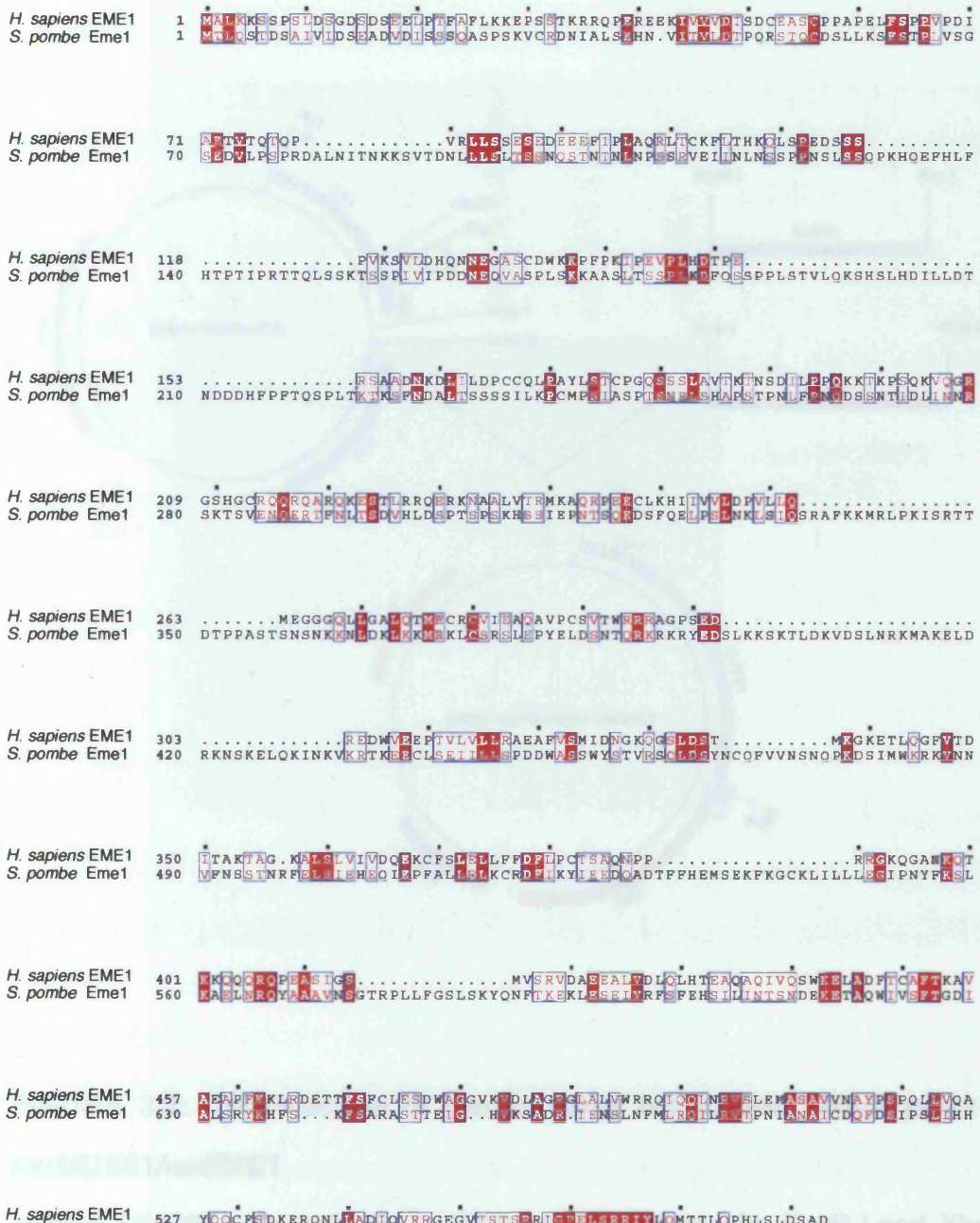

FIGURE 3.1: Sequence alignment between *H. sapiens* EME1 and *S. pombe* Eme1

Identical and similar residues are indicated in filled and unfilled red boxes, respectively. Sequence alignments were carried out using ClustalW.

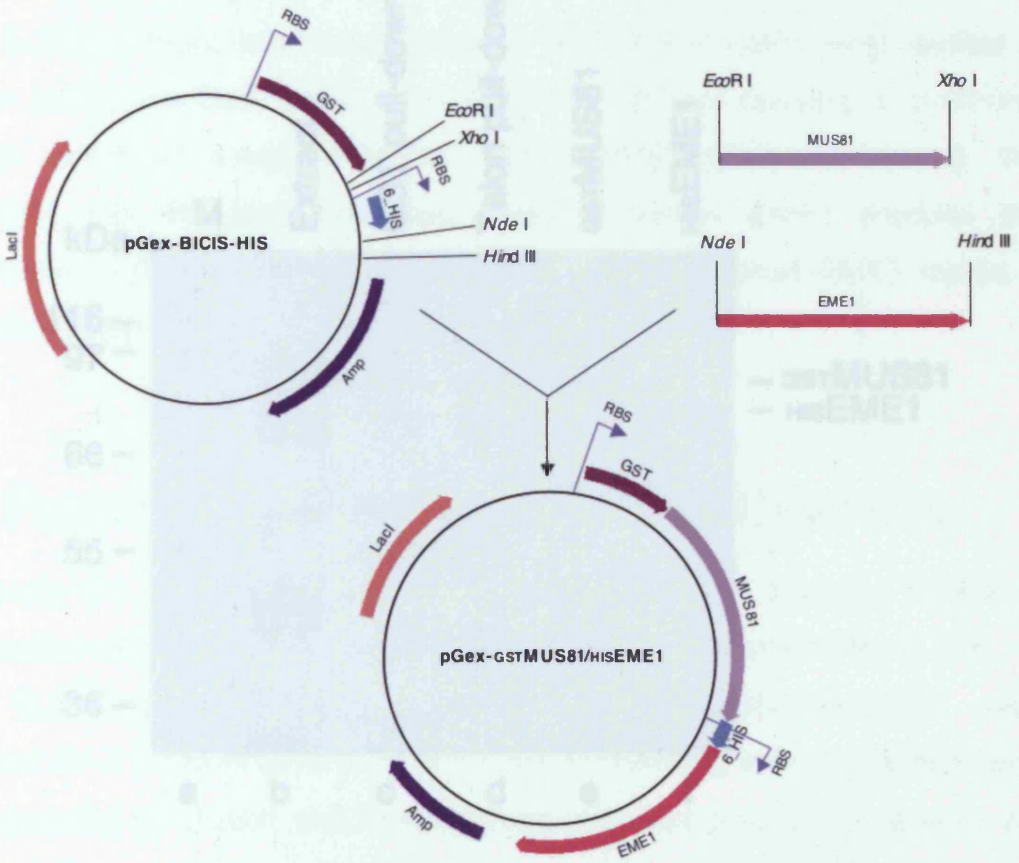

FIGURE 3.2: Construction of the bacterial bicistronic vector pGex-GSTMUS81/HISEME1

Human *MUS81* was amplified by PCR and cloned into the *Eco*R I and *Xho* I sites of pGex-BICIS-HIS (Section 2.6). Human *EME1* was cloned by PCR and inserted into the *Nde* I and *Hin*d III sites of a pGex-BICIS-HIS containing *MUS81*. *MUS81* is represented by a violet arrow, *EME1* by a red arrow. GST tag (GST), 6HIS tag (6HIS), ribosomal binding sites (RBS), Ampicillin resistance (Amp) and *LacI* repressor gene (LacI) are indicated.

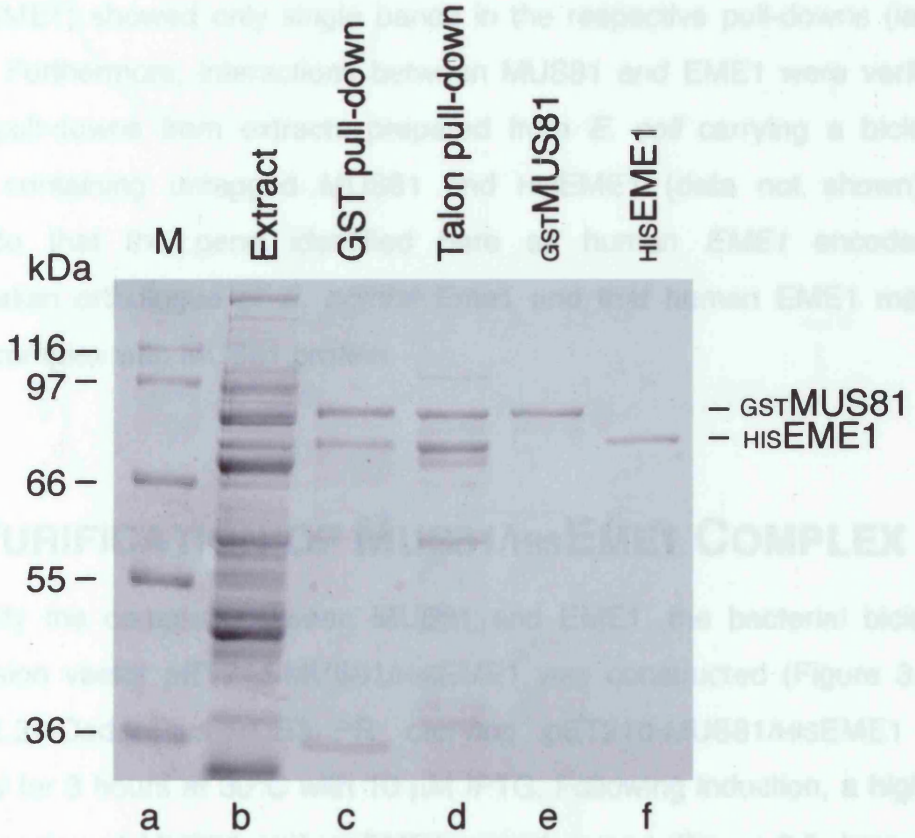

FIGURE 3.3: Interaction of human MUS81 with EME1

Cell-free extracts were prepared from *E. coli* carrying the bicistronic vector pGex-GSTMUS81/HISEME1 (lane b; Section 2.6), and pull-down assays were carried out using GST-sepharose (lane c) or Talon (lane d) beads. Marker proteins GSTMUS81 (lane e) and HISEME1 (lane f) were purified as described in Sections 2.30 and 2.28, respectively. Proteins were separated by 10% SDS-PAGE and the gel was stained with Coomassie blue.

incubation of histidine-binding Talon beads with the extract led to the co-precipitation of both GSTMUS81 and HISEME1 (lane d). As expected, extracts prepared from *E. coli* expressing only one of the two proteins (either GSTMUS81 or HISEME1) showed only single bands in the respective pull-downs (lanes e and f). Furthermore, interactions between MUS81 and EME1 were verified in Talon pull-downs from extracts prepared from *E. coli* carrying a bicistronic vector containing untagged MUS81 and HISEME1 (data not shown). We conclude that the gene identified here as human *EME1* encodes the mammalian orthologue of *S. pombe* Eme1 and that human EME1 makes a stable complex with MUS81 protein.

III. PURIFICATION OF MUS81/HISEME1 COMPLEX

To purify the complex between MUS81 and EME1, the bacterial bicistronic expression vector pET21d-MUS81/HISEME1 was constructed (Figure 3.4). *E. coli* BL21-CodonPlus (DE3)-PR carrying pET21d-MUS81/HISEME1 were induced for 3 hours at 30°C with 10 μM IPTG. Following induction, a high level of expression of MUS81 and HISEME1 was observed (Figure 3.5, lane c), but most of the over-expressed protein was found to be insoluble and precipitated during high-speed centrifugation. The clear supernatant (lane d) was loaded on a 10 ml phosphocellulose column and MUS81/HISEME1 complex was eluted with 0.5 – 1.5 M NaCl gradient. Peak fractions for MUS81/HISEME1 were pooled (lane e) and mixed with 1.5 ml of Talon beads for 2 hours at 4°C. The complex was then eluted from the beads with 0.5 M imidazole (lane f), dialysed and stored in aliquots at –80°C.

IV. SUBSTRATE SPECIFICITY OF HUMAN MUS81/HISEME1 COMPLEX

As previously reported, recombinant *S. cerevisiae* Mus81/Mms4 and *S. pombe*

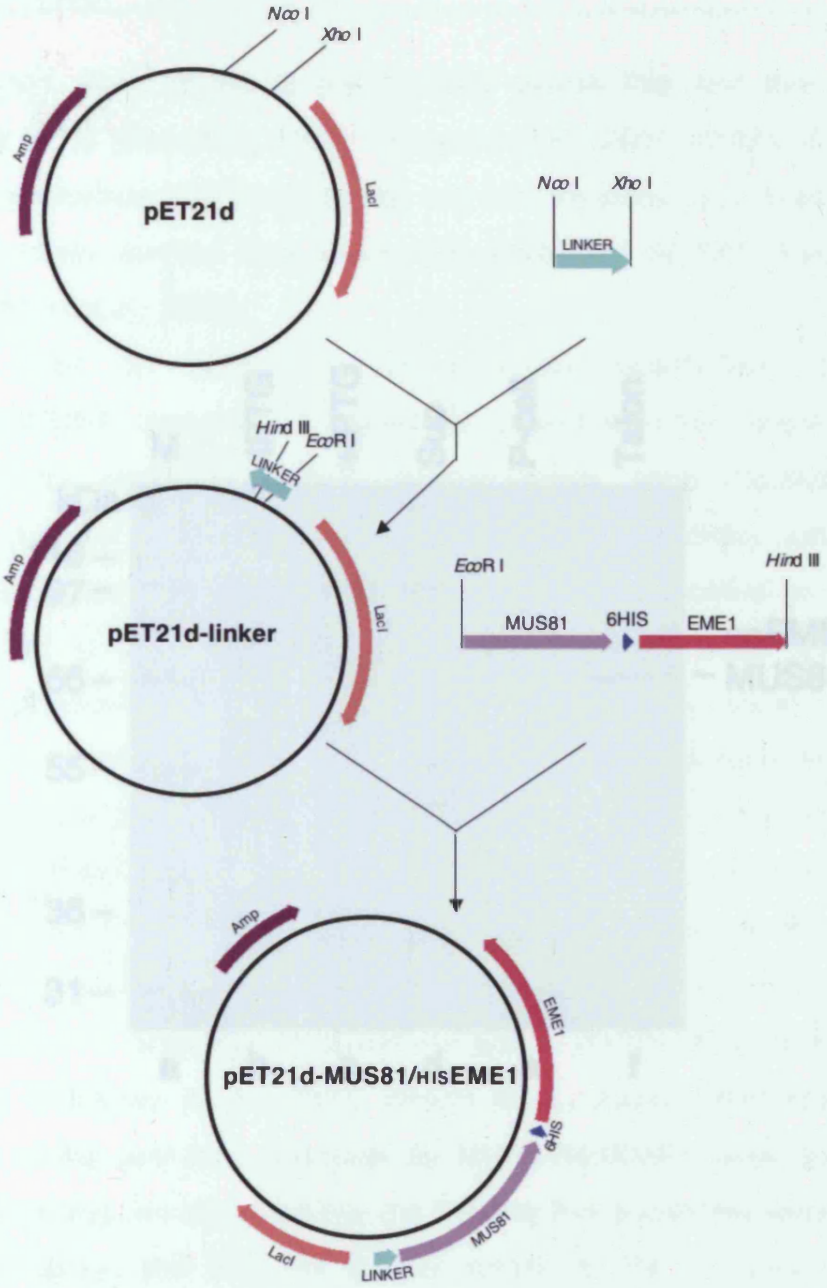

FIGURE 3.4: Construction of the bacterial bicistronic vector pET21d-MUS81/HISEME1

A linker containing *Eco*R I and *Hin*d III sites was inserted into the *Nco* I and *Xho* I sites of pET21d (Section 2.6). An *Eco*R I-*Hin*d III fragment encoding MUS81/HISEME1 was cloned from pGEX-GSTMUS81/HISEME1 into the *Eco*R I and *Hin*d III sites of pET21d-linker. *MUS81* is represented by a violet arrow, *EME1* by a red arrow. 6HIS tag (6HIS), linker, Ampicillin resistance (Amp) and *LacI* repressor gene (LacI) are indicated.

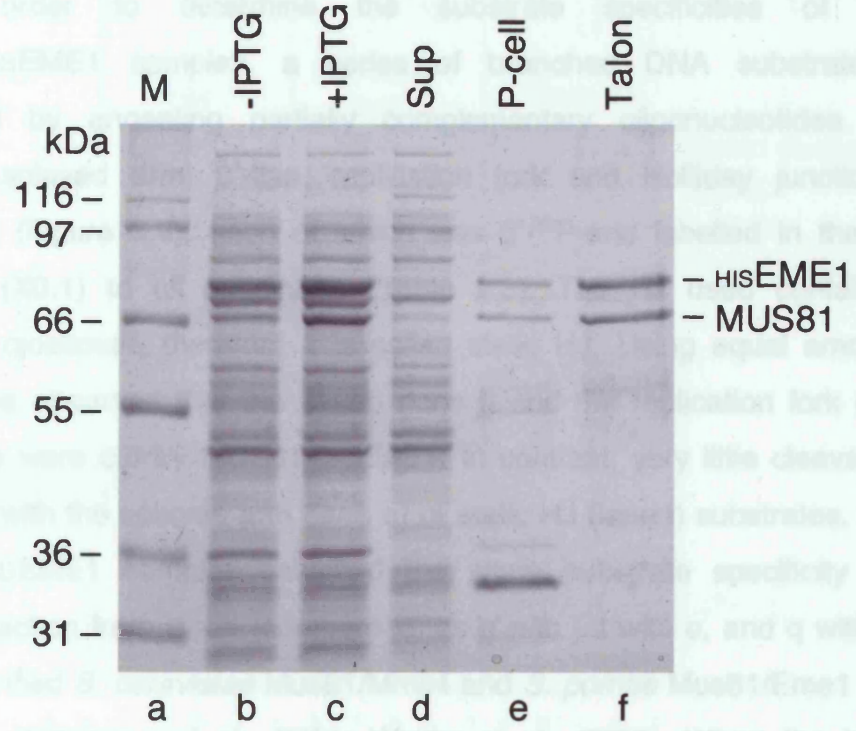

FIGURE 3.5: Purification of MUS81/HISEME1 complex

MUS81/HISEME1 was purified following over-expression in *E. coli* cells carrying pET21d-MUS81/HISEME1 (Section 2.31). Lane a, marker proteins; lanes b and c, total cellular proteins before and after 3 hours induction with IPTG; lane d, supernatant (Sup) after high-speed spin; lanes e and f, fractions eluted from phosphocellulose and Talon beads. Proteins were analysed by 10% SDS-PAGE and visualised by Coomassie blue staining.

Mus81/Eme1 were shown to preferentially cleave flap and fork structures compared to HJ (Doe et al., 2002; Kaliraman et al., 2001; Whitby et al., 2003). The same substrate specificity for flap and fork structures was described for a fraction partially purified from HeLa cells containing MUS81 (Section 2.41) (Constantinou et al., 2002).

In order to determine the substrate specificities of human MUS81/HISEME1 complex, a series of branched DNA substrates was generated by annealing partially complementary oligonucleotides. These included splayed arm, 3'-flap, replication fork and Holliday junction (HJ) structures (Figure 3.6), each of which was 5'-^{32}P-end labelled in the strand common (X0.1) to all substrates (Table 2.3). The HJ used contained an immobile crossover, therefore it is called static HJ. Using equal amounts of protein, we observed that the 3'-flap (lane j) and the replication fork (lane o) substrates were cut by MUS81/HISEME1. In contrast, very little cleavage was observed with the splayed arm (lane e) or static HJ (lane t) substrates. Purified MUS81/HISEME1 complex exhibited the same substrate specificity as the MUS81 fraction from HeLa (compare lanes g with j, l with o, and q with t) and that of purified *S. cerevisiae* Mus81/Mms4 and *S. pombe* Mus81/Eme1 (Doe et al., 2002; Kaliraman et al., 2001; Whitby et al., 2003). When the levels of cleavage of flap and fork structures by MUS81/HISEME1 were quantified by phosphorimaging, we observed that the flap and fork substrates were cut with a similar efficiency, and that the specific activity of the nuclease with these substrates was approximately 75x greater than that observed with the synthetic HJ (Figure 3.7).

Whereas purified MUS81/HISEME1 exhibited flap and fork endonuclease activity, neither HISEME1 (Figure 3.6, lanes c, h, m and r) nor HISMUS81 (lanes d, i, n and s) alone exhibited nuclease activity. We conclude that human MUS81/EME1, like its yeast orthologues, is functional as a heterodimer. To date, attempts to reconstitute nuclease activity by mixing separately purified recombinant HISEME1 and HISMUS81 subunits have not been successful (data not shown).

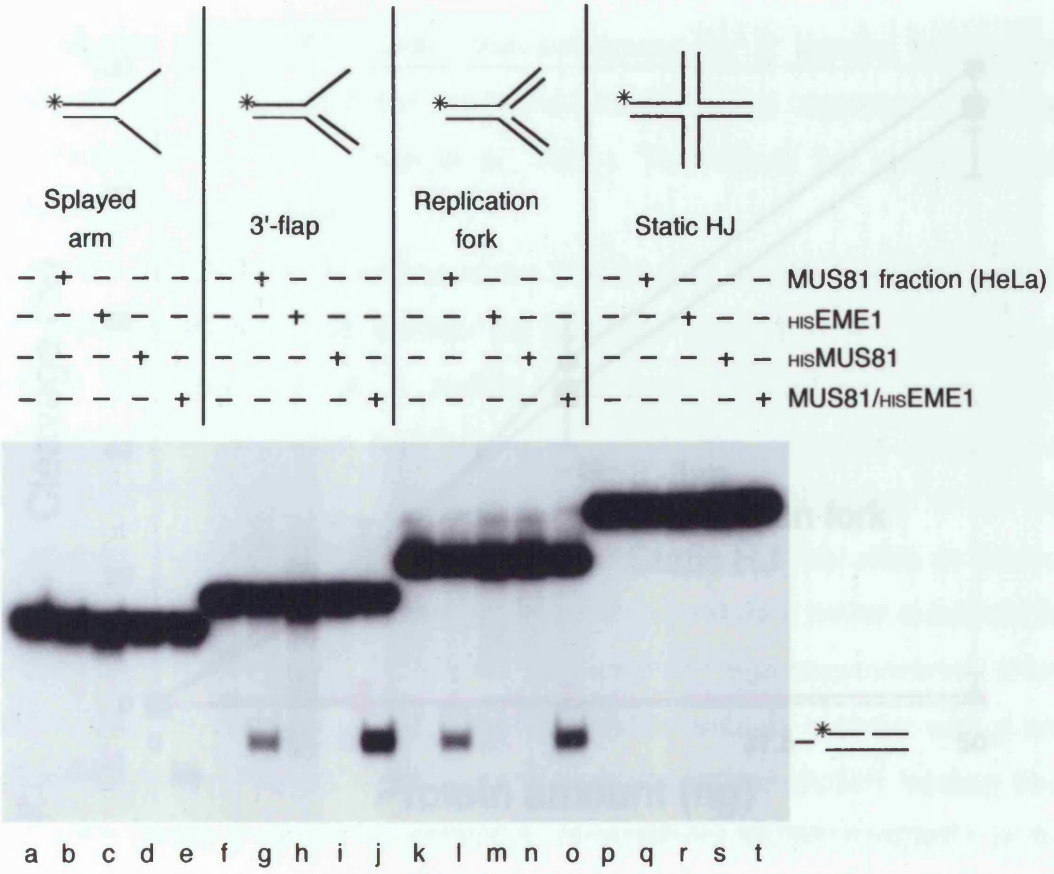

FIGURE 3.6: Substrate specificity of human MUS81/HISEME1 endonuclease

Reactions contained the indicated ^{32}P-labelled substrates (approx 3 ng) and purified HISEME1 (15 ng), HISMUS81 (15 ng) or MUS81/HISEME1 (30 ng)(Sections 2.28, 2.26 and 2.31, respectively). A MUS81-containing fraction prepared from HeLa cell-free extracts was used as a positive control (Section 2.41). Reactions were incubated at 37°C for 30 min (Section 2.45). DNA products were analysed by neutral PAGE followed by autoradiography. ^{32}P-labels are indicated with asterisks.

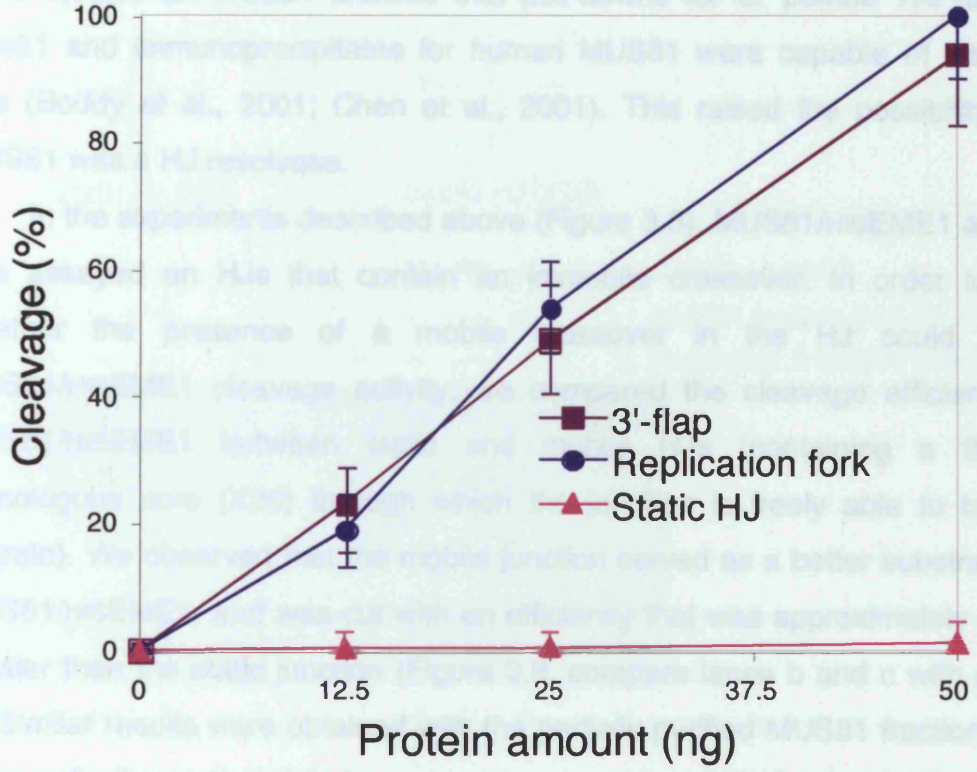

FIGURE 3.7: Quantification of the cleavage efficiency with the fork, flap and Holliday junction substrates

Reactions were carried out as described in Fig. 3.6 using purified MUS81/HISEME1 and ^{32}P-labelled 3'-flap, replication fork and static Holliday junction (X0) substrates. The reaction products were separated by PAGE and the amount of cleavage quantified by phosphorimaging (Section 2.12). Cleavage is expressed as a percentage relative to that observed with the replication fork substrate. The data presented is an average of 5 independent experiments.

V. HUMAN MUS81/HISEME1 AND HOLLIDAY JUNCTIONS

Initial studies on MUS81 showed that pull-downs for *S. pombe* TAP-tagged Mus81 and immunoprecipitates for human MUS81 were capable of cleaving HJs (Boddy et al., 2001; Chen et al., 2001). This raised the possibility that MUS81 was a HJ resolvase.

In the experiments described above (Figure 3.6), MUS81/HISEME1 activity was assayed on HJs that contain an immobile crossover. In order to test whether the presence of a mobile crossover in the HJ could affect MUS81/HISEME1 cleavage activity, we compared the cleavage efficiency of MUS81/HISEME1 between static and mobile HJs (containing a 26 bp homologous core (X26) through which the junction is freely able to branch migrate). We observed that the mobile junction served as a better substrate for MUS81/HISEME1, and was cut with an efficiency that was approximately 6-fold greater than the static junction (Figure 3.8, compare lanes b and c with g and h). Similar results were obtained with the partially purified MUS81 fraction from HeLa cells (lanes d and i). In contrast to recombinant MUS81/HISEME1 or the HeLa MUS81 fraction, fractionated extracts from HeLa cells enriched for the human HJ Resolvase A (Constantinou et al., 2002) cleaved static and mobile junctions equally and efficiently (lanes e and j).

Taken together, these results show that the endonuclease activity of MUS81/EME1 complex is specifically targeted to flap/fork structures. Although MUS81/EME1 is relatively inactive on HJs, the efficiency of cleavage can be enhanced by inclusion of homologous sequences. Previously, using chemical probes that could detect the formation of transient regions of single-stranded DNA, it was observed that mobile junctions exhibit a transient single-stranded character suggestive of base-pair breathing (West, 1995). We therefore suggest that the ability of MUS81/EME1 to cut four-way junctions is likely to be due to the recognition of transient flap structures that are formed as the junction undergoes spontaneous thermal denaturation. Consistent with this proposal, it was shown that cleavage of Holliday junctions by MUS81 fractions prepared

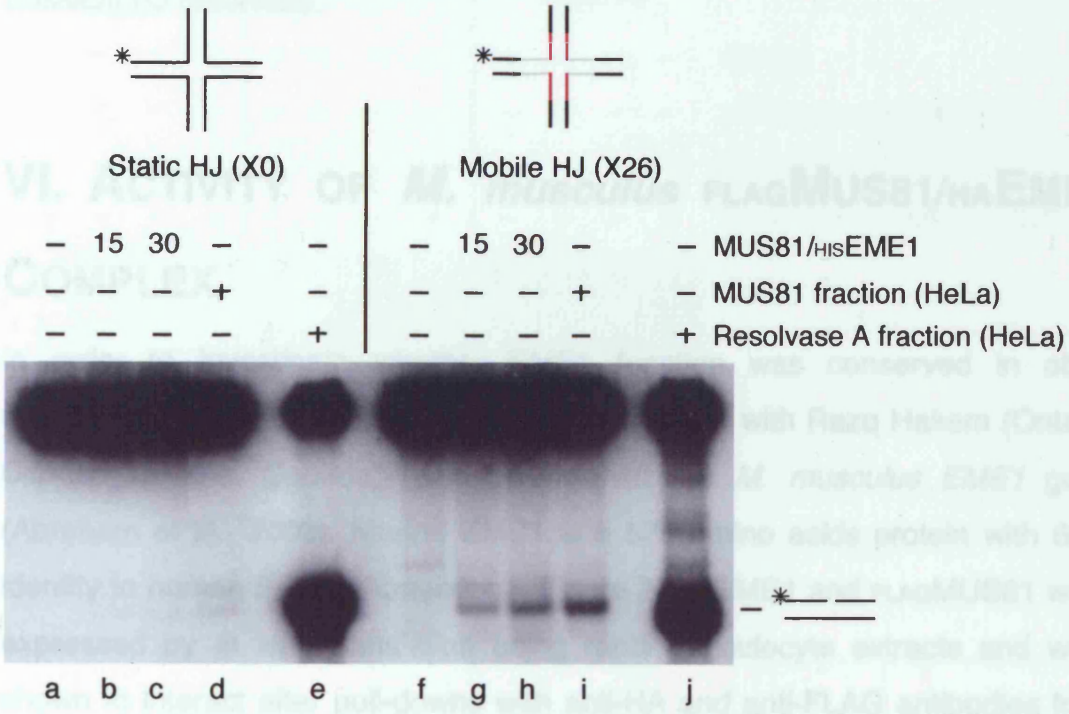

FIGURE 3.8: Comparison of human MUS81/HISEME1 activity on static and mobile Holliday junctions

Reactions contained ^{32}P-labelled synthetic Holliday junction (approx 3 ng) and purified MUS81/HISEME1 complex (Section 2.31). MUS81-containing fraction and Resolvase A (0.5 μl), both partially purified from HeLa cell-free extracts, were used as controls (Section 2.41). Reactions were incubated at 37°C for 30 min (Section 2.45). DNA products were analysed by neutral PAGE followed by autoradiography. ^{32}P-labels are indicated with asterisks. Complementary DNA strands in the homologous core of the mobile HJ are represented in red or grey (Table 2.3).

from HeLa extracts occurred at the 5'-side of the substrate and that the nicks were introduced without symmetry leading to the formation of non-ligatable products (Constantinou et al., 2002). We conclude that HJ cleavage by MUS81/EME1 is a secondary effect of its flap activity, rather than the sign of a classical HJ resolvase.

VI. ACTIVITY OF *M. musculus* FLAGMUS81/HAEME1 COMPLEX

In order to investigate whether EME1 function was conserved in other mammalian species, we established a collaboration with Razq Hakem (Ontario Cancer Institute, Canada), who had cloned the *M. musculus EME1* gene (Abraham et al., 2003). Murine EME1 is a 570 amino acids protein with 66% identity to human EME1 (Appendix 1, Figure 2). HAEME1 and FLAGMUS81 were expressed by *in vitro* translation using rabbit reticulocyte extracts and were shown to interact after pull-downs with anti-HA and anti-FLAG antibodies from the *in vitro* translation mixtures (Abraham et al., 2003). To test whether murine FLAGMUS81/HAEME1 had similar substrate specificity to human MUS81/HISEME1, we assayed the activity of HAEME1 or FLAGMUS81/HAEME1, both pulled-down with anti-HA beads from *in vitro* translation reactions. We found that FLAGMUS81/HAEME1 cleaved 3'-flap (Figure 3.9, lane h) and replication fork substrates efficiently (data not shown). In contrast, little or no cleavage was observed for the static HJ (lane l). A MUS81 fraction from HeLa (Section 2.41) was used as a positive control.

From this experiment we can conclude that murine MUS81/EME1 preferentially cleaves the same substrates as yeast Mus81/Eme1(Mms4) and human MUS81/EME1. It is therefore likely that the MUS81/EME1 substrate specificity is conserved among all eukaryotic species.

The work described in this chapter has been published (Abraham et al., 2003; Ciccia et al., 2003).

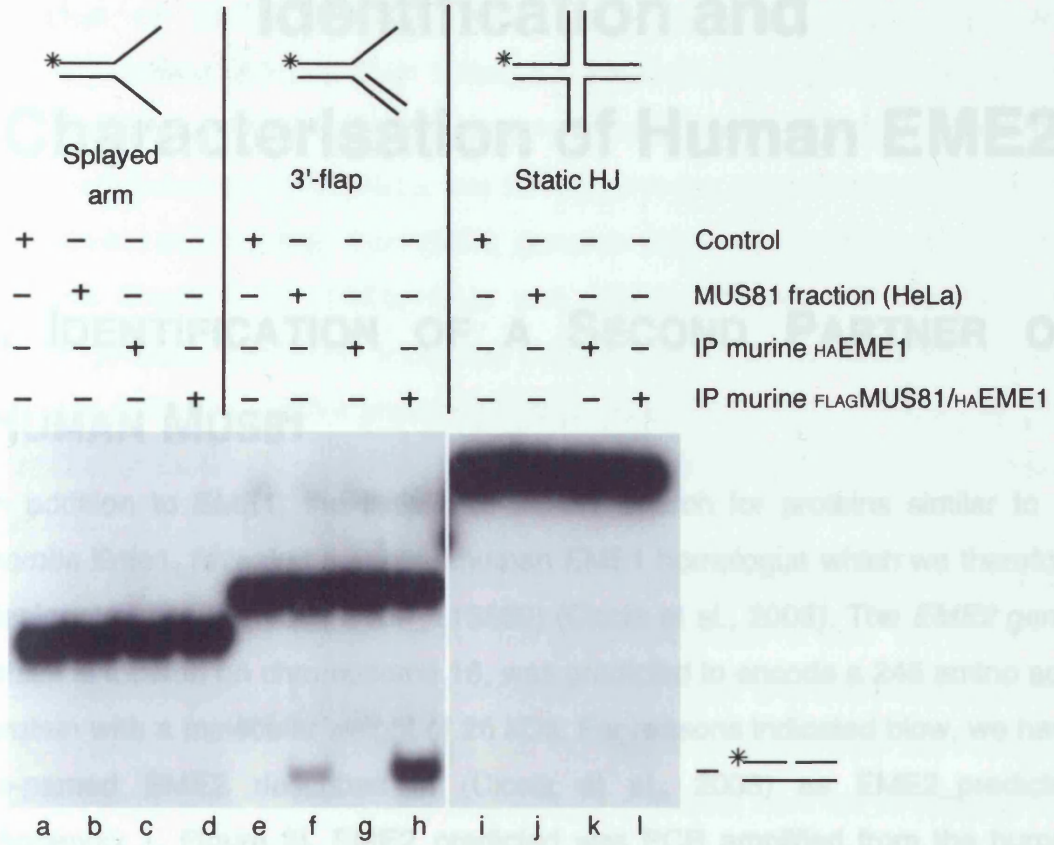

FIGURE 3.9: Substrate specificity of murine FLAGMUS81/HAEME1 endonuclease

Reactions contained a variety of ^{32}P-labelled substrates (approx 3 ng) and murine HAEME1 immunocomplex or murine FLAGMUS81/HAEME1 immunocomplex, as indicated. Both HAEME1 and murine FLAGMUS81/HAEME1 were obtained by *in vitro* translation reaction in reticulocyte extracts followed by immunoprecipitation with anti-HA antibody (Abraham et al., 2003). A human MUS81-containing fraction prepared from HeLa cell-free extracts was used as a positive control (Section 2.41). Reactions were incubated at 37°C for 30 min (Section 2.45). DNA products were analysed by neutral PAGE followed by autoradiography. ^{32}P-labels are indicated with asterisks.

CHAPTER FOUR

Identification and Characterisation of Human EME2

I. IDENTIFICATION OF A SECOND PARTNER OF HUMAN MUS81

In addition to EME1, the initial PSI-BLAST search for proteins similar to *S. pombe* Eme1, revealed a second human EME1 homologue which we therefore designated EME2 (NCBI # XM_113869) (Ciccia et al., 2003). The *EME2* gene, which is located on chromosome 16, was predicted to encode a 245 amino acid protein with a molecular weight of 26 kDa. For reasons indicated blow, we have re-named EME2 described in (Ciccia et al., 2003) as EME2_predicted (Appendix 1, Figure 3). EME2_predicted was PCR amplified from the human cDNA # AK074080 using DNA oligonucleotides 27 and 28 (Table 2.1). In order to test whether EME2_predicted interacts with MUS81, the bicistronic vector pGex-GSTMUS81/HISEME2_predicted was constructed (Section 2.6). Purification of GSTMUS81/HISEME2_predicted proved to be unsuccessful because the two proteins failed to form a stable complex (data not shown).

Further attempts to clone a different *EME2* splice variant were carried out according to the Genscan prediction NT_037887.92 (NCBI # NP_001010865) that subsequently replaced the EME2_predicted record in the NCBI database. DNA oligonucleotides 17 and 18 (Table 2.1) corresponding to the 5' and 3' ends of the Genscan prediction NT_037887.92, here designated EME2_genescan, were used in a PCR amplification reaction from a ProQuest HeLa Cell cDNA library (Section 2.2). The PCR clone obtained from the ProQuest HeLa Cell cDNA library encodes a 379 amino acid protein, designated EME2_HeLa, with a molecular weight of 41 kDa (Appendix 1, Figure 3). Alignment between EME2_HeLa and EME2_predicted (Appendix 1, Figure 3) revealed that the C-

terminal region of EME2_HeLa (amino acids 189-379) is identical to the C-terminus of EME2_predicted (amino acids 57-245). EME2_HeLa and EME2_predicted differ in their N-terminal regions, since EME2_HeLa is 134 amino acids longer than EME2_predicted (Appendix 1, Figure 3). Sequence alignment between EME2_HeLa and EME2_genscan showed that EME2_HeLa is 65 amino acids shorter than EME2_genscan (Appendix 1, Figure 4). Both the N- and C-termini of EME2_HeLa and EME2_genscan are identical, but EME2_genscan has three additional regions (amino acids 193-236, 267-273 and 312-325) that are not present in EME2_HeLa (Appendix 1, Figure 4). This is probably due to an inaccurate prediction of exons and introns by the Genscan software.

To verify whether EME2 cDNA had tissue-specific splice variants, additional PCR amplifications with DNA oligonucleotides 17 and 18 (Table 2.1) were performed from the ProQuest Human Fetal Brain and SuperScript Human Testis cDNA libraries (Section 2.2). The PCR clone obtained from the ProQuest Human Fetal Brain cDNA library encodes for a protein identical to EME2_HeLa (data not shown). The PCR clone obtained from the SuperScript Human Testis cDNA library, instead, encodes for a protein, designated EME2_testis, that is slightly different from EME2_HeLa. Although EME2_testis cDNA is longer than EME2_HeLa cDNA (1322 bp for EME2_testis cDNA and 1140 bp for EME2_HeLa cDNA), EME2_testis results in a protein that is 76 amino acids shorter than EME2_HeLa. This is due to a stop codon present at nucleotides 910-912 of EME2_testis cDNA. The N-terminus of EME2_testis (amino acids 1-190) is identical to the N-terminus of EME2_HeLa (Appendix 1, Figure 5), but an unspliced intron between nucleotides 570 and 753 of the EME2_testis cDNA altered the protein sequence of the C-terminus of EME2_testis compared to EME2_HeLa.

EME2_HeLa is 39% identical and 23% similar to human EME1, with the C-terminal regions being the most conserved (Figure 4.1). On the other hand, EME2_testis is only 20% identical and 26% similar to human EME1 because it has lost the similarity with the C-terminus of EME1 (Appendix 1, Figure 6). To determine whether the human EME1 and EME2_HeLa C-terminal sequences

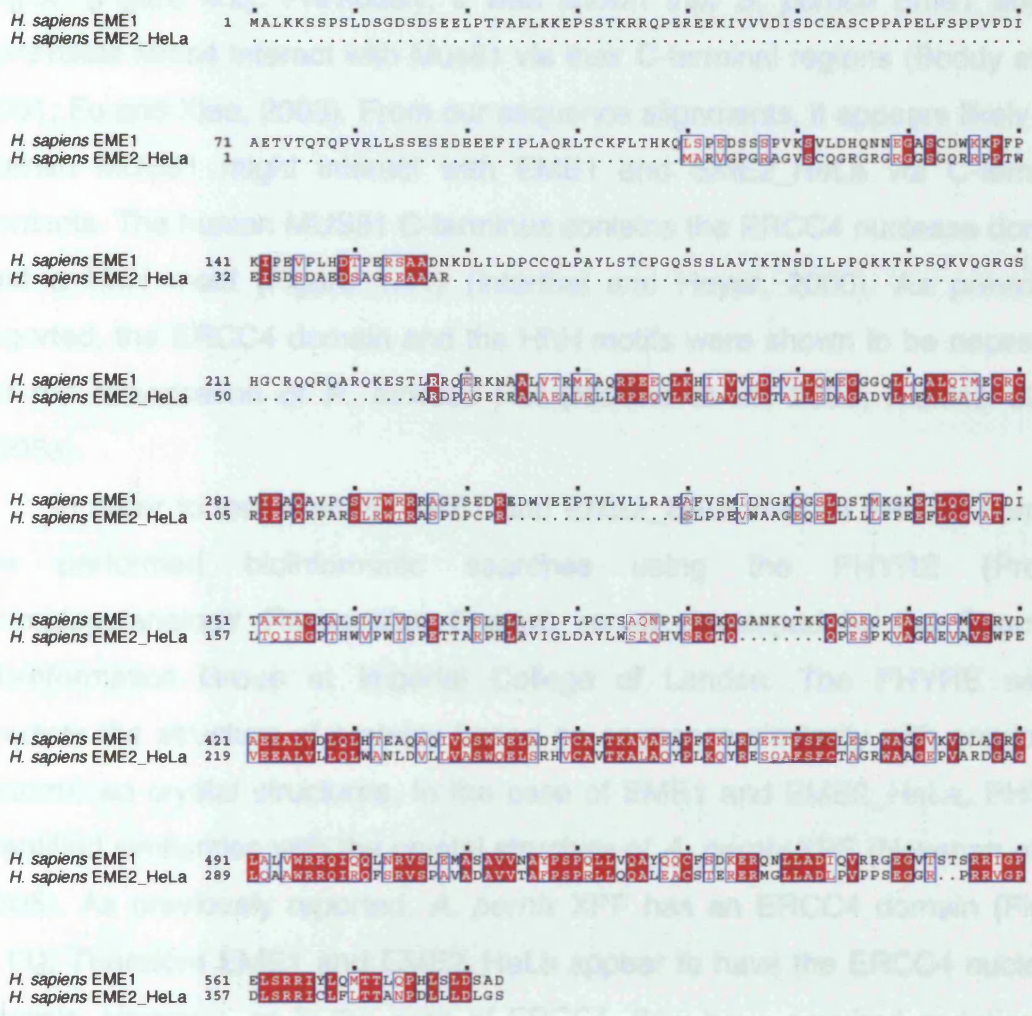

FIGURE 4.1: Sequence alignment between *H. sapiens* EME1 and *H. sapiens* EME2_HeLa

Sequence alignments were carried out as described in Figure 3.1.

were conserved in other proteins, a PSI-BLAST search was initiated using the last 160 amino acids of EME1 and EME2_HeLa. Remarkably, a close match was identified with human MUS81 protein. Alignment of MUS81, EME1 and EME2_HeLa confirmed that these three proteins have a conserved C-terminal region (Figure 4.2). Previously, it was shown that *S. pombe* Eme1 and *S. cerevisiae* Mms4 interact with Mus81 via their C-terminal regions (Boddy et al., 2001; Fu and Xiao, 2003). From our sequence alignments, it appears likely that human MUS81 might interact with EME1 and EME2_HeLa via C-terminal contacts. The human MUS81 C-terminus contains the ERCC4 nuclease domain and a HhH motif (Figure 1.11) (Interthal and Heyer, 2000). As previously reported, the ERCC4 domain and the HhH motifs were shown to be necessary for the dimerisation of *P. furiosus* Hef (Nishino et al., 2003; Nishino et al., 2005a).

In order to test whether EME1 and EME2_HeLa had an ERCC4 domain, we performed bioinformatic searches using the PHYRE (Protein Homology/analogY Recognition Engine) server developed by the Structural Bioinformatics Group at Imperial College of London. The PHYRE server predicts the structure of proteins based on sequence similarity with previously determined crystal structures. In the case of EME1 and EME2_HeLa, PHYRE identified similarities with the crystal structure of *A. pernix* XPF (Newman et al., 2005). As previously reported, *A. pernix* XPF has an ERCC4 domain (Figure 1.11). Therefore EME1 and EME2_HeLa appear to have the ERCC4 nuclease domain. However, as in the case of ERCC1, they have acquired mutations in the catalytic motif. When EME1 and EME2_HeLa were aligned with MUS81, it was apparent that they do not contain the $ERKX_3D$ catalytic motif (Figure 4.2, compare amino acids 333-339 of MUS81 with the corresponding amino acids of EME1 and EME2_HeLa). The PHYRE server also predicted the presence of a single HhH motif in human EME1 and EME2_HeLa, as also reported for MUS81 (Interthal and Heyer, 2000).

As described previously, EME2_predicted was unable to form a stable complex with MUS81, even though it is identical to EME2_Hela for the C-terminal 190 amino acids (Appendix 1, Figure 3). Based on the database

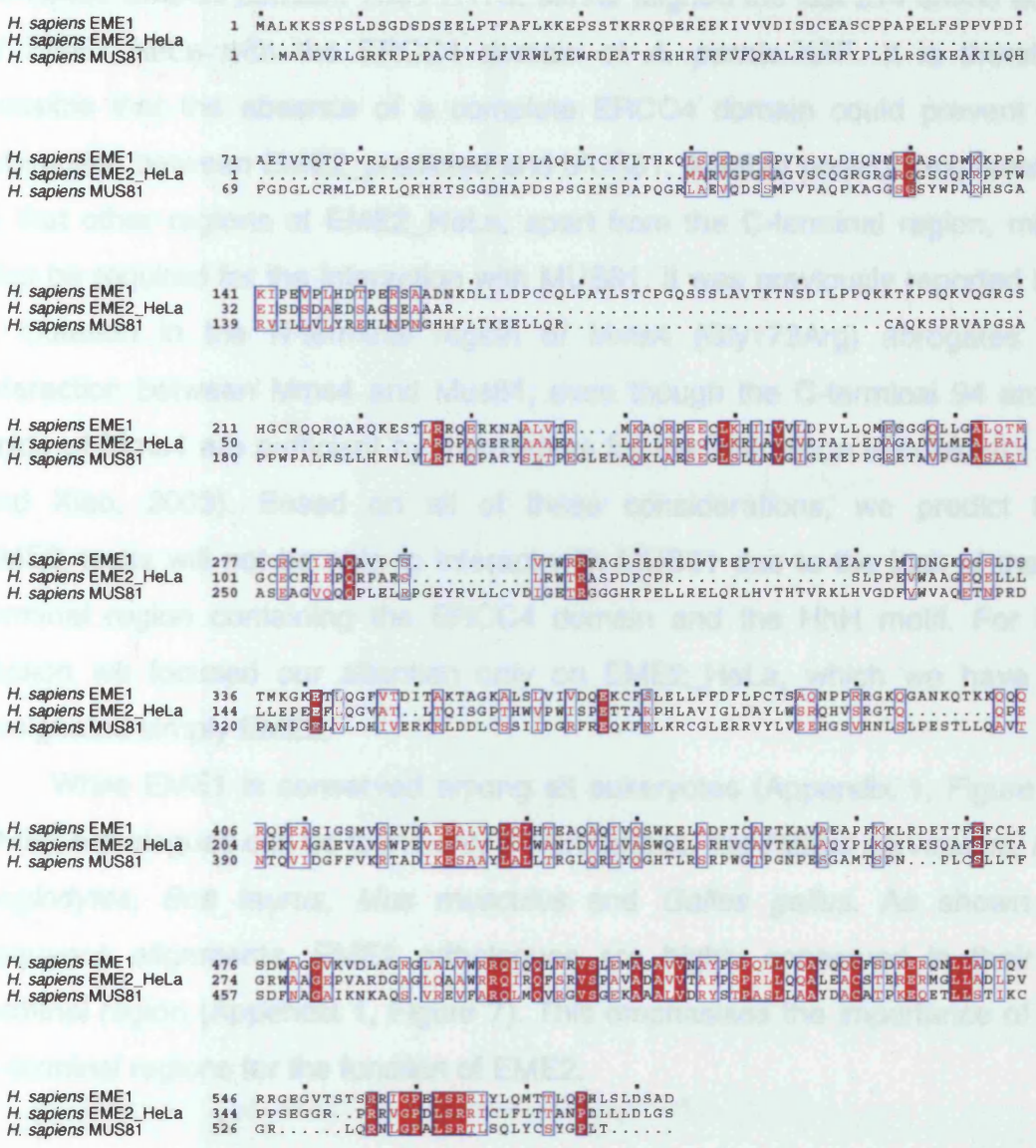

FIGURE 4.2: Sequence alignment of *H. sapiens* EME1, *H. sapiens* EME2_HeLa and *H. sapiens* MUS81

Sequence alignments were carried out as described using ClustalW.

searches performed with the PHYRE server, the last 190 amino acids contain a truncated ERCC4 domain. The PHYRE server aligned the last 214 amino acids of EME2_HeLa with the ERCC4 domain of *A. pernix* XPF. It is therefore possible that the absence of a complete ERCC4 domain could prevent the interaction between EME2_predicted and MUS81. Another possible explanation is that other regions of EME2_HeLa, apart from the C-terminal region, might also be required for the interaction with MUS81. It was previously reported that a mutation in the N-terminal region of Mms4 (Gly173Arg) abrogates the interaction between Mms4 and Mus81, even though the C-terminal 94 amino acids of Mms4 are sufficient by themselves for the interaction with Mus81 (Fu and Xiao, 2003). Based on all of these considerations, we predict that EME2_testis will not be able to interact with MUS81 due to the lack of the C-terminal region containing the ERCC4 domain and the HhH motif. For this reason we focused our attention only on EME2_HeLa, which we have re-designated simply EME2.

While EME1 is conserved among all eukaryotes (Appendix 1, Figure 2), EME2 orthologues can be found only in vertebrates, like *Rattus norvegicus*, *Pan troglodytes*, *Bos taurus*, *Mus musculus* and *Gallus gallus*. As shown by sequence alignments, EME2 orthologues are highly conserved in their C-terminal region (Appendix 1, Figure 7). This emphasises the importance of the C-terminal regions for the function of EME2.

II. INTERACTION OF HUMAN EME2 WITH MUS81

In order to test whether EME2 interacted with MUS81, the bicistronic vector pGex-MUS81/HISEME2 was constructed as described in Section 2.6. Cell-free extracts were prepared from *E. coli* BL21-CodonPlus (DE3)-PR carrying pGex-GSTMUS81/HISEME2 as indicated in Section 2.39 and pull-downs were performed either with GST-sepharose beads or Talon beads. We observed that GST-sepharose beads pulled-down both GSTMUS81 and HISEME2, as determined by SDS-PAGE followed by Coomassie blue staining (Figure 4.3, lane b). In addition, GSTMUS81 co-precipitated with HISEME2 when the cell-free

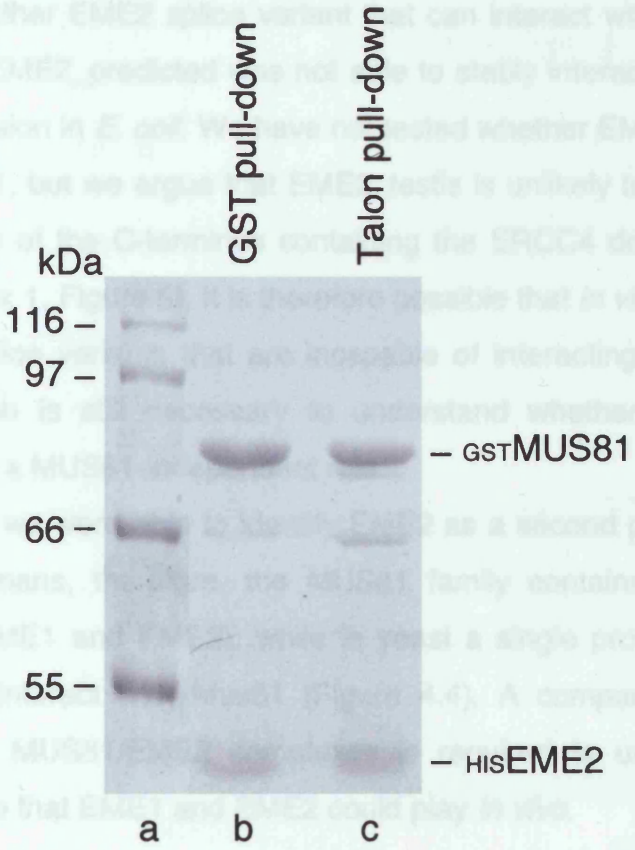

FIGURE 4.3: Interaction of human MUS81 with EME2

Cell-free extracts were prepared from *E. coli* carrying the bicistronic vector pGex-GSTMUS81/HISEME2 (Section 2.6), and pull-down assays were carried out using GST-sepharose (lane b) or Talon (lane c) beads (Section 2.39). Proteins were separated by 10% SDS-PAGE and visualised by staining with Coomassie blue.

extracts were mixed with Talon beads (Figure 4.3, lane c). This experiment indicates that MUS81 and EME2 form a stable complex. At the present time, we have not found another EME2 splice variant that can interact with MUS81. As mentioned above, EME2_predicted was not able to stably interact with MUS81 following co-expression in *E. coli*. We have not tested whether EME2_testis can interact with MUS81, but we argue that EME2_testis is unlikely to bind MUS81 due to the absence of the C-terminus containing the ERCC4 domain and the HhH motif (Appendix 1, Figure 5). It is therefore possible that *in vivo* there might be some EME2 splice variants that are incapable of interacting with MUS81. Further investigation is still necessary to understand whether these splice variants might have a MUS81-independent role.

In conclusion, we were able to identify EME2 as a second partner protein for MUS81. In humans, therefore, the MUS81 family contains two MUS81 partner proteins (EME1 and EME2), while in yeast a single protein (Eme1 or Mms4) is able to interact with Mus81 (Figure 4.4). A comparison between MUS81/EME1 and MUS81/EME2 complexes is required to understand the possibly diverse role that EME1 and EME2 could play *in vivo*.

III. COMPARISON OF THE ACTIVITIES OF HUMAN MUS81/HISEME1 AND MUS81/HISEME2 COMPLEXES

In order to test whether the MUS81/EME2 complex was active, the bicistronic vector pET21d-MUS81/HISEME2 was constructed (Section 2.6). MUS81/HISEME2 was purified from *E. coli* BL21-CodonPlus (DE3)-PR carrying pET21d-MUS81/HISEME2 by phosphocellulose and Talon column chromatography, as described in Section 2.32. MUS81/HISEME2 complex was incubated with 3'-flap and replication fork substrates (Figure 4.5) that were prepared by annealing partially complementary oligonucleotides (Table 2.3). Both substrates contained a common 5'-^{32}P labelled oligonucleotide (X0.1). We observed that MUS81/HISEME2 cleaved both the 3'-flap and replication fork substrates with similar efficiency (compare lane b with lane d). MUS81/HISEME1

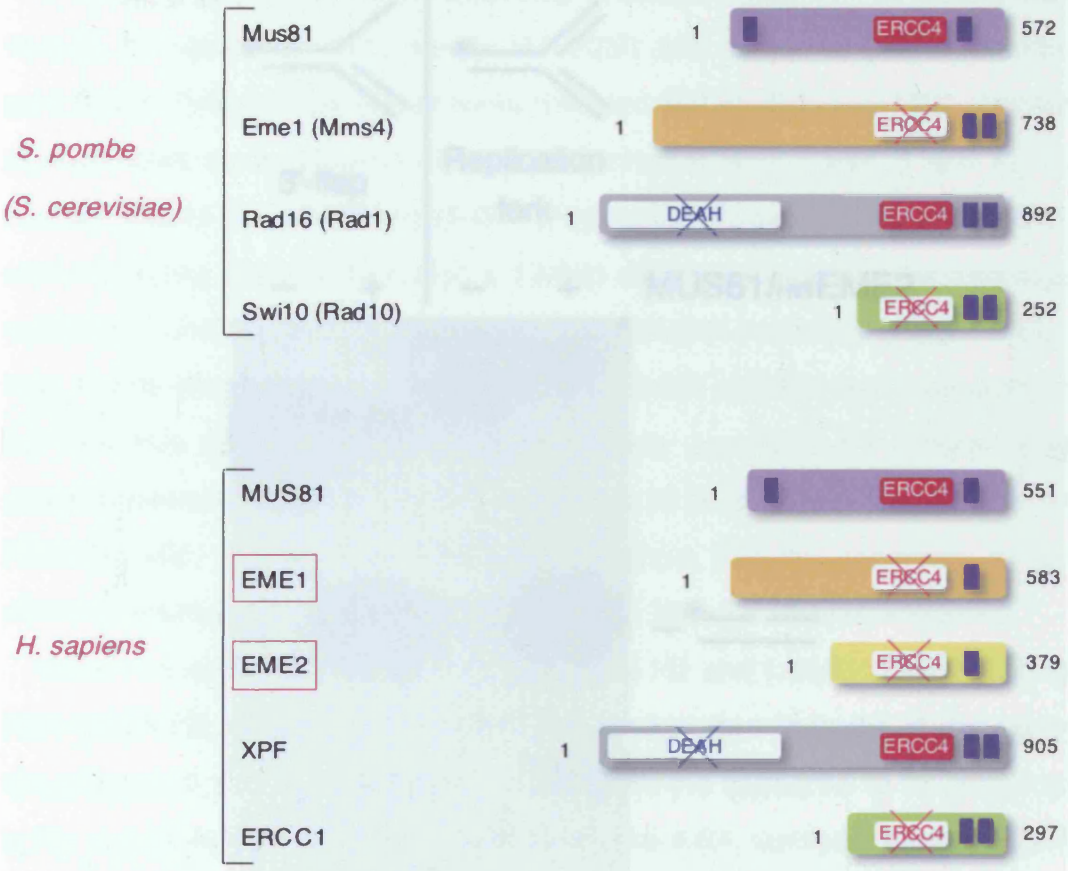

FIGURE 4.4: Comparison of yeast and human MUS81 family of proteins

The MUS81 family of proteins in *S. pombe* and *H. sapiens* are represented. *S. cerevisiae* orthologues of *S. pombe* proteins are shown in brackets. Novel human proteins of the MUS81 family are highlighted by red boxes. *H. sapiens* EME2 corresponds to *H. sapiens* EME2_HeLa (Figure 4.1). ERCC4 nuclease domains (red), HhH motifs (dark violet) and DEAH helicase domains (blue) are indicated with boxes. Inactive ERCC4 and DEAH domains are indicated with red and blue crosses, respectively.

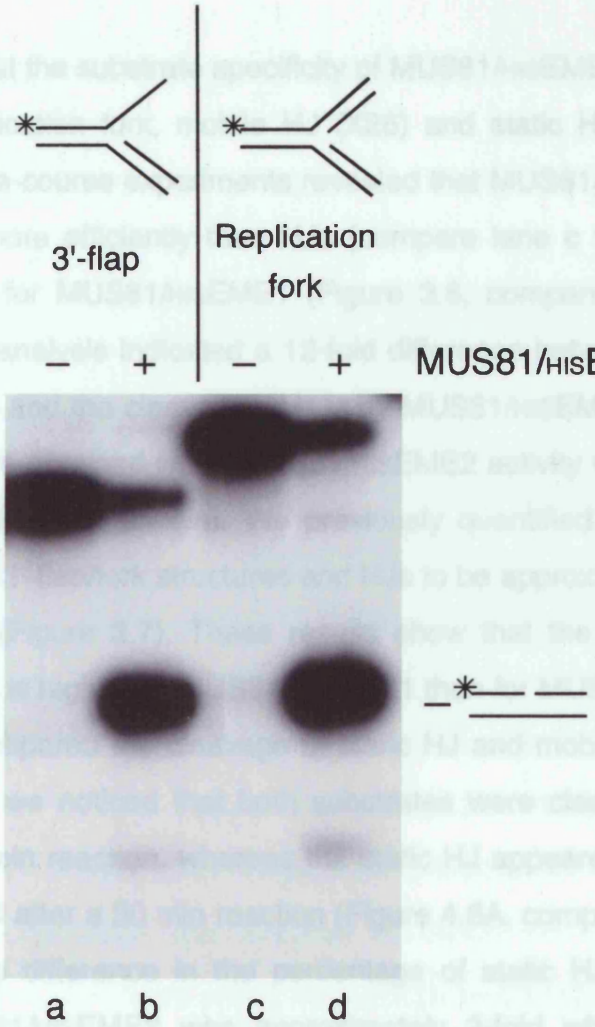

FIGURE 4.5: MUS81/HISEME2 activity on 3'-flap and replication fork structures

Reactions contained ^{32}P-labelled synthetic substrates (approx 3 ng of 3'-flap or replication fork) and purified MUS81/HISEME2 complex (10 nM; lanes b and d). MUS81/HISEME2 was purified as described in Section 2.32. Reactions were incubated at 37°C for 30 min (Section 2.45). DNA products were analysed by neutral PAGE followed by autoradiography. ^{32}P-labels are indicated with asterisks.

also showed equal cleavage efficiency of 3'-flap and replication fork substrates (Figure 3.7).

In order to test the substrate specificity of MUS81/HISEME2, its activity was compared on replication fork, mobile HJ (X26) and static HJ (X0) structures (Figure 4.6A). Time-course experiments revealed that MUS81/HISEME2 cleaved replication forks more efficiently than HJs (compare lane c with g and k), as previously shown for MUS81/HISEME1 (Figure 3.6, compare lanes o and t). Phosphorimaging analysis indicated a 12-fold difference between the cleavage of replication forks and the cleavage of HJs by MUS81/HISEME2 (Figure 4.6B). Similar results were obtained when MUS81/HISEME2 activity was compared on 3'-flap and HJs (data not shown). We previously quantified the difference of cleavage between 3'-flap/fork structures and HJs to be approximately 75-fold for MUS81/HISEME1 (Figure 3.7). These results show that the specificity for 3'-flap/fork structures is higher for MUS81/HISEME1 than for MUS81/HISEME2.

When we compared the cleavage of static HJ and mobile HJ induced by MUS81/HISEME2, we noticed that both substrates were cleaved to the same extent after a 10 min reaction, whereas the static HJ appeared to be preferred over the mobile HJ after a 30 min reaction (Figure 4.6A, compare lanes g and h with k and l). The difference in the percentage of static HJs or mobile HJs cleaved by MUS81/HISEME2 was approximately 2-fold when quantified by phosphorimaging (Figure 4.6B). In the case of MUS81/HISEME1, we observed that mobile HJs were cleaved approximately 6-fold more efficiently than static HJs (Figure 3.8). We cannot explain, at the present time, the observation that MUS81/HISEME1 and MUS81/HISEME2 prefer different types of HJs. We have not tested whether this might be due to a different binding affinity for static or mobile HJs between MUS81/HISEME1 and MUS81/HISEME2.

To compare the cleavage efficiency of MUS81/HISEME1 and MUS81/HISEME2 on the same substrate, we incubated equal amounts of MUS81/HISEME1 or MUS81/HISEME2 complex in the presence of a replication fork substrate (Figure 4.7A). Time-course experiments revealed that MUS81/HISEME2 is more active than MUS81/HISEME1 on the replication fork substrate (compare lanes b and f). Quantification by phosphorimaging revealed

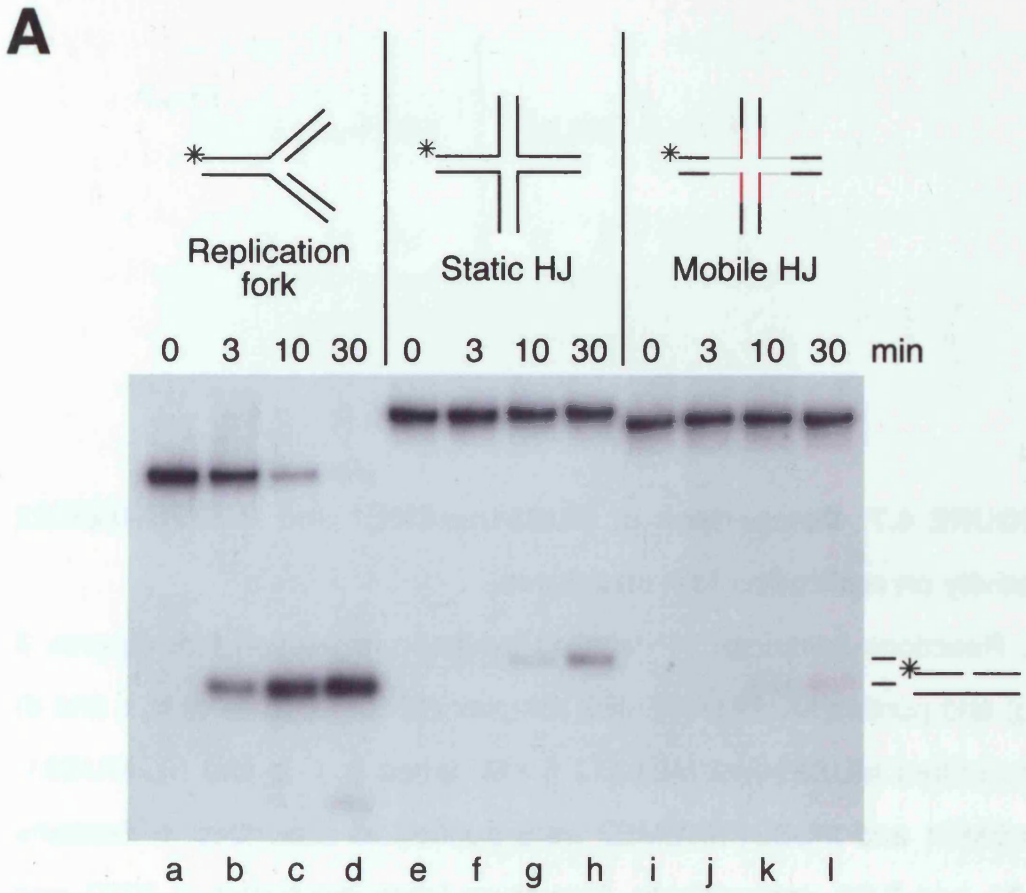
A
Replication fork
Static HJ
Mobile HJ
0 3 10 30 0 3 10 30 0 3 10 30 min
a b c d e f g h i j k l

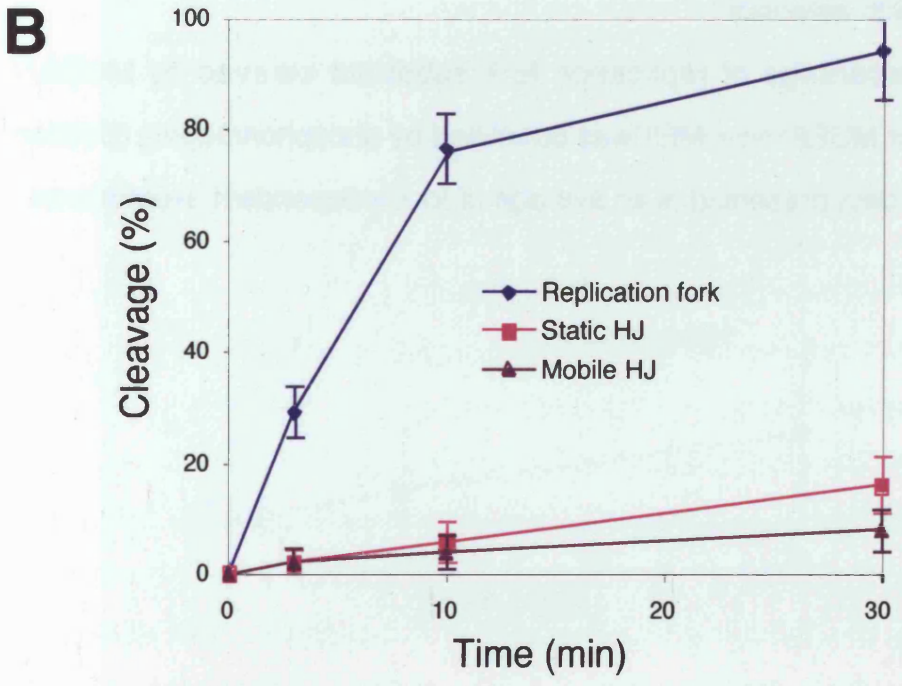
B
Cleavage (%)
100
80
60
40
20
0
0
10
20
30
Time (min)
Replication fork
Static HJ
Mobile HJ


A
MUS81/HISEME2
MUS81/HISEME1
0 3 10 30 0 3 10 30 min
a b c d e f g h

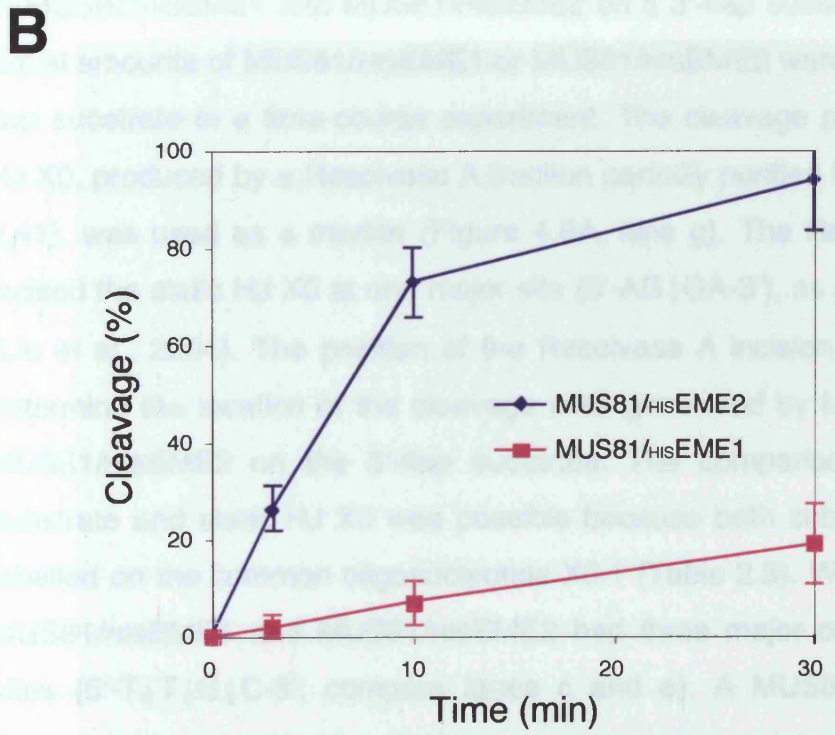
B
Cleavage (%)
100
80
60
40
20
0
0
10
20
30
Time (min)
MUS81/HISEME2
MUS81/HISEME1

a 10-fold difference in the percentage of replication fork cleaved by MUS81/HISEME2 or MUS81/HISEME1 (Figure 4.7B). Similar results were obtained when 3'-flap was used as a substrate (data not shown). It is possible that the higher activity of MUS81/HISEME2 compared to MUS81/HISEME1 might be a consequence of a more efficient binding of MUS81/HISEME2 to 3'-flap/fork compared to MUS81/HISEME1. An alternative explanation could be that EME2, through the interaction with MUS81, stimulates the catalytic domain of MUS81 more efficiently than EME1. Further experiments will be required to test these hypotheses.

IV. DNA CLEAVAGE MECHANISM OF HUMAN MUS81/HISEME1 AND MUS81/HISEME2 COMPLEXES

To investigate if there was any difference in the cleavage mechanism of MUS81/HISEME1 and MUS81/HISEME2, we compared the pattern of cleavage of MUS81/HISEME1 and MUS81/HISEME2 on a 3'-flap substrate (Figure 4.8A). Equal amounts of MUS81/HISEME1 or MUS81/HISEME2 were incubated with 3'-flap substrate in a time-course experiment. The cleavage pattern of the static HJ X0, produced by a Resolvase A fraction partially purified from HeLa (Section 2.41), was used as a marker (Figure 4.8A, lane g). The Resolvase A fraction incised the static HJ X0 at one major site (5'-AG↓GA-3'), as previously reported (Liu et al., 2004). The position of the Resolvase A incision site allowed us to determine the location of the cleavage sites generated by MUS81/HISEME1 or MUS81/HISEME2 on the 3'-flap substrate. The comparison between 3'-flap substrate and static HJ X0 was possible because both substrates were 5'-^{32}P labelled on the common oligonucleotide X0.1 (Table 2.3). We noticed that both MUS81/HISEME1 and MUS81/HISEME2 had three major consecutive incision sites (5'-T↓T↓G↓C-3'; compare lanes c and e). A MUS81 fraction partially purified from HeLa (Section 2.41) showed the same incision pattern (lane f). In addition to these three incision sites, MUS81/HISEME2 displayed a unique major cleavage site (5'-GC↓CT-3'; lane e). The three incision sites common to

HISEME2 cle

of the 3'-flap

8 nucleotide

is indicated

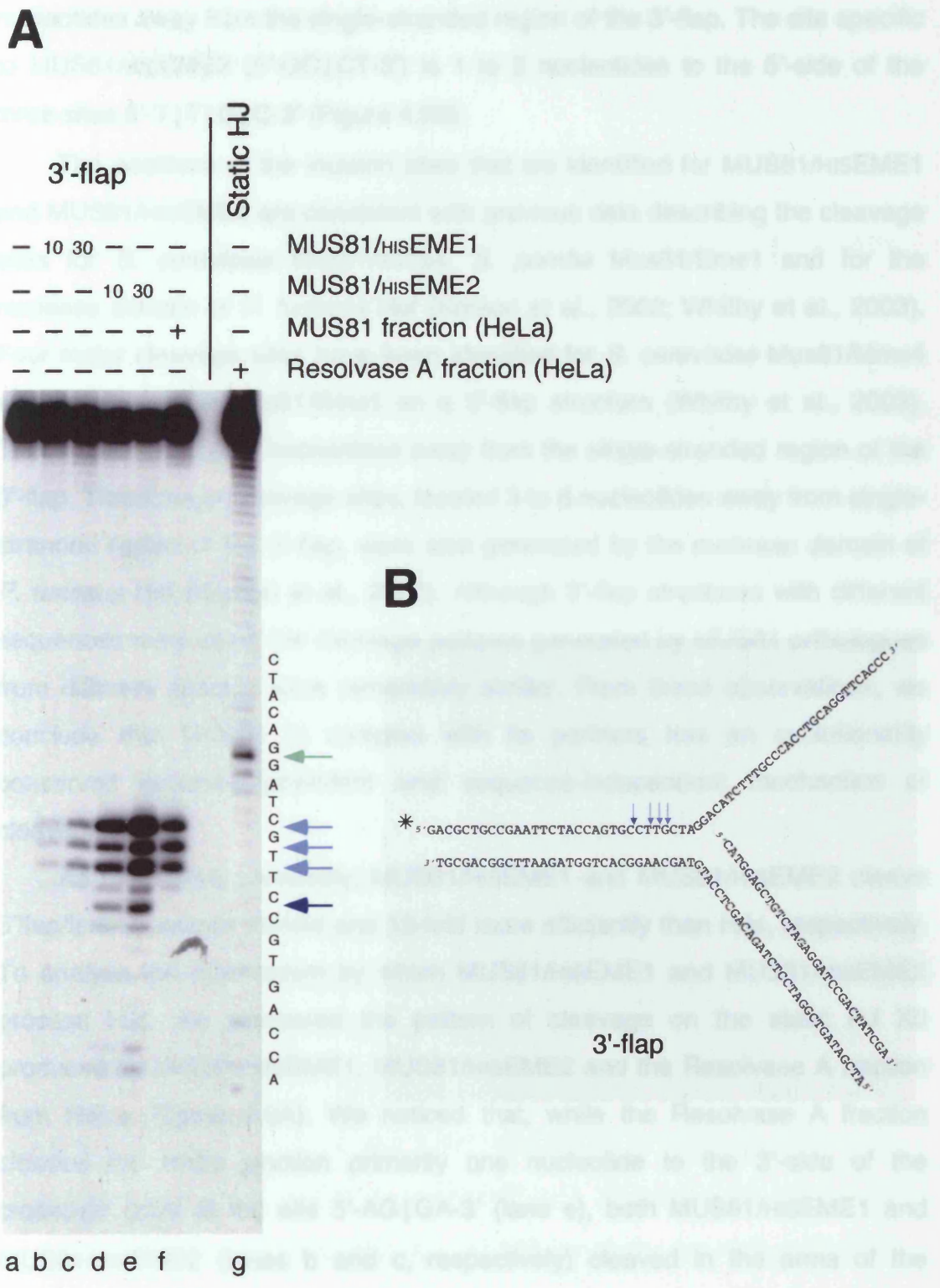
A
3'-flap
Static HJ
– 10 30 – – – – MUS81/HISEME1
– – – 10 30 – – MUS81/HISEME2
– – – – – + – MUS81 fraction (HeLa)
– – – – – – + Resolvase A fraction (HeLa)
a b c d e f g
B
3'-flap

both MUS81/HISEME1 and MUS81/HISEME2 (5'-T↓T↓G↓C-3') are 3 to 6 nucleotides away from the single-stranded region of the 3'-flap. The site specific to MUS81/HISEME2 (5'-GC↓CT-3') is 1 to 2 nucleotides to the 5'-side of the three sites 5'-T↓T↓G↓C-3' (Figure 4.8B).

The positions of the incision sites that we identified for MUS81/HISEME1 and MUS81/HISEME2 are consistent with previous data describing the cleavage sites for *S. cerevisiae* Mus81/Mms4, *S. pombe* Mus81/Eme1 and for the nuclease domain of *P. furiosus* Hef (Komori et al., 2002; Whitby et al., 2003). Four major cleavage sites have been identified for *S. cerevisiae* Mus81/Mms4 and for *S. pombe* Mus81/Eme1 on a 3'-flap structure (Whitby et al., 2003). These sites are 3 to 7 nucleotides away from the single-stranded region of the 3'-flap. Three major cleavage sites, located 3 to 6 nucleotides away from single-stranded region of the 3'-flap, were also generated by the nuclease domain of *P. furiosus* Hef (Komori et al., 2002). Although 3'-flap structures with different sequences were used, the cleavage patterns generated by MUS81 orthologues from different species were remarkably similar. From these observations, we conclude that MUS81 in complex with its partners has an evolutionarily conserved structure-dependent and sequence-independent mechanism of cleavage.

As mentioned previously, MUS81/HISEME1 and MUS81/HISEME2 cleave 3'flap/fork structures 75-fold and 12-fold more efficiently than HJs, respectively. To analyse the mechanism by which MUS81/HISEME1 and MUS81/HISEME2 process HJs, we compared the pattern of cleavage on the static HJ X0 produced by MUS81/HISEME1, MUS81/HISEME2 and the Resolvase A fraction from HeLa (Figure 4.9A). We noticed that, while the Resolvase A fraction cleaved the static junction primarily one nucleotide to the 3'-side of the crossover point at the site 5'-AG↓GA-3' (lane e), both MUS81/HISEME1 and MUS81/HISEME2 (lanes b and c, respectively) cleaved in the arms of the junction, away from the crossover point. In particular, we identified one incision site (5'-CT↓TG-3') common to both MUS81/HISEME1 and MUS81/HISEME2 and two consecutive major incision sites (5'-G↓C↓CT-3') specific for MUS81/HISEME2. Comparing the intensity of the incisions generated by

away from the

otide away from

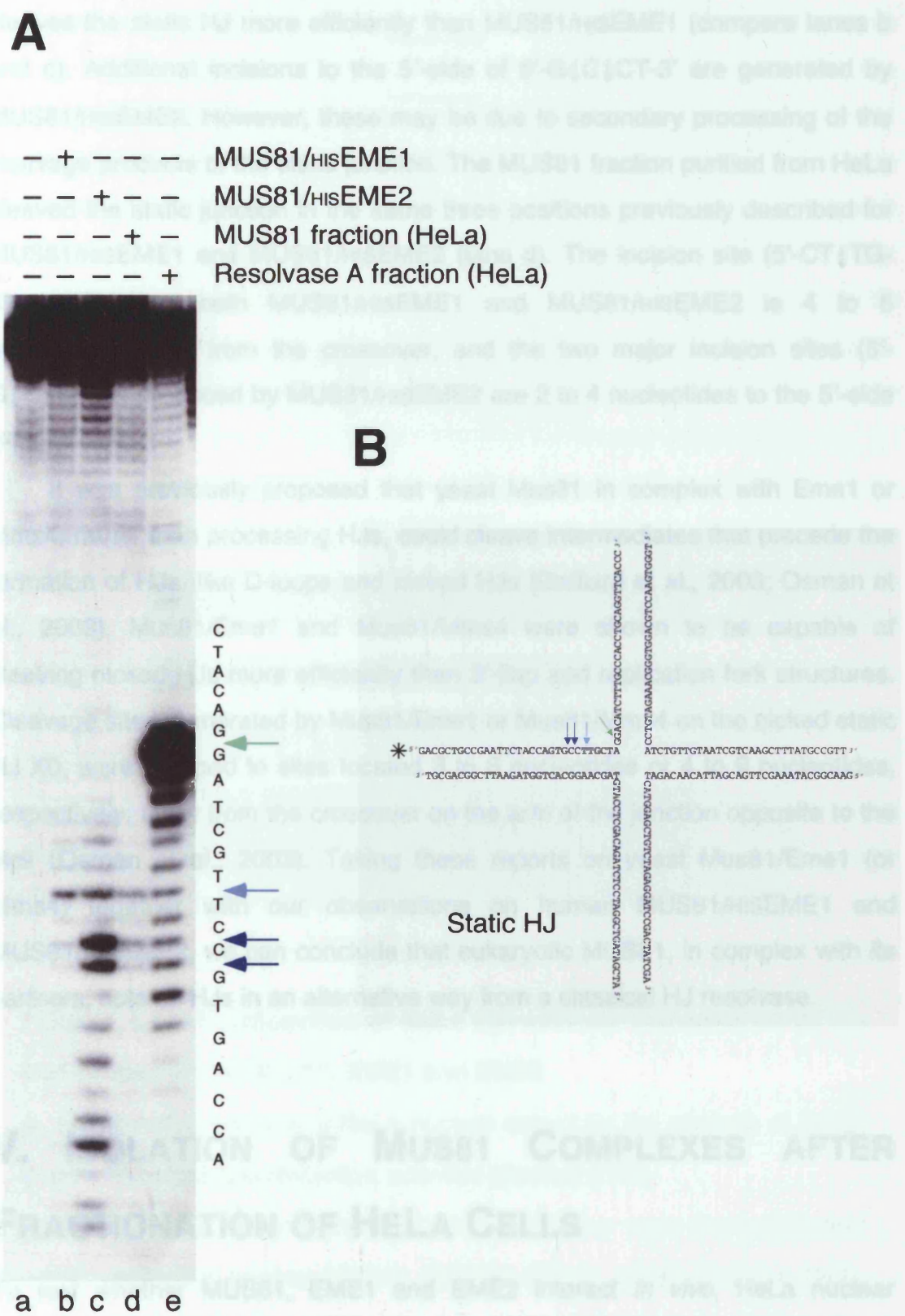
A
– + – – – MUS81/HISEME1
– – + – – MUS81/HISEME2
– – – + – MUS81 fraction (HeLa)
– – – – + Resolvase A fraction (HeLa)
C T A C A G G A T C G T T C C G T G A C C A
a b c d e
B
GACGCTGCCGAATTCTACCAGTGCCTTGCTA
TGCGACGGCTTAAGATGGTCACGGAACGAT
ATCTGTTGTAATCGTCAAGCTTTATGCCGTT
TAGACAACATTAGCAGTTCGAAATACGGCAAG
Static HJ

MUS81/HISEME1 and MUS81/HISEME2, it is apparent that MUS81/HISEME2 cleaves the static HJ more efficiently than MUS81/HISEME1 (compare lanes b and c). Additional incisions to the 5'-side of 5'-G↓C↓CT-3' are generated by MUS81/HISEME2. However, these may be due to secondary processing of the cleavage products of the static junction. The MUS81 fraction purified from HeLa cleaved the static junction in the same three positions previously described for MUS81/HISEME1 and MUS81/HISEME2 (lane d). The incision site (5'-CT↓TG-3') common to both MUS81/HISEME1 and MUS81/HISEME2 is 4 to 5 nucleotides away from the crossover, and the two major incision sites (5'-G↓C↓CT-3') produced by MUS81/HISEME2 are 2 to 4 nucleotides to the 5'-side (Figure 4.9B).

It was previously proposed that yeast Mus81 in complex with Eme1 or Mms4, rather than processing HJs, could cleave intermediates that precede the formation of HJs, like D-loops and nicked HJs (Gaillard et al., 2003; Osman et al., 2003). Mus81/Eme1 and Mus81/Mms4 were shown to be capable of cleaving nicked HJs more efficiently than 3'-flap and replication fork structures. Cleavage sites, generated by Mus81/Eme1 or Mus81/Mms4 on the nicked static HJ X0, were mapped to sites located 3 to 6 nucleotides or 4 to 9 nucleotides, respectively, away from the crossover on the arm of the junction opposite to the nick (Osman et al., 2003). Taking these reports on yeast Mus81/Eme1 (or Mms4) together with our observations on human MUS81/HISEME1 and MUS81/HISEME2, we can conclude that eukaryotic MUS81, in complex with its partners, acts on HJs in an alternative way from a classical HJ resolvase.

V. ISOLATION OF MUS81 COMPLEXES AFTER FRACTIONATION OF HELA CELLS

To test whether MUS81, EME1 and EME2 interact *in vivo*, HeLa nuclear extracts were fractionated according to the previous scheme developed in our lab (Liu et al., 2004) and the elution profile of MUS81, EME1, EME2 was followed (Figure 4.10A). HeLa nuclear extracts precipitated by a 25% - 55%

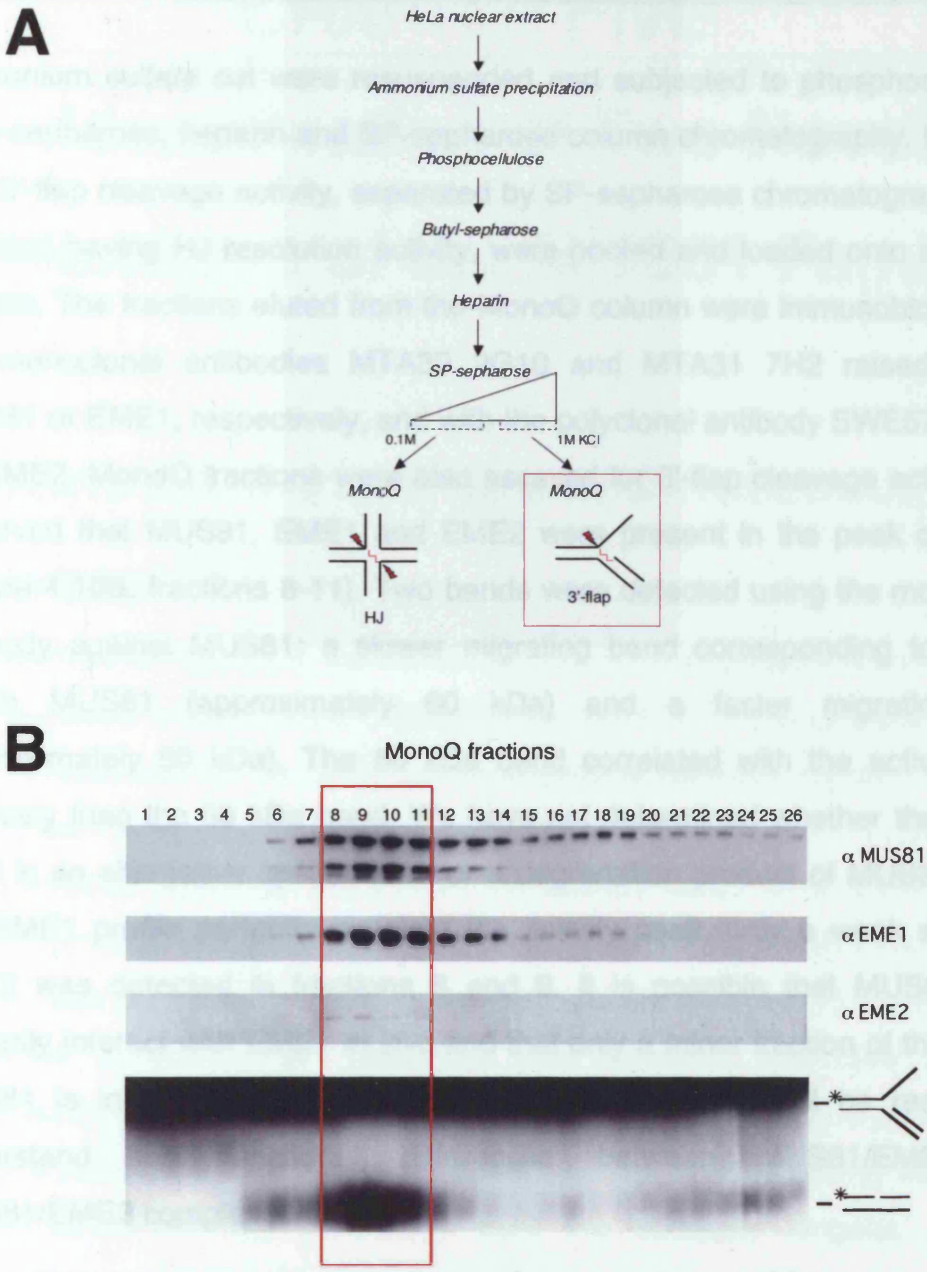

FIGURE 4.10: Fractionation of HeLa cell extracts and analysis of the elution profiles of MUS81, EME1 and EME2

A. Fractionation scheme of HeLa nuclear extract for the analysis of 3'-flap and Holliday junction resolution activities (Section 2.41).

B. Fractions eluted from the final MonoQ column were immunoblotted using antibodies against MUS81 (MTA30 2G10), EME1 (MTA31 7H2), EME2 (SWE57; Section 2.22) and were assayed for 3'-flap cleavage activity (Section 2.45). DNA products were analysed by neutral PAGE followed by autoradiography.

ammonium sulfate cut were resuspended and subjected to phosphocellulose, butyl-sepharose, heparin and SP-sepharose column chromatography. Fractions with 3'-flap cleavage activity, separated by SP-sepharose chromatography from fractions having HJ resolution activity, were pooled and loaded onto a MonoQ column. The fractions eluted from the MonoQ column were immunoblotted with the monoclonal antibodies MTA30 2G10 and MTA31 7H2 raised against MUS81 or EME1, respectively, and with the polyclonal antibody SWE57 specific for EME2. MonoQ fractions were also assayed for 3'-flap cleavage activity. We observed that MUS81, EME1 and EME2 were present in the peak of activity (Figure 4.10B, fractions 8-11). Two bands were detected using the monoclonal antibody against MUS81: a slower migrating band corresponding to the full length MUS81 (approximately 60 kDa) and a faster migrating band (approximately 50 kDa). The 50 kDa band correlated with the activity more precisely than the 60 kDa band. We have not determined whether the 50 kDa band is an alternative spliced form or a degradation product of MUS81. While the EME1 profile perfectly matched the activity peak, only a weak signal for EME2 was detected in fractions 8 and 9. It is possible that MUS81 could primarily interact with EME1 *in vivo* and that only a minor fraction of the pool of MUS81 is in complex with EME2. Further experiments will be required to understand the functional differences between MUS81/EME1 and MUS81/EME2 complexes *in vivo*.

CHAPTER FIVE

Identification of Two Novel Members of the MUS81 Family

I. IDENTIFICATION OF A HUMAN ORTHOLOGUE OF *P. furiosus* HEF

As described in Figure 4.4, the human MUS81 family of proteins is composed of five members: MUS81, EME1, EME2, XPF and ERCC1. All of these proteins are characterised by the presence of an ERCC4 nuclease domain. However, this domain is active only in MUS81 and XPF proteins (Figure 4.4). In order to verify whether additional proteins of the MUS81 family were present in the human genome, a domain search for proteins containing the ERCC4 nuclease domain was performed in the InterPro database. Besides MUS81 and XPF, an additional protein, called KIAA1596, was identified. KIAA1596 (NCBI # BAB13422) is a 1151 amino acid protein, which is encoded by a partial cDNA (NCBI # AB046816) missing the ATG start codon. A clone coding for the full-length KIAA1596 was purchased from the company Origene (clone # TC125463). We re-designated KIAA1596 as human HEF because of the similarity with the *P. furiousus* Hef (Section 1.10). The *HEF* gene is located in chromosome 14 and encodes a 2048 amino acid protein with a predicted molecular weight of 250 kDa. Human HEF, like *P. furiousus* Hef, has the DEAH helicase domain and the ERCC4 nuclease domain (compare Figure 1.11 and Figure 5.1). Sequence alignment showed that the DEAH domain of human HEF (amino acids 70-611) is 28% identical and 24% similar to the DEAH domain of *P. furiousus* Hef and that the ERCC4 domain of human HEF (amino acids 1830-2030) is 23% identical and 27% similar to the ERCC4 domain of *P. furiousus* (Appendix 1, Figure 8). The ERCC4 nuclease domain of human HEF has been

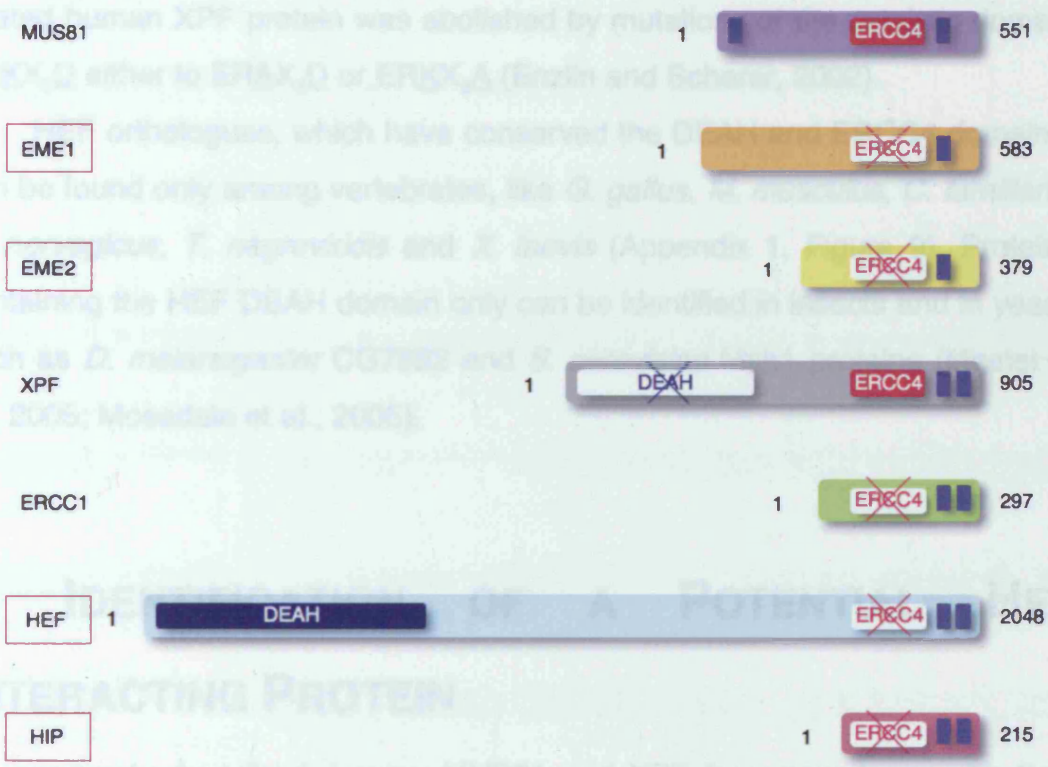

FIGURE 5.1: The human MUS81 family of proteins

Members of the human MUS81 family are represented. Novel members identified in this study are highlighted by red boxes. ERCC4 nuclease domains (red), HhH motifs (dark violet), DEAH helicase domains (blue) are indicated with boxes. Inactive ERCC4 and DEAH domains are indicated with red and blue crosses, respectively.

proposed to be inactive due to mutation of the catalytic motif ERKX$_3$D to ERRX$_3$E (amino acids 1864-1870 of human HEF) (Meetei et al., 2005). This hypothesis was based on the observation that the endonuclease activity of the related human XPF protein was abolished by mutations of the catalytic domain ERKX$_3$D either to ERAX$_3$D or ERKX$_3$A (Enzlin and Scharer, 2002).

HEF orthologues, which have conserved the DEAH and ERCC4 domains, can be found only among vertebrates, like *G. gallus*, *M. musculus*, *C. familiaris*, *R. norvegicus*, *T. negroviridis* and *X. laevis* (Appendix 1, Figure 9). Proteins containing the HEF DEAH domain only can be identified in insects and in yeast, such as *D. melanogaster* CG7922 and *S. cerevisiae* Mph1 proteins (Meetei et al., 2005; Mosedale et al., 2005).

II. IDENTIFICATION OF A POTENTIAL HEF INTERACTING PROTEIN

As previously described, human MUS81 and XPF form complexes with their partner proteins EME1 (or EME2) and ERCC1, respectively. EME1 and EME2 share homology with the C-terminus of MUS81 and ERCC1 is related to the C-terminus of XPF (Aravind et al., 1999; Gaillard and Wood, 2001). In order to test whether HEF could also form a heterodimer with partner proteins that have a related C-terminus, we performed a PSI-BLAST search for proteins homologous to the C-terminal 300 amino acids of human HEF. Following three PSI-BLAST iterations, we identified a human protein named MGC32020 (NCBI # NP_689479) as a potential HEF partner. We re-designated MGC32020 as HIP (HEF Interacting Protein) based on the experiments described below. The *HIP* gene localises to chromosome 19 and encodes a 215 amino acid protein, which has a predicted molecular weight of 24 kDa. HIP is 20% identical and 31% similar to the C-terminal 300 amino acids of human HEF (Figure 5.2). Human HIP orthologues can be found exclusively in vertebrates, such as *B. taurus*, *M. musculus*, *D. rerio*, *G. gallus* and *X. leavis* (Appendix 1, Figure 10). We were not able to identify HIP orthologues in species that express proteins lacking the C-

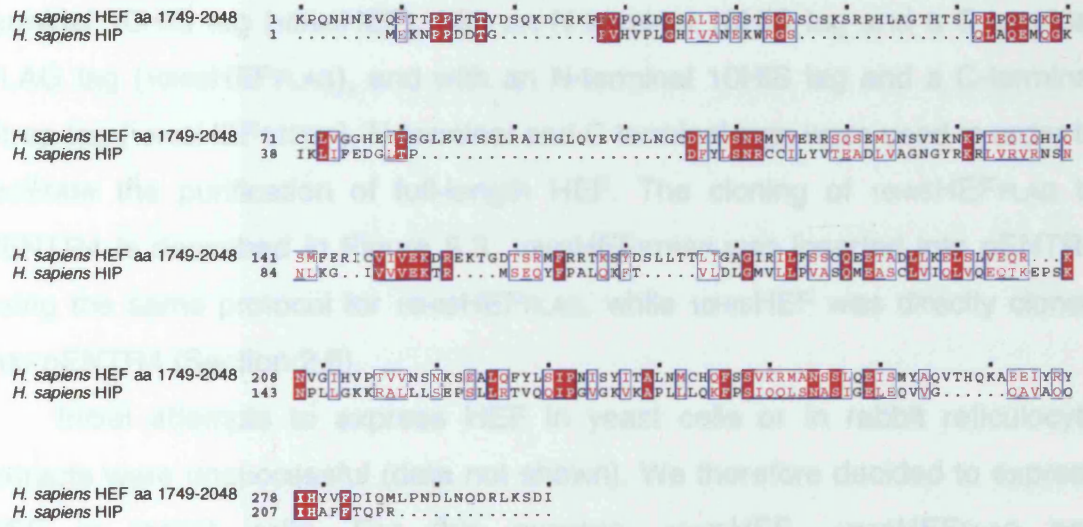

FIGURE 5.2: Sequence alignment between the C-terminus of *H. sapiens* HEF (amino acids 1749-2048) and *H. sapiens* HIP

Sequence alignments were carried out as using ClustalW.

terminal ERCC4 nuclease domain of HEF, such as *D. melanogaster* CG7922 and *S. cerevisiae* Mph1 proteins.

III. INTERACTION OF HUMAN HIP WITH HEF

In order to test whether HIP was forming a complex with HEF, we expressed and purified HEF alone or in the presence of HIP. Three different HEF constructs were cloned into the Gateway entry vector pENTR4: HEF with an N-terminal 10HIS tag (10HISHEF), with an N-terminal 10HIS tag and a C-terminal FLAG tag (10HISHEFFLAG), and with an N-terminal 10HIS tag and a C-terminal Strep tag (10HISHEFSTREP). N-terminal and C-terminal tags were used in order to facilitate the purification of full-length HEF. The cloning of 10HISHEFFLAG in pENTR4 is described in Figure 5.3. 10HISHEFSTREP was inserted into pENTR4 using the same protocol for 10HISHEFFLAG, while 10HISHEF was directly cloned into pENTR4 (Section 2.6).

Initial attempts to express HEF in yeast cells or in rabbit reticulocyte extracts were unsuccessful (data not shown). We therefore decided to express HEF in insect cells. For this purpose, 10HISHEF, 10HISHEFFLAG and 10HISHEFSTREP were recombined from the Gateway entry vector pENTR4 into the expression vector pDEST8 (Section 2.6). pDEST8-10HISHEF, pDEST8-10HISHEFFLAG and pDEST8-10HISHEFSTREP were used to generate three baculoviruses expressing 10HISHEF, 10HISHEFFLAG and 10HISHEFSTREP, respectively (Section 2.23). 10HISHEF, 10HISHEFFLAG and 10HISHEFSTREP were all expressed equally well in High Five insect cells, as detected by immunoblotting with anti-HEF SWE98 antibody (Figure 5.4A, lanes a, b and c, respectively) and anti-HIS tag antibody (data not shown). Anti-HEF antibody, in addition to detecting the full-length 10HISHEF, 10HISHEFFLAG and 10HISHEFSTREP (approximately 250 kDa), recognised several smaller bands that are most likely HEF degradation products. Anti-FLAG antibody specifically recognised 10HISHEFFLAG (Figure 5.4B, lane b), while anti-Strep tag antibody failed to detect 10HISHEFSTREP (data not shown). We therefore focused our attention on the baculovirus expressing 10HISHEFFLAG.

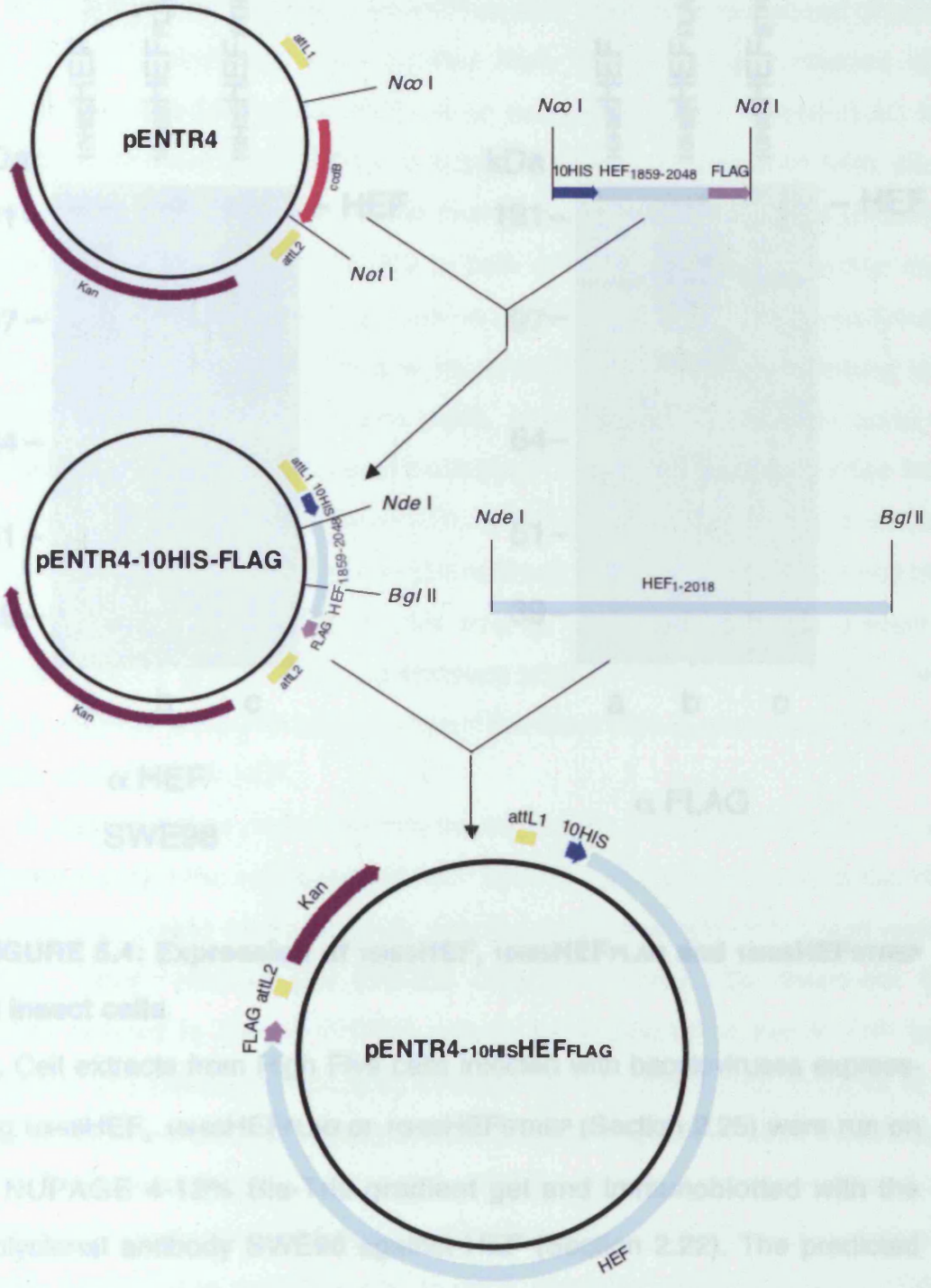
pENTR4
attL1
Nco I
ccdB
attL2
Not I
Kan
Nco I
Not I
10HIS HEF1859-2048 FLAG
pENTR4-10HIS-FLAG
attL1 10HIS
Nde I
HEF1859-2048
Bgl II
FLAG
attL2
Kan
Nde I
Bgl II
HEF1-2018
attL1
10HIS
Kan
FLAG attL2
pENTR4-10HISHEFFLAG
HEF

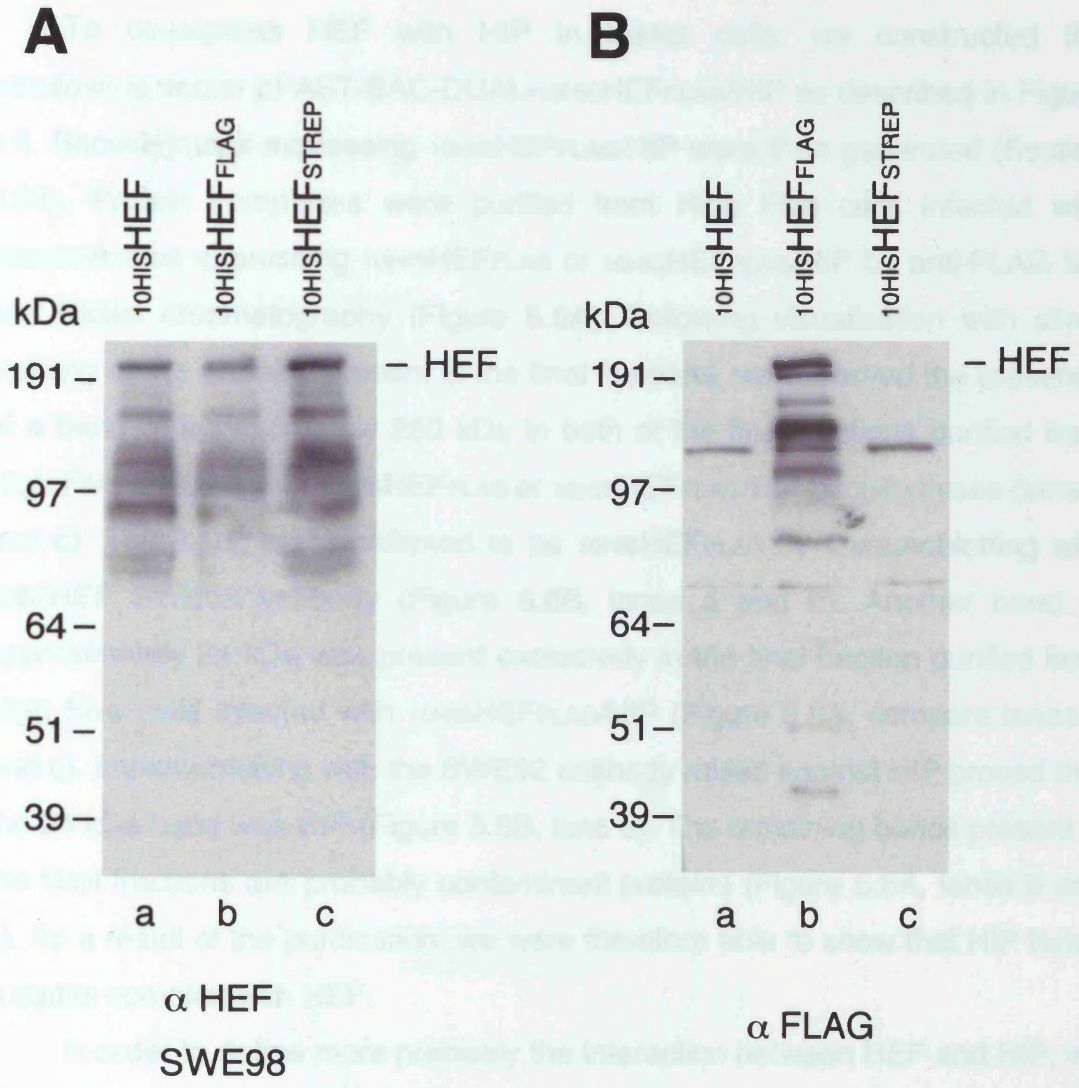

FIGURE 5.4: Expression of 10HISHEF, 10HISHEFFLAG and 10HISHEFSTREP in insect cells

A. Cell extracts from High Five cells infected with baculoviruses expressing 10HISHEF, 10HISHEFFLAG or 10HISHEFSTREP (Section 2.25) were run on a NUPAGE 4-12% Bis-Tris gradient gel and immunoblotted with the polyclonal antibody SWE98 against HEF (Section 2.22). The predicted molecular weight for 10HISHEF, 10HISHEFFLAG or 10HISHEFSTREP (lanes a, b and c, respectively) is approx 250 kDa.

B. Cell extracts described in (A) were immunoblotted with anti-FLAG antibody (Section 2.22).

To co-express HEF with HIP in insect cells, we constructed the baculovirus vector pFAST-BAC-DUAL-$_{10HIS}$HEF$_{FLAG}$/HIP as described in Figure 5.5. Baculoviruses expressing $_{10HIS}$HEF$_{FLAG}$/HIP were then generated (Section 2.23). Protein complexes were purified from High Five cells infected with baculoviruses expressing $_{10HIS}$HEF$_{FLAG}$ or $_{10HIS}$HEF$_{FLAG}$/HIP by anti-FLAG M2 and Nickel chromatography (Figure 5.6A). Following visualisation with silver staining of the proteins present in the final fractions, we observed the presence of a band of approximately 250 kDa in both of the final fractions purified from High Five infected with $_{10HIS}$HEF$_{FLAG}$ or $_{10HIS}$HEF$_{FLAG}$/HIP baculoviruses (lane b and c). This band was confirmed to be $_{10HIS}$HEF$_{FLAG}$ by immunoblotting with anti-HEF SWE98 antibody (Figure 5.6B, lanes a and b). Another band of approximately 24 kDa was present exclusively in the final fraction purified from High Five cells infected with $_{10HIS}$HEF$_{FLAG}$/HIP (Figure 5.6A, compare lanes b and c). Immunoblotting with the SWE92 antibody raised against HIP proved that the 24 kDa band was HIP (Figure 5.6B, lane b). The remaining bands present in the final fractions are probably contaminant proteins (Figure 5.6A, lanes b and c). As a result of the purification, we were therefore able to show that HIP forms a stable complex with HEF.

In order to define more precisely the interaction between HEF and HIP, we analysed in detail the sequences of HEF and HIP. As indicated previously, HIP was identified based on its similarity with the C-terminal 300 amino acid region of HEF, which contains the ERCC4 nuclease domain. To determine the domains present in HIP, a PHYRE search for structures similar to HIP was performed. We identified a similarity between HIP and the crystal structure of *A. pernix* XPF (Newman et al., 2005). As observed with ERCC1, EME1, EME2 and HEF, HIP appears to have an inactive ERCC4 nuclease domain (Figure 5.1). The PHYRE server also predicted the presence of 2 HhH motifs both in HIP and in HEF. According to previous reports on *P. furiosus* Hef (Nishino et al., 2003; Nishino et al., 2005a), we expect that the ERCC4 domain and the HhH motifs are necessary for the interaction between HEF and HIP.

To test this hypothesis, we constructed a bicistronic bacterial vector to co-express HIP and a 322 amino acid region of HEF ($HEF_{1727-2048}$) containing both

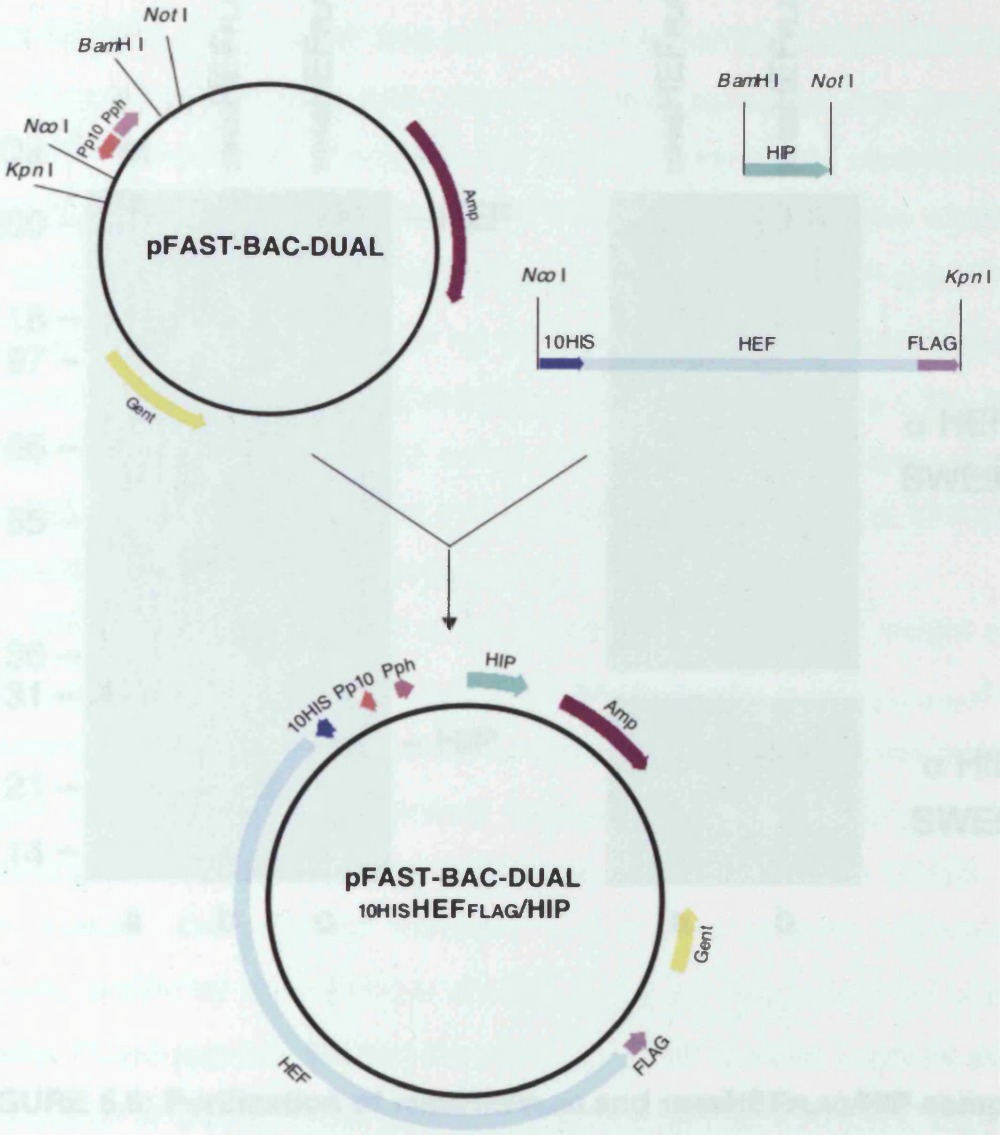

FIGURE 5.5: Construction of the baculovirus vector pFAST-BAC-DUAL-10HISHEFFLAG/HIP

HIP was cloned into the *Bam*H I and *Not* I sites of pFAST-BAC-DUAL followed by the insertion of 10HISHEFFLAG into the *Nco* I and *Kpn* I sites to generate the vector pFAST-BAC-DUAL-10HISHEFFLAG/HIP (Section 2.6). p10 promoter (Pp10), polyhedrin promoter (Pph), Ampicillin resistance (Amp), Gentamicin resistance (Gent), 10HIS tag (10HIS), FLAG tag (FLAG), HEF and HIP are indicated.

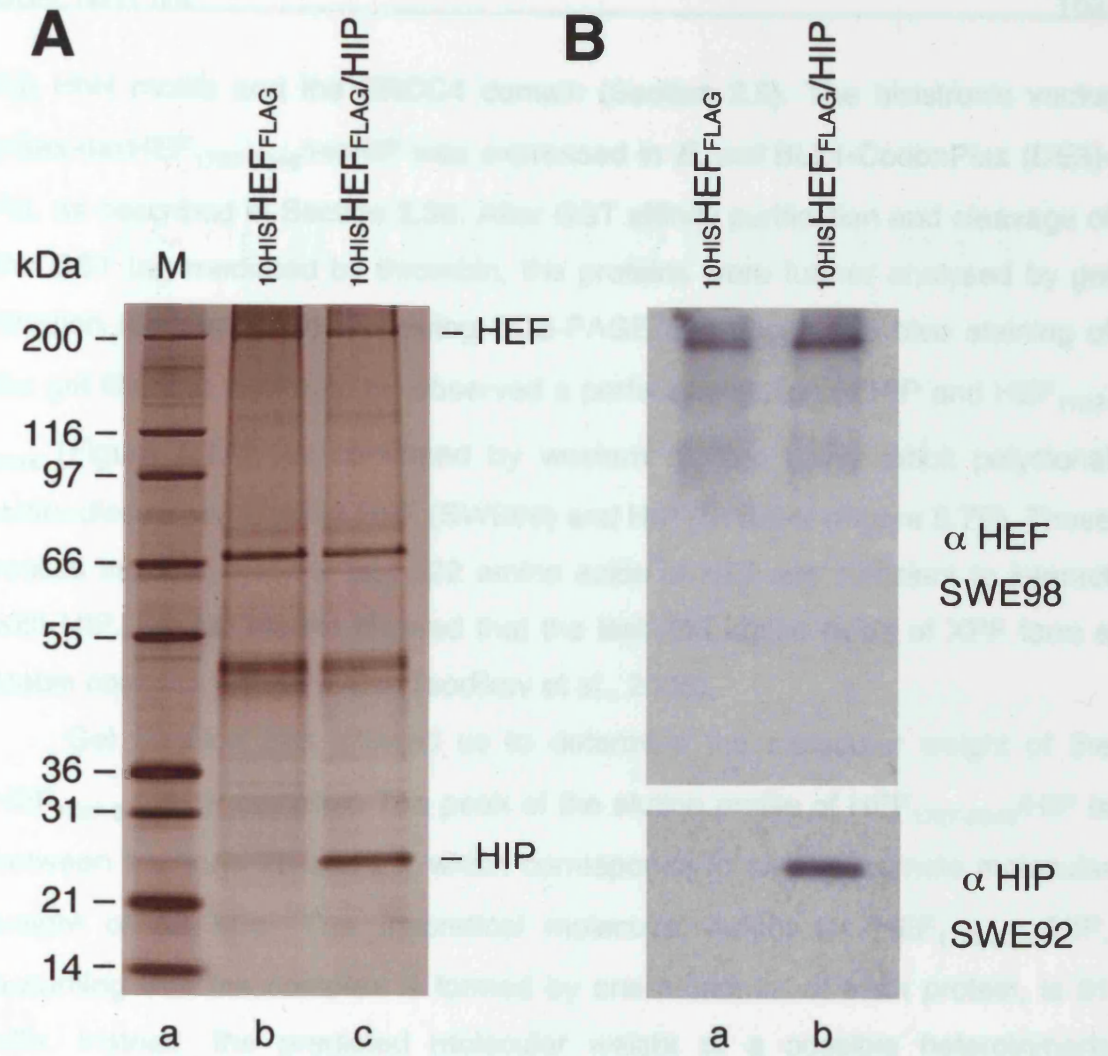

FIGURE 5.6: Purification of 10HISHEFFLAG and 10HISHEFFLAG/HIP complex from insect cells

A. Cell extracts from High Five cells infected with baculoviruses expressing 10HISHEFFLAG or 10HISHEFFLAG/HIP were subjected to anti-FLAG M2 chromatography followed by Nickel chromatography as described in Sections 2.36 and 2.37. Final fractions of 10HISHEFFLAG or 10HISHEFFLAG/HIP were pooled, run on a NUPAGE 4-12% Bis-Tris gradient gel and the proteins were visualised by silver staining (lanes b and c).

B. Final fractions of 10HISHEFFLAG or 10HISHEFFLAG/HIP described in (A) were immunoblotted with SWE98 and SWE92 antibodies against HEF and HIP, respectively (Section 2.22).

the HhH motifs and the ERCC4 domain (Section 2.6). The bicistronic vector pGex-GSTHEF$_{1727-2048}$/HISHIP was expressed in *E. coli* BL21-CodonPlus (DE3)-RIL as described in Section 2.38. After GST affinity purification and cleavage of the GST tag mediated by thrombin, the proteins were further analysed by gel filtration (Section 2.38). Following SDS-PAGE and coomassie blue staining of the gel filtration fractions, we observed a perfect co-elution of HIP and HEF$_{1727-2048}$ (Figure 5.7A), as confirmed by western blotting using rabbit polyclonal antibodies raised against HEF (SWE98) and HIP (SWE94) (Figure 5.7B). These results indicate that the last 322 amino acids of HEF are sufficient to interact with HIP. Similar results showed that the last 250 amino acids of XPF form a stable complex with ERCC1 (Tsodikov et al., 2005).

Gel filtration has allowed us to determine the molecular weight of the HEF$_{1727-2048}$/HIP complex. The peak of the elution profile of HEF$_{1727-2048}$/HIP is between fractions 28 and 29, which corresponds to an approximate molecular weight of 80 kDa. The theoretical molecular weight for HEF$_{1727-2048}$/HIP, assuming that the complex is formed by one monomer of each protein, is 61 kDa. Instead, the predicted molecular weight of a possible heterotrimeric complex formed by one monomer of HEF$_{1727-2048}$ and two monomers of HIP is 85 kDa. These data indicate that the HEF$_{1727-2048}$/HIP complex might be either a heterotrimer or a heterodimer with a slightly extended conformation. We favour the latter hypothesis, based on the observation that other members of the MUS81 family, such as XPF and ERCC1, form a 1:1 heterodimeric complex, as determined by gel filtration analysis and crystallographic studies (Choi et al., 2005; Tripsianes et al., 2005).

IV. ACTIVITY TEST FOR HEF$_{1727-2048}$/HIP

As previously mentioned, it has been hypothesised that the ERCC4 domain of HEF is inactive due to the mutation of the catalytic domain ER<u>K</u>X$_3$<u>D</u> to ER<u>R</u>X$_3$<u>E</u>. However, the substitutions of Lysine (K) into Arginine (R) and Aspartate (D) into

FIGURE 5.7: Gel filtration profile of the $HEF_{1727-2048}$/HIP complex

A. $HEF_{1727-2048}$/HIP complex was purified by gel filtration chromatography as described in Section 2.38. Fractions 21 to 34 were run on a NUPAGE 4-12% Bis-Tris gradient gel and the proteins were visualised by Coomassie blue staining. The positions of the gel filtration markers are indicated in red.

B. Gel filtration fractions of $HEF_{1727-2048}$/HIP described in (A) were immunoblotted with SWE98 and SWE94 antibodies against HEF and HIP, respectively (Section 2.22).

Glutamate (E) could be conservative, because both K and R are positively charged amino acids and both D and E are negatively charged. To determined whether HEF has nuclease activity, the activity of $HEF_{1727-2048}$/HIP complex was assayed. The activity of the full-length HEF/HIP complex has not yet been tested because the large molecular weight of HEF has prevented the purification of sufficient amount of full-length HEF/HIP complex from insect cells. However, in the case of XPF, it was previously reported that a complex between the last 250 amino acids of XPF ($XPF_{\Delta 655}$) and the last 202 amino acids of ERCC1 ($ERCC1_{\Delta 95}$) exhibits the same nuclease activity as full length XPF/ ERCC1, although the cleavage efficiency of $XPF_{\Delta 655}$/$ERCC1_{\Delta 95}$ is significantly reduced (Tsodikov et al., 2005). In the same study it was noted that a fraction of $XPF_{\Delta 655}$/$ERCC1_{\Delta 95}$ complex formed inactive aggregates, such that it was necessary to purify the heterodimeric fraction of the $XPF_{\Delta 655}$/$ERCC1_{\Delta 95}$ complex (Tsodikov et al., 2005). In order to purify $HEF_{1727-2048}$/HIP without nuclease contaminations, the bicistronic vector pGex-GSTHEF$_{1727-2048}$/HISHIP was expressed in *E. coli* STL5827 BL21 (DE3)-ExoI$^-$ EndoI$^-$ (Section 2.4). $HEF_{1727-2048}$/HIP was then purified by GST affinity chromatography followed by thrombin cleavage of the GST tag and gel filtration (Section 2.38). Purified $HEF_{1727-2048}$/HIP was assayed on 3'-flap substrate but no nuclease activity was detected (Figure 5.8, lane b). Similar results were obtained with splayed arm and replication fork substrates (data not shown). We think it is unlikely that the absence of nuclease activity is due to the use of inappropriate substrates. As previously shown, MUS81/EME1 (or EME2) is able to efficiently cleave 3'-flap and replication fork substrates (Figure 5.8, lane c; Figure 3.6, lanes j and o; Figure 4.5, lanes b and d) and XPF/ERCC1 has been reported to nick splayed arm and 3'-flap substrates (De Laat et al., 1998a). Based on these considerations, we assumed that if HEF has nuclease activity, it should be able to process substrates cleaved by the related nucleases MUS81 and XPF. In addition to that, we do not think that $HEF_{1727-2048}$/HIP is inactive because HEF is not full-length. As mentioned above, in the case of XPF, the fraction of

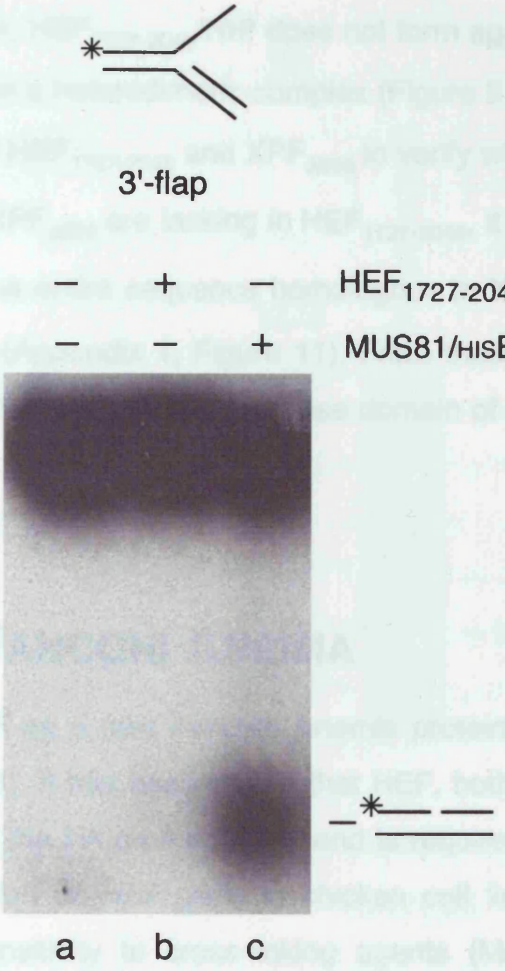

FIGURE 5.8: Activity test for $HEF_{1727-2048}$/HIP complex on 3'-flap substrate

Reactions contained ^{32}P-labelled synthetic 3'-flap substrate (approx 3 ng) and purified $HEF_{1727-2048}$/HIP complex (50 nM; lane b) or purified MUS81/HISEME1 (50 nM; lane c). $HEF_{1727-2048}$/HIP and MUS81/HISEME1 were purified as described in Sections 2.38 and 2.31, respectively. Reactions were incubated at 37°C for 30 min (Section 2.45). DNA products were analysed by neutral PAGE followed by autoradiography. ^{32}P-labels are indicated with asterisks.

$XPF_{\Delta 655}$/$ERCC1_{\Delta 95}$ that forms a heterodimeric complex is active (Tsodikov et al., 2005). In our preparation, $HEF_{1727-2048}$/HIP does not form aggregates and is present in what is likely to be a heterodimeric complex (Figure 5.7A). Moreover, if we align the sequences of $HEF_{1727-2048}$ and $XPF_{\Delta 655}$ to verify whether potential critical residues present in $XPF_{\Delta 655}$ are lacking in $HEF_{1727-2048}$, it can be noticed that $HEF_{1727-2048}$ contains the entire sequence homologous to $XPF_{\Delta 655}$ with the addition of 77 amino acids (Appendix 1, Figure 11). From these observations, we can therefore conclude that the ERCC4 nuclease domain of HEF is likely to be inactive.

V. HEF/HIP AND FANCONI ANEMIA

Recent reports identify HEF as a new Fanconi Anemia protein (Meetei et al., 2005; Mosedale et al., 2005). It has been shown that HEF, both in human and chicken cell lines, is part of the FA core complex and is required for FANC-D2 monoubiquitination. Disruption of *HEF* gene in chicken cell lines resulted in genomic instability and sensitivity to cross-linking agents (Mosedale et al., 2005). *HEF* has been re-designated *FANC-M* because it is defective in the FA complementation group M (Meetei et al., 2005). In addition, FLAGFANC-M purified from human cells was shown to have translocase but not helicase activity, which is mediated by the DEAH helicase domain (Meetei et al., 2005).

The identification of HEF as FANC-M raised the possibility that HIP could also be part of the FA pathway. In order to investigate whether HIP could interact with HEF/FANC-M and other FA proteins *in vivo*, antibodies against HEF/FANC-M and HIP were raised. Anti-HEF/FANC-M SWE98 and anti-HIP SWE94 recognised full-length HEF/FANC-M (approximately 250 kDa; Figure 5.9A) and HIP (approximately 24 kDa; Figure 5.9B) from HeLa cell extracts, respectively.

In collaboration with Weidong Wang (National Institute of Aging/NIH) we have shown that HIP interacts with HEF/FANC-M *in vivo* when immunocomplexes from cells stably expressing FLAGHEF/FANC-M were

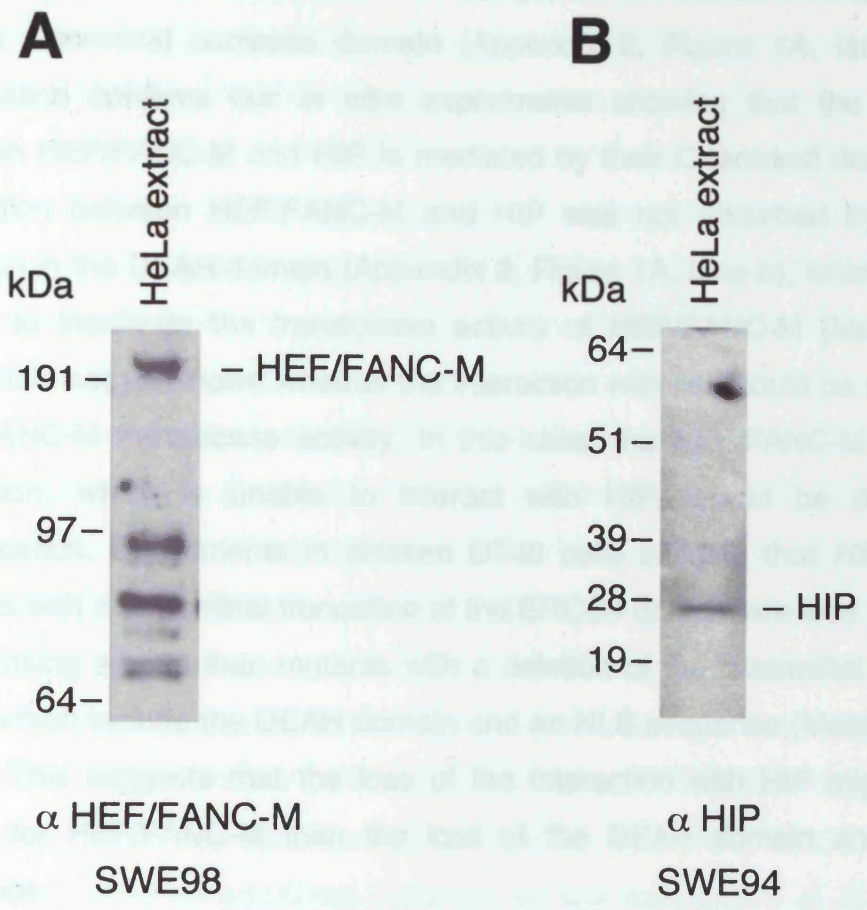

FIGURE 5.9: Visualisation of HEF/FANC-M and HIP by western blotting of HeLa extract

A. HeLa extract (Section 2.41) was run on a NUPAGE 4-12% Bis-Tris gradient gel and immunoblotted with the rabbit polyclonal antibody SWE98 raised against GSTHEF$_{1727-2048}$ (Section 2.22). The predicted molecular weight for HEF/FANC-M is 250 kDa.

B.The HeLa extract described in (A) was immunoblotted with rabbit polyclonal antibody SWE94 raised against HISHIP (Section 2.22). The predicted molecular weight for HIP is 24 kDa.

immunoprecipitated with anti-FLAG antibody (Appendix 2, Figure 1A, lane a). Interestingly, HIP did not interact with complexes of FLAGHEF/FANC-M deleted for the C-terminal nuclease domain (Appendix 2, Figure 1A, lane c). This observation confirms our *in vitro* experiments showing that the interaction between HEF/FANC-M and HIP is mediated by their C-terminal domains. The interaction between HEF/FANC-M and HIP was not disturbed by a K117R mutation in the DEAH domain (Appendix 2, Figure 1A, lane b), which has been shown to inactivate the translocase activity of HEF/FANC-M (Meetei et al., 2005). It is not yet known whether the interaction with HIP could be required for HEF/FANC-M translocase activity. In this case, the HEF/FANC-M C-terminal truncation, which is unable to interact with HIP, would be defective in translocation. Experiments in chicken DT40 cells indicate that *HEF/FANC-M* mutants with a C-terminal truncation of the ERCC4 domain are less sensitive to cross-linking agents than mutants with a deletion of the N-terminal 725 amino acids, which include the DEAH domain and an NLS sequence (Mosedale et al., 2005). This suggests that the loss of the interaction with HIP might be less critical for HEF/FANC-M than the loss of the DEAH domain and the NLS sequence.

To test whether HEF/FANC-M and HIP are part of the same complex in mammalian cells, HeLa nuclear extracts were fractionated by gel filtration chromatography. As shown in Appendix 2, Figure 1B, HEF/FANC-M and HIP co-fractionated in a single peak, with an apparent molecular weight of 800 kDa. Because the calculated molecular weight of the complex between HEF/FANC-M and HIP is approximately 275 kDa, this result suggests that HEF/FANC-M and HIP belong to a high molecular weight complex.

To identify the components of the HEF/FANC-M high molecular weight complex, the peak gel filtration fractions containing HEF/FANC-M were collected and immunoprecipitated with a rabbit polyclonal antibody raised against HEF/FANC-M (Meetei et al., 2005). About 10 major polypeptides were obtained based on SDS-PAGE followed by Coomassie blue staining (Appendix 2, Figure 2A, lane b). Mass spectrometric analysis identified the major polypeptide with an apparent molecular weight of about 250 kDa as

HEF/FANCM. Three other major polypeptides between 40-60 kDa were similarly identified as FANC-C, FANC-E and FANC-F, all of which are components of the FA core complex. Other FA core components, such as FANC-A, FANC-G, FANC-B and FANC-L were identified by immunoblotting analysis (Appendix 2, Figure 2B, lane a). The fact that HEF/FANCM co-immunoprecipitates with multiple components of the core complex is consistent with the previous data showing that HEF/FANCM is an integral part of the FA core complex (Meetei et al., 2005). It also implies that the other major polypeptides isolated could be components of the same complex.

Mass spectrometry also identified the 75 kDa polypeptide as the BLAP75 protein (Appendix 2, Figure 2A, lane b), which interacts with BLM/TOPOIIIα complex (Yin et al., 2005) and stimulates the Holliday junction dissolution activity of BLM/TOPOIIIα by recruiting TOPOIIIα to dHJs (Wu et al., 2006). BLAP75 has been previously identified in the FA core complex purified by the FANCA antibody (Meetei et al., 2003b). We have also detected the presence of BLM and TOPOIIIα in the immunoprecipitate by HEF/FANCM antibody (data not shown). Thus, the identification of BLAP75 as a HEF/FANCM-associated polypeptide provides additional evidence for the association of BLM and FA complexes.

In addition to the FA core components and BLAP75, mass spectrometric analysis identified the 25 kDa polypeptide as HIP (Appendix 2, Figure 2A, lane b). HIP was also detected by immunoblotting of the HEF/FANC-M immunocomplex with the anti-HIP SWE94 antibody (Appendix 2, Figure 2B, lane a). In order to confirm the possibility that HIP might be part of the FA core complex, nuclear extracts were immunoprecipitated with the anti-HIP SWE94 antibody and immunoblotted for FA core components. As shown in Appendix 2, Figure 2B, HIP immunocomplexes contained the FA core complex proteins HEF/FANC-M, FANC-A, FANC-B, FANC-G and FANC-L (lane b). Similarly, HIP and the FA core components were detected in the FANC-A immunocomplexes (Appendix 2, Figure 2B, lane c). Altogether, these results suggest that HIP is a novel component of the FA core complex.

The FA core complex is required for FANC-D2 monoubiquitination after treatment with cross-linking agents and for subsequent FANC-D2 localisation to foci together with BRCA1, BRCA2/FANC-D1 and RAD51 (Section 1.6). The absence of any of the Fanconi core complex proteins results in impaired FANC-D2 monoubiquitination. To determine whether depletion of HIP results in defective FANC-D2 monoubiquitination after cross-linking agent treatment, mammalian cells were transfected with siRNA oligonucleotides against HIP and control siRNA (Appendix 2, Figure 3). After treatment with MMC, cells were lysed and the protein lysate was immunblotted for HEF/FANC-M, FANC-D2 and HIP. Preliminary data indicate that depletion of HIP with both siRNA resulted in reduced FANC-D2 monoubiquitination and reduced HEF/FANC-M hyper-phosphorylation after MMC treatment (Appendix 2, Figure 3, compare lanes d and f with b). Because HIP has no recognisable kinase domain, HIP might affect HEF/FANC-M hyper-phosphorylation indirectly. HEF/FANC-M hyper-phosphorylation was shown to be stimulated in response to genotoxic stress, such as MMC or HU (Meetei et al., 2005), but the function of this HEF/FANC-M modification is still unknown. Future experiments using *HIP*$^{-/-}$ cell lines will be necessary to confirm whether HIP is required for FANC-D2 monoubiquitination and HEF/FANC-M hyper-phosphorylation.

Among the twelve FA complementation groups so far classified, only the *FANC-I* gene remains to be identified (Section 1.6). To test whether *HIP* might correspond to *FANC-I*, FANC-I patients were screened for *HIP* mutations in collaboration with Johan De Winter and Hans Joenje (Free University Medical Center, Amsterdam). However, no defects in the *HIP* gene or in HIP protein levels were detected in FANC-I patients (data not shown). In contrast, two independent cell lines from FANC-B patients displayed reduced protein levels of both HEF/FANC-M and HIP (Appendix 2, Figure 4, compare lanes e, f, g and h with a and b). Similarly, reduced levels of FANC-L have been detected in cell lines depleted for FANC-B (Meetei et al., 2004). These results indicate that FANC-B might be required for the stabilisation of FANC-L (Section 1.6), and it is possible that FANC-B could also regulate the stability of HEF/FANC-M and HIP proteins. The observation that HIP is unaffected even in the absence of

HEF/FANC-M (Appendix 2, Figure 4, compare lanes c and d with a and b) indicates that the decreased levels of HIP in FANC-B cells might not simply be a consequence of HEF/FANC-M destabilisation. Taken together, these data provide evidence that HIP is an integral part of the FA core complex.

VI. THE MUS81 FAMILY OF PROTEINS

Based on our database searches, we have identified four novel members of the human MUS81 family: EME1, EME2, HEF and HIP (Figure 5.1). We and others have previously described four interactions among the members of the MUS81 family: MUS81/EME1 (Chapter 3), MUS81/EME2 (Chapter 4), XPF/ERCC1 (Sijbers et al., 1996a) and HEF/HIP (Chapter 5). In order to test whether additional interactions are present among the MUS81 family of proteins, bicistronic vectors were constructed to co-express twelve combinations of the MUS81 family of proteins in *E. coli* (Figure 5.10 and Section 2.6). Due to the difficulty of expressing large proteins such as HEF and XPF in bacteria (250 kDa and 110 kDa, respectively), C-terminal fragments encoding $HEF_{1727-2048}$ and $XPF_{606-905}$ were cloned in the expression vector pGex-BICIS-HIS (Section 2.6). $XPF_{606-905}$, $HEF_{1727-2048}$ or MUS81 were expressed as N-terminal GST-tagged proteins in combination with EME1, EME2, HIP or ERCC1, all HIS-tagged in their N-termini. All proteins expressed equally well, as detected by western blotting with antibodies against the GST tag, EME1, EME2, HIP and ERCC1 (Figure 5.11A). Two forms of EME2 were visualised by immunoblotting, the lower form probably being a degradation product. Cell-free extracts from *E. coli* strains carrying the twelve bicistronic vectors were subjected to GST pull-downs with GST-sepharose beads and protein complexes were immunoblotted with antibodies against the GST tag, EME1, EME2, HIP and ERCC1 (Figure 5.11B). As expected, we observed that HISEME2 preferentially interacted with GSTMUS81 (compare lane j with b and f), HISERCC1 with $GSTXPF_{606-905}$ (compare lane d with h and l) and HISHIP with $GSTHEF_{1727-2048}$ (compare lane g with c and k). Coomassie blue staining of the GST pull-down complexes (Figure

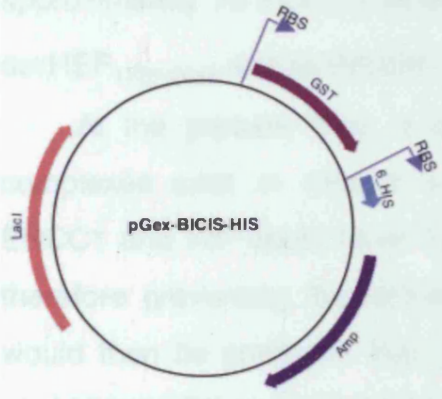

1) pGex-GSTXPF$_{606-905}$/HISEME1

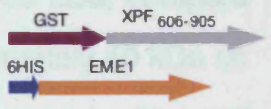

2) pGex-GSTXPF$_{606-905}$/HISEME2

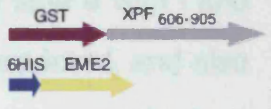

3) pGex-GSTXPF$_{606-905}$/HISHIP

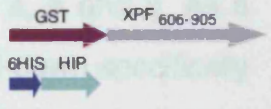

4) pGex-GSTXPF$_{606-905}$/HISERCC1

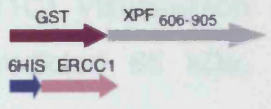

5) pGex-GSTHEF$_{1727-2048}$/HISEME1

6) pGex-GSTHEF$_{1727-2048}$/HISEME2

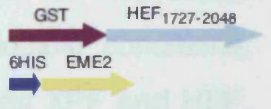

7) pGex-GSTHEF$_{1727-2048}$/HISHIP

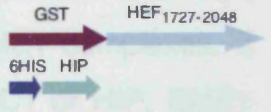

8) pGex-GSTHEF$_{1727-2048}$/HISERCC1

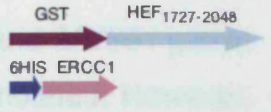

9) pGex-GSTMUS81/HISEME1

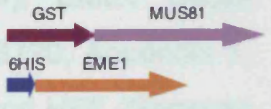

10) pGex-GSTMUS81/HISEME2

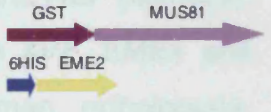

11) pGex-GSTMUS81/HISHIP

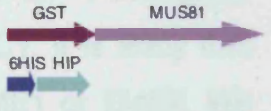

12) pGex-GSTMUS81/HISERCC1

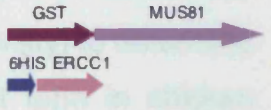

5.12) confirmed that HISEME2 (approximately 41 kDa) specifically interacted with GSTMUS81 (approximately 87 kDa; compare lane k with c and g), HISHIP (approximately 24 kDa) with GSTHEF$_{1727-2048}$ (approximately 63 kDa; compare lane h with d and l) and HISERCC1 (predicted 32 kDa, approximately 40 kDa on SDS gel) with GSTXPF$_{606-905}$ (approximately 65 kDa; compare lane e with i and m). In contrast, HISEME1 co-precipitated with GSTMUS81, as expected, and also with GSTXPF$_{606-905}$ and GSTHEF$_{1727-2048}$ (Figure 5.11B, lanes a, e and i). As a control, we showed that HISEME1 expressed alone was pulled-down specifically by Nickel beads and not by GST-sepharose beads (Figure 5.11C). Visualisation by Coomassie blue staining confirmed that HISEME1 (predicted 65 kDa, approximately 75 kDa on SDS gel) interacted equally well with GSTXPF$_{606-905}$, GSTHEF$_{1727-2048}$ and GSTMUS81 (Figure 5.12, lanes b, f and j).

At the present time, it is unknown whether XPF/EME1 or HEF/EME1 complexes exist *in vivo*. It is possible that, under physiological conditions, ERCC1 and HIP could have higher affinity than EME1 towards XPF and HEF, therefore preventing the formation of XPF/EME1 or HEF/EME1 complexes. It would then be predicted that, in the absence of either ERCC1 or HIP, EME1 could bind XPF or HEF. Interestingly, in chicken no *ERCC1* and *MUS81* genes have been reported, although the genome has been fully annotated. However, there are genes coding for XPF (NCBI # XP_414734), EME1 (NCBI #XP_420107, Appendix 1, Figure 2), EME2 (NCBI # XP_593720, Appendix 1, Figure 7), HIP (NCBI # XP_414132, Appendix 1, Figure 10) and HEF (Genscan gene prediction chr5_12.11, Appendix 1, Figure 9). Chicken XPF, EME1 and EME2 are 76%, 49% and 49% identical to their human orthologues, respectively. Due to the absence of both MUS81 and ERCC1, it is likely that chicken XPF could form a functional complex either with EME1 or EME2. We are currently collaborating with Shunichi Takeda (Kyoto University) to determine whether active XPF/EME1 or XPF/EME2 complexes might form in chicken DT40 cell lines. It is tempting to speculate, based on our interactions studies, that in mammalian cells, under pathological conditions leading to inactivation

sample buffer and

MTA31 7H2.

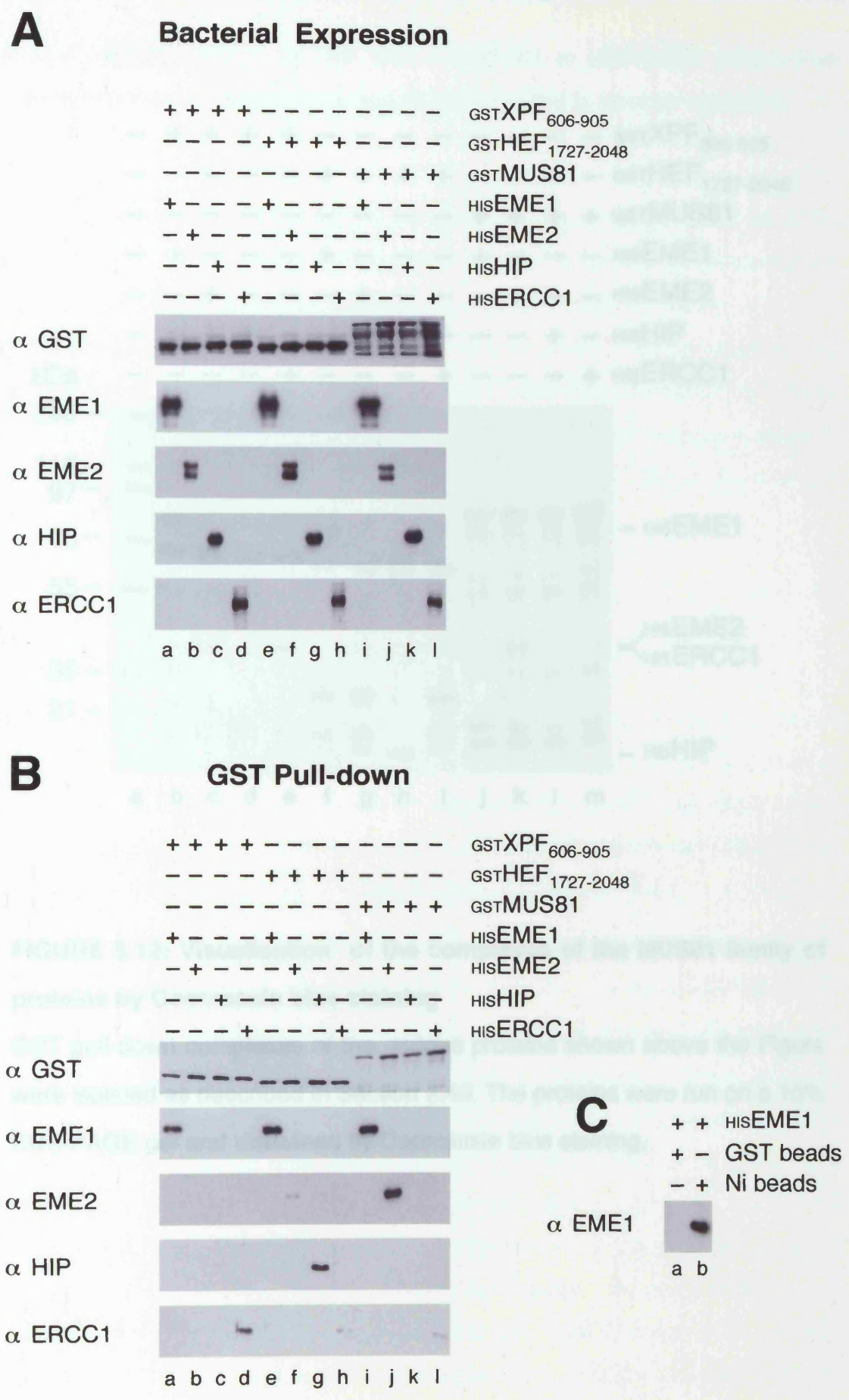
A
Bacterial Expression
+ + + + − − − − − − − − GSTXPF606-905
− − − − + + + + − − − − GSTHEF1727-2048
− − − − − − − − + + + + GSTMUS81
+ − − − + − − − + − − − HISEME1
− + − − − + − − − + − − HISEME2
− − + − − − + − − − + − HISHIP
− − − + − − − + − − − + HISERCC1
α GST
α EME1
α EME2
α HIP
α ERCC1
a b c d e f g h i j k l
B
GST Pull-down
+ + + + − − − − − − − − GSTXPF606-905
− − − − + + + + − − − − GSTHEF1727-2048
− − − − − − − − + + + + GSTMUS81
+ − − − + − − − + − − − HISEME1
− + − − − + − − − + − − HISEME2
− − + − − − + − − − + − HISHIP
− − − + − − − + − − − + HISERCC1
α GST
α EME1
α EME2
α HIP
α ERCC1
a b c d e f g h i j k l
C
+ + HISEME1
+ − GST beads
− + Ni beads
α EME1
a b

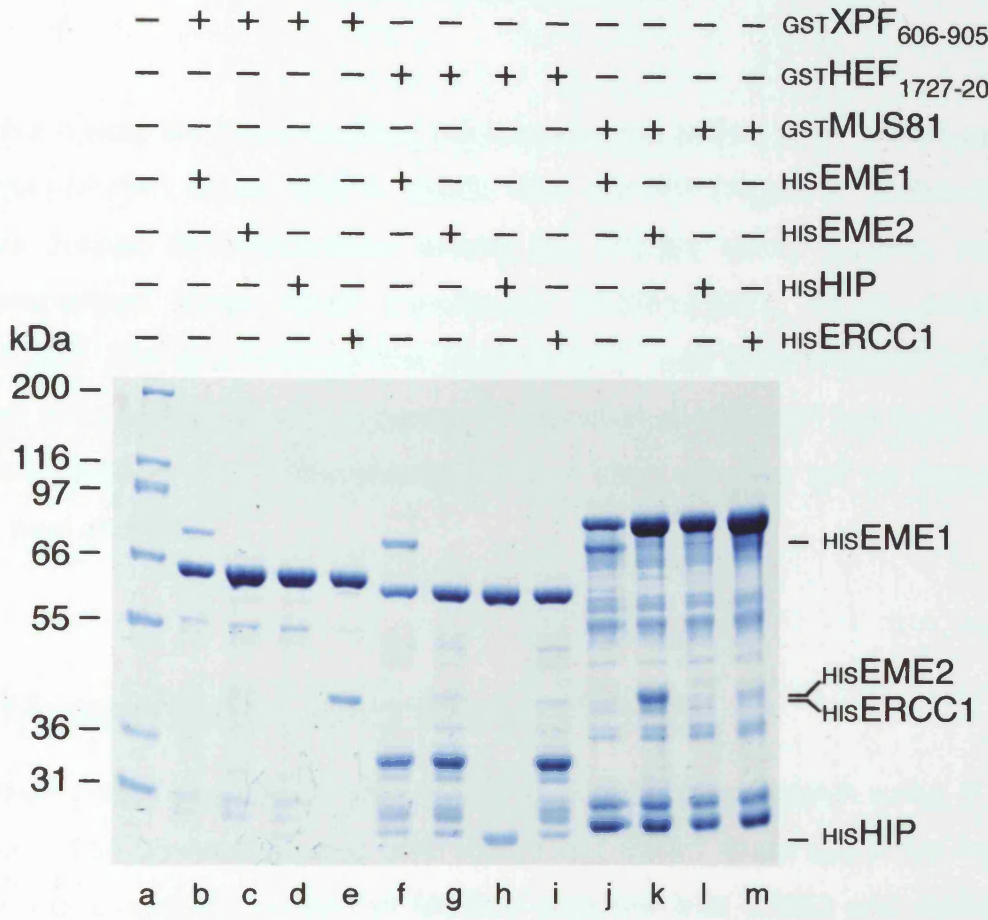

FIGURE 5.12: Visualisation of the complexes of the MUS81 family of proteins by Coomassie blue staining

GST pull-down complexes of the various proteins shown above the Figure were isolated as described in Section 2.40. The proteins were run on a 10% SDS-PAGE gel and visualised by Coomassie blue staining.

either of MUS81, ERCC1 or HIP, new XPF/EME1 or HEF/EME1 heterodimer could form. Whether these complexes might be active is an open question.

CHAPTER SIX

Discussion

In this thesis, we have reported the identification of four novel members of the human MUS81 family: EME1, EME2, HEF and HIP (Figure 5.1). Moreover, we have defined the interactions among the MUS81 family proteins and have characterised three novel complexes: MUS81/EME1, MUS81/EME2 and HEF/HIP. The properties of the MUS81/EME1 and MUS81/EME2 complexes have been studied *in vitro*, whereas the function of HEF/HIP has been primarily investigated *in vivo*. The characteristics of each complex will be discussed in the next sections.

I. MUS81/EME1 AND MUS81/EME2

Human *EME1* and *EME2* were identified in a database search using *S. pombe EME1*. The observation that both EME1 and EME2 share sequence homology with the C-terminal portion of MUS81 suggests that *EME1* and *EME2* might have evolved from gene duplication of the 3'-region of *MUS81*, as proposed for *ERCC1* and *XPF* (Aravind et al., 1999; Gaillard and Wood, 2001).

MUS81/EME1 and MUS81/EME2 heterodimeric complexes contain a single subunit (MUS81) with an active ERCC4 nuclease domain. This characteristic is typical of all of the MUS81 family of proteins. As previously described, even though archaeal MUS81 family proteins form homodimers with two potentially active ERCC4 domains, the homodimeric complex has a single active monomer (Figure 1.12) (Newman et al., 2005; Nishino et al., 2005a). In eukaryotes, the requirement for a single active nuclease domain in the dimeric complex has led to evolutionary-driven divergence of the nuclease domain sequence of the inactive subunit. As a consequence, the eukaryotic inactive subunit of the heterodimer has acquired other specialised functions. In the case of XPF/ERCC1, the inactive ERCC1 subunit is required for DNA-binding,

which is mediated by the ERCC1 HhH motifs (Figure 1.13B) (Tripsianes et al., 2005). Similarly, EME1 and EME2 might be involved in targeting MUS81 to DNA. The presence of a single HhH motif in EME1 (or EME2), compared to the two HhH motifs of ERCC1 (Figure 5.1), could be responsible for the different substrate specificities of MUS81/EME1 (or EME2) and XPF/ERCC1 complexes (Figure 1.10).

6.1 ACTIVITIES OF MUS81/EME1 AND MUS81/EME2 COMPLEXES

Recombinant human MUS81/EME1 and MUS81/EME2 complexes exhibit nuclease activities very similar to recombinant *S. pombe* Mus81/Eme1 and *S. cerevisiae* Mus81/Mms4 (Doe et al., 2002; Kaliraman et al., 2001; Whitby et al., 2003). Human MUS81/EME1 and MUS81/EME2 cleave 3'-flap and replication fork structures, while exhibiting approximately 75-fold or 12-fold reduced activity on HJs, respectively (Figures 3.6, 4.5 and 4.6). Therefore, MUS81/EME1 is approximately 6-fold more specific for flaps and fork structures compared to MUS81/EME2.

MUS81/EME2 is approximately 10-fold more active than MUS81/EME1, when compared on flap/fork substrates (Figure 4.7). The mechanism by which these substrates are cleaved by MUS81/EME1 or MUS81/EME2 is similar. Indeed, both MUS81/EME1 and MUS81/EME2 exhibit almost identical cleavage pattern of 3'-flap structures (Figure 4.8), which is consistent with previous reports on the activities of archaeal and yeast MUS81 orthologues (Komori et al., 2002; Whitby et al., 2003). Therefore, similar to the archaeal MUS81 family of proteins (Newman et al., 2005; Nishino et al., 2005a), human MUS81/EME1 or MUS81/EME2 complex might bridge the duplex arms of the flap/fork structure allowing the ERCC4 nuclease domain of MUS81 to bind and cleave near the branch point. The incisions are then introduced by human MUS81/EME1 or MUS81/EME2 on the duplex region 3 to 6 nucleotides away from the branch (Figure 4.8). This is consistent with the observation that *S. cerevisiae*

Mus81/Mms4 recognises the 5'-end of the DNA strand downstream of the branch point of a 3'-flap structure and introduces nicks into the duplex region between 5 and 6 nucleotides upstream of the branch point (Bastin-Shanower et al., 2003). As a consequence, the 3'-flap structure is converted by Mus81/Mms4 into a duplex with a 5 nucleotide gap. It has been shown that Mus81/Mms4 is unable to cleave structures with the 5'-end of the downstream DNA strand more than 5 nucleotides away from the branch point (Bastin-Shanower et al., 2003). Due to the similarity between the cleavage mechanism of yeast and human MUS81 complexes, it is likely that similar structures are processed by human MUS81/EME1 or MUS81/EME2.

MUS81/EME2 is significantly more efficient than MUS81/EME1 in processing HJs (Figure 4.9). Also, MUS81/EME2 has a 2-fold greater preference for static HJs, as compared to mobile HJs (Figure 4.6). In contrast, MUS81/EME1 exhibits a 6-fold preference for mobile HJs over static HJs (Figure 3.8). We have suggested that the ability of MUS81/EME1 to cut mobile HJs might be due to the recognition of transient flap structures that are formed as the mobile, but not static HJ, undergoes spontaneous thermal denaturation (Ciccia et al., 2003). However, this hypothesis does not explain the cleavage of static HJs by MUS81/EME2. It is possible that MUS81/EME2 recognises HJs in a manner that is different from MUS81/EME1. Interestingly, MUS81/EME2 exhibits a different pattern of cleavage of static HJs compared to MUS81/EME1 (Figure 4.9). This could be due to a distinct folding of the HJ induced by MUS81/EME2.

Both MUS81/EME1 and MUS81/EME2 cleave HJs with a pattern that is quite different from that produced by a HeLa cell fraction containing Resolvase A (Figure 4.9). These results are consistent with the observation that MUS81 and Resolvase A, partially purified from HeLa cells, have distinct activities (Constantinou et al., 2002). MUS81 fractions purified from HeLa cells by a

similar protocol contain primarily the MUS81/EME1 complex, with only traces of EME2 (Figure 4.10). In agreement with this, a MUS81 peak fraction has weak activity on static HJ, similar to the recombinant MUS81/EME1 complex (Figure 4.9). HeLa fractions enriched for MUS81/EME2 have not yet been purified. It is therefore uncertain whether an activity similar to MUS81/EME2 is present in significant amounts in mammalian cells.

Taken together, these results suggest that human MUS81, in complex with either EME1 or EME2, is a flap/fork endonuclease. Intact HJs are cleaved by MUS81/EME1 or MUS81/EME2 significantly less efficiently than flap/fork structures and with a different pattern from a classical RuvC-like HJ resolvase. Other flap endonucleases, such as Slx1/Slx4, have been shown to cleave HJs by a mechanism distinct from authentic HJ resolvases (Fricke and Brill, 2003). The ability of human MUS81/EME1 or MUS81/EME2 to cleave D-loops and nicked HJs, as suggested for yeast Mus81/Eme1(Mms4) (Gaillard et al., 2003; Osman et al., 2003), has not as yet been tested. However, based on the observation that such activities are conserved both in archaeal (Roberts and White, 2005) and yeast MUS81 orthologues, it is likely that human MUS81/EME1 and MUS81/EME2 complexes will be able to efficiently process D-loops and nicked HJs.

6.2 POSSIBLE *IN VIVO* FUNCTIONS OF MUS81, EME1 AND EME2

As previously described in Section 1.10, yeast Mus81 plays a role both during mitosis and meiosis, whereas mammalian MUS81 is exclusively involved in mitosis. In particular, mammalian MUS81 is required to prevent genomic instability during an unperturbed cell cycle (Dendouga et al., 2005; Hiyama et al., 2006; McPherson et al., 2004), suggesting that *MUS81* is a caretaker gene. It is still an object of debate whether *MUS81* is a tumour suppressor that can predispose to cancer development even when a single copy is mutated (Dendouga et al., 2005; McPherson et al., 2004).

Our biochemical data suggest that the defects seen in mammalian cell lines and animals deficient for MUS81 might be due to aberrant processing of intermediates arising during the repair of stalled DNA replication forks. Similar to its yeast orthologue, mammalian MUS81 could promote the cleavage of blocked replication forks (Figure 1.4, step h), D-loop structures (Figure 1.4, step f) and 3'-flaps after SDSA (Figure 1.3, step j). It is not known whether any of these substrates are preferentially processed by mammalian MUS81 *in vivo*. The observation that *MUS81*$^{-/-}$ or *EME1*$^{-/-}$ mammalian cell lines and animals are primarily sensitive to DNA cross-linking agents (Abraham et al., 2003; Dendouga et al., 2005; Hiyama et al., 2006; McPherson et al., 2004), such as MMC, indicates that the substrates cleaved by MUS81/EME1 are intermediates generated during ICL repair.

In particular, MUS81/EME1 could cleave replication forks blocked at ICLs (Figure 1.8, step 2). However, there is currently no evidence that MUS81/EME1 generates DSBs at replication forks blocked after MMC treatment. Indeed, the formation of DSBs appears to be normal in *MUS81*$^{-/-}$ cells (Dendouga et al., 2005), as also observed with *ERCC1*$^{-/-}$ cells (Niedernhofer et al., 2004). The possibility that XPF/ERCC1 could have redundant functions with MUS81/EME1 needs further investigation. Given that chicken cells have XPF, but not MUS81, may indicate that XPF could compensate for the absence of MUS81. In an alternative to the cleavage of blocked replication fork described above, MUS81/EME1 could play a late role in ICL repair and process D-loop structures promoted by RAD51 (Figure 1.8, step 11), as suggested by the persistence of RAD51 foci in *MUS81*$^{-/-}$ cells (Dendouga et al., 2005).

The *in vivo* role of EME2 is still unknown. Whereas EME1 orthologues are present among most of eukaryotes species, EME2 is exclusively present in vertebrates. Therefore, EME2 might be required for more specialised functions than EME1. Sequence analysis of the N-terminal region of most of the EME2 orthologues has identified the presence of the AP2 clathrin adaptor domain (data not shown). This domain plays a central role in linking proteins to clathrin, which is responsible for coating vesicles during endocytosis (Owen et al., 2000; Pearse et al., 2000). The possible connection between EME2 and clathrin is

completely unknown. Preliminary *in vivo* experiments indicate that GFP-EME2 decorates mammalian cells with a punctated cytoplasmic pattern, which is quite different from the nuclear and nucleolar localisation of both GFP-MUS81 and GFP-EME1 (data not shown). Moreover, GFP-EME2 appears to localise to the actin-myosin ring that separates the two daughter cells during cytokinesis (data not shown). It has not yet been determined whether these observations are real or are artefacts due to protein over-expression. However, in the case of MUS81, the cellular localisation is similar between native (Gao et al., 2003) and GFP-tagged protein. To date, EME2-GFP cell lines have not been treated with any DNA damaging agents to determine whether EME2-GFP might re-localise into the nucleus together with MUS81 upon damage induction. Moreover, *in vivo* interaction studies between MUS81 and EME2 have yet to be performed.

One possibility is that EME2 might have both MUS81-dependent and independent functions. The observation that the EME2_testis splice variant contains the N-terminal region with the AP2 clathrin adaptor domain but not the C-terminal ERCC4 domain and the HhH motif (Appendix 1, Figure 5) suggests that the two domains might be functionally separate and that EME2_testis might have exclusively a MUS81-independent role. Future genetic experiments are required to test the epistatic relationship between EME2 and MUS81.

Taken together, our observations indicate that mammalian MUS81 appears to interact primarily with EME1. Indeed, both proteins form a stable complex after several purification steps from HeLa cells (Figure 4.10), have similar cellular localisation and give rise to similar phenotypes when mutated. In contrast, EME2 might interact with MUS81 only under specific (and still undetermined) conditions.

II. HEF/HIP

Human HEF has been identified in a database search for human proteins containing the ERCC4 nuclease domain. The subsequent search for proteins homologous to the C-terminal domain of HEF has led to the identification of HIP. We have shown that HIP interacts with the C-terminal region of HEF, both

in vitro (Figure 5.7) and *in vivo* (Appendix 2, Figure 1A), and that the HEF/HIP complex is likely to be a heterodimer (Figure 5.7). Moreover, the regions promoting the interaction between HEF and HIP contain the ERCC4 domain and two HhH motifs. Altogether, these observations indicate that HEF and HIP interact by a mechanism similar to other MUS81 family proteins and therefore HEF/HIP represent a novel heterodimeric complex of the MUS81 family.

In vitro interaction experiments among all of the MUS81 family proteins have shown that HIP interacts with HEF, but not with XPF or MUS81 (Figure 5.11). The specificity of the interaction between HEF and HIP might be guaranteed by the homology of their C-terminal regions, as observed also in the case of MUS81/EME2 and XPF/ERCC1 complexes (Figure 5.11).

6.3 POSSIBLE BIOCHEMICAL FUNCTIONS OF HEF/HIP COMPLEX

Previous studies have shown that human HEF complexes purified from mammalian cells have a translocase, but not a helicase activity, which is dependent on the N-terminal DEAH helicase domain (Meetei et al., 2005). In contrast, the homologous DEAH helicase domains of both *P. furiosus* Hef and *S. cerevisiae* Mph1 have functional helicase activities (Komori et al., 2004; Prakash et al., 2005). The lack of helicase activity in human HEF might be due to amino acid changes that impair the helicase activity without interfering with the translocase activity. In support of this hypothesis, it has previously been shown for the bacterial PcrA protein that mutations that affect dsDNA binding can inhibit the helicase activity, leaving the translocase activity intact (Soultanas et al., 2000).

The presence of the ERCC4 domain suggests that human HEF might have nuclease activity in complex with HIP. However, based on sequence analysis, the human HEF nuclease domain has been proposed to be non-functional (Meetei et al., 2005). In agreement with this hypothesis, we have not been able to detect any nuclease activity for a C-terminally truncated human HEF in complex with HIP (Figure 5.8). Given that a similarly truncated XPF was previously shown to retain nuclease activity in complex with ERCC1 (Tsodikov et al., 2005), we suggest that the lack of nuclease activity seen for the truncated

HEF/HIP complex might also be a characteristic of the full-length HEF/HIP. However, future experiments are necessary to confirm this hypothesis.

Alternatively, the interaction between HEF and HIP might be important for DNA binding. In particular, HIP could be required to target HEF to branched DNA structures, similar to the recent model proposed for ERCC1 and XPF (Tripsianes et al., 2005). The important residues for XPF/ERCC1 binding to branched DNA structures have been identified in the HhH motifs of ERCC1. In particular, the second HhH motif contains a classical Glycine–Hydrophobic residue–Glycine (GhG) hairpin, which is important for interacting with DNA (Figures 1.13A and 6.1). No DNA contacts have been detected for XPF, probably because XPF does not contain classical GhG hairpins in either of the two HhH motifs (Figures 1.13A and 6.1). In the case of HIP, the first HhH motif has a GhG hairpin (sequence GVG at amino acids 168-170, Figure 6.1), whereas a hairpin with a Valine to Glycine substitution is present in the second HhH motif (VVG sequence at amino acids 198-200, Figure 6.1). These regions have been maintained almost perfectly identical across many species throughout evolution (Appendix 1, Figure 10). In contrast, none of the two hairpins of human HEF has a GhG motif (Figure 6.1). Moreover, the two hairpins of human HEF have remained less conserved during evolution. In fact, comparing amino acids 2013-2015 of human HEF with the respective sequences of HEF from other species, it is apparent that QVT is changed to RVS in *G. gallus*, CMS in *T. negroviridis* or KHR in *X. laevis* (Appendix 1, Figure 9). Taken together, these observations indicate that HIP is the only subunit of the HEF/HIP complex that contains the critical residues for DNA binding to branched DNA structures.

The HEF/HIP complex may also interact with DNA through the DEAH helicase domain of HEF. The crystal structure of the N-terminal DEAH domain of *P. furiosus* Hef has identified a novel DNA binding domain, which is inserted in between two domains containing the seven helicase motifs of SF2 helicases (Nishino et al., 2005b). This DNA binding domain plays a critical role for the recognition of branched DNA structures, such as replication fork substrates. Indeed, the DEAH helicase domain of *P. furiosus* Hef can bind and unwind

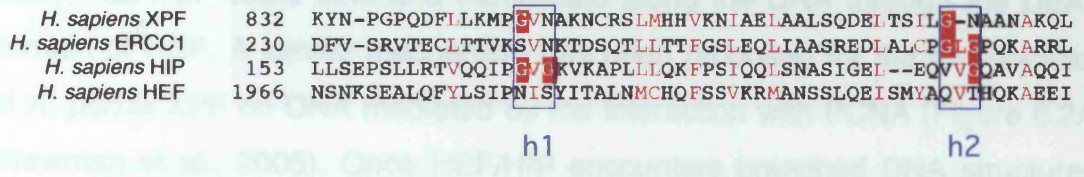

FIGURE 6.1: Sequence alignment between the C-termini of *H. sapiens* XPF (amino acids 832-886), *H. sapiens* ERCC1 (amino acids 230-285), *H. sapiens* HIP (amino acids 153-207) and *H. sapiens* HEF (amino acids 1966-2022)

The two hairpin sequences (h1 and h2) of the HhH motifs are indicated in blue boxes. Conserved hydrophobic residues are in red and Glycine residues of the hairpins are highlighted by red filled boxes. Sequence alignments were carried out using ClustalW.

replication fork structures (Komori et al., 2004). In contrast, although the DEAH domain of human HEF possesses a DNA binding domain similar to *P. furiosus* Hef, it binds replication fork structures very weakly (Mosedale et al., 2005). It may be that amino acid changes in the DEAH DNA binding domain of human HEF, compared to the same domain of *P. furiosus* Hef, have decreased the interaction with branched DNA substrates. The ability of human HEF to bind these structures could therefore depend primarily on HIP.

Despite binding fork structures poorly, the DEAH domain of human HEF interacts strongly with ssDNA (Mosedale et al., 2005). This interaction might be relevant for the translocase activity of HEF. In one possible model (Figure 6.2B), HEF/HIP could bind and translocate along the DNA through the DEAH domain of HEF. A similar mechanism has been proposed for the translocation of *A. pernix* XPF on DNA mediated by the interaction with PCNA (Figure 6.2A) (Newman et al., 2005). Once HEF/HIP encounters branched DNA structures, which could arise from replication fork blockage, the complex could recognise them by the HIP HhH motifs (Figure 6.2B) and then promote the repair of blocked replication forks, as described in the next section.

6.4 ROLE OF HEF/HIP IN FANCONI ANEMIA

HEF has been previously shown to correspond to FANC-M and to be part of the FA core complex (Meetei et al., 2005). We have reported that HIP is a novel component of the FA core complex, since it can be identified in HEF/FANC-M or FANC-A immunocomplexes (Appendix 2, Figure 2). Moreover, preliminary data indicate that depletion of HIP might affect the levels of FANC-D2 monoubiquitination after MMC treatment (Appendix 2, Figure 3). The absence of HIP could result in defective recognition of blocked replication fork structures by the FA core complex. This could possibly decrease the efficiency by which FANC-D2 might be monoubiquitinated by FANC-L. In agreement with this hypothesis, HEF depletion in chicken cells reduces the ability of the FA core complex to bind to chromatin after MMC treatment (Mosedale et al., 2005). Future experiments are required to test whether the FA core complex can localise to chromatin without HIP.

as describe

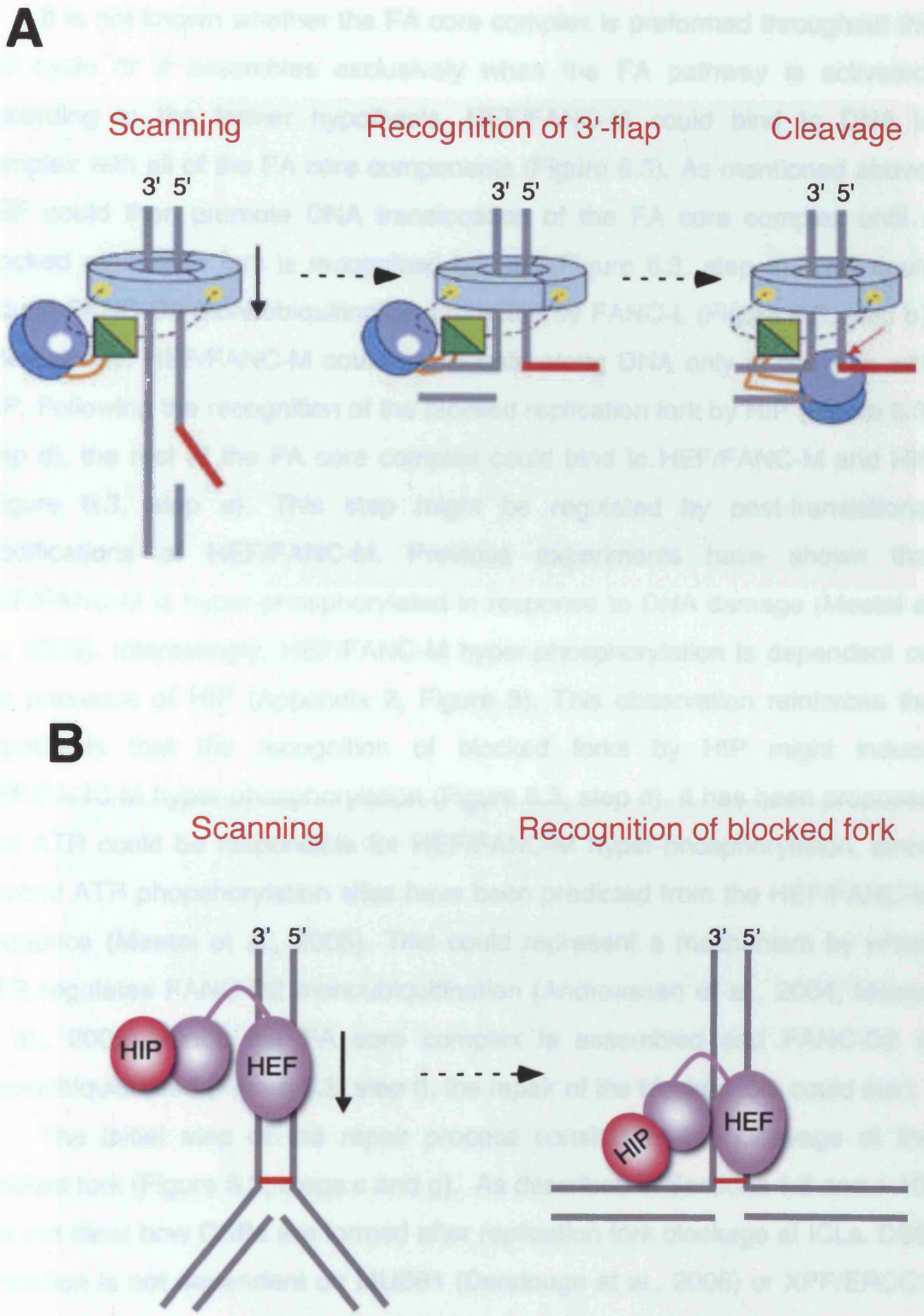
A
Scanning
Recognition of 3'-flap
Cleavage
3' 5'
3' 5'
3' 5'
B
Scanning
Recognition of blocked fork
3' 5'
3' 5'
HIP
HEF
HIP
HEF

It is not known whether the FA core complex is preformed throughout the cell cycle or it assembles exclusively when the FA pathway is activated. According to the former hypothesis, HEF/FANC-M could bind to DNA in complex with all of the FA core components (Figure 6.3). As mentioned above, HEF could then promote DNA translocation of the FA core complex until a blocked replication fork is recognised by HIP (Figure 6.3, step a). This could induce FANC-D2 monoubiquitination promoted by FANC-L (Figure 6.3, step b). Alternatively, HEF/FANC-M could translocate along DNA only in complex with HIP. Following the recognition of the blocked replication fork by HIP (Figure 6.3, step d), the rest of the FA core complex could bind to HEF/FANC-M and HIP (Figure 6.3, step e). This step might be regulated by post-translational modifications of HEF/FANC-M. Previous experiments have shown that HEF/FANC-M is hyper-phosphorylated in response to DNA damage (Meetei et al., 2005). Interestingly, HEF/FANC-M hyper-phosphorylation is dependent on the presence of HIP (Appendix 2, Figure 3). This observation reinforces the hypothesis that the recognition of blocked forks by HIP might induce HEF/FANC-M hyper-phosphorylation (Figure 6.3, step d). It has been proposed that ATR could be responsible for HEF/FANC-M hyper-phosphorylation, since several ATR phopshorylation sites have been predicted from the HEF/FANC-M sequence (Meetei et al., 2005). This could represent a mechanism by which ATR regulates FANC-D2 monoubiquitination (Andreassen et al., 2004; Meetei et al., 2005). Once the FA core complex is assembled and FANC-D2 is monoubiquitinated (Figure 6.3, step f), the repair of the blocked fork could start.

The initial step of the repair process consists of the cleavage of the blocked fork (Figure 6.3, steps c and g). As described in Sections 1.6 and 1.10, it is not clear how DSBs are formed after replication fork blockage at ICLs. DSB formation is not dependent on MUS81 (Dendouga et al., 2005) or XPF/ERCC1 (Niedernhofer et al., 2004). Our biochemical data on HEF/FANC-M do not support the hypothesis that HEF/FANC-M in complex with HIP might cleave blocked replication forks. However, it would be interesting to test whether *FANC-M* deficient cell lines are proficient in DSB formation after MMC

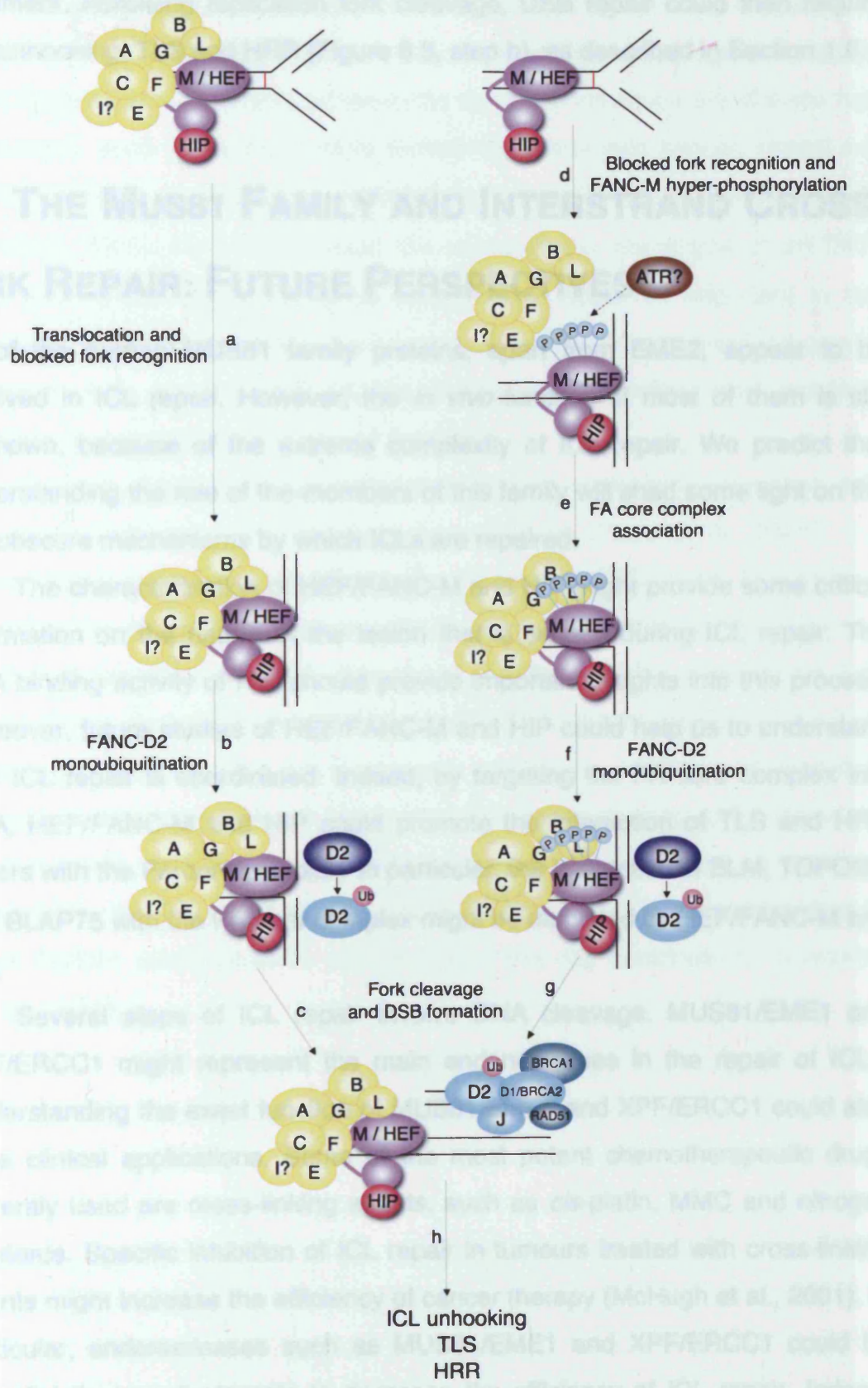
B
A G L
C F
I? E
M / HEF
HIP
Translocation and
blocked fork recognition
a
d
Blocked fork recognition and
FANC-M hyper-phosphorylation
ATR?
P P P P P
e
FA core complex
association
FANC-D2
monoubiquitination
b
f
FANC-D2
monoubiquitination
D2
Ub
Fork cleavage
and DSB formation
c
g
BRCA1
D1/BRCA2
RAD51
J
h
ICL unhooking
TLS
HRR

treatment. Following replication fork cleavage, DSB repair could then require ICL unhooking, TLS and HRR (Figure 6.3, step h), as described in Section 1.6.

III. THE MUS81 FAMILY AND INTERSTRAND CROSS-LINK REPAIR: FUTURE PERSPECTIVES

All of the human MUS81 family proteins, apart from EME2, appear to be involved in ICL repair. However, the *in vivo* function of most of them is still unknown, because of the extreme complexity of ICL repair. We predict that understanding the role of the members of this family will shed some light on the still obscure mechanisms by which ICLs are repaired.

The characterisation of HEF/FANC-M and HIP might provide some critical information on the nature of the lesion that is sensed during ICL repair. The DNA binding activity of HIP should provide important insights into this process. Moreover, future studies of HEF/FANC-M and HIP could help us to understand how ICL repair is coordinated. Indeed, by targeting the FA core complex into DNA, HEF/FANC-M and HIP could promote the interaction of TLS and HRR factors with the FA core complex. In particular, the interaction of BLM, TOPOIIIα and BLAP75 with the FA core complex might be mediated by HEF/FANC-M and HIP.

Several steps of ICL repair involve DNA cleavage. MUS81/EME1 and XPF/ERCC1 might represent the main endonucleases in the repair of ICLs. Understanding the exact function of MUS81/EME1 and XPF/ERCC1 could also have clinical applications. Some of the most potent chemotherapeutic drugs currently used are cross-linking agents, such as *cis*-platin, MMC and nitrogen mustards. Specific inhibition of ICL repair in tumours treated with cross-linking agents might increase the efficiency of cancer therapy (McHugh et al., 2001). In particular, endonucleases such as MUS81/EME1 and XPF/ERCC1 could be potential therapeutic targets to decrease the efficiency of ICL repair. Indeed, MUS81 and XPF have well defined nuclease domains, which could be suitable targets for developing specific inhibitors.

The study of MUS81 family proteins could also prove to be important for understanding the etiology of cancer. It is possible that heterozygous mutations in *HEF/FANC-M* or *HIP* might increase the risk of the development of some type of cancers, such as acute myeloid leukaemia, pancreatic cancer, breast and ovarian cancer, as previously reported for other FA genes (Kennedy and D'Andrea, 2005). Moreover, should the cancer-prone phenotype of *MUS81*$^{-/-}$ mice (McPherson et al., 2004) be confirmed, it would be important to test whether *MUS81* mutations could predispose to cancer development in humans. Therefore it is possible that MUS81 family proteins might have caretaker functions that protect against cancer formation.

Recently, it has been suggested that tumours could arise from stem cells that accumulate mutations and become cancerous (Reya et al., 2001). It is known that mammalian cells deficient for FA genes, *ERCC1* and *MUS81* have defects in the proliferation of stem cells (Agoulnik et al., 2002; Dendouga et al., 2005; Park and Gerson, 2005; Prasher et al., 2005), which might derive from spontaneous genomic instability. Under these conditions, genomic instability could select for cells that have a growth advantage, which could potentially become cancer stem cells. It would therefore be interesting to investigate in detail the role of MUS81 family proteins during the proliferation of stem cell progenitors. We hope that further understanding of the basic mechanism by which MUS81 family proteins operate might one day contribute to ameliorate human health.

APPENDIX ONE

Sequence Alignments

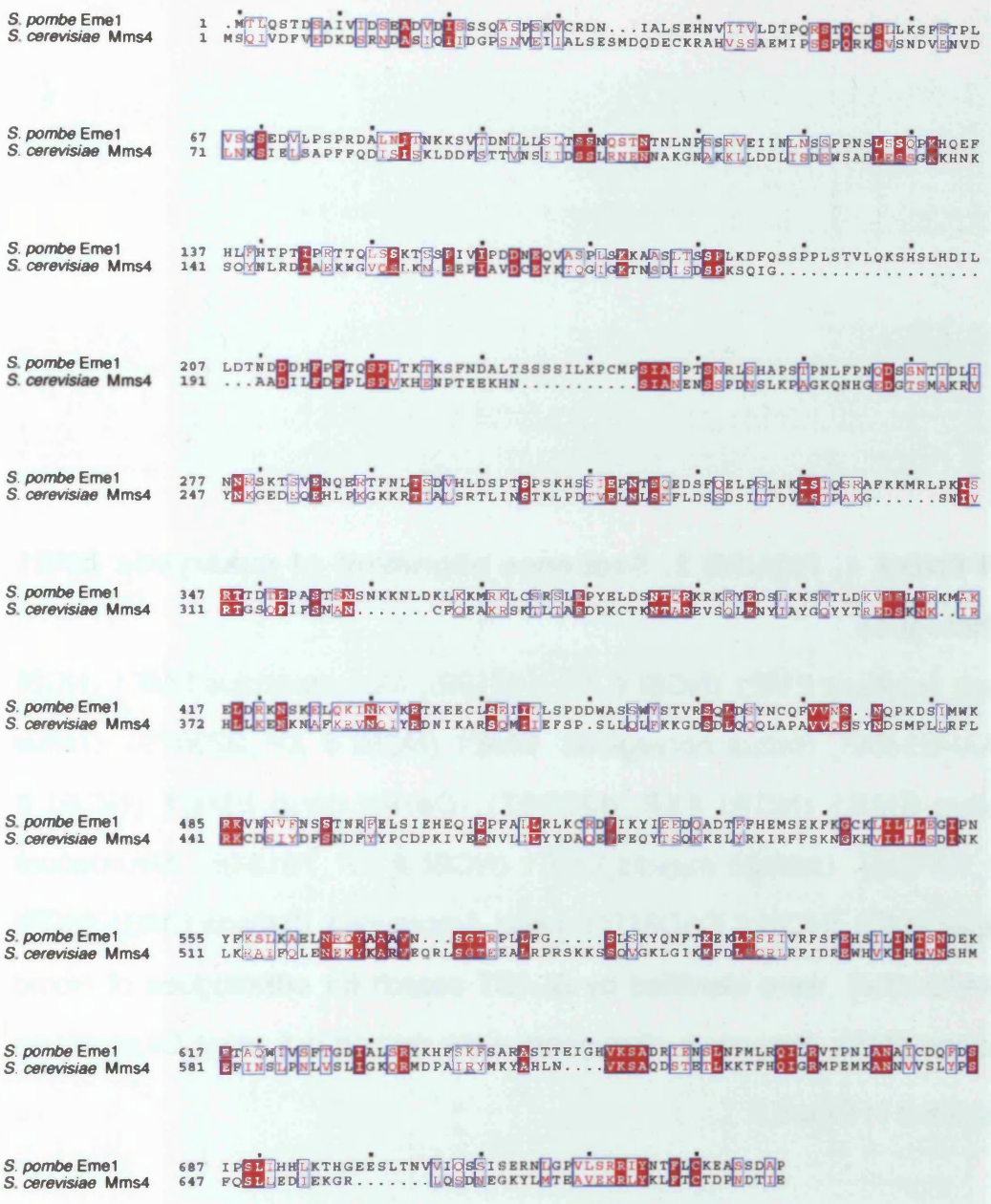

APPENDIX 1, FIGURE 1: Sequence alignment between *S. pombe* Eme1 and *S. cerevisiae* Mms4

Identical and similar residues are indicated in filled and unfilled red boxes, respectively. Sequence alignments were carried out using ClustalW.

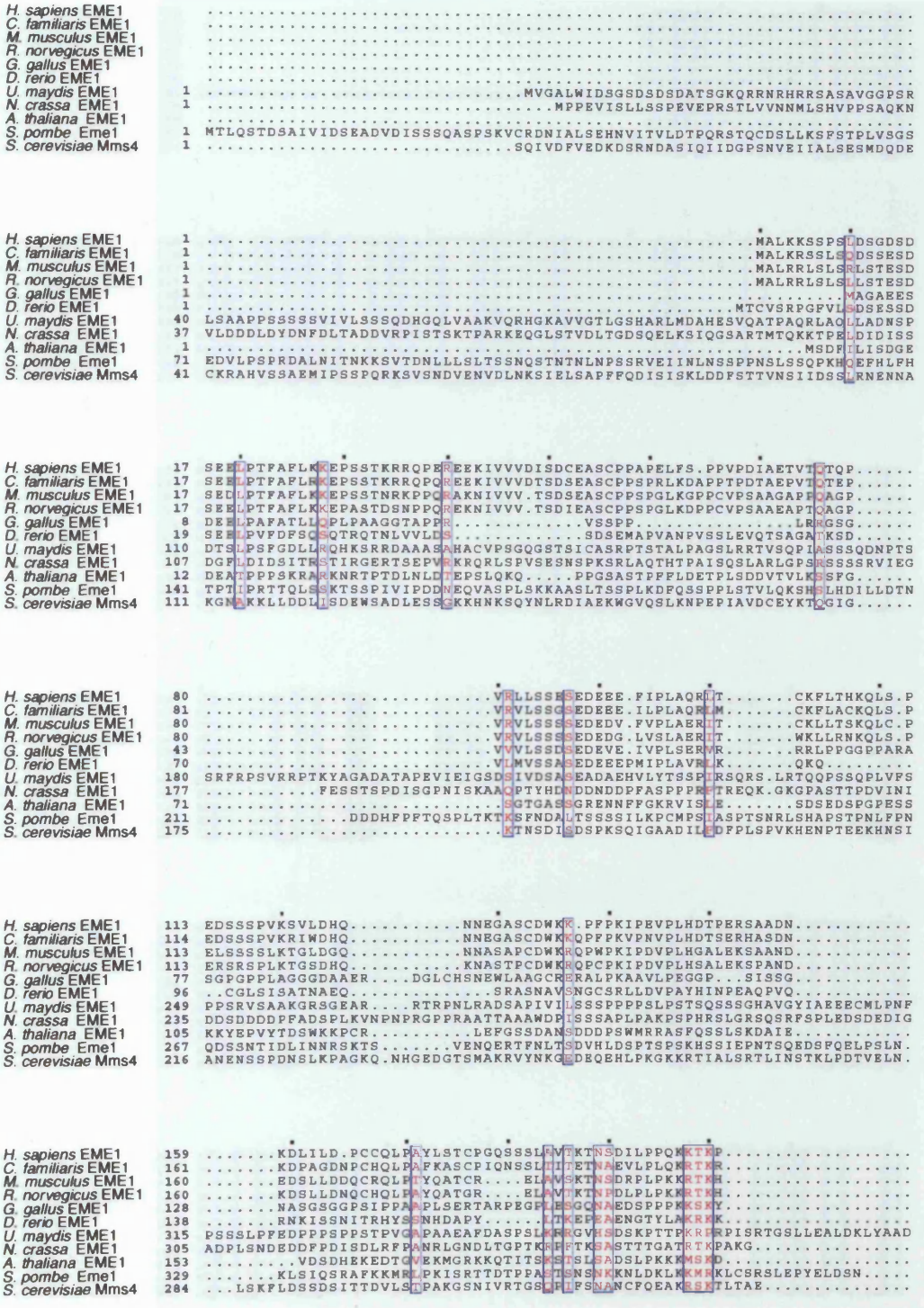
H. sapiens EME1
C. familiaris EME1
M. musculus EME1
R. norvegicus EME1
G. gallus EME1
D. rerio EME1
U. maydis EME1
N. crassa EME1
A. thaliana EME1
S. pombe Eme1
S. cerevisiae Mms4

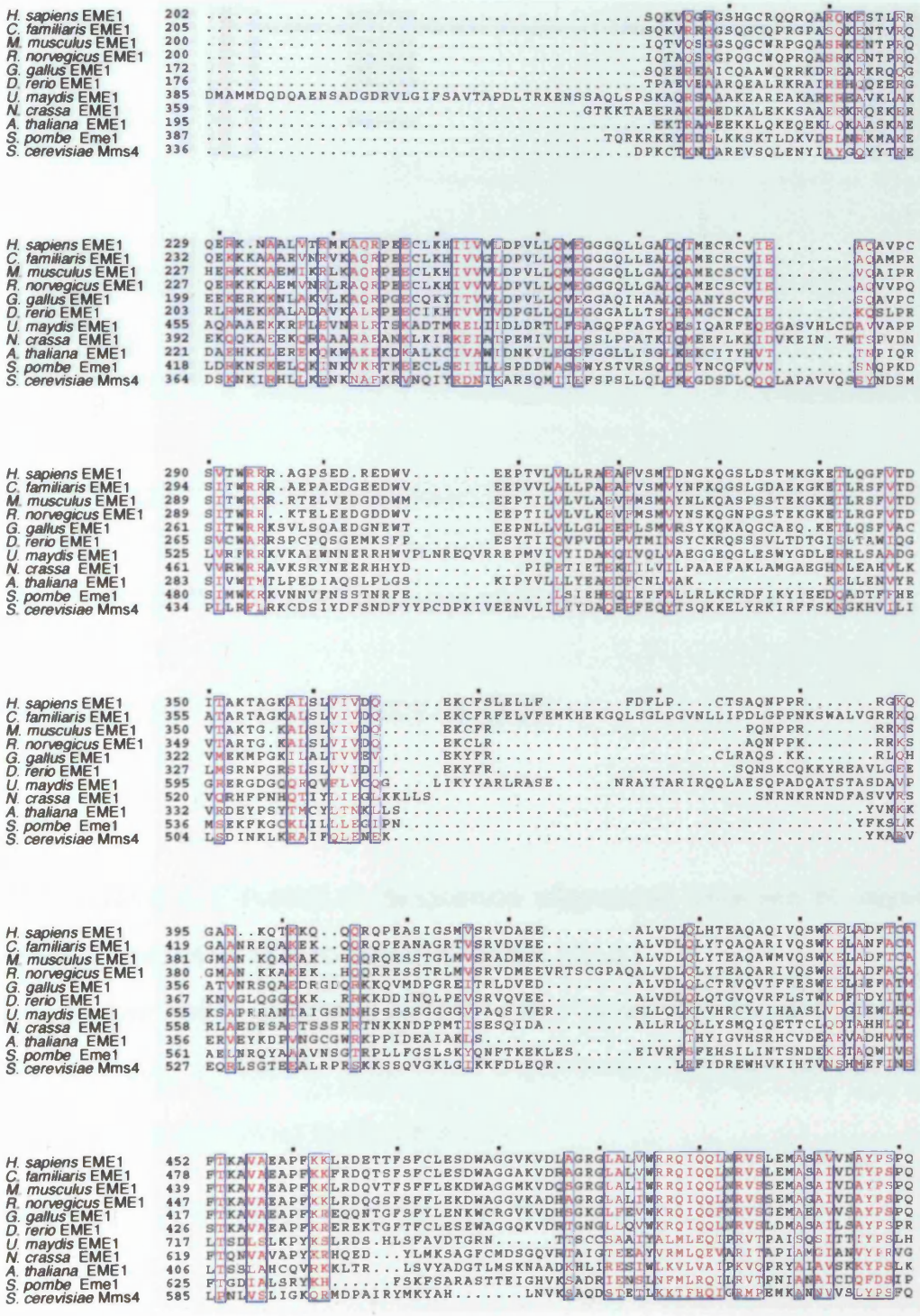
H. sapiens EME1
C. familiaris EME1
M. musculus EME1
R. norvegicus EME1
G. gallus EME1
D. rerio EME1
U. maydis EME1
N. crassa EME1
A. thaliana EME1
S. pombe Eme1
S. cerevisiae Mms4

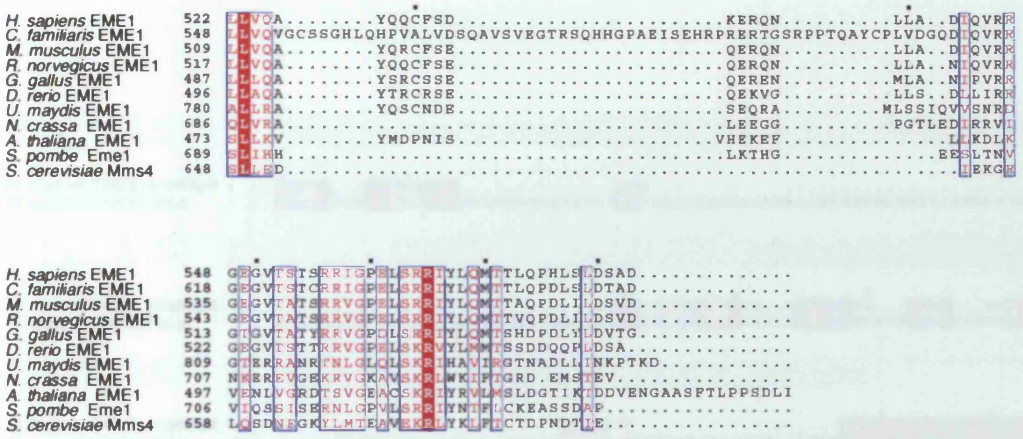
H. sapiens EME1 522
C. familiaris EME1 548
M. musculus EME1 509
R. norvegicus EME1 517
G. gallus EME1 487
D. rerio EME1 496
U. maydis EME1 780
N. crassa EME1 686
A. thaliana EME1 473
S. pombe Eme1 689
S. cerevisiae Mms4 648
H. sapiens EME1 548
C. familiaris EME1 618
M. musculus EME1 535
R. norvegicus EME1 543
G. gallus EME1 513
D. rerio EME1 522
U. maydis EME1 809
N. crassa EME1 707
A. thaliana EME1 497
S. pombe Eme1 706
S. cerevisiae Mms4 658

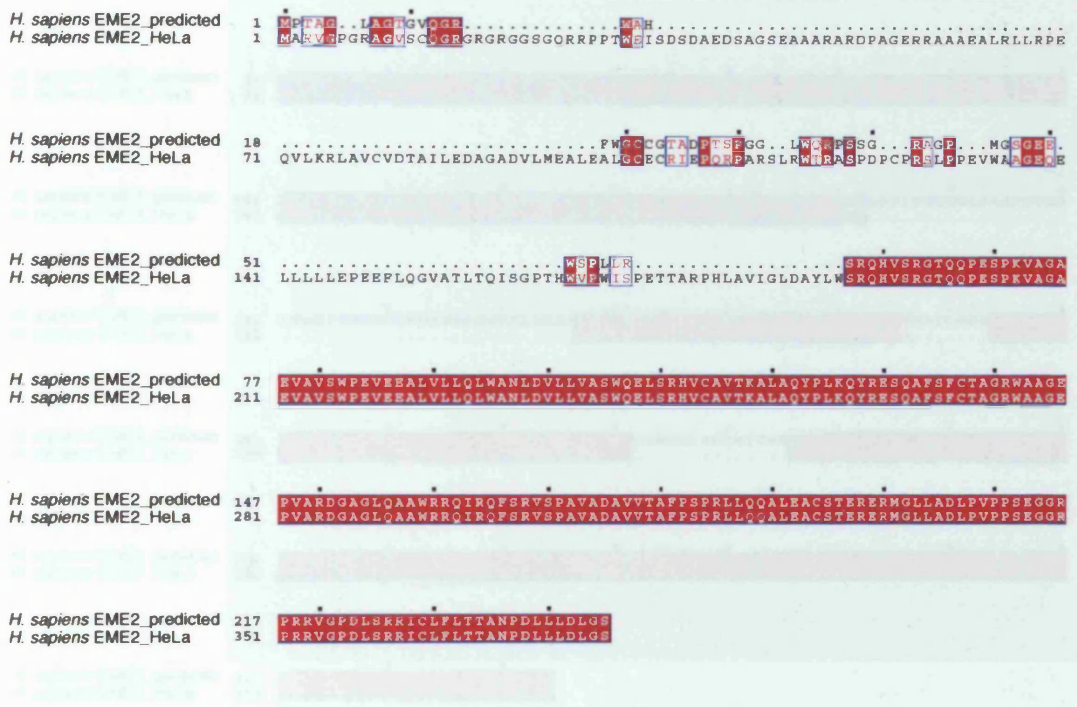

APPENDIX 1, FIGURE 3: Sequence alignment between *H. sapiens* EME2_predicted and *H. sapiens* EME2_HeLa

H. sapiens EME2_predicted (NCBI # XM_113869) was identified based to its similarity to EME1. Sequence alignments were carried out using ClustalW as described in Figure 3.1.

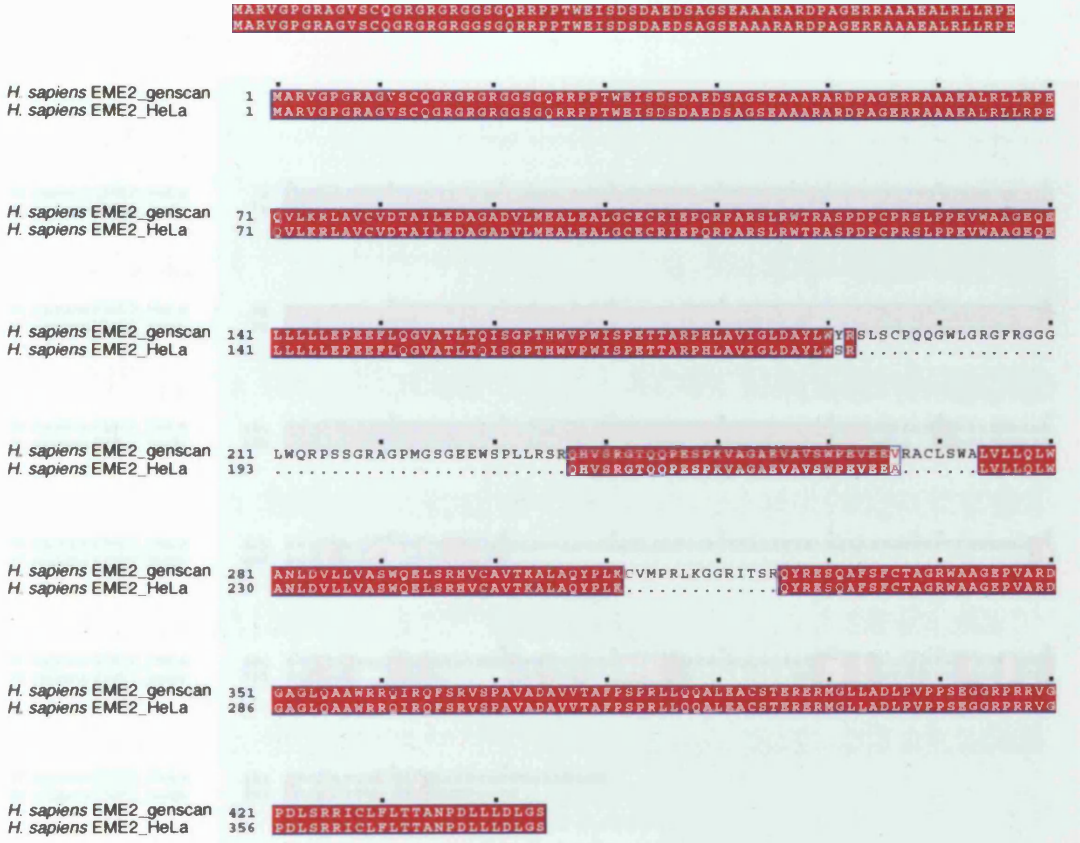

APPENDIX 1, FIGURE 4: Sequence alignment between *H. sapiens* EME2_genscan and *H. sapiens* EME2_HeLa

H. sapiens EME2 genescan prediction NT_037887.92 (NCBI # NP_001010865) is indicated as EME2_genscan. Sequence alignments were carried out using ClustalW as described in Figure 3.1.

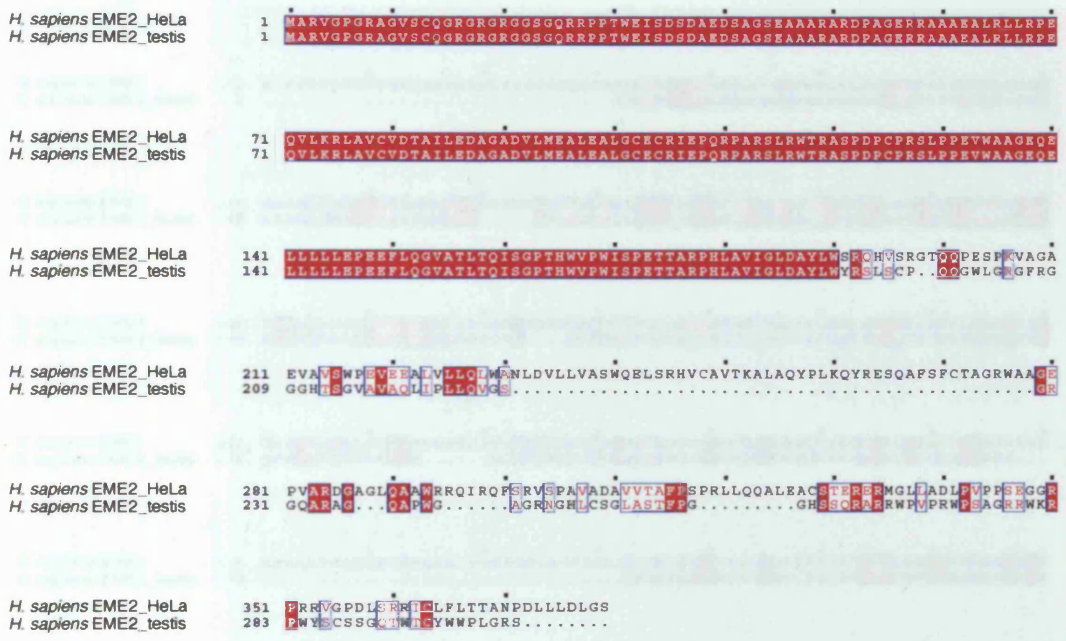

APPENDIX 1, FIGURE 5: Sequence alignment between *H. sapiens* EME2_HeLa and *H. sapiens* EME2_testis

Sequence alignments were carried out using ClustalW.

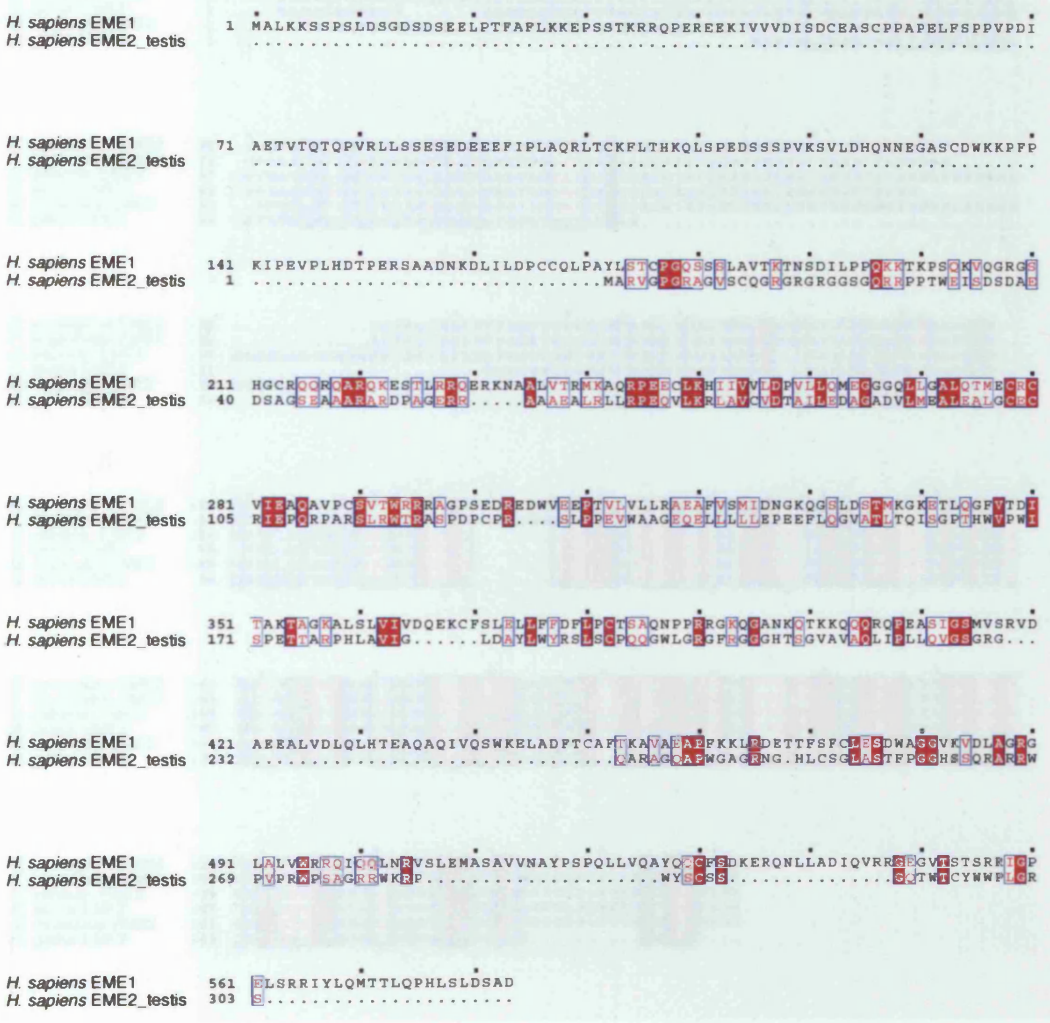

APPENDIX 1, FIGURE 6: Sequence alignment between *H. sapiens* EME1 and *H. sapiens* EME2_testis

Sequence alignments were carried out using ClustalW.

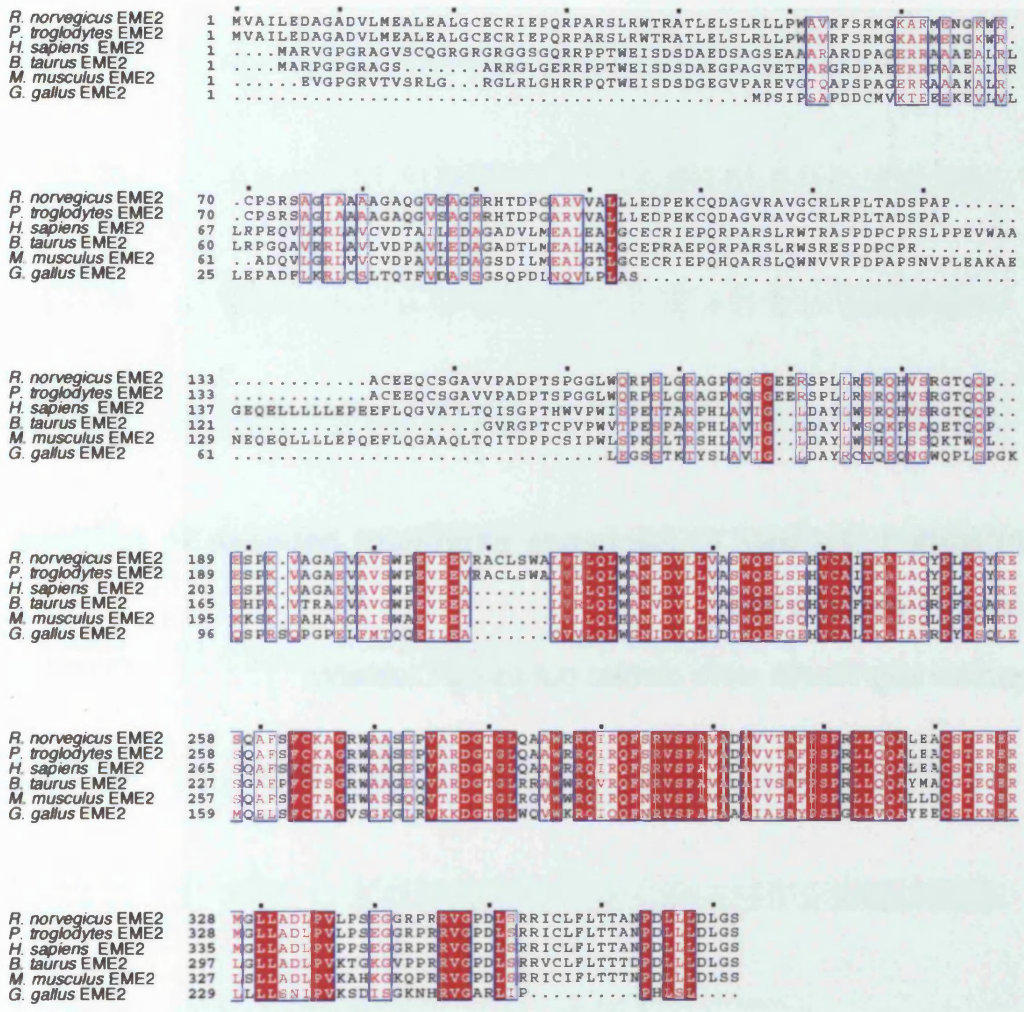

APPENDIX 1, FIGURE 7: Sequence alignment of vertebrate EME2 orthologues

Homo sapiens EME2 corresponds to *Homo sapiens* EME2_HeLa (Figure 7.3). *Rattus norvegicus* EME2 (NCBI # XP_220231), *Pan troglodytes* EME2 (NCBI # XP_523262), *Bos taurus* EME2 (NCBI # XP_593720) *Mus musculus* EME2 (NCBI # AAH92228) and *Gallus gallus* EME2 (NCBI # XP_414715) were identified by BLAST search for orthologues of *H. sapiens* EME2. Sequence alignments were carried using ClustalW.

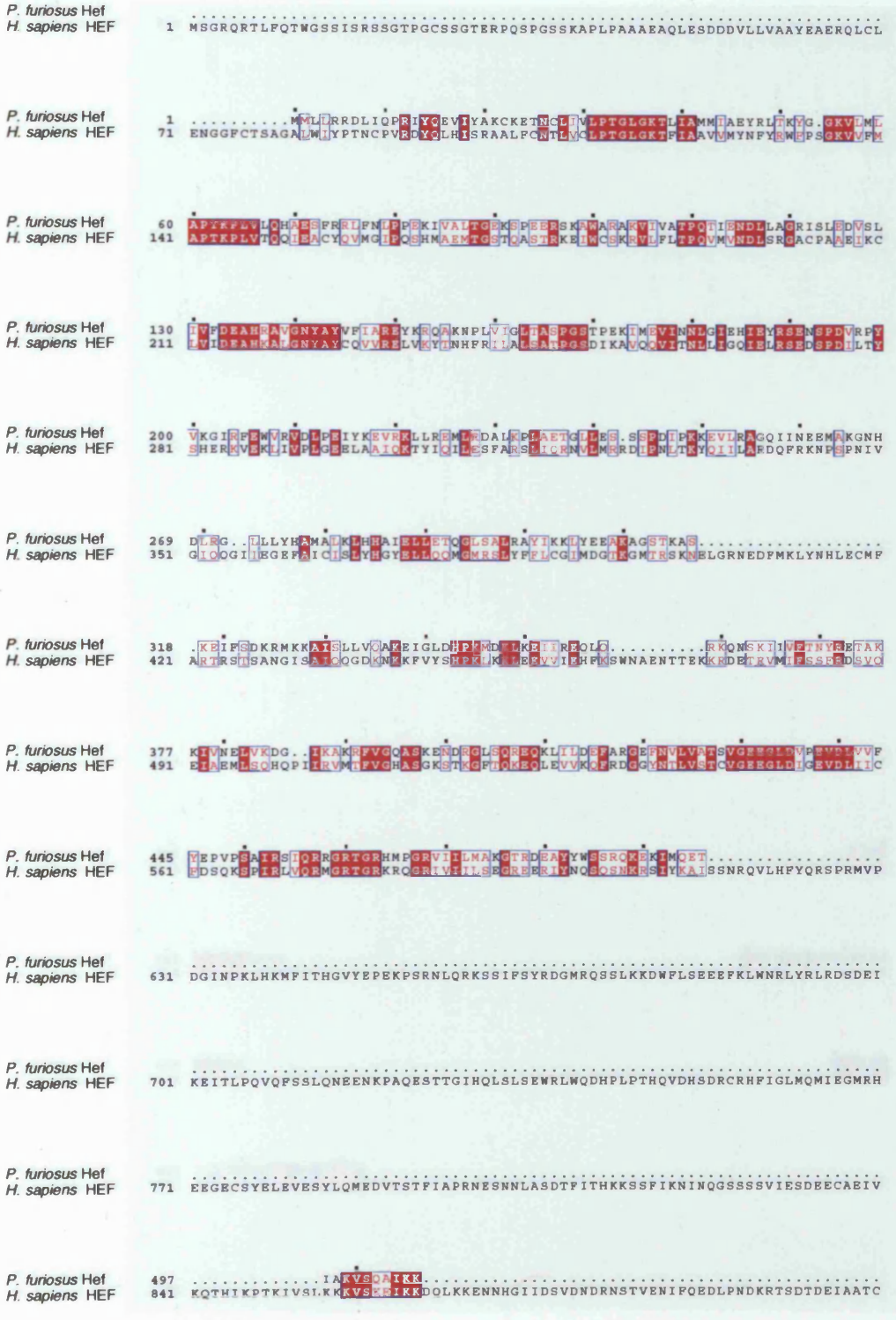
P. furiosus Hef
H. sapiens HEF
1 MSGRQRTLFQTWGSSISRSSGTPGCSSGTERPQSPGSSKAPLPAAAEAQLESDDDVLLVAAYEAERQLCL
P. furiosus Hef
H. sapiens HEF
1 ..........MMLLRRDLIQPRIYQEVIYAKCKETNGLIVLPTGLGKTLIAMMIAEYRLTKYG.GKVLML
71 ENGGPCTSAGALWIYPTNCPVRDYQLHISRAALFCNILVCLPTGLGKTFIAAVVMYNFYRWFPSGKVVFM
P. furiosus Hef
H. sapiens HEF
60 APYKPLVLQHAESFRRLFNLPPEKIVALTGEKSPEERSKAWARAKVIVATPQTIENDLLAGRISLEDVSL
141 APTKPLVTQQIEACYQVMGIPQSHMAEMTGSTQASTRKEIWCSKRVLFLTPQVMVNDLSRGACPAAEIKC
P. furiosus Hef
H. sapiens HEF
130 IVFDEAHRAVGNYAYVFIAREYKRQAKNPLVIGLTASPGSTPEKIMEVINNLGIEHIEYRSENSPDVRPY
211 IVIDEAHKALGNYAYCQVVRELVKYTNHFRIIALSATPGSDIKAVQQVINNLLISGQIELRSESDPDILTY
P. furiosus Hef
H. sapiens HEF
200 VKGIRFSWVRVDLPEIYKEVRKLLREMMWDALKPLAETGLLES.SSPDIPKKEVLRAGQIINEEMAKGNH
281 SHERKVLKLIVPLGEELAAIQKTYIQILESFARSLICRNVLMHRDIPNLTKYQIILARDQFRKNPSPNIV
P. furiosus Hef
H. sapiens HEF
269 DLRG..LLLYHAMALKPHHAIELLETQGLSALRAYIKKLYEEAAAGSTKAS.....................
351 GIQQGIIEGEFAICISLYHGYSLLQQMGMRSLYPFLCGIMDGMGMTRSKNELGRNEDFMKLYNHLECMF
P. furiosus Hef
H. sapiens HEF
318 .KEIFSDKRMKKAISLLVQAKEIGLDHPKMDTLKEIIREQLQ.........RKQNSKIIVETNYRETAK
421 ARTRSTSANGISAIQQGDKNKKFVYSHPKLKKLEFVVIFHFKSWNAENTTEKKRDETRVMIFSSFRDSVQ
P. furiosus Hef
H. sapiens HEF
377 KIVNELVKDG..IKAKRFVGQASKENDRGLSQREQKLILDSFARGEGNVLVATSVGEEGLDVPEVDLVVF
491 EHAEMLSQHQPIIRVMIFVGHASGKSTKQFTQKEQLEVVKQFRDGGYNHLVSTCVGEEGLDIGEVDLIIC
P. furiosus Hef
H. sapiens HEF
445 VEPVPSAIRSIQRRGRTGRHMPGRVIILMAKGTRDEAYYWSSRQKEKIMQET.....................
561 HDSQKSPIRLVQRMGRTGRKRQGRIVILSEGREERIYNQSQSNKRSHYKAISSNRQVLHFYQRSPRMVP
P. furiosus Hef
H. sapiens HEF
631 DGINPKLHKMFITHGVYEPEKPSRNLQRKSSIFSYRDGMRQSSLKKDWFLSEEEFKLWNRLYRLRDSDEI
P. furiosus Hef
H. sapiens HEF
701 KEITLPQVQFSSLQNEENKPAQESTTGIHQLSLSEWRLWQDHPLPTHQVDHSDRCRHFIGLMQMIEGMRH
P. furiosus Hef
H. sapiens HEF
771 EEGECSYELEVESYLQMEDVTSTFIAPRNESNNLASDTFITHKKSSFIKNINQGSSSSVIESDEECAEIV
P. furiosus Hef
H. sapiens HEF
497 ....IAKVSQAIKK...
841 KQTHIKPTKIVSLKKKVSEEIKKDQLKKENNHGIIDSVDNDRNSTVENIFQEDLPNDKRTSDTDEIAATC

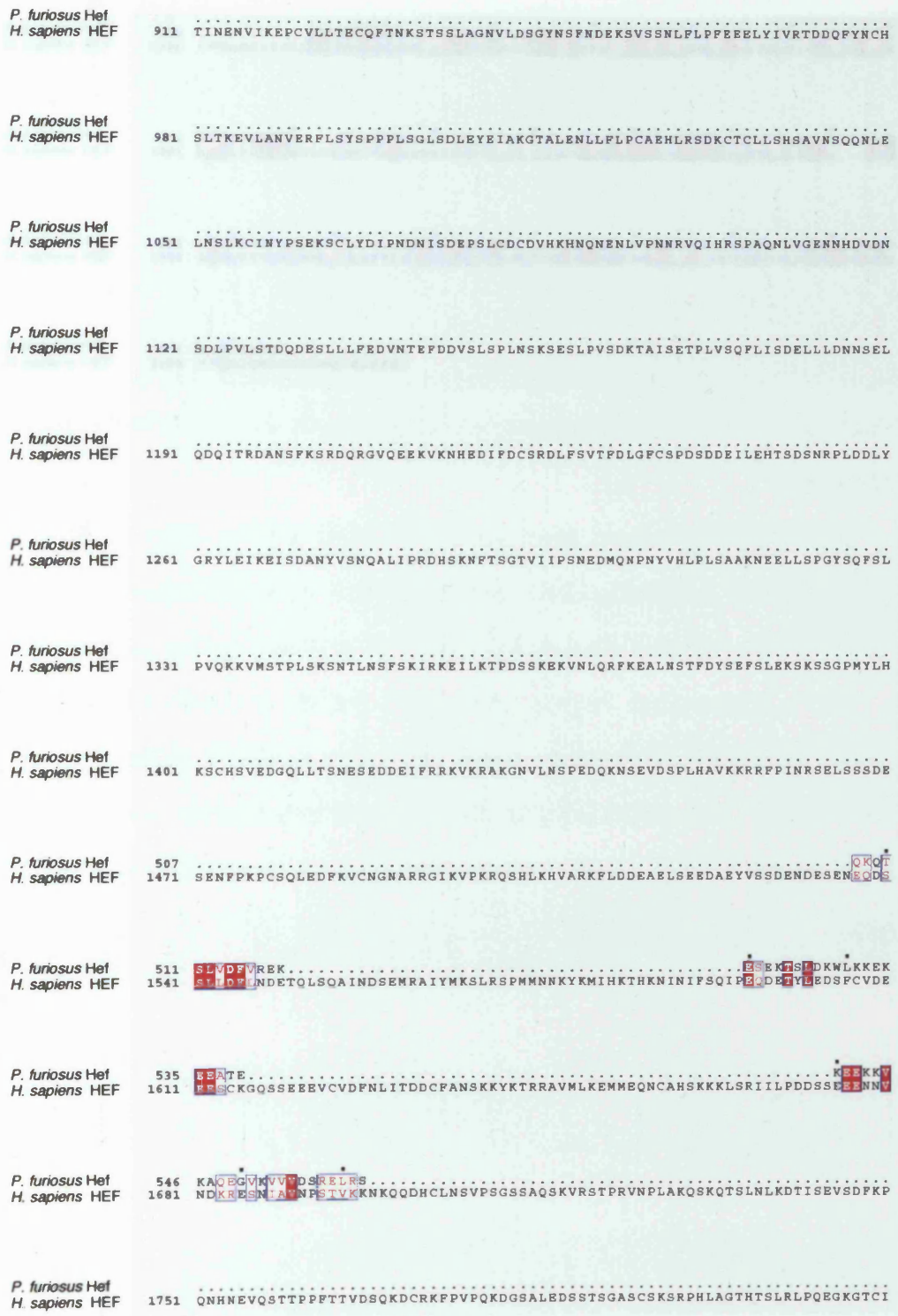
P. furiosus Hef
H. sapiens HEF
911 TINENVIKEPCVLLTECQFTNKSTSSLAGNVLDSGYNSFNDEKSVSSNLFLPFEEELYIVRTDDQFYNCH
981 SLTKEVLANVERFLSYSPPPLSGLSDLEYEIAKGTALENLLFLPCAEHLRSDKCTCLLSHSAVNSQQNLE
1051 LNSLKCINYPSEKSCLYDIPNDNISDEPSLCDCDVHKHNQNENLVPNNRVQIHRSPAQNLVGENNHDVDN
1121 SDLPVLSTDQDESLLLFEDVNTEFDDVSLSPLNSKSESLPVSDKTAISETPLVSQFLISDELLLDNNSEL
1191 QDQITRDANSFKSRDQRGVQEEKVKNHEDIFDCSRDLFSVTFDLGFCSPDSDDEILEHTSDSNRPLDDLY
1261 GRYLEIKEISDANYVSNQALIPRDHSKNFTSGTVIIPSNEDMQNPNYVHLPLSAAKNEELLSPGYSQFSL
1331 PVQKKVMSTPLSKSNTLNSFSKIRKEILKTPDSSKEKVNLQRFKEALNSTFDYSEFSLEKSKSSGPMYLH
1401 KSCHSVEDGQLLTSNESEDDEIFRRKVKRAKGNVLNSPEDQKNSEVDSPLHAVKKRRFPINRSELSSSDE
507 QKQT
1471 SENFPKPCSQLEDFKVCNGNARRGIKVPKRQSHLKHVARKFLDDEAELSEEDAEYVSSDENDESENEQDS
511 SLVDFVREK EEEKTSLDKWLKKEK
1541 SLIDFLNDETQLSQAINDSEMRAIYMKSLRSPMMNNKYKMIHKTHKNINIFSQIPEQDETYLEDSFCVDE
535 EEATE KEEKKV
1611 EESCKGQSSEEEVCVDPNLITDDCFANSKKYKTRRAVMLKEMMEQNCAHSKKKLSRIILPDDSSEEENNV
546 KAQEGVKKVVDSRELRS
1681 NDKREGNIAINPSTVKKNKQQDHCLNSVPSGSSAQSKVRSTPRVNPLAKQSKQTSLNLKDTISEVSDFKP
1751 QNHNEVQSTTPPFTTVDSQKDCRKFPVPQKDGSALEDSSTSGASCSKSRPHLAGTHTSLRLPQEGKGTCI

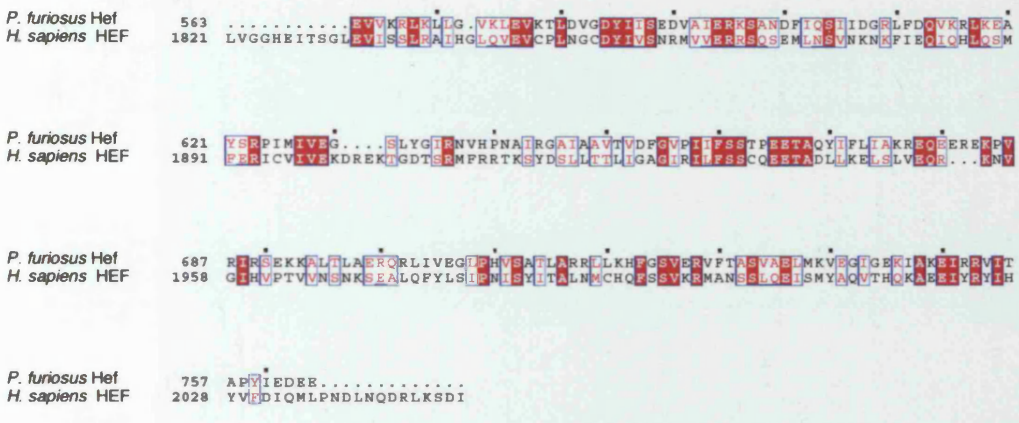
P. furiosus Hef
H. sapiens HEF
563
1821
P. furiosus Hef
H. sapiens HEF
621
1891
P. furiosus Hef
H. sapiens HEF
687
1958
P. furiosus Hef
H. sapiens HEF
757
2028

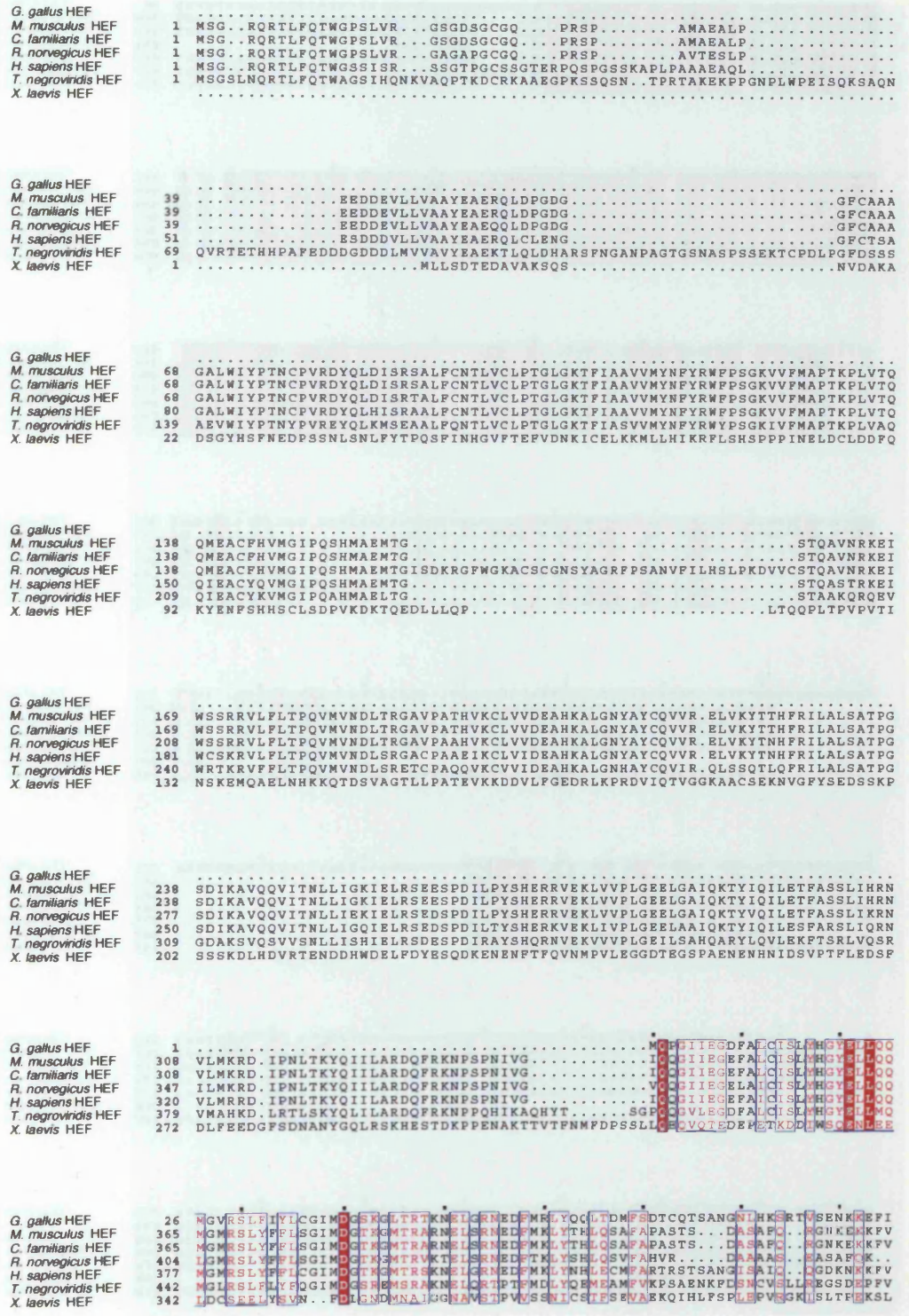
G. gallus HEF
M. musculus HEF
C. familiaris HEF
R. norvegicus HEF
H. sapiens HEF
T. negroviridis HEF
X. laevis HEF

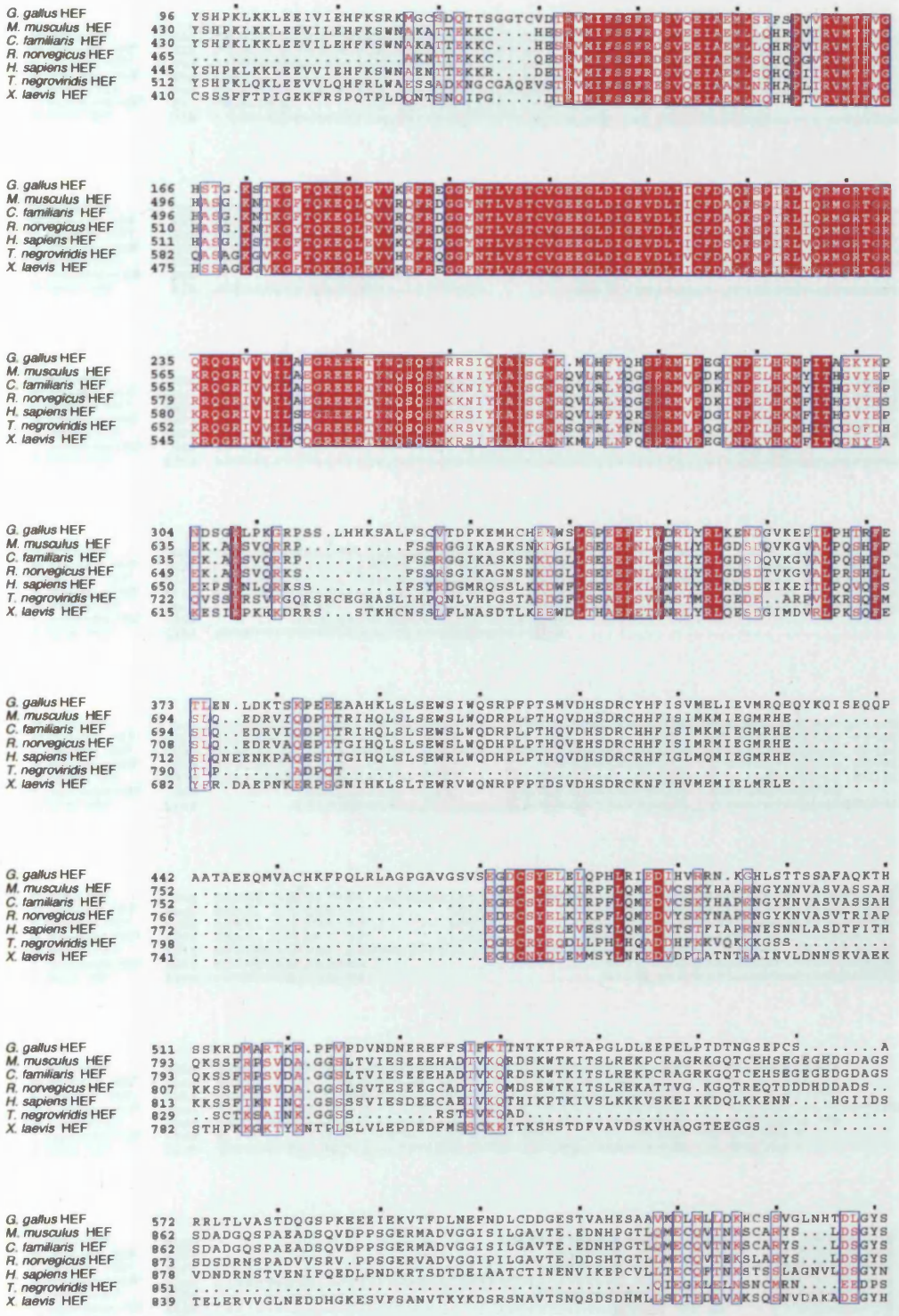
G. gallus HEF
M. musculus HEF
C. familiaris HEF
R. norvegicus HEF
H. sapiens HEF
T. negroviridis HEF
X. laevis HEF

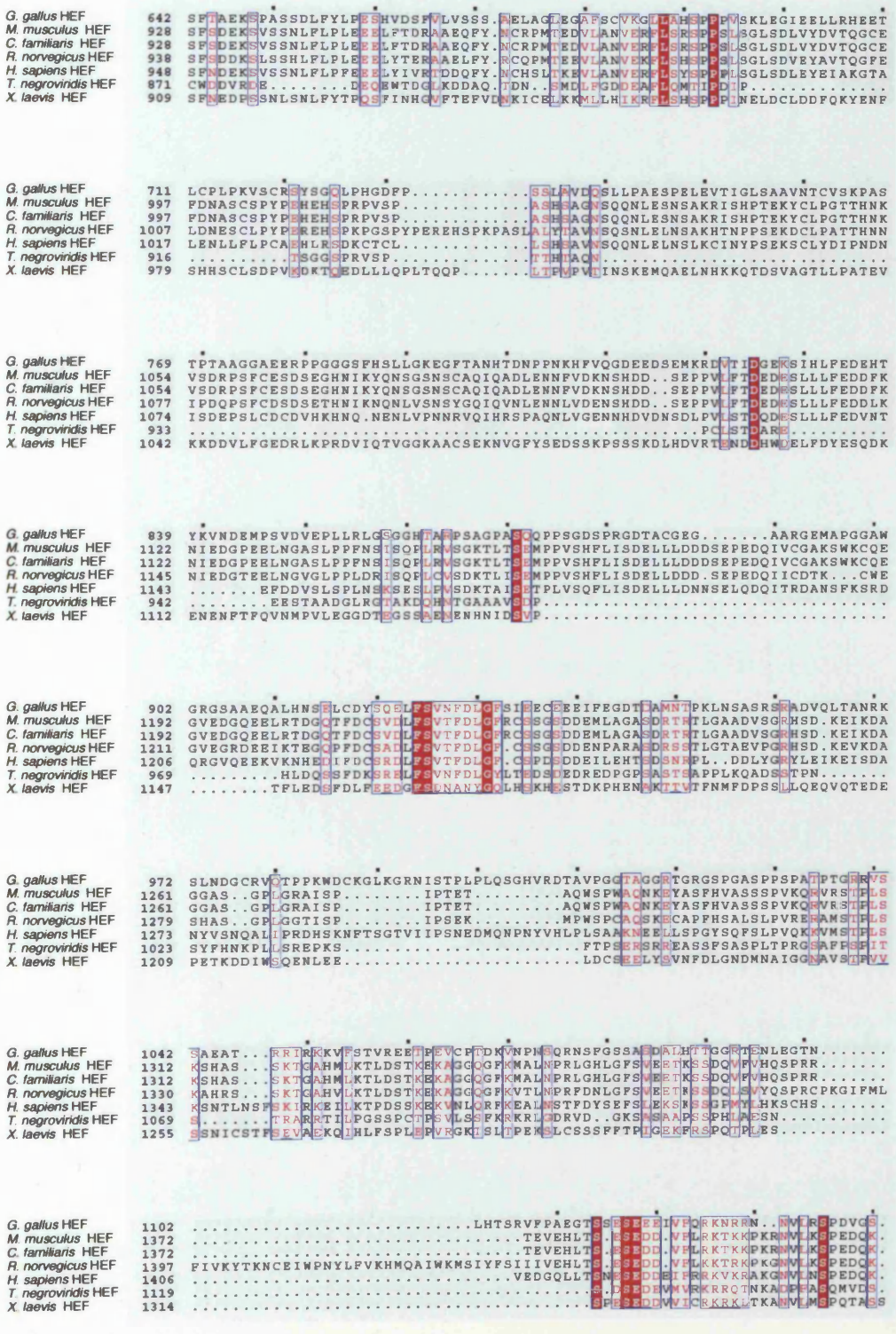
G. gallus HEF
M. musculus HEF
C. familiaris HEF
R. norvegicus HEF
H. sapiens HEF
T. negroviridis HEF
X. laevis HEF

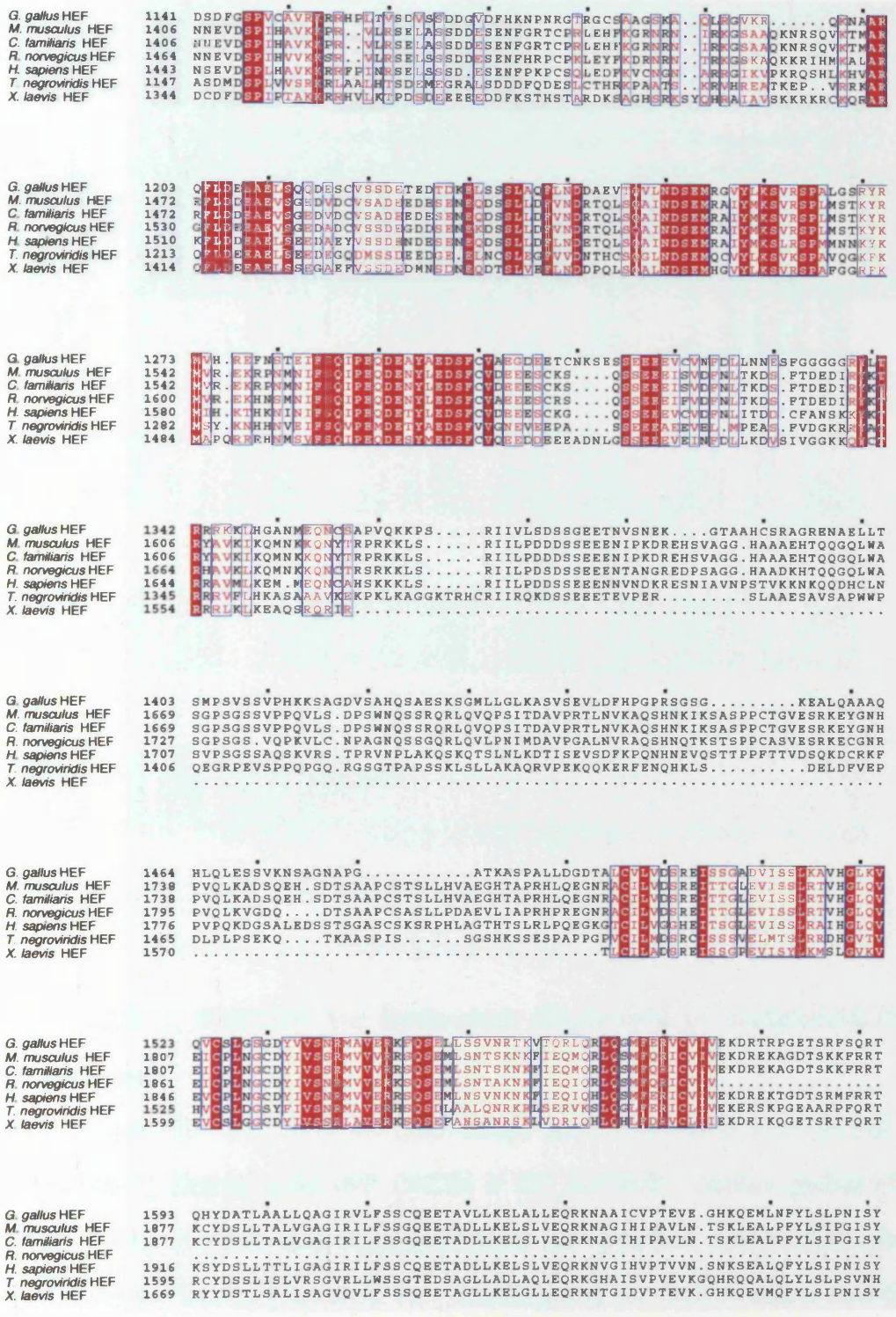
G. gallus HEF 1141
M. musculus HEF 1406
C. familiaris HEF 1406
R. norvegicus HEF 1464
H. sapiens HEF 1443
T. negroviridis HEF 1147
X. laevis HEF 1344
G. gallus HEF 1203
M. musculus HEF 1472
C. familiaris HEF 1472
R. norvegicus HEF 1530
H. sapiens HEF 1510
T. negroviridis HEF 1213
X. laevis HEF 1414
G. gallus HEF 1273
M. musculus HEF 1542
C. familiaris HEF 1542
R. norvegicus HEF 1600
H. sapiens HEF 1580
T. negroviridis HEF 1282
X. laevis HEF 1484
G. gallus HEF 1342
M. musculus HEF 1606
C. familiaris HEF 1606
R. norvegicus HEF 1664
H. sapiens HEF 1644
T. negroviridis HEF 1345
X. laevis HEF 1554
G. gallus HEF 1403
M. musculus HEF 1669
C. familiaris HEF 1669
R. norvegicus HEF 1727
H. sapiens HEF 1707
T. negroviridis HEF 1406
X. laevis HEF
G. gallus HEF 1464
M. musculus HEF 1738
C. familiaris HEF 1738
R. norvegicus HEF 1795
H. sapiens HEF 1776
T. negroviridis HEF 1465
X. laevis HEF 1570
G. gallus HEF 1523
M. musculus HEF 1807
C. familiaris HEF 1807
R. norvegicus HEF 1861
H. sapiens HEF 1846
T. negroviridis HEF 1525
X. laevis HEF 1599
G. gallus HEF 1593
M. musculus HEF 1877
C. familiaris HEF 1877
R. norvegicus HEF
H. sapiens HEF 1916
T. negroviridis HEF 1595
X. laevis HEF 1669

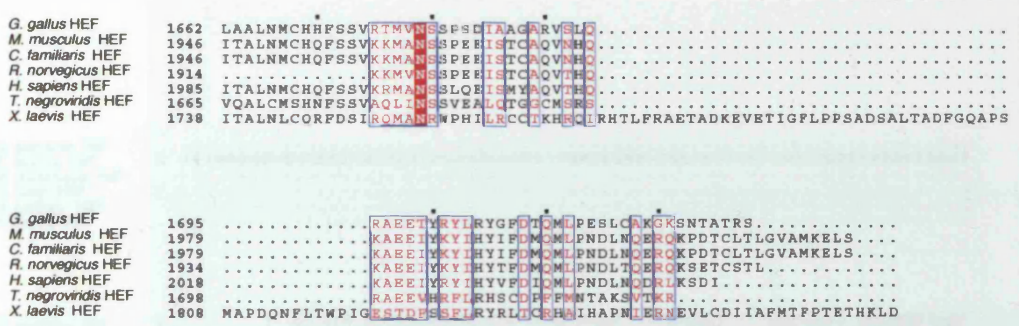
G. gallus HEF 1662 LAALNMCHHFSSVRTMVNSSPSDIAAGARVSLQ
M. musculus HEF 1946 ITALNMCHQFSSVKKMANSSPEEISTCAQVNHQ
C. familiaris HEF 1946 ITALNMCHQFSSVKKMANSSPEEISTCAQVNHQ
R. norvegicus HEF 1914 KKMVNSSPEEISTCAQVTHQ
H. sapiens HEF 1985 ITALNMCHQFSSVKRMANSSLQEISMYAQVTHQ
T. negroviridis HEF 1665 VQALCMSHNFSSVAQLINSSVEALQTGGCMSRS
X. laevis HEF 1738 ITALNLCQRFDSIRQMANSWPHILRCCTKHRQLRHTLFRAETADKEVETIGFLPPSADSALTADFGQAPS
G. gallus HEF 1695 RAEETYRYLRYGFDTQMLPESLCAKGKSNTATRS
M. musculus HEF 1979 KAEEIYKYIHYIFDMQMLPNDLNQERQKPDTCLTLGVAMKELS
C. familiaris HEF 1979 KAEEIYKYIHYIFDMQMLPNDLNQERQKPDTCLTLGVAMKELS
R. norvegicus HEF 1934 KAEEIYKYIHYTFDMQMLPNDLTQERQKSETCSTL
H. sapiens HEF 2018 KAEEIYRYIHYVFDIQMLPNDLNQDRLKSDI
T. negroviridis HEF 1698 RAEEVWRFLRHSCDPFFMNTAKSVTKR
X. laevis HEF 1808 MAPDQNFLTWPIGESTDFSSFLRYRLTCRHAIHAPNLERNEVLCDIIAFMTFPTETHKLD

APPENDIX 1, FIGURE 10: Sequence alignment of vertebrate HIP orthologues

Bos taurus HIP (NCBI # XP_587996), *Mus musculus* HIP (NCBI # AAH96687), *Danio rerio* HIP (NCBI # XP_687903), *Gallus gallus* HIP (NCBI # XP_414132) and *Xenopus laevis* HIP (NCBI # AAH87430) were identified by BLAST search for orthologues of *Homo sapiens* HIP. Sequence alignments were carried out using ClustalW.

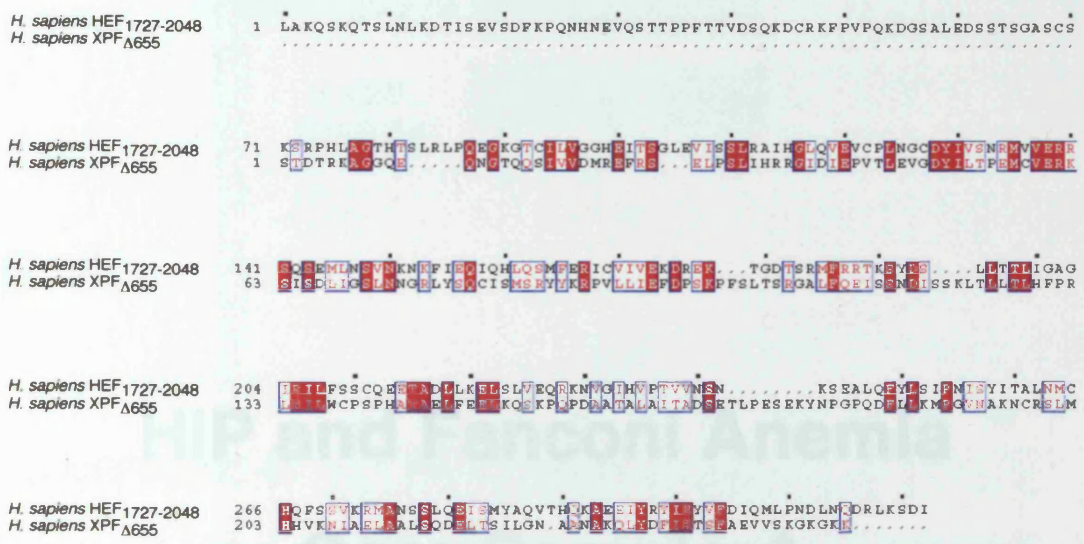

APPENDIX 1, FIGURE 11: Sequence alignment between *H. sapiens* $HEF_{1727-2048}$ and *H. sapiens* $XPF_{\Delta 655}$

Sequence alignments were carried out using ClustalW.

APPENDIX TWO

HIP and Fanconi Anemia Core Complex*

The experiments described in the figures of this appendix have been performed in Weidong Wang's lab (National Institute of Aging/NIH)

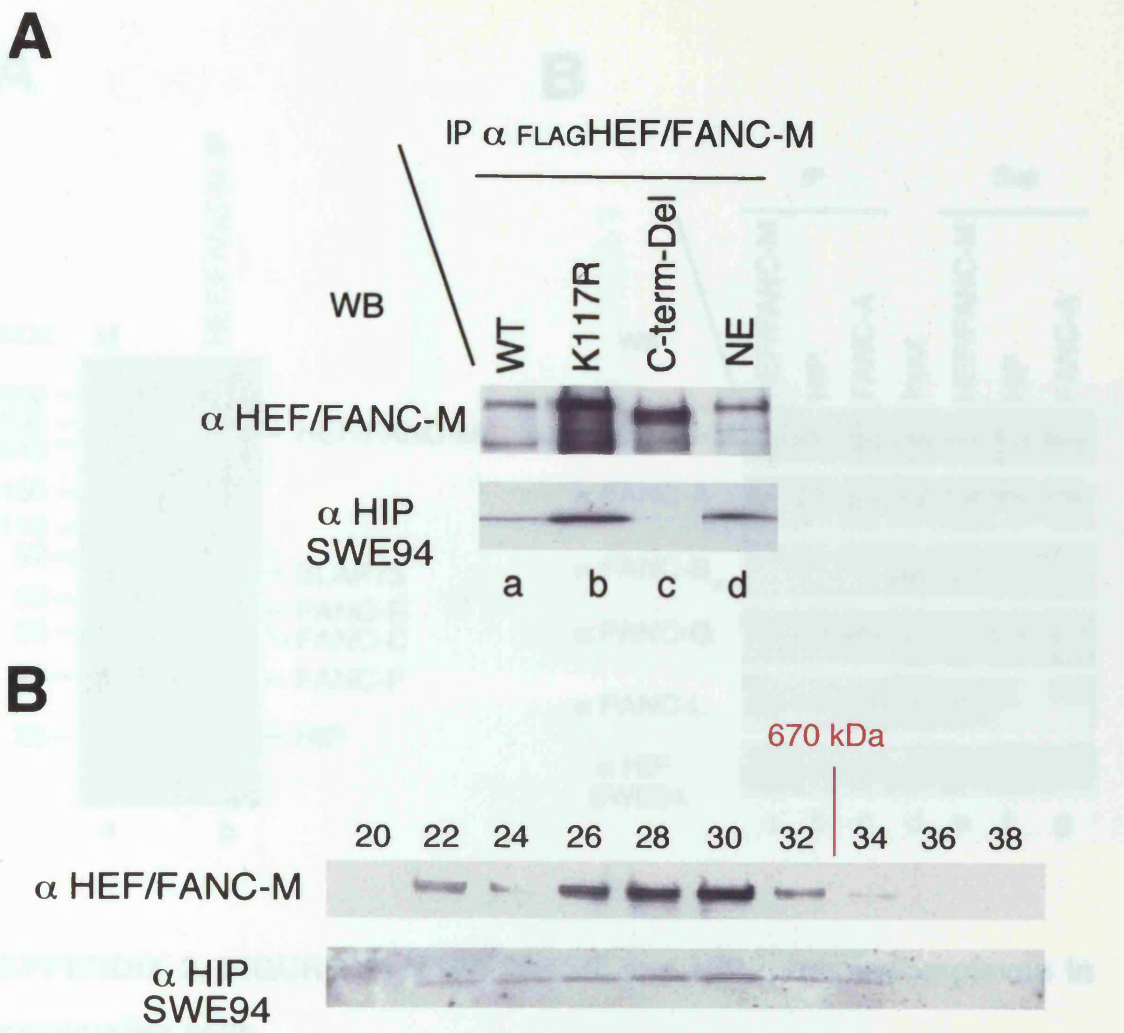

APPENDIX 2, FIGURE 1: Interaction of HEF/FANC-M and HIP in mammalian cells

A. Extracts from HeLa cells expressing either FLAGHEF/FANC-M or K117R mutant FLAGHEF/FANC-M or C-terminal deleted FLAGHEF/FANC-M (lanes a, b, and c respectively) were immunoprecipitated using anti-FLAG antibody and immunoblotted using rabbit polyclonal antibodies raised against HEF/FANC-M (Meetei et al., 2005) and HIP (SWE94). Nuclear extract (NE) was used as a control (lane d).

B. The final fractions of HeLa nuclear extracts subjected to Superose 6 gel filtration chromatography were immunoblotted against HEF/FANC-M and HIP, as described in (A). The fraction number and the position of the 670 kDa gel filtration marker is indicated.

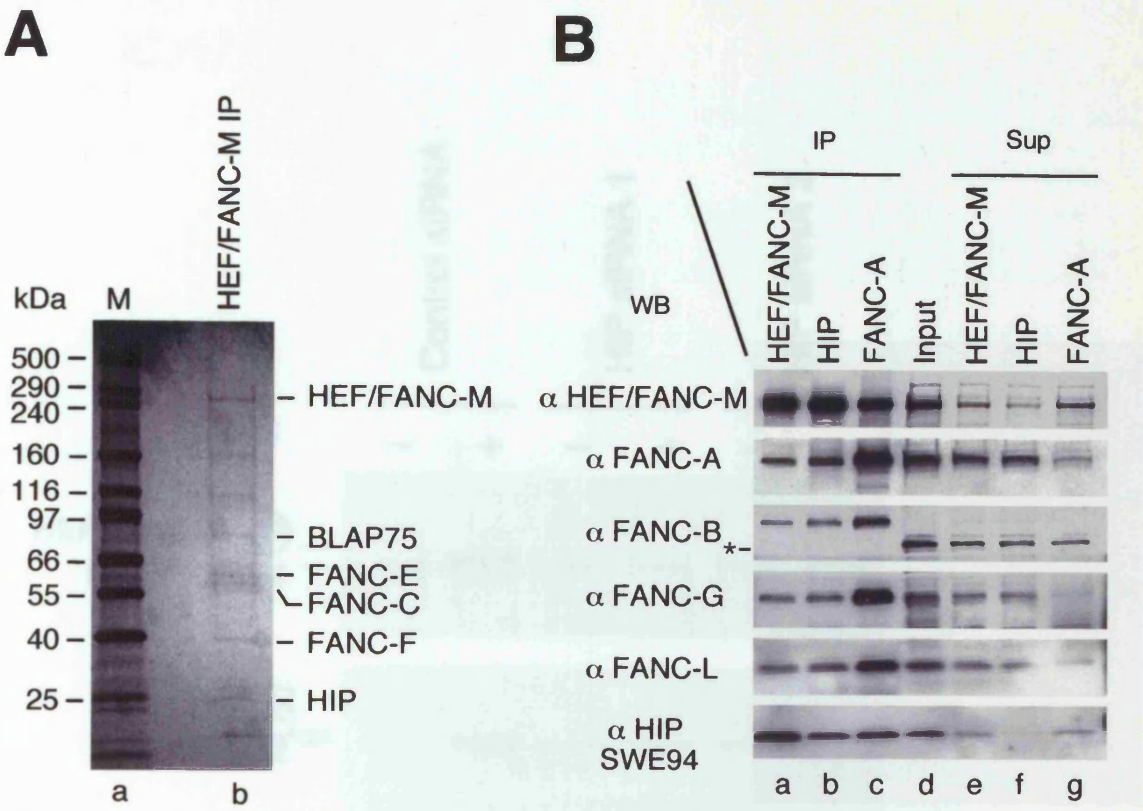

APPENDIX 2, FIGURE 2: HEF/FANC-M and HIP immunocomplexes in mammalian cells

A. Complexes immunoprecipitated from HeLa nuclear extract with a rabbit polyclonal anti-HEF/FANC-M antibody (Meetei et al., 2005) were run on SDS-PAGE and visualised with Coomassie blue staining (lane b). The identities of the polypeptides in the HEF/FANC-M immunocomplex, as detected by mass-spectrometric analysis, are indicated on the right side of the gel.

B. Extracts from mammalian cells were immunoprecipitated with rabbit polyclonal antibodies against HEF/FANC-M (Meetei et al., 2005), FANC-A (Waisfisz et al., 1999) and HIP (SWE94). Supernatant and immunoprecipitated fractions (lanes e-g and a-c, respectively) were immunoblotted with antibodies against HEF/FANC-M (Meetei et al., 2005), FANC-A (Waisfisz et al., 1999), FANC-B (Meetei et al., 2004), FANC-G (Waisfisz et al., 1999), FANC-L (Meetei et al., 2003a) and HIP (SWE94). Input fraction was used as a control (lane d). The asterisk indicates a non-specific band recognised by the FANC-B antibody.

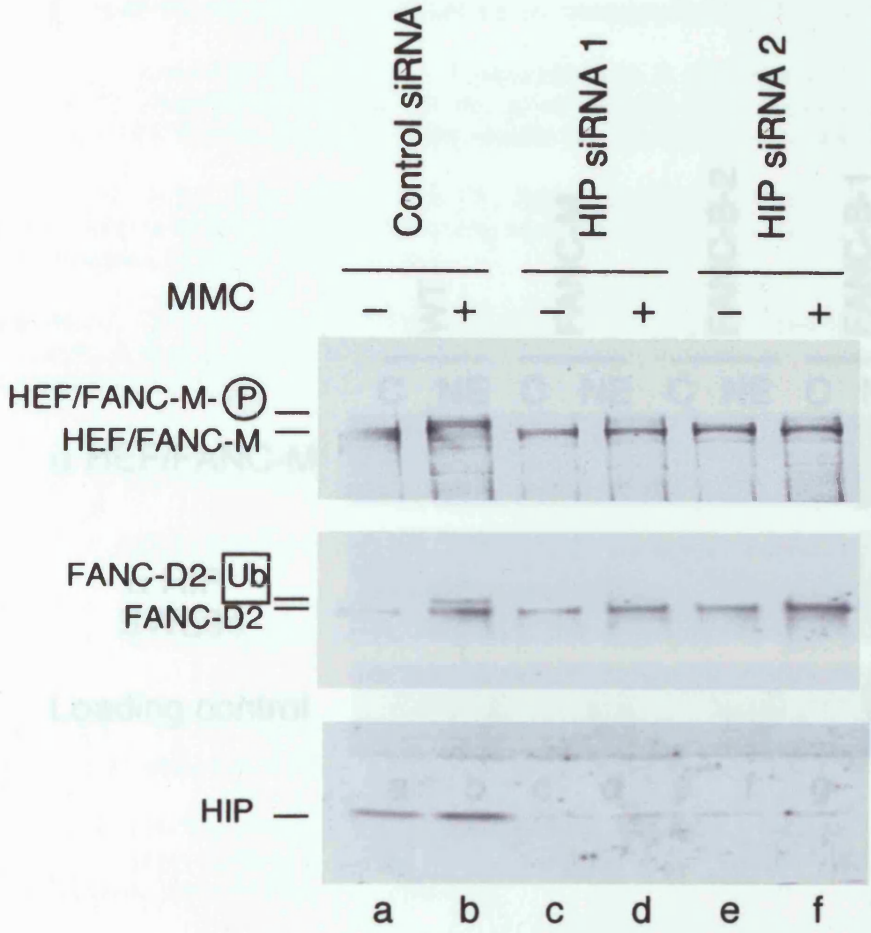

APPENDIX 2, FIGURE 3: Depletion of HIP by siRNA in mammalian cells

Mammalian cells were transfected with siRNA 1 or 2 against HIP or with control siRNA. Extracts from siRNA transfected cells, with or without mitomycin C (MMC) treatment (lanes b, d and f or a, c and e, respectively), were immunoblotted with antibodies against HEF/FANC-M (Meetei et al., 2005), FANC-D2 (Meetei et al., 2003a) and HIP (SWE94). The phosphorylated form of HEF/FANC-M (HEF/FANC-M-Ⓟ) and the monoubiquitinated form of FANC-D2 (FANC-D2-Ub) are indicated.

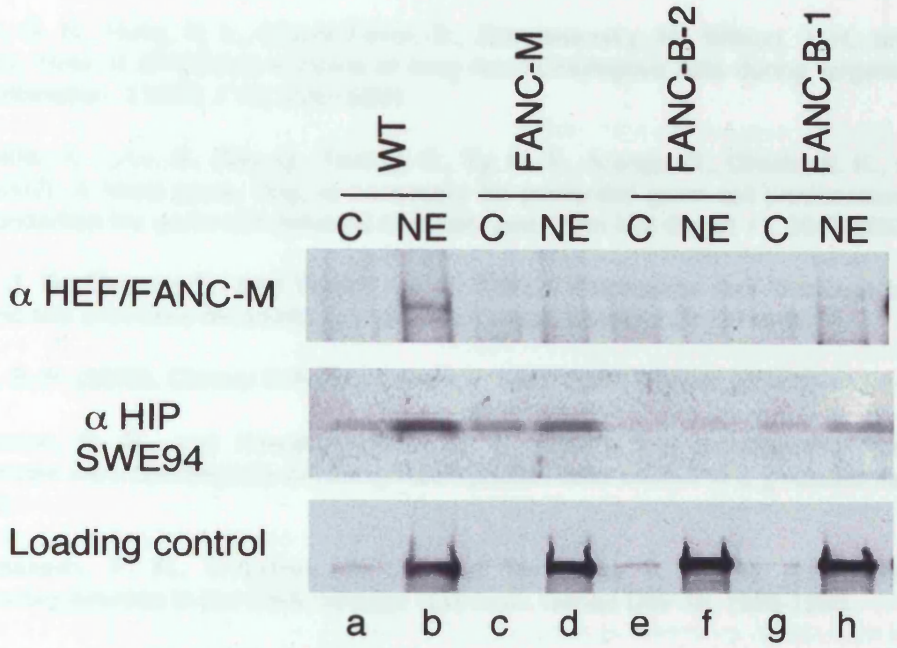

APPENDIX 2, FIGURE 4: Protein levels of HEF/FANC-M and HIP in Fanconi Anemia cell lines

Cytoplasmic (C) and nuclear extracts (NE) from WT (lanes a and b), FANC-M (lanes c and d) and two FANC-B cell lines (FANC-B-2, lanes e and f; FANC-B-1, lanes g and h) were run on SDS-PAGE and immuno-blotted with rabbit polyclonal antibodies against HEF/FANC-M (Meetei et al., 2005) and HIP (SWE94). A control for equal loading of cytoplasmic or nuclear extracts is shown.

BIBLIOGRAPHY

Aboussekhra, A., Biggerstaff, M., Shivji, M. K. K., Vilpo, J. A., Moncollin, V., Podust, V. N., Protic, M., Hubscher, U., Egly, J. M., and Wood, R. D. (1995). Mammalian DNA nucleotide excision repair reconstituted with purified protein components. Cell *80*, 859-868.

Abraham, J., Lemmers, B., Hande, M. P., Moynahan, M. E., Chahwan, C., Ciccia, A., Essers, J., Hanada, K., Chahwan, R., Khaw, A. K., *et al.* (2003). Eme1 is involved in DNA damage processing and maintenance of genomic stability in mammalian cells. EMBO J *22*, 6137-6147.

Adair, G. R., Rolig, R. L., Moore-Faver, D., Zabelshansky, M., Wilson, J. H., and Nairn, R. S. (2000). Role of ERCC1 in removal of long non-homologous tails during targeted homologous recombination. EMBO J *19*, 5552-5561.

Agoulnik, A. I., Lu, B., Zhu, Q., Truong, C., Ty, M. T., Arango, N., Chada, K. K., and Bishop, C. E. (2002). A novel gene, Pog, is necessary for primordial germ cell proliferation in the mouse and underlies the germ cell deficient mutation, gcd. Hum Mol Genet *11*, 3047-3053.

Ahn, J. S., Osman, F., and Whitby, M. C. (2005). Replication fork blockage by RTS1 at an ectopic site promotes recombination in fission yeast. EMBO J *24*, 2011-2023.

Alter, B. P. (2003). Cancer in Fanconi anemia, 1927-2001. Cancer *97*, 425-440.

Anderson, D. G., and Kowalczykowski, S. C. (1997). The translocating RecBCD enzyme stimulates recombination by directing RecA protein onto ssDNA in a χ-related manner. Cell *90*, 77-86.

Andreassen, P. R., D'Andrea, A. D., and Taniguchi, T. (2004). ATR couples FANCD2 monoubiquitination to the DNA-damage response. Genes Dev *18*, 1958-1963.

Aravind, L., and Koonin, E. V. (2001). Prokaryotic homologs of the eukaryotic DNA-end-binding protein Ku, novel domains in the Ku protein and prediction of a prokaryotic double-strand break repair system. Genome Res *11*, 1365-1374.

Aravind, L., Makarova, K. S., and Koonin, E. V. (2000). Holliday junction resolvases and related nucleases: identification of new families, phyletic distribution and evolutionary trajectories. Nucl Acids Res *28*, 3417-3432.

Aravind, L., Walker, D. R., and Koonin, E. V. (1999). Conserved domains in DNA repair proteins and evolution of repair systems. Nucl Acids Res *27*, 1223-1242.

Ariyoshi, M., Vassylyev, D. G., Iwasaki, H., Nakamura, H., Shinagawa, H., and Morikawa, K. (1994). Atomic structure of the RuvC resolvase: A Holliday junction-specific endonuclease from E. coli. Cell *78*, 1063-1072.

Baker, B. S., and Carpenter, A. T. (1972). Genetic analysis of sex chromosomal meiotic mutants in Drosophilia melanogaster. Genetics *71*, 255-286.

Barber, L. J., Ward, T. A., Hartley, J. A., and McHugh, P. J. (2005). DNA interstrand cross-link repair in the Saccharomyces cerevisiae cell cycle: Overlapping roles for PSO2 (SNM1) with MutS factors and EXO1 during S phase. Mol Cell Biol *25*, 2297-2309.

Bastin-Shanower, S. A., Fricke, W. M., Mullen, J. R., and Brill, S. J. (2003). The mechanism of Mus81-Mms4 cleavage site selection distinguishes it from the homologous endonuclease Rad1-Rad10. Mol Cell Biol *23*, 3487-3496.

Baumann, P., Benson, F. E., and West, S. C. (1996). Human Rad51 protein promotes ATP-dependent homologous pairing and strand transfer reactions in vitro. Cell *87*, 757-766.

Benbow, R. M., Zuccarelli, A. J., and Sinsheimer, R. L. (1975). Recombinant DNA molecules of ØX174. Proc Natl Acad Sci USA *72*, 235-239.

Benkovic, S. J., Valentine, A. M., and Salinas, F. (2001). Replisome-mediated DNA replication. Annu Rev Biochem *70*, 181-208.

Bennett, R. J., Dunderdale, H. J., and West, S. C. (1993). Resolution of Holliday junctions by RuvC resolvase: Cleavage specificity and DNA distortion. Cell *74*, 1021-1031.

Bennett, R. J., and West, S. C. (1995). Structural analysis of the RuvC-Holliday junction complex reveals an unfolded junction. J Mol Biol *252*, 213-226.

Berardini, M., Foster, P. L., and Loechler, E. L. (1999). DNA polymerase II (polB) is involved in a new DNA repair pathway for DNA interstrand cross-links in Escherichia coli. J Bacteriol *181*, 2878-2882.

Bernstein, D. A., Zittel, M. C., and Keck, J. L. (2003). High-resolution structure of the E.coli RecQ helicase catalytic core. EMBO J *22*, 4910-4921.

Bianchi, V., Pontis, E., and Reichard, P. (1986). Changes of deoxyribonucleoside triphosphate pools induced by hydroxyurea and their relation to DNA synthesis. J Biol Chem *261*, 16037-16042.

Bienko, M., Green, C. M., Crosetto, N., Rudolf, F., Zapart, G., Coull, B., Kannouche, P., Wider, G., Peter, M., Lehmann, A. R., *et al.* (2005). Ubiquitin-binding domains in Y-family polymerases regulate translesion synthesis. Science *310*, 1821-1824.

Blais, V., Gao, H., Elwell, C. A., Boddy, M. N., Gaillard, P. H. L., Russell, P., and McGowan, C. H. (2004). RNA interference inhibition of Mus81 reduces mitotic recombination in human cells. Mol Biol Cell *15*, 552-562.

Blom, E., van de Vrugt, H. J., de Vries, Y., de Winter, J. P., Arwert, F., and Joenje, H. (2004). Multiple TPR motifs characterize the Fanconi anemia FANCG protein. DNA Repair (Amst) *3*, 77-84.

Boddy, M. N., Gaillard, P. H. L., McDonald, W. H., Shanahan, P., Yates, J. R., and Russell, P. (2001). Mus81-Eme1 are essential components of a Holliday junction resolvase. Cell *107*, 537-548.

Boddy, M. N., Lopez-Girona, A., Shanahan, P., Interthal, H., Heyer, W. D., and Russell, P. (2000). Damage tolerance protein Mus81 associates with the FHA1 domain of checkpoint kinase Cds1. Mol Cell Biol *20*, 8758-8766.

Bootsma, D., and Hoeijmakers, J. H. (1994). The molecular basis of nucleotide excision repair syndromes. Mutat Res *307*, 15-23.

Bradford, M. M. (1976). A rapid and sensitive method for the quantitation of microgram quantities of protein utilizing the principle of protein-dye binding. Anal Biochem *72*, 248-254.

Bregman, D. B., Halaban, R., Van Gool, A. J., Henning, K. A., Friedberg, E. C., and Warren, S. L. (1996). UV-induced ubiquitination of RNA polymerase II: A novel modification deficient in Cockayne syndrome cells. Proc Natl Acad Sci USA *93*, 11586-11590.

Brendel, M., and Ruhland, A. (1984). Relationships between functionality and genetic toxicology of selected DNA damaging agents Mutat Res *133*, 51-85.

Brewer, B. J., and Fangman, W. L. (1988). A replication fork barrier at the 3' end of yeast ribosomal RNA genes. Cell *55*, 637-643.

Bridge, W. L., Vandenberg, C. J., Franklin, R. J., and Hiom, K. (2005). The BRIP1 helicase functions independently of BRCA1 in the Fanconi anemia pathway for DNA crosslink repair. Nat Genet *37*, 953-957.

Burkhalter, M. D., and Sogo, J. M. (2004). rDNA enhancer affects replication initiation and mitotic recombination: Fob1 mediates nucleolytic processing independently of replication. Mol Cell *15*, 409-421.

Buschta-Hedayat, N., Buterin, T., Hess, M. T., Missura, M., and Naegeli, H. (1999). Recognition of nonhybridizing base pairs during nucleotide excision repair of DNA. Proc Natl Acad Sci U S A *96*, 6090-6095.

Calzada, A., Hodgson, B., Kanemaki, M., Bueno, A., and Labib, K. (2005). Molecular anatomy and regulation of a stable replisome at a paused eukaryotic DNA replication fork. Genes Dev *19*, 1905-1919.

Cantor, S., Drapkin, R., Zhang, F., Lin, Y. F., Han, J. L., Pamidi, S., and Livingston, D. M. (2004). The BRCA1-associated protein BACH1 is a DNA helicase targeted by clinically relevant inactivating mutations. Proc Natl Acad Sci U S A *101*, 2357-2362.

Cassuto, E., West, S. C., and Howard-Flanders, P. (1980). Initiation of genetic recombination: Pairing of duplex DNA molecules promoted by RecA protein, In Mechanistic Studies of DNA Replication and Genetic Recombination. UCLA Symposia on Molecular and Cellular Biology, B. Alberts, ed. (New York: Academic Press), pp. 871-880.

Ceschini, S., Keeley, A., McAlister, M. S. B., Oram, M., Phelan, J., Pearl, L. H., Tsaneva, I. R., and Barrett, T. E. (2001). Crystal structure of the fission yeast mitochondrial Holliday junction resolvase Ydc2. EMBO J *20*, 6601-6611.

Chaganti, R. S., Schonberg, S., and German, J. (1974). A manyfold increase in sister chromatid exchanges in Bloom's syndrome lymphocytes. Proc Natl Acad Sci U S A *71*, 4508-4512.

Chen, X. B., Melchionna, R., Denis, C. M., Gaillard, P. H. L., Blasina, A., Van de Weyer, I., Boddy, M. N., Russell, P., Vialard, J., and McGowan, C. H. (2001). Human Mus81-associated endonuclease cleaves Holliday junctions in vitro. Mol Cell *8*, 1117-1127.

Choi, Y. J., Ryu, K. S., Ko, Y. M., Chae, Y. K., Pelton, J. G., Wemmer, D. E., and Choi, B. S. (2005). Biophysical characterization of the interaction domains and mapping of the contact residues in the XPF-ERCC1 complex. J Biol Chem *280*, 28644-28652.

Ciccia, A., Constantinou, A., and West, S. C. (2003). Identification and characterization of the human Mus81/Eme1 endonuclease. J Biol Chem *278*, 25172-25178.

Cleaver, J. E. (2005). Cancer in xeroderma pigmentosum and related disorders of DNA repair. Nat Rev Cancer *7*, 564-573.

Cleaver, J. E., Cortés, F., Karentz, D., Lutze, L. H., Morgan, W. F., Player, A. N., Vuksanovic, L., and Mitchell, D. L. (1988). The relative biological importance of cyclobutane and (6-4) pyrimidine-pyrimidone dimer photoproducts in human cells: Evidence from a xeroderma pigmentosum revertant. Photochem Photobiol *48*, 41-49.

Clegg, R. M., Murchie, A. I. H., and Lilley, D. M. J. (1994). The solution structure of the four-way DNA junction at low salt conditions: A fluorescence resonance energy transfer analysis. Biophys J *66*, 99-109.

Collins, A. R. (1993). Mutant rodent cell lines sensitive to ultraviolet light, ionizing radiation and cross-linking agents: a comprehensive survey of genetic and biochemical characteristics. Mutat Res *293*, 99-118.

Constantinou, A., Chen, X.-B., McGowan, C. H., and West, S. C. (2002). Holliday junction resolution in human cells: Two junction endonucleases with distinct substrate specificities. EMBO J *21*, 5577-5585.

Constantinou, A., Davies, A. A., and West, S. C. (2001). Branch migration and Holliday junction resolution catalyzed by activities from mammalian cells. Cell *104*, 259-268.

Coulon, S., Gaillard, P. H. L., Chahwan, C., McDonald, W. H., Yates, J. R., and Russell, P. (2004). Slx1-Slx4 are subunits of a structure-specific endonuclease that maintains ribosomal DNA in fission yeast. Mol Biol Cell *15*, 71-80.

Coulon, S., Noguchi, E., Noguchi, C., Du, L. L., Nakamura, T. M., and Russell, P. (2006). Rad22Rad52-dependent Repair of Ribosomal DNA Repeats Cleaved by Slx1-Slx4 Endonuclease. Mol Biol Cell.

Cox, M. M., Goodman, M. F., Kreuzer, K. N., Sherratt, D. J., Sandler, S. J., and Marians, K. J. (2000). The importance of repairing stalled replication forks. Nature *404*, 37-41.

Cui, X., Brenneman, M., Meyne, J., Oshimura, M., Goodwin, E. H., and Chen, D. J. (1999). The XRCC2 and XRCC3 repair genes are required for chromosome stability in mammalian cells. Mutat Res DNA Repair *434*, 75-88.

Cunningham, R. P., DasGupta, C., Shibata, T., and Radding, C. M. (1980). Homologous pairing in genetic recombination: RecA protein makes joint molecules of gapped circular DNA and closed circular DNA. Cell *20*, 223-235.

D'Andrea, A. D., and Grompe, M. (2003). The Fanconi anaemia BRCA pathway. Nat Rev Canc *3*, 23-34.

Dalgaard, J. Z., and Klar, A. J. (2001). A DNA replication-arrest site RTS1 regulates imprinting by determining the direction of replication at mat1 in S. pombe. Genes Dev *15*, 2060-2068.

Davies, A. A., Masson, J.-Y., McIlwraith, M. J., Stasiak, A. Z., Stasiak, A., Venkitaraman, A. R., and West, S. C. (2001). Role of BRCA2 in control of the RAD51 recombination and DNA repair protein. Molec Cell *7*, 273-282.

de Boer, J., and Hoeijmakers, J. H. (2000). Nucleotide excision repair and human syndromes. Carcinogenesis *21*, 453-460.

De Laat, W. L., Appeldoorn, E., Jaspers, N. G. J., and Hoeijmakers, J. H. J. (1998a). DNA structural elements required for ERCC1-XPF endonuclease activity. J Biol Chem *273*, 7835-7842.

De Laat, W. L., Sijbers, A. M., Odijk, H., Jaspers, N. G. J., and Hoeijmakers, J. H. J. (1998b). Mapping of interaction domains between human repair proteins ERCC1 and XPF. Nucl Acids Res *26*, 4146-4152.

de los Santos, T., Hunter, N., Lee, C., Larkin, B., Loidl, J., and Hollingsworth, N. M. (2003). The Mus81/Mms4 endonuclease acts independently of double-Holliday junction resolution to promote a distinct subset of crossovers during meiosis in budding yeast. Genetics *164*, 81-94.

de los Santos, T., Loidl, J., Larkin, B., and Hollingsworth, N. M. (2001). A role for MMS4 in the processing of recombination intermediates during meiosis in Saccharomyces cerevisiae. Genetics *159*, 1511-1525.

De Silva, I. U., McHugh, P. J., Clingen, P. H., and Hartley, J. A. (2000). Defining the roles of nucleotide excision repair and recombination in the repair of DNA interstrand cross-links in mammalian cells. Mol Cell Biol *20*, 7980-7990.

de Vries, A., van Oostrom, C. T., Hofhuis, F. M., Dortant, P. M., Berg, R. J., de Gruijl, F. R., Wester, P. W., van Kreijl, C. F., Capel, P. J., van Steeg, H., and et al. (1995). Increased susceptibility to ultraviolet-B and carcinogens of mice lacking the DNA excision repair gene XPA. Nature *377*, 169-173.

de Vries, S. S., Baart, E. B., Dekker, M., Siezen, A., de Rooij, D. G., de Boer, P., and te Riele, H. (1999). Mouse MutS-like protein Msh5 is required for proper chromosome synapsis in male and female meiosis. Genes Dev *13*, 523-531.

de Winter, J. P., van der Weel, L., de Groot, J., Stone, S., Waisfisz, Q., Arwert, F., Scheper, R. J., Kruyt, F. A., Hoatlin, M. E., and Joenje, H. (2000). The Fanconi anemia protein FANCF forms a nuclear complex with FANCA, FANCC and FANCG. Hum Mol Genet *9*, 2665-2674.

Dendouga, N., Gao, H., Moechars, D., Janicot, M., Vialard, J., and McGowan, C. H. (2005). Disruption of murine Mus81 increases genomic instability and DNA damage sensitivity but does not promote tumorigenesis. Mol Cell Biol *25*, 7569-7579.

Digweed, M., Rothe, S., Demuth, I., Scholz, R., Schindler, D., Stumm, M., Grompe, M., Jordan, A., and Sperling, K. (2002). Attenuation of the formation of DNA-repair foci containing RAD51 in Fanconi anaemia. Carcinogenesis *23*, 1121-1126.

Doe, C. L., Ahn, J. S., Dixon, J., and Whitby, M. C. (2002). Mus81-Eme1 and Rqh1 involvement in processing stalled and collapsed replication forks. J Biol Chem *277*, 32753-32759.

Doe, C. L., Dixon, J., Osman, F., and Whitby, M. C. (2000). Partial suppression of the fission yeast rqh1(-) phenotype by expression of a bacterial Holliday junction resolvase. EMBO J *19*, 2751-2762.

Doe, C. L., Osman, F., Dixon, J., and Whitby, M. C. (2004). DNA repair by a Rad22-Mus81-dependent pathway that is independent of Rhp51. Nucleic Acids Res *32*, 5570-5581.

Doe, C. L., and Whitby, M. C. (2004). The involvement of Srs2 in post-replication repair and homologous recombination in fission yeast. Nucl Acids Res *32*, 1480-1491.

Doherty, A. J., Serpell, L. C., and Ponting, C. P. (1996). The helix-hairpin-helix DNA-binding motif: a structural basis for non-sequence-specific recognition of DNA. Nucleic Acids Res *24*, 2488-2497.

Doniger, J., Warner, R. C., and Tessman, I. (1973). Role of circular dimer DNA in the primary recombination mechanism of bacteriophage S13. Nature New Biol *242*, 9-12.

Dronkert, M. L. G., and Kanaar, R. (2001). Repair of DNA interstrand cross-links. Mutat Res DNA Repair *486*, 217-247.

Duckett, D. R., Murchie, A. I. H., Diekmann, S., Von Kitzing, E., Kemper, B., and Lilley, D. M. J. (1988). The structure of the Holliday junction and its resolution. Cell *55*, 79-89.

Dunderdale, H. J., Benson, F. E., Parsons, C. A., Sharples, G. J., Lloyd, R. G., and West, S. C. (1991). Formation and resolution of recombination intermediates by E. coli RecA and RuvC proteins. Nature *354*, 506-510.

Dyda, F., Hickman, A. B., Jenkins, T. M., Engelman, A., Craigie, R., and Davies, D. R. (1994). Crystal structure of the catalytic domain of HIV-1 integrase: similarity to other polynucleotidyl transferases. Science *266*, 1981-1986.

Easton, D. F., Hopper, J. L., Thomas, D. C., Antoniou, A., Pharoah, P. D. P., Whittemore, A. S., and Haile, R. W. (2004). Breast cancer risks for BRCA1/2 carriers. Science *306*, 2187-2188.

Echols, H., and Goodman, M. F. (1991). Fidelity mechanisms in DNA replication. Ann Rev Biochem *60*, 477-511.

Edelmann, W., Cohen, P. E., Kneitz, B., Winand, N., Lia, M., Heyer, J., Kolodner, R., Pollard, J. W., and Kucherlapati, R. (1999). Mammalian MutS homologue 5 is required for chromosome pairing in meiosis. Nature Genet *21*, 123-127.

Eichman, B. F., Vargason, J. M., Mooers, B. H. M., and Ho, P. S. (2000). The Holliday junction in an inverted repeat DNA sequence: Sequence effects on the structure of four-way junctions. Proc Natl Acad Sci USA *97*, 3971-3976.

Ensch-Simon, I., Burgers, P. M., and Taylor, J. S. (1998). Bypass of a site-specific cis-syn thymine dimer in an SV40 vector during in vitro replication by HeLa and XPV cell-free extracts. Biochemistry *37*, 8218-8226.

Enzlin, J. H., and Scharer, O. D. (2002). The active site of the DNA repair endonuclease XPF-ERCC1 forms a highly conserved nuclease motif. EMBO J *21*, 2045-2053.

Esashi, F., Christ, N., Gannon, J., Liu, Y., Hunt, T., Jasin, M., and West, S. C. (2005). CDK-dependent phosphorylation of BRCA2 as a regulatory mechanism for recombinational repair. Nature *434*, 598-604.

Evans, D. H., and Kolodner, R. (1988). Effect of DNA structure and nucleotide sequence on Holliday junction resolution by a Saccharomyces cerevisiae endonuclease. J Mol Biol *201*, 69-80.

Evans, E., Fellows, J., Coffer, A., and Wood, R. D. (1997a). Open complex formation around a lesion during nucleotide excision repair provides a structure for cleavage by human XPG protein. EMBO J *16*, 625-638.

Evans, E., Moggs, J. G., Hwang, J. R., Egly, J. M., and Wood, R. D. (1997b). Mechanism of open complex and dual incision formation by human nucleotide excision repair factors. EMBO J *16*, 6559-6573.

Fabre, F., Chan, A., Heyer, W. D., and Gangloff, S. (2002). Alternate pathways involving Sgs1/Top3, Mus81/Mus81, and Srs2 prevent formation of toxic recombination intermediates from single-stranded gaps created by DNA replication. Proc Natl Acad Sci U S A *99*, 16887-16892.

Fei, P. W., Yin, J. H., and Wang, W. D. (2005). New advances in the DNA damage response network of Fanconi anemia and BRCA proteins - FAAP95 replaces BRCA2 as the true FANCB protein. Cell Cycle *4*, 80-86.

Flores, M. J., Bierne, H., Ehrlich, S. D., and Michel, B. (2001). Impairment of lagging strand synthesis triggers the formation of a RuvABC substrate at replication forks. EMBO J *20*, 619-629.

Fricke, W. M., and Brill, S. J. (2003). Slx1-Slx4 is a second structure-specific endonuclease functionally redundant with Sgs1-Top3. Genes Dev *17*, 1768-1778.

Friedberg, E. C. (2001). How nucleotide excision repair protects against cancer. Nat Rev Cancer *1*, 22-33.

Friedberg, E. C. (2003). DNA damage and repair. Nature *421*, 436-440.

Friedberg, E. C. (2005). Suffering in silence: the tolerance of DNA damage. Nat Rev Mol Cell Biol *6*, 943-953.
Fu, Y., and Xiao, W. (2003). Functional domains required for the Saccharomyces cerevisiae Mus81-Mms4 endonuclease complex formation and nuclear localization. DNA Repair *2*, 1435-1447.

Gaillard, P.-H. L., Noguchi, E., Shanahan, P., and Russell, P. (2003). The endogenous Mus81-Eme1 complex resolves Holliday junctions by a nick and couternick mechanism. Molec Cell *12*, 747-759.

Gaillard, P. H., and Wood, R. D. (2001). Activity of individual ERCC1 and XPF subunits in DNA nucleotide excision repair. Nucleic Acids Res *29*, 872-879.

Gao, H., Chen, X. B., and McGowan, C. H. (2003). Mus81 endonuclease localizes to nucleoli and to regions of DNA damage in human S-phase cells. Mol Biol Cell *14*, 4826-4834.

Garcia-Higuera, I., Kuang, Y., Denham, J., and D'Andrea, A. D. (2000). The fanconi anemia proteins FANCA and FANCG stabilize each other and promote the nuclear accumulation of the Fanconi anemia complex. Blood *96*, 3224-3230.

Garcia-Higuera, I., Taniguchi, T., Ganesan, S., Meyn, M. S., Timmers, C., Hejna, J., Grompe, M., and D'Andrea, A. D. (2001). Interaction of the Fanconi anemia proteins and BRCA1 in a common pathway. Mol Cell *7*, 249-262.

Gerber, J. K., Gogel, E., Berger, C., Wallisch, M., Muller, F., Grummt, I., and Grummt, F. (1997). Termination of mammalian rDNA replication: polar arrest of replication fork movement by transcription termination factor TTF-I. Cell *90*, 559-567.

Godthelp, B. C., Artwert, F., Joenje, H., and Zdzienicka, M. Z. (2002a). Impaired DNA damage-induced nuclear RAD51 foci formation uniquely characterizes Fanconi anemia group D1. Oncogene *21*, 5002-5005.

Godthelp, B. C., Wiegant, W. W., A., v. D.-G., Scharer, O. D., van Buul, P. P. W., Kanaar, R., and Zdzienicka, M. Z. (2002b). Mammalian Rad51C contributes to DNA cross-link resistance, sister chromatid cohesion and genomic stability. Nucl Acids Res *30*, 2172-2182.

Godthelp, B. C., Wiegant, W. W., Waisfisz, Q., Medhurst, A. L., Arwert, F., Joenje, H., and Zdzienicka, M. Z. (2006). Inducibility of nuclear Rad51 foci after DNA damage distinguishes all Fanconi anemia complementation groups from D1/BRCA2. Mutat Res *594*, 39-48.

Gordon, S. M., Alon, N., and Buchwald, M. (2005). FANCC, FANCE, and FANCD2 form a ternary complex essential to the integrity of the Fanconi anemia DNA damage response pathway. J Biol Chem *280*, 36118-36125.

Gruver, A. M., Miller, K. A., Rajesh, C., Smiraldo, P. G., Kaliyaperumal, S., Balder, R., Stiles, K. M., Albala, J. S., and Pittman, D. L. (2005). The ATPase motif in RAD51D is required for resistance to DNA interstrand crosslinking agents and interaction with RAD51C. Mutagenesis *20*, 433-440.

Gupta, R., Sharma, S., Sommers, J. A., Jin, Z., Cantor, S. B., and Brosh, R. M. (2005). Analysis of the DNA substrate specificity of the human BACH1 helicase associated with breast cancer. J Biol Chem *280*, 25450-25460.

Gurtan, A. M., Stuckert, P., and D'Andrea, A. D. (2006). The WD40-repeats of FANCL are required for Fanconi anemia core complex assembly. J Biol Chem.

Harrington, J. J., and Lieber, M. R. (1994). The characterization of a mammalian DNA structure specific endonuclease. EMBO J *13*, 1235-1246.

Hashizume, R., Fukuda, M., Maeda, I., Nishikawa, H., Oyake, D., Yabuki, Y., Ogata, F., and Ohta, T. (2001). The RING heterodimer BRCA1-BARD1 is a ubiquitin ligase inactivated by a breast cancer-derived mutation. J Biol Chem *276*, 14537-14540.

Heller, R. C., and Marians, K. J. (2006). Replication fork reactivation downstream of a blocked nascent leading strand. Nature *439*, 557-562.

Henneke, G., Friedrich-Heineken, E., and Hubscher, U. (2003). Flap endonuclease 1: a novel tumour suppresser protein. Trends Biochem Sci *28*, 384-390.

Higuchi, K., Katayama, T., Iwai, S., Hidaka, M., Horiuchi, T., and Maki, H. (2003). Fate of DNA replication fork encountering a single DNA lesion during oriC plasmid DNA replication in vitro. Genes Cells *8*, 437-449.

Hindges, R., and Hubscher, U. (1997). DNA polymerase delta, an essential enzyme for DNA transactions. Biol Chem *378*, 345-362.

Hirano, S., Yamamoto, K., Ishiai, M., Yamazoe, M., Seki, M., Matsushita, N., Ohzeki, M., Yamashita, Y. M., Arakawa, H., Buerstedde, J. M., *et al.* (2005). Functional relationships of FANCC to homologous recombination, translesion synthesis, and BLM. EMBO J *24*, 418-427.

Hiyama, T., Katsura, M., Yoshihara, T., Ishida, M., Kinomura, A., Tonda, T., Asahara, T., and Miyagawa, K. (2006). Haploinsufficiency of the Mus81-Eme1 endonuclease activates the intra-S-phase and G2/M checkpoints and promotes rereplication in human cells. Nucleic Acids Res *34*, 880-892.

Hoeijmakers, J. H. (2000). Genome maintenance mechanisms for preventing cancer. Nature *411*, 366-374.

Hohl, M., Thorel, F., Clarkson, S. G., and Scharer, O. D. (2003). Structural determinants for substrate binding and catalysis by the structure-specific endonuclease XPG. J Biol Chem *278*, 19500-19508.

Holliday, R. (1964). A mechanism for gene conversion in fungi. Genet Res Camb *5*, 282-304.

Hollingsworth, N. M., and Brill, S. J. (2004). The Mus81 solution to resolution: generating meiotic crossovers without Holliday junctions. Genes and Dev *18*, 117-125.

Houghtaling, S., Newell, A., Akkari, Y., Taniguchi, T., Olson, S., and Grompe, M. (2005). Fancd2 functions in a double strand break repair pathway that is distinct from non-homologous end joining. Hum Mol Genet *14*, 3027-3033.

Houghtaling, S., Timmers, C., Noll, M., Finegold, M. J., Jones, S. N., Meyn, M. S., and Grompe, M. (2003). Epithelial cancer in Fanconi anemia complementation group D2 (FancD2) knockout mice. Genes Dev *17*, 2021-2035.

Howard-Flanders, P., and West, S. C. (1983). Enzymatic mechanism of postreplication repair, In Cellular Responses to DNA Damage" UCLA Symposium on Molecular and Cellular Biology, New Series, E. C. Friedberg, and B. A. Bridges, eds. (New York: Liss), pp. 399-407.

Howlett, N. G., Taniguchi, T., Durkin, S. G., D'Andrea, A. D., and Glover, T. W. (2005). The Fanconi anemia pathway is required for the DNA replication stress response and for the regulation of common fragile site stability. Hum Mol Genet *14*, 693-701.

Howlett, N. G., Taniguchi, T., Olson, S., Cox, B., Waisfisz, Q., de Die-Smulders, C., Persky, N., Grompe, M., Joenje, H., Pals, G., *et al.* (2002). Biallelic inactivation of BRCA2 in Fanconi anemia. Science *297*, 606-609.

Hsia, K. T., Millar, M. R., King, S., Selfridge, J., Redhead, N. J., Melton, D. W., and Saunders, P. T. (2003). DNA repair gene Ercc1 is essential for normal spermatogenesis and oogenesis and for functional integrity of germ cell DNA in the mouse. Development *130*, 369-378.

Hubscher, U., and Seo, Y. S. (2001). Replication of the lagging strand: a concert of at least 23 polypeptides. Mol Cells *12*, 149-157.

Hussain, S., Wilson, J. B., Medhurst, A. L., Hejna, J., Witt, E., Anath, A., Davies, A., Masson, J. Y., Moses, R., West, S. C., *et al.* (2004). Direct interaction of FANCD2 with BRCA2 in DNA damage response pathways. Hum Mol Genet *13*, 1241-1248.

Hutchinson, F. (1985). Chemical changes induced in DNA by ionizing radiation. Prog Nucleic Acid Res *32*, 115-154.

Imlay, J. A., and Linn, S. (1988). DNA damage and oxygen radical toxicity. Science *240*, 1302-1309.

Interthal, H., and Heyer, W. D. (2000). MUS81 encodes a novel helix-hairpin-helix protein involved in the response to UV- and methylation-induced DNA damage in Saccharomyces cerevisiae. Mol Gen Genet *263*, 812-827.

Ira, G., Malkova, A., Liberi, G., Foiani, M., and Haber, J. E. (2003). Srs2 and Sgs1-Top3 suppress crossovers during double-strand break repair in yeast. Cell *115*, 401-411.

Ishida, R., and Buchwald, M. (1982). Susceptibility of Fanconi's anemia lymphoblasts to DNA-cross-linking and alkylating agents. Cancer Res *42*, 4000-4006.

Jachymczyk, W. J., von Borstel, R. C., Mowat, M. R., and Hastings, P. J. (1981). Repair of interstrand cross-links in DNA of Saccharomyces cerevisiae requires two systems for DNA repair: the RAD3 system and the RAD51 system. Mol Gen Genet *182*, 196-205.

Jackson, P. K. (2001). A new RING for SUMO: wrestling transcriptional responses into nuclear bodies with PIAS family E3 SUMO ligases. Genes Dev *15*, 3053-3058.

Johnson, R. D., Liu, N., and Jasin, M. (1999a). Mammalian XRCC2 promotes the repair of DNA double-strand breaks by homologous recombination. Nature *401*, 397-399.

Johnson, R. E., Kondratick, C. M., Prakash, S., and Prakash, L. (1999b). hRAD30 mutations in the variant form of Xeroderma pigmentosum. Science *285*, 263-265.

Kai, M., Boddy, M. N., Russell, P., and Wang, T. S. (2005). Replication checkpoint kinase Cds1 regulates Mus81 to preserve genome integrity during replication stress. Genes Dev *19*, 919-932.

Kaliraman, V., and Brill, S. J. (2002). Role of SGS1 and SLX4 in maintaining rDNA structure in Saccharomyces cerevisiae. Curr Genet *41*, 389-400.

Kaliraman, V., Mullen, J. R., Fricke, W. M., Bastin-Shanower, S. A., and Brill, S. J. (2001). Functional overlap between Sgs1-Top3 and the Mms4-Mus81 endonuclease. Genes Dev *15*, 2730-2740.

Kannouche, P., Broughton, B. C., Volker, M., Hanaoka, F., Mullenders, L. H. F., and Lehmann, A. R. (2001). Domain structure, localization, and function of DNA polymerase h defective in xeroderma pigmentosum variant cells. Genes Dev *15*, 158-172.

Kannouche, P., Fernandez de Henestrosa, A. R., Coull, B., Vidal, A. E., Gray, C., Zicha, D., Woodgate, R., and Lehmann, A. R. (2002). Localization of DNA polymerases eta and iota to the replication machinery is tightly co-ordinated in human cells. Embo J *21*, 6246-6256.
Kannouche, P. L., Wing, J., and Lehmann, A. R. (2004). Interaction of human DNA polymerase eta with monoubiquitinated PCNA: a possible mechanism for the polymerase switch in response to DNA damage. Mol Cell *14*, 491-500.

Kao, H. I., Henricksen, L. A., Liu, Y., and Bambara, R. A. (2002). Cleavage specificity of Saccharomyces cerevisiae flap endonuclease 1 suggests a double-flap structure as the cellular substrate. J Biol Chem *277*, 14379-14389.

Karow, J. K., Constantinou, A., Li, J.-L., West, S. C., and Hickson, I. D. (2000). The Bloom's Syndrome gene product promotes branch migration of Holliday junctions. Proc Natl Acad Sci USA *97*, 6504-6508.

Kato, T., and Shinoura, Y. (1977). Isolation and characterization of mutants of Escherichia coli deficient in induction of mutations by ultraviolet light. Mol Gen Genet *156*, 121-131.

Kawamoto, T., Araki, K., Sonoda, E., Yamashita, Y. M., Harada, K., Kikuchi, K., Masutani, C., Hanaoka, F., Nozaki, K., Hashimoto, N., and Takeda, S. (2006). Dual roles for DNA polymerase h in homologous DNA recombination and translesion DNA synthesis. Molec Cell, submitted for publication.

Keeney, S., Giroux, C. N., and Kleckner, N. (1997). Meiosis-specific DNA double-strand breaks are catalyzed by Spo11, a member of a widely conserved protein family. Cell *88*, 375-384.

Kennedy, R. D., and D'Andrea, A. D. (2005). The Fanconi Anemia/BRCA pathway: new faces in the crowd. Genes Dev *19*, 2925-2940

.

Kitagawa, Y., Akaboshi, E., Shinagawa, H., Horii, T., Ogawa, H., and Kato, T. (1985). Structural analysis of the umu operon required for inducible mutagenesis in Escherichia coli. Proc Natl Acad Sci U S A *82*, 4336-4340.

Kneitz, B., Cohen, P. E., Avdievich, E., Zhu, L., Kane, M. F., Hou, H., Jr., Kolodner, R. D., Kucherlapati, R., Pollard, J. W., and Edelmann, W. (2000). MutS homolog 4 localization to meiotic chromosomes is required for chromosome pairing during meiosis in male and female mice. Genes Dev *14*, 1085-1097.

Komori, K., Fujikane, R., Shinagawa, H., and Ishino, Y. (2002). Novel endonuclease in Archaea cleaving DNA with various branched structure. Genes Genet Syst *77*, 227-241.

Komori, K., Hidaka, M., Horiuchi, T., Fujikane, R., Shinagawa, H., and Ishino, Y. (2004). Cooperation of the N-terminal helicase and C-terminal endonuclease activities of archaeal Hef protein in processing stalled replication forks. J Biol Chem *279*, 53175-53185.

Komori, K., Sakae, S., Shinagawa, H., Morikawa, K., and Ishino, Y. (1999). A Holliday junction resolvase from Pyrococcus furiosus: Functional similarity to Escherichia coli RuvC provides evidence for conserved mechanism of homologous recombination in Bacteria, Eukarya, and Archaea. Proc Natl Acad Sci USA *96*, 8873-8878.

Kondo, S., Mamada, A., Miyamoto, C., Keong, C. H., Satoh, Y., and Fujiwara, Y. (1989). Late onset of skin cancers in 2 xeroderma pigmentosum group F siblings and a review of 30 Japanese xeroderma pigmentosum patients in groups D, E and F. Photodermatol *6*, 89-95.

Kook, H. (2005). Fanconi anemia: current management. Hematology *10 Suppl 1*, 108-110.

Kowalczykowski, S. C. (2000). Initiation of genetic recombination and recombination-dependent replication. Trends Biochem Sci *25*, 156-165.

Krejci, L., Van Komen, S., Li, Y., Villemain, J., Reddy, M. S., Klein, H., Ellenberger, T., and Sung, P. (2003). DNA helicase Srs2 disrupts the Rad51 presynaptic filament. Nature *423*, 305-309.

Kunkel, T. A. (1995). DNA mismatch repair: the intricacies of eukaryotic spell checking. Curr Biol *5*, 1091-1094.

Kuraoka, I., Kobertz, W. R., Ariza, R. R., Biggerstaff, M., Essigmann, J. M., and Wood, R. D. (2000). Repair of an interstrand DNA cross-link initiated by ERCC1-XPF repair/recombination nuclease. J Biol Chem *275*, 26632-26636.

Kuzminov, A. (2001a). DNA replication meets genetic exchange: Chromosomal damage and its repair by homologous recombination. Proc Natl Acad Sci U S A *98*, 8461-8468.

Kuzminov, A. (2001b). Single-strand interruptions in replicating chromosomes cause double-strand breaks. Proc Natl Acad Sci U S A *98*, 8241-8246.

Kvaratskhelia, M., and White, M. F. (2000). An archaeal Holliday junction resolving enzyme from Sulfolobus solfataricus exhibits unique properties. J Mol Biol *295*, 193-202.

Laemmli, U. K. (1970). Cleavage of structural proteins during the assembly of the head of bacteriophage T4. Nature *227*, 680-685.

Lambert, S., and Carr, A. M. (2005). Checkpoint responses to replication fork barriers. Biochimie *87*, 591-602.

Lambert, S., Watson, A., Sheedy, D. M., Martin, B., and Carr, A. M. (2005). Gross chromosomal rearrangements and elevated recombination at an inducible site-specific replication fork barrier. Cell *121*, 689-702.

Latonen, L., and Laiho, M. (2005). Cellular UV damage responses--functions of tumor suppressor p53. Biochim Biophys Acta *1755*, 71-89.

Lehmann, A. R. (1972). Postreplication repair of DNA in ultraviolet-irradiated mammalian cells. J Mol Biol *66*, 319-337.

Lehmann, A. R. (2005). Replication of damaged DNA by translesion synthesis in human cells. FEBS Lett *579*, 873-876.

Leveille, F., Blom, E., Medhurst, A. L., Bier, P., Laghmani el, H., Johnson, M., Rooimans, M. A., Sobeck, A., Waisfisz, Q., Arwert, F., *et al.* (2004). The Fanconi anemia gene product FANCF is a flexible adaptor protein. J Biol Chem *279*, 39421-39430.

Levitus, M., Rooimans, M. A., Steltenpool, J., Cool, N. F., Oostra, A. B., Mathew, C. G., Hoatlin, M. E., Waisfisz, Q., Arwert, F., de Winter, J. P., and Joenje, H. (2004). Heterogeneity in Fanconi anemia: evidence for 2 new genetic subtypes. Blood *103*, 2498-2503.

Levitus, M., Waisfisz, Q., Godthelp, B. C., de Vries, Y., Hussain, S., Wiegant, W. W., Elghalbzouri-Maghrani, E., Steltenpool, J., Rooimans, M. A., Pals, G., *et al.* (2005). The DNA helicase BRIP1 is defective in Fanconi anemia complementation group J. Nat Genet *37*, 934-935.

Levran, O., Attwooll, C., Henry, R. T., Milton, K. L., Neveling, K., Rio, P., Batish, S. D., Kalb, R., Velleuer, E., Barral, S., *et al.* (2005). The BRCA1-interacting helicase BRIP1 is deficient in Fanconi anemia. Nat Genet *37*, 931-933.

Lieber, M. R. (1997). The Fen-1 family of structure-specific nucleases in eukaryotic DNA replication, recombination and repair. BioEssays *19*, 233-240.
Lilley, D. M. J., and White, M. F. (2000). Resolving the relationships of resolving enzymes. Proc Natl Acad Sci USA *97*, 9351-9353.

Lilley, D. M. J., and White, M. F. (2001). The junction-resolving enzymes. Nat Revs Mol Cell Biol *2*, 433-443.

Lindahl, T. (1993). Instability and decay of the primary structure of DNA. Nature *362*, 709-715.

Lindahl, T., and Wood, R. D. (1999). Quality control by DNA repair. Science *286*, 1897-1905.

Litman, R., Peng, M., Jin, Z., Zhang, F., Zhang, J., Powell, S., Andreassen, P. R., and Cantor, S. B. (2005). BACH1 is critical for homologous recombination and appears to be the Fanconi anemia gene product FANCJ. Cancer Cell *8*, 255-265.

Liu, L. F., Desai, S. D., Li, T. K., Mao, Y., Sun, M., and Sim, S. P. (2000). Mechanism of action of camptothecin. Ann N Y Acad Sci *922*, 1-10.

Liu, Y., Masson, J.-Y., Shah, R., O'Regan, P., and West, S. C. (2004). RAD51C is required for Holliday junction processing in mammalian cells. Science *303*, 243-246.

Liu, Y., and West, S. C. (2004). Happy Hollidays: 40th Anniversary of the Holliday junction. Nat Rev Mol Cell Biol *5*, 937-944.

Lopes, M., Cotta-Ramusino, C., Pellicioli, A., Liberi, G., Plevani, P., Muzi-Falconi, M., Newlon, C. S., and Foiani, M. (2001). The DNA replication checkpoint response stabilizes stalled replication forks. Nature *412*, 557-561.

Lopes, M., Foiani, M., and Sogo, J. M. (2006). Multiple mechanisms control chromosome integrity after replication fork uncoupling and restart at irreparable UV lesions. Mol Cell *21*, 15-27.

Mace, G., Bogliolo, M., Guervilly, J. H., Dugas du Villard, J. A., and Rosselli, F. (2005). 3R coordination by Fanconi anemia proteins. Biochimie *87*, 647-658.

Masson, J.-Y., Tarsounas, M. C., Stasiak, A. Z., Stasiak, A., Shah, R., McIlwraith, M. J., Benson, F. E., and West, S. C. (2001). Identification and purification of two distinct complexes containing the five RAD51 paralogs. Genes Dev *15*, 3296-3307.

Masutani, C., Kusumoto, R., Yamada, A., Dohmae, N., Yokoi, M., Yuasa, M., Araki, M., Iwai, S., Takio, K., and Hanaoka, F. (1999). The XPV (xeroderma pigmentosum variant) gene encodes human DNA polymerase eta. Nature *399*, 700-704.

Matsumura, Y., Nishigori, C., Yagi, T., Imamura, S., and Takebe, H. (1998). Characterization of molecular defects in xeroderma pigmentosum group F in relation to its clinically mild symptoms. Hum Mol Genet *7*, 969-974.

Matsushita, N., Kitao, H., Ishiai, M., Nagashima, N., Hirano, S., Okawa, K., Ohta, T., Yu, D. S., McHugh, P. J., Hickson, I. D., *et al.* (2005). A FancD2-monoubiquitin fusion reveals hidden functions of Fanconi anemia core complex in DNA repair. Mol Cell *19*, 841-847.

Mazina, O. M., and Mazin, A. V. (2004). Human Rad54 protein stimulates DNA strand exchange activity of hRad51 protein in the presence of Ca2+. J Biol Chem *279*, 52042-52051.

McGlynn, P., and Lloyd, R. G. (2000). Modulation of RNA polymerase by (p)ppGpp reveals a RecG-dependent mechanism for replication fork progression. Cell *101*, 35-45.

McGlynn, P., and Lloyd, R. G. (2001). Rescue of stalled replication forks by RecG: Simultaneous translocation on the leading and lagging strand templates supports an active DNA unwinding model of fork reversal and Holliday junction formation. Proc Natl Acad Sci U S A *98*, 8227-8234.

McGlynn, P., and Lloyd, R. G. (2002a). Genome stability and the processing of damaged replication forks by RecG. Trends Genet *18*, 413-419.

McGlynn, P., and Lloyd, R. G. (2002b). Recombinational repair and the restart of damaged replication forks. Nat Rev Mol Cell Biol *3*, 859-870.

McHugh, P. J., Gill, R. D., Waters, R., and Hartley, J. A. (1999). Excision repair of nitrogen mustard-DNA adducts in Saccharomyces cerevisiae. Nucleic Acids Res *27*, 3259-3266.

McHugh, P. J., Sones, W. R., and Hartley, J. A. (2000). Repair of intermediate structures produced at DNA interstrand crosslinks in S. cerevisiae. Molec Cell Biol *20*, 3425-3433.

McHugh, P. J., Spanswick, V. J., and Hartley, J. A. (2001). Repair of DNA interstrand crosslinks: molecular mechanisms and clinical relevance. Lancet Oncol *2*, 483-490.

McIlwraith, M., Vaisman, A., Liu, Y., Fanning, E., Woodgate, R., and West, S. C. (2005). Human DNA polymerase η promotes DNA synthesis from strand invasion intermediates of homologous recombination. Mol Cell *20*, 783-792.

McPherson, J. P., Lemmers, B., Chahwan, R., Pamidi, A., Migon, E., Maytysiak-Zablocki, E., Moynahan, M. E., Essers, J., Hanada, K., Poonepalli, A., Sanchez-Sweatman, O., *et al.* (2004). Involvement of mammalian Mus81 in genome integrity and tumor suppression. Science *304*, 1822-1826.

Medhurst, A. L., Huber, P. A., Waisfisz, Q., de Winter, J. P., and Mathew, C. G. (2001). Direct interactions of the five known Fanconi anaemia proteins suggest a common functional pathway. Hum Mol Genet *10*, 423-429.

Meetei, A. R., de Winter, J. P., Medhurst, A. L., Wallisch, M., Waisfisz, Q., van de Vrugt, H. J., Oostra, A. B., Yan, Z. J., Ling, C., Bishop, C. E., *et al.* (2003a). A novel ubiquitin ligase is deficient in Fanconi anemia. Nat Genet *35*, 165-170.

Meetei, A. R., Levitus, M., Xue, Y. T., Medhurst, A. L., Zwaan, M., Ling, C., Rooimans, M. A., Bier, P., Hoatlin, M., Pals, G., *et al.* (2004). X-linked inheritance of Fanconi anemia complementation group B. Nat Genet *36*, 1219-1224.

Meetei, A. R., Medhurst, A. L., Ling, C., Xue, Y., Singh, T. R., Bier, P., Steltenpool, J., Stone, S., Dokal, I., Mathew, C. G., *et al.* (2005). A human ortholog of archaeal DNA repair protein Hef is defective in Fanconi anemia complementation group M. Nat Genet *37*, 958-963.

Meetei, A. R., Sechi, S., Wallisch, M., Yang, D. F., Young, M. K., Joenje, H., Hoatlin, M. E., and Wang, W. D. (2003b). A multiprotein nuclear complex connects Fanconi anemia and Bloom syndrome. Mol Cell Biol *23*, 3417-3426.

Meniel, V., Magana-Schwencke, N., Averbeck, D., and Waters, R. (1997). Preferential incision of interstrand crosslinks induced by 8-methoxypsoralen plus UVA in yeast during the cell cycle. Mutat Res *384*, 23-32.

Michel, B., Grompone, G., Flores, M. J., and Bidnenko, V. (2004). Multiple pathways process stalled replication forks. Proc Natl Acad Sci U S A *101*, 12783-12788.

Middleton, C. L., Parker, J. L., Richard, D. J., White, M. F., and Bond, C. S. (2004). Substrate recognition and catalysis by the Holliday junction resolving enzyme Hje. Nucleic Acids Res *32*, 5442-5451.

Miller, R. D., Prakash, L., and Prakash, S. (1982). Genetic control of excision of Saccharomyces cerevisiae interstrand DNA cross-links induced by psoralen plus near-UV light. Mol Cell Biol *2*, 939-948.

Mizuuchi, K., Kemper, B., Hays, J., and Weisberg, R. A. (1982). T4 endonuclease VII cleaves Holliday structures. Cell *29*, 357-365.

Moggs, J. G., Yarema, K. J., Essigmann, J. M., and Wood, R. D. (1996). Analysis of incision sites produced by human cell extracts and purified proteins during nucleotide excision repair of a 1,3-intrastrand d(GpTpG)-cisplatin adduct. J Biol Chem *271*, 7177-7186.

Montes de Oca, R., Andreassen, P. R., Margossian, S. P., Gregory, R. C., Taniguchi, T., Wang, X., Houghtaling, S., Grompe, M., and D'Andrea, A. D. (2005). Regulated interaction of the Fanconi anemia protein, FANCD2, with chromatin. Blood *105*, 1003-1009.

Morimatsu, K., and Kowalczykowski, S. C. (2003). RecFOR proteins load RecA protein onto gapped DNA to accelerate DNA strand exchange: A universal step of recombinational repair. Mol Cell *11*, 1337-1347.

Mortensen, U. H., Bendixen, C., Sunjevaric, I., and Rothstein, R. (1996). DNA strand annealing is promoted by the yeast Rad52 protein. Proc Natl Acad Sci USA *93*, 10729-10734.

Mosedale, G., Niedzwiedz, W., Alpi, A., Perrina, F., Pereira-Leal, J. B., Johnson, M., Langevin, F., Pace, P., and Patel, K. J. (2005). The vertebrate Hef ortholog is a component of the Fanconi anemia tumor-suppressor pathway. Nat Struct Mol Biol *12*, 763-771.

Moynahan, M. E., Cui, T. Y., and Jasin, M. (2001a). Homology-directed DNA repair, mitomycin-C resistance, and chromosome stability is restored with correction of a BRCA1 mutation. Cancer Res *61*, 4842-4850.

Moynahan, M. E., Pierce, A. J., and Jasin, M. (2001b). BRCA2 is required for homology-directed repair of chromosomal breaks. Molec Cell *7*, 263-272.

Mozzherin, D. J., and Fisher, P. A. (1996). Human DNA polymerase epsilon: enzymologic mechanism and gap-filling synthesis. Biochemistry *35*, 3572-3577.

Mu, D., Hsu, D. S., and Sancar, A. (1996). Reaction mechanism of human DNA repair excision nuclease. J Biol Chem *271*, 8285-8294.

Mullen, J. R., Kaliraman, V., Ibrahim, S. S., and Brill, S. J. (2001). Requirement for three novel protein complexes in the absence of the Sgs1 DNA helicase in Saccharomyces cerevisiae. Genetics *157*, 103-118.

Nakane, H., Takeuchi, S., Yuba, S., Saijo, M., Nakatsu, Y., Murai, H., Nakatsuru, Y., Ishikawa, T., Hirota, S., Kitamura, Y., and et al. (1995). High incidence of ultraviolet-B-or chemical-carcinogen-induced skin tumours in mice lacking the xeroderma pigmentosum group A gene. Nature *377*, 165-168.

Nakanishi, K., Yang, Y. G., Pierce, A. J., Taniguchi, T., Digweed, M., D'Andrea, A. D., Wang, Z. Q., and Jasin, M. (2005). Human Fanconi anemia monoubiquitination pathway promotes homologous DNA repair. Proc Natl Acad Sci U S A *102*, 1110-1115.

New, J. H., Sugiyama, T., Zaitseva, E., and Kowalczykowski, S. C. (1998). Rad52 protein stimulates DNA strand exchange by Rad51 and replication protein-A. Nature *391*, 407-410.

Newman, M., Murray-Rust, J., Lally, J., Rudolf, J., Fadden, A., Knowles, P. P., White, M. F., and McDonald, N. Q. (2005). Structure of an XPF endonuclease with and without DNA suggests a model for substrate recognition. EMBO J *24*, 895-905.

Niedernhofer, L. J., Essers, J., Weeda, G., Beverloo, B., de Wit, J., Muijtjens, M., Odijk, H., Hoeijmakers, J. H. J., and Kanaar, R. (2001). The structure-specific endonuclease Ercc1-Xpf is required for targeted gene replacement in embryonic stem cells. EMBO J *20*, 6540-6549.

Niedernhofer, L. J., Lalai, A. S., and Hoeijmakers, J. H. (2005). Fanconi anemia (cross)linked to DNA repair. Cell *123*, 1191-1198.

Niedernhofer, L. J., Odijk, H., Budzowska, M., van Drunen, E., Maas, A., Theil, A. F., de Wit, J., Jaspers, N. G. J., Beverloo, H. B., Hoeijmakers, J. H. J., and Kanaar, R. (2004). The structure-specific endonuclease Ercc1-Xpf is required to resolve DNA interstrand cross-link-induced double-strand breaks. Mol Cell Biol *24*, 5776-5787.

Niedzwiedz, W., Mosedale, G., Johnson, M., Ong, C. Y., Pace, P., and Patel, K. J. (2004). The Fanconi anaemia gene FANCC promotes homologous recombination and error-prone DNA repair. Mol Cell *15*, 607-620.

Nijman, S. M. B., Huang, T. T., Dirac, A. M. G., Brummelkamp, T. R., Kerkhoven, R. M., D'Andrea, A. D., and Bernards, R. (2005). The deubiquitinating enzyme USP1 regulates the Fanconi anemia pathway. Mol Cell *17*, 331-339.

Nishino, T., Ishino, Y., and Morikawa, K. (2006). Structure-specific DNA nucleases: structural basis for 3D-scissors. Curr Opin Struct Biol *16*, 60-67.

Nishino, T., Komori, K., Ishino, Y., and Morikawa, K. (2003). X-ray and biochemical anatomy of an archaeal XPF/Rad1/Mus81 family nuclease: Similarity between its endonuclease domain and restriction enzymes. Structure (Camb) *11*, 445-457.

Nishino, T., Komori, K., Ishino, Y., and Morikawa, K. (2005a). Structural and functional analyses of an archaeal XPF/Rad1/Mus81 nuclease: asymmetric DNA binding and cleavage mechanisms. Structure (Camb) *13*, 1183-1192.

Nishino, T., Komori, K., Tsuchiya, D., Ishino, Y., and Morikawa, K. (2001). Crystal structure of the archaeal Holliday Junction resolvase Hjc and implications for DNA recognition. Structure *9*, 197-204.

Nishino, T., Komori, K., Tsuchiya, D., Ishino, Y., and Morikawa, K. (2005b). Crystal structure and functional implications of Pyrococcus furiosus hef helicase domain involved in branched DNA processing. Structure (Camb) *13*, 143-153.

O'Donovan, A., Davies, A. A., Moggs, J. G., West, S. C., and Wood, R. D. (1994). XPG endonuclease makes the 3' incision in human DNA nucleotide excision repair. Nature *371*, 432-435.

Ogawa, T., Yu, X., Shinohara, A., and Egelman, E. H. (1993). Similarity of the yeast Rad51 filament to the bacterial RecA filament. Science *259*, 1896-1899.

Ohashi, A., Zdzienicka, M. Z., Chen, J. J., and Couch, F. J. (2005). Fanconi anemia complementation group D2 (FANCD2) functions independently of BRCA2- and RAD51-associated homologous recombination in response to DNA damage. J Biol Chem *280*, 14877-14883.

Osborn, A. J., Elledge, S. J., and Zou, L. (2002). Checking on the fork: the DNA-replication stress-response pathway. Trends Cell Biol *12*, 509-516.

Osman, F., Dixon, J., Doe, C. L., and Whitby, M. C. (2003). Generating crossovers by resolution of nicked Holliday junctions: A role of Mus81-Eme1 in meiosis. Molec Cell *12*, 761-774.

Owen, D. J., Vallis, Y., Pearse, B. M., McMahon, H. T., and Evans, P. R. (2000). The structure and function of the beta 2-adaptin appendage domain. Embo J *19*, 4216-4227.

Pace, P., Johnson, M., Tan, W. M., Mosedale, G., Sng, C., Hoatlin, M., de Winter, J., Joenje, H., Gergely, F., and Patel, K. J. (2002). FANCE: the link between Fanconi anaemia complex assembly and activity. EMBO J *21*, 3414-3423.

Pages, V., and Fuchs, R. P. (2003). Uncoupling of leading- and lagging-strand DNA replication during lesion bypass in vivo. Science *300*, 1300-1303.

Papadopoulo, D., Guillouf, C., Mohrenweiser, H., and Moustacchi, E. (1990a). Hypomutability in Fanconi anemia cells is associated with increased deletion frequency at the HPRT locus. Proc Natl Acad Sci U S A *87*, 8383-8387.

Papadopoulo, D., Porfirio, B., and Moustacchi, E. (1990b). Mutagenic response of Fanconi's anemia cells from a defined complementation group after treatment with photoactivated bifunctional psoralens. Cancer Res *50*, 3289-3294.

Paques, F., and Haber, J. E. (1999). Multiple pathways of recombination induced by double-strand breaks in Saccharomyces cerevisiae. Microbiol Molec Biol Revs *63*, 349-404.

Park, Y., and Gerson, S. L. (2005). DNA repair defects in stem cell function and aging. Annu Rev Med *56*, 495-508.

Parsons, C. A., Stasiak, A., Bennett, R. J., and West, S. C. (1995). Structure of a multisubunit complex that promotes DNA branch migration. Nature *374*, 375-378.

Paull, T. T., and Gellert, M. (1998). The 3'-exonuclease to 5'-exonuclease activity of Mre11 facilitates repair of DNA double-strand breaks. Mol Cell *1*, 969-979.

Paull, T. T., and Gellert, M. (1999). Nbs1 potentiates ATP-driven DNA unwinding and endonuclease cleavage by the Mre11/Rad50 complex. Genes Dev *13*, 1276-1288.

Pearse, B. M., Smith, C. J., and Owen, D. J. (2000). Clathrin coat construction in endocytosis. Curr Opin Struct Biol *10*, 220-228.

Petukhova, G., Stratton, S., and Sung, P. (1998). Catalysis of homologous DNA pairing by yeast Rad51 and Rad54 proteins. Nature *393*, 91-94.

Pichierri, P., Averbeck, D., and Rosselli, F. (2002). DNA cross-link-dependent RAD50/MRE11/NBS1 subnuclear assembly requires the Fanconi anemia C protein. Hum Mol Genet *11*, 2531-2546.

Pichierri, P., Franchitto, A., and Rosselli, F. (2004). BLM and the FANC proteins collaborate in a common pathway in response to stalled replication forks. EMBO J *23*, 3154-3163.

Pichierri, P., and Rosselli, F. (2004). The DNA crosslink-induced S-phase checkpoint depends on ATR-CHK1 and ATR-NBS1-FANCD2 pathways. EMBO J *23*, 1178-1187.

Pierce, A. J., Johnson, R. D., Thompson, L. H., and Jasin, M. (1999). XRCC3 promotes homology-directed repair of DNA damage in mammalian cells. Genes Dev *13*, 2633-2638.

Prado, F., and Aguilera, A. (2005). Impairment of replication fork progression mediates RNA polII transcription-associated recombination. Embo J *24*, 1267-1276.

Prakash, L. (1981). Characterization of postreplication repair in Saccharomyces cerevisiae and effects of rad6, rad18, rev3 and rad52 mutations. Mol Gen Genet *184*, 471-478.

Prakash, R., Krejci, L., Van Komen, S., Schurer, K. A., Kramer, W., and Sung, P. (2005). Saccharomyces cerevisiae MPH1 gene, required for homologous recombination-mediated mutation avoidance, encodes a 3 ' to 5 ' DNA helicase. J Biol Chem *280*, 7854-7860.

Prasher, J. M., Lalai, A. S., Heijmans-Antonissen, C., Ploemacher, R. E., Hoeijmakers, J. H., Touw, I. P., and Niedernhofer, L. J. (2005). Reduced hematopoietic reserves in DNA interstrand crosslink repair-deficient Ercc1-/- mice. Embo J *24*, 861-871.

Raaijmakers, H., Vix, O., Toro, I., Golz, S., Kemper, B., and Suck, D. (1999). X-ray structure of T4 endonuclease VII: a DNA junction resolvase with a novel fold and unusual domain-swapped dimer architecture. EMBO J *18*, 1447-1458.

Radford, S. J., Goley, E., Baxter, K., McMahan, S., and Sekelsky, J. (2005). Drosophila ERCC1 is required for a subset of MEI-9-dependent meiotic crossovers. Genetics *170*, 1737-1745.

Rafferty, J. B., Bolt, E. L., Muranova, T. A., Sedelnikova, S. E., Leonard, P., Pasquo, A., Baker, P. J., Rice, D. W., Sharpies, G. J., and Lloyd, R. G. (2003). The structure of Escherichia coli RusA endonuclease reveals a new Holliday junction DNA binding fold. Structure (Camb) *11*, 1557-1567.

Rahman, N., and Stratton, M. R. (1998). The genetics of breast cancer susceptibility. Annu Rev Genet *32*, 95-121.

Ratner, J. N., Balasubramanian, B., Corden, J., Warren, S. L., and Bregman, D. B. (1998). Ultraviolet radiation-induced ubiquitination and proteasomal degradation of the large subunit of RNA polymerase II. Implications for transcription-coupled DNA repair. J Biol Chem *273*, 5184-5189.

Reya, T., Morrison, S. J., Clarke, M. F., and Weissman, I. L. (2001). Stem cells, cancer, and cancer stem cells. Nature *414*, 105-111.

Ristic, D., Wyman, C., Paulusma, C., and Kanaar, R. (2001). The architecture of the human RAD54-DNA complex provides evidence for protein translocation along DNA. Proc Natl Acad Sci U S A *98*, 8454-8460.

Roberts, J. A., Bell, S. D., and White, M. F. (2003). An archaeal XPF repair endonuclease dependent on a heterotrimeric PCNA. Mol Microbiol *48*, 361-371.

Roberts, J. A., and White, M. F. (2005). An archaeal endonuclease displays key properties of both eukaryal XPF-ERCC1 and Mus81. J Biol Chem *280*, 5924-5928.

Rothfuss, A., and Grompe, M. (2004). Repair kinetics of genomic interstrand DNA cross-links: Evidence for DNA double-strand break-dependent activation of the Fanconi anemia/BRCA pathway. Mol Cell Biol *24*, 123-134.

Rupp, W. D., and Howard-Flanders, P. (1968). Discontinuities in the DNA synthesized in an excision-defective strain of Escherichia coli following ultraviolet irradiation. J Mol Biol *31*, 291-304.

Rupp, W. D., Wilde, C. E., Reno, D. L., and Howard-Flanders, P. (1971). Exchanges between DNA strands in ultraviolet-irradiated Escherichia coli. J Mol Biol *61*, 25-44.

Saito, A., Iwasaki, H., Ariyoshi, M., Morikawa, K., and Shinagawa, H. (1995). Identification of four acidic amino acids that constitute the catalytic center of the RuvC Holliday junction resolvase. Proc Natl Acad Sci USA *92*, 7470-7474.

Sands, A. T., Abuin, A., Sanchez, A., Conti, C. J., and Bradley, A. (1995). High susceptibility to ultraviolet-induced carcinogenesis in mice lacking XPC. Nature *377*, 162-165.

Scheller, J., Schurer, A., Rudolph, C., Hettwer, S., and Kramer, W. (2000). MPH1, a yeast gene encoding a DEAH protein, plays a role in protection of the genome from spontaneous and chemically induced damage. Genetics *155*, 1069-1081.

Schurer, K. A., Rudolph, C., Ulrich, H. D., and Kramer, W. (2004). Yeast MPH1 gene functions in an error-free DNA damage bypass pathway that requires genes from homologous recombination, but not from postreplicative repair. Genetics *166*, 1673-1686.

Seigneur, M., Bidnenko, V., Ehrlich, S. D., and Michel, B. (1998). RuvAB acts at arrested replication forks. Cell *95*, 419-430.

Selby, C. P., Drapkin, R., Reinberg, D., and Sancar, A. (1997). RNA polymerase II stalled at a thymine dimer: footprint and effect on excision repair. Nucleic Acids Res *25*, 787-793.

Setlow, R. B. (1966). Cyclobutane-type pirimidine dimers in polynucleotides. Science *22*, 379-386.

Sgouros, J., Gaillard, P. H. L., and Wood, R. D. (1999). A relationship between a DNA-repair/recombination nuclease family and archaeal helicases. Trends Biochem Sci *24*, 95-97.

Shah, R., Bennett, R. J., and West, S. C. (1994). Genetic recombination in E. coli: RuvC protein cleaves Holliday junctions at resolution hotspots in vitro. Cell *79*, 853-864.

Shah, R., Cosstick, R., and West, S. C. (1997). The RuvC dimer resolves Holliday junctions by a dual incision mechanism that involves base-specific contacts. EMBO J *16*, 1464-1472.

Shannon, M., Lamerdin, J. E., Richardson, L., McCutchen-Maloney, S. L., Hwang, M. H., Handel, M. A., Stubbs, L., and Thelen, M. P. (1999). Characterization of the mouse XPF DNA repair gene and differential expression during spermatogenesis. Genomics *62*, 427-435.

Sharp, P. A., Sugden, B., and Sambrook, J. (1973). Detection of two restriction endonuclease activities in Haemophilus parainfluenzae using analytical agarose--ethidium bromide electrophoresis. Biochemistry *12*, 3055-3063.

Sharples, G. J. (2001). The X philes: structure-specific endonucleases that resolve Holliday junctions. Mol Microbiol *39*, 823-834.

Sharples, G. J., Chan, S. N., Mahdi, A. A., Whitby, M. C., and Lloyd, R. G. (1994). Processing of intermediates in recombination and DNA repair: Identification of a new endonuclease that specifically cleaves Holliday junctions. EMBO J *13*, 6133-6142.

Shen, Z. Y., Cloud, K. G., Chen, D. J., and Park, M. S. (1996). Specific interactions between the human Rad51 and Rad52 proteins. J Biol Chem *271*, 148-152.

Shevchenko, A., Wilm, M., Vorm, O., and Mann, M. (1996). Mass spectrometric sequencing of proteins silver-stained polyacrylamide gels. Anal Chem *68*, 850-858.

Shibata, T., Cunningham, R. P., DasGupta, C., and Radding, C. M. (1979). Homologous pairing in genetic recombination: complexes of RecA protein and DNA. Proc Nat Acad Sci USA *76*, 5100-5104.

Siddique, M. A., Nakanishi, K., Taniguchi, T., Grompe, M., and D'Andrea, A. D. (2001). Function of the Fanconi anemia pathway in Fanconi anemia complementation group F and D1 cells. Exp Hematol *29*, 1448-1455.

Sigurdsson, S., Van Komen, S., Petukhovan, G., and Sung, P. (2002). Homologous DNA pairing by human recombination factors RAD51 and RAD54. J Biol Chem *277*, 42790-42794.

Sijbers, A. M., Delaat, W. L., Ariza, R. R., Biggerstaff, M., Wei, Y. F., Moggs, J. G., Carter, K. C., Shell, B. K., Evans, E., De Jong, M. C., *et al.* (1996a). Xeroderma pigmentosum group F caused by a defect in a structure-specific DNA repair endonuclease. Cell *86*, 811-822.

Sijbers, A. M., Van der Spek, P. J., Odijk, H., Van den Berg, J., Van Duin, M., Westerveld, A., Jaspers, N. G. J., Bootsma, D., and Hoeijmakers, J. H. J. (1996b). Mutational analysis of the human nucleotide excision repair gene ERCC1. Nucl Acids Res *24*, 3370-3380.

Singer, B. (1975). The chemical effects of nucleic acid alkylation and their relation to mutagenesis and carcinogenesis. Cancer Res *15*, 219-284.

Singleton, M. R., Scaife, S., and Wigley, D. B. (2001). Structural analysis of DNA replication fork reversal by RecG. Cell *107*, 79-89.

Singleton, M. R., and Wigley, D. B. (2002). Modularity and specialization in superfamily 1 and 2 helicases. J Bacteriol *184*, 1819-1826.

Sladek, F. M., Munn, M. M., Rupp, W. D., and Howard-Flanders, P. (1989). In vitro repair of psoralen-DNA cross-links by RecA, UvrABC, and the 5'-exonuclease of DNA polymerase I. J Biol Chem *264*, 6755-6765.

Smith, G. R., Boddy, M. N., Shanahan, P., and Russell, P. (2003). Fission yeast Mus81-Eme1 Holliday junction resolvase is required for meiotic crossing over but not for gene conversion. Genetics *165*, 2289-2293.

Sobeck, A., Stone, S., Costanzo, V., de Graaf, B., Reuter, T., de Winter, J., Wallisch, M., Akkari, Y., Olson, S., Wang, W., *et al.* (2006). Fanconi anemia proteins are required to prevent accumulation of replication-associated DNA double-strand breaks. Mol Cell Biol *26*, 425-437.

Sogo, J. M., Lopes, M., and Foiani, M. (2002). Fork reversal and ssDNA accumulation at stalled replication forks owing to checkpoint defects. Science *297*, 599-602.

Soultanas, P., Dillingham, M. S., Wiley, P., Webb, M. R., and Wigley, D. B. (2000). Uncoupling DNA translocation and helicase activity in PcrA: direct evidence for an active mechanism. EMBO J *19*, 3799-3810.

Sridharan, D., Brown, M., Lambert, W. C., McMahon, L. W., and Lambert, M. W. (2003). Nonerythroid alphaII spectrin is required for recruitment of FANCA and XPF to nuclear foci induced by DNA interstrand cross-links. J Cell Sci *116*, 823-835.

Sugasawa, K., Masutani, C., Uchida, A., Maekawa, T., Van der Spek, P. J., Bootsma, D., Hoeijmakers, J. H. J., and Hanaoka, F. (1996). HHR23b, a human RAD23 homolog, stimulates XPC protein in nucleotide excision repair in vitro. Mol Cell Biol *16*, 4852-4861.

Sugasawa, K., Ng, J. M. Y., Masutani, C., Iwai, S., Van der Spek, P. J., Eker, A. P. M., Hanaoka, F., Bootsma, D., and Hoeijmakers, J. H. J. (1998). Xeroderma pigmentosum group C protein complex is the initiator of global genome nucleotide excision repair. Mol Cell *2*, 223-232.

Sung, P. (1994). Catalysis of ATP-dependent homologous DNA pairing and strand exchange by yeast Rad51 protein. Science *265*, 1241-1243.

Symington, L. S., and Kolodner, R. (1985). Partial purification of an enzyme from Saccharomyces cerevisiae that cleaves Holliday junctions. Proc Natl Acad Sci USA *82*, 7247-7251.

Szostak, J. W., Orr-Weaver, T. L., Rothstein, R. J., and Stahl, F. W. (1983). The double-strand break repair model for recombination. Cell *33*, 25-35.

Takeuchi, Y., Horiuchi, T., and Kobayashi, T. (2003). Transcription-dependent recombination and the role of fork collision in yeast rDNA. Genes Dev *17*, 1497-1506.

Tan, T. L. R., Essers, J., Cittero, E., Swagemakers, S. M. A., de Wit, J., Benson, F. E., Hoeijmakers, J. H. J., and Kanaar, R. (1999). Mouse Rad54 affects DNA conformation and DNA-damage-induced Rad51 foci formation. Curr Biol *9*, 325-328.

Tang, M. J., Shen, X., Frank, E. G., O'Donnell, M., Woodgate, R., and Goodman, M. F. (1999). UmuD'C2 is an error-prone DNA polymerase, Escherichia coli pol V. Proc Natl Acad Sci USA *96*, 8919-8924.

Taniguchi, T., and D' Andrea, A. D. (2002). The Fanconi Anemia protein, FANCE, promotes the nuclear accumulation of FANCC. Blood *100*, 2457-2462.

Taniguchi, T., I., G.-H., Andreassen, P. R., Gregory, R. C., Grompe, M., and D'Andrea, A. D. (2002). S-phase-specific interaction of the Fanconi anemia protein, FANCD2, with BRCA1 and RAD51. Blood *100*, 2414-2420.

Tarsounas, M., Davies, A. A., and West, S. C. (2004). RAD51 localization and activation following DNA damage. Phil Trans R Soc Lond B *359*, 87-93.

Tarsounas, M., Davies, D., and West, S. C. (2003). BRCA2-dependent and independent formation of RAD51 nuclear foci. Oncogene *22*, 1115-1123.

Teoule, R. (1987). Radiation-induced DNA damage and its repair. Int J Radiat Biol *51*, 573-589.

Tercero, J. A., and Diffley, J. F. X. (2001). Regularion of DNA replication fork progression through damaged DNA by Mec1/Rad53 checkpoint. Nature *412*, 553-557.

Thacker, J. (2005). The RAD51 gene family, genetic instability and cancer. Cancer Lett *219*, 125-135.

Thompson, B. J., Escarmis, C., Parker, B., Slater, W. C., Doniger, J., Tessman, I., and Warner, R. C. (1975). Figure-8 configuration of dimers of S13 and ØX174 replicative form DNA. J Mol Biol *91*, 409-419.

Tian, M., Shinkura R., Shinkura N., and Alt, F. W. (2004). Growth retardation, early death, and DNA repair defects in mice deficient for the nucleotide excision repair enzyme XPF. Mol Cell Biol *24*, 1200-1205.

Tornaletti, S., Patrick, S. M., Turchi, J. J., and Hanawalt, P. C. (2003). Behavior of T7 RNA polymerase and mammalian RNA polymerase II at site-specific cisplatin adducts in the template DNA. J Biol Chem *278*, 35791-35797.

Tremeau-Bravard, A., Riedl, T., Egly, J. M., and Dahmus, M. E. (2004). Fate of RNA polymerase II stalled at a cisplatin lesion. J Biol Chem *279*, 7751-7759.

Tripsianes, K., Folkers, G., Ab, E., Das, D., Odijk, H., Jaspers, N. G., Hoeijmakers, J. H., Kaptein, R., and Boelens, R. (2005). The structure of the human ERCC1/XPF interaction domains reveals a complementary role for the two proteins in nucleotide excision repair. Structure *13*, 1849-1858.

Truglio, J. J., Croteau, D. L., Van Houten, B., and Kisker, C. (2006). Prokaryotic nucleotide excision repair: the UvrABC system. Chem Rev *106*, 233-252.

Tsaneva, I. R., Müller, B., and West, S. C. (1992). ATP-dependent branch migration of Holliday junctions promoted by the RuvA and RuvB proteins of E. coli. Cell *69*, 1171-1180.

Tsodikov, O. V., Enzlin, J. H., Scharer, O. D., and Ellenberger, T. (2005). Crystal structure and DNA binding functions of ERCC1, a subunit of the DNA structure-specific endonuclease XPF-ERCC1. Proc Natl Acad Sci U S A *102*, 11236-11241.

Tsubouchi, H., and Ogawa, H. (2000). Exo1 roles for repair of DNA double-strand breaks and meiotic crossing over in Saccharomyces cerevisiae. Mol Biol Cell *11*, 2221-2233.

Vaisman, A., Frank, E. G., Iwai, S., Ohashi, E., Ohmori, H., Hanaoka, F., and Woodgate, R. (2003). Sequence context-dependent replication of DNA templates containing UV-induced lesions by human DNA polymerase iota. DNA Repair (Amst) *2*, 991-1006.

Van Houten, B., Gamper, H., Holbrook, S. R., Hearst, J. E., and Sancar, A. (1986). Action mechanism of ABC excision nuclease on a DNA substrate containing a psoralen crosslink at a defined position. Proc Natl Acad Sci U S A *83*, 8077-8081.

Van Komen, S., Petukhova, G., Sigurdsson, S., Stratton, S., and Sung, P. (2000). Superhelicity-driven homologous DNA pairing by yeast recombination factors Rad51 and Rad54. Mol Cell *6*, 563-572.

Vandenberg, C. J., Gergely, F., Ong, C. Y., Pace, P., Mallery, D. L., Hiom, K., and Patel, K. J. (2003). BRCA1-independent ubiquitination of FANCD2. Mol Cell *12*, 247-254.

Veaute, X., Jeusset, J., Soustelle, C., Kowalczykowski, S. C., Le Cam, E., and Fabre, F. (2003). The Srs2 helicase prevents recombination by disrupting Rad51 nucleoprotein filaments. Nature *423*, 309-312.

Waisfisz, Q., de Winter, J. P., Kruyt, F. A. E., de Groot, J., van der Weel, L., Dijkmans, L. M., Zhi, Y., Arwert, F., Scheper, R. J., Youssoufian, H., *et al.* (1999). A physical complex of the Fanconi anemia proteins FANCG/XRCC9 and FANCA. Proc Natl Acad Sci USA *96*, 10320-10325.

Walker, J. E., Saraste, M., Runswick, M. J., and Gay, N. J. (1982). Distantly related sequences in the a- and b-subunits of ATP synthase, myosin, kinases and other ATP-requiring enzymes and a common nucleotide binding fold. EMBO J *1*, 945-951.

Wang, T. C. (2005). Discontinuous or semi-discontinuous DNA replication in Escherichia coli? Bioessays *27*, 633-636.

Wang, T. C., and Chen, S. H. (1992). Similar-sized daughter-strand gaps are produced in the leading and lagging strands of DNA in UV-irradiated E. coli uvrA cells. Biochem Biophys Res Commun *184*, 1496-1503.

Wang, X., Andreassen, P. R., and D'Andrea, A. D. (2004). Functional interaction of monoubiquitinated FANCD2 and BRCA2/FANCD1 in chromatin. Mol Cell Biol *24*, 5850-5862.

Wang, Z., Jones, G. M., and Prelich, G. (2005). Genetic analysis connects SLX5 and SLX8 to the SUMO pathway in Saccharomyces cerevisiae. Genetics.

Weeda, G., Donker, I., de Wit, J., Morreau, H., Janssens, R., Vissers, C. J., Nigg, A., van Steeg, H., Bootsma, D., and Hoeijmakers, J. H. (1997). Disruption of mouse ERCC1 results in a novel

repair syndrome with growth failure, nuclear abnormalities and senescence. Curr Biol *7*, 427-439.

West, S. C. (1995). Holliday junctions cleaved by Rad1? Nature *373*, 27-28.

West, S. C. (1997). Processing of recombination intermediates by the RuvABC proteins. Ann Rev Genet *31*, 213-244.

West, S. C. (2003). Molecular views of recombination proteins and their control. Nat Rev Mol Cell Biol *4*, 435-445.

West, S. C., Cassuto, E., and Howard-Flanders, P. (1982). Postreplication repair in E. coli: Strand exchange reactions of gapped DNA by RecA protein. Mol Gen Genet *187*, 209-217.

Westermark, U. K., Reyngold, M., Olshen, A. B., Baer, R., Jasin, M., and Moynahan, M. E. (2003). BARD1 participates with BRCA1 in homology-directed repair of chromosome breaks. Mol, Cell, Biol *23*, 7926-7936.

Whitby, M. C. (2005). Making crossovers during meiosis. Biochem Soc Trans *33*, 1451-1455.

Whitby, M. C., Bolt, E. L., Chan, S. N., and Lloyd, R. G. (1996). Interactions between RuvA and RuvC at Holliday junctions: inhibition of junction cleavage and formation of a RuvA-RuvC-DNA complex. J Mol Biol *264*, 878-890.

Whitby, M. C., and Dixon, J. (1997). A new Holliday junction resolving enzyme from Schizosaccharomyces pombe that is homologous to Cce1 from Saccharomyces cerevisiae. J Mol Biol *272*, 509-522.

Whitby, M. C., Osman, F., and Dixon, J. (2003). Cleavage of model replication forks by fission yeast Mus81-Eme1 and budding yeast Mus81-Mms4. J Biol Chem *278*, 6928-6935.

White, M. F. (2003). Archaeal DNA repair: paradigms and puzzles. Biochem Soc Trans *31*, 690-693.

White, M. F., and Lilley, D. M. J. (1997). Characterization of a Holliday junction-resolving enzyme from Schizosaccharomyces pombe. Mol Cell Biol *17*, 6465-6471.

Wong, A. K. C., Pero, R., Ormonde, P. A., Tavtigian, S. V., and Bartel, P. L. (1997). Rad51 interacts with the evolutionarily conserved BRC motifs in the human breast cancer susceptibility gene BRCA2. J Biol Chem *272*, 31941-31944.

Wu, L., Bachrati, C. Z., Ou, J., Xu, C., Yin, J., Chang, M., Wang, W., Li, L., Brown, G. W., and Hickson, I. D. (2006). BLAP75/RMI1 promotes the BLM-dependent dissolution of homologous recombination intermediates. Proc Natl Acad Sci U S A *103*, 4068-4073.

Wu, L., and Hickson, I. D. (2003). The Bloom's syndrome helicase suppresses crossing over during homologous recombination. Nature *426*, 870-874.

Yamada, K., Miyata, T., Tsuchiya, D., Oyama, T., Fujiwara, Y., Ohnishi, T., Iwasaki, H., Shinagawa, H., Ariyoshi, M., Mayanagi, K., and Morikawa, K. (2002). Crystal structure of the RuvA-RuvB complex: A structural basis for the Holliday junction migrating motor machinery. Mol Cell *10*, 671-681.

Yamamoto, K., Hirano, S., Ishiai, M., Morishima, K., Kitao, H., Namikoshi, K., Kimura, M., Matsushita, N., Arakawa, H., Buerstedde, J. M., *et al.* (2005). Fanconi anemia protein FANCD2 promotes immunoglobulin gene conversion and DNA repair through a mechanism related to homologous recombination. Mol Cell Biol *25*, 34-43.

Yamamoto, K., Ishiai, M., Matsushita, N., Arakawa, H., Lamerdin, J. E., Buerstedde, J. M., Tanimoto, M., Harada, M., Thompson, L. H., and Takata, M. (2003). Fanconi anemia FANCG protein in mitigating radiation- and enzyme-induced DNA double-strand breaks by homologous recombination in vertebrate cells. Mol Cell Biol *23*, 5421-5430.

Yang, Y. G., Herceg, Z., Nakanishi, K., Demuth, I., Piccoli, C., Michelon, J., Hildebrand, G., Jasin, M., Digweed, M., and Wang, Z. Q. (2005). The Fanconi anemia group A protein modulates homologous repair of DNA double-strand breaks in mammalian cells. Carcinogenesis *26*, 1731-1740.

Yildiz, O., Kearney, H., Kramer, B. C., and Sekelsky, J. J. (2004). Mutational analysis of the Drosophila DNA repair and recombination gene mei-9. Genetics *167*, 263-273.

Yildiz, O., Majumder, S., Kramer, B., and Sekelsky, J. J. (2002). Drosophila MUS312 interacts with the nucleotide excision repair endonuclease MEI-9 to generate meiotic crossovers. Mol Cell *10*, 1503-1509.

Yin, J. H., Sobeck, A., Xu, C., Meetei, A. R., Hoatlin, M., Li, L., and Wang, W. (2005). BLAP75, an essential component of Bloom's syndrome protein complexes that maintain genome integrity. EMBO J *24*, 1465-1476.

Yu, X., Jacobs, S. A., West, S. C., Ogawa, T., and Egelman, E. H. (2001). Domain structure and dynamics in the helical filaments formed by RecA and RAD51 on DNA. Proc Natl Acad Sci USA *98*, 8419-8424.

Yuan, S.-S. F., Lee, S.-Y., Chen, G., Song, M., Tomlinson, G. E., and Lee, E. Y. (1999). BRCA2 is required for ionizing radiation-induced assembly of Rad51 complex in vivo. Cancer Res *59*, 3547-3551.

Yun, J. H., Zhong, Q., Kwak, J. Y., and Lee, W. H. (2005). Hypersensitivity of BRCA1-deficient MEF to the DNA interstrand crosslinking agent mitomycin C is associated with defect in homologous recombination repair and aberrant S-phase arrest. Oncogene *24*, 4009-4016.

Zhang, C., Roberts, T. M., Yang, J., Desai, R., and Brown, G. W. (2006). Suppression of genomic instability by SLX5 and SLX8 in Saccharomyces cerevisiae. DNA Repair (Amst) *5*, 336-346.

Zhang, R., Sengupta, S., Yang, Q., Linke, S. P., Yanaihara, N., Bradsher, J., Blais, V., McGowan, C. H., and Harris, C. C. (2005). BLM helicase facilitates MUS81 endonuclease activity in human cells. Cancer Res *65*, 2526-2531.

Zurita, M., and Merino, C. (2003). The transcriptional complexity of the TFIIH complex. Trends Genet *19*, 578-584.